WOMEN IN GASTROINTESTINAL SCIENCES: 2021

EDITED BY: Kathleen E. DelGiorno and Natalie Luhtala
PUBLISHED IN: Frontiers in Physiology and Frontiers in Oncology

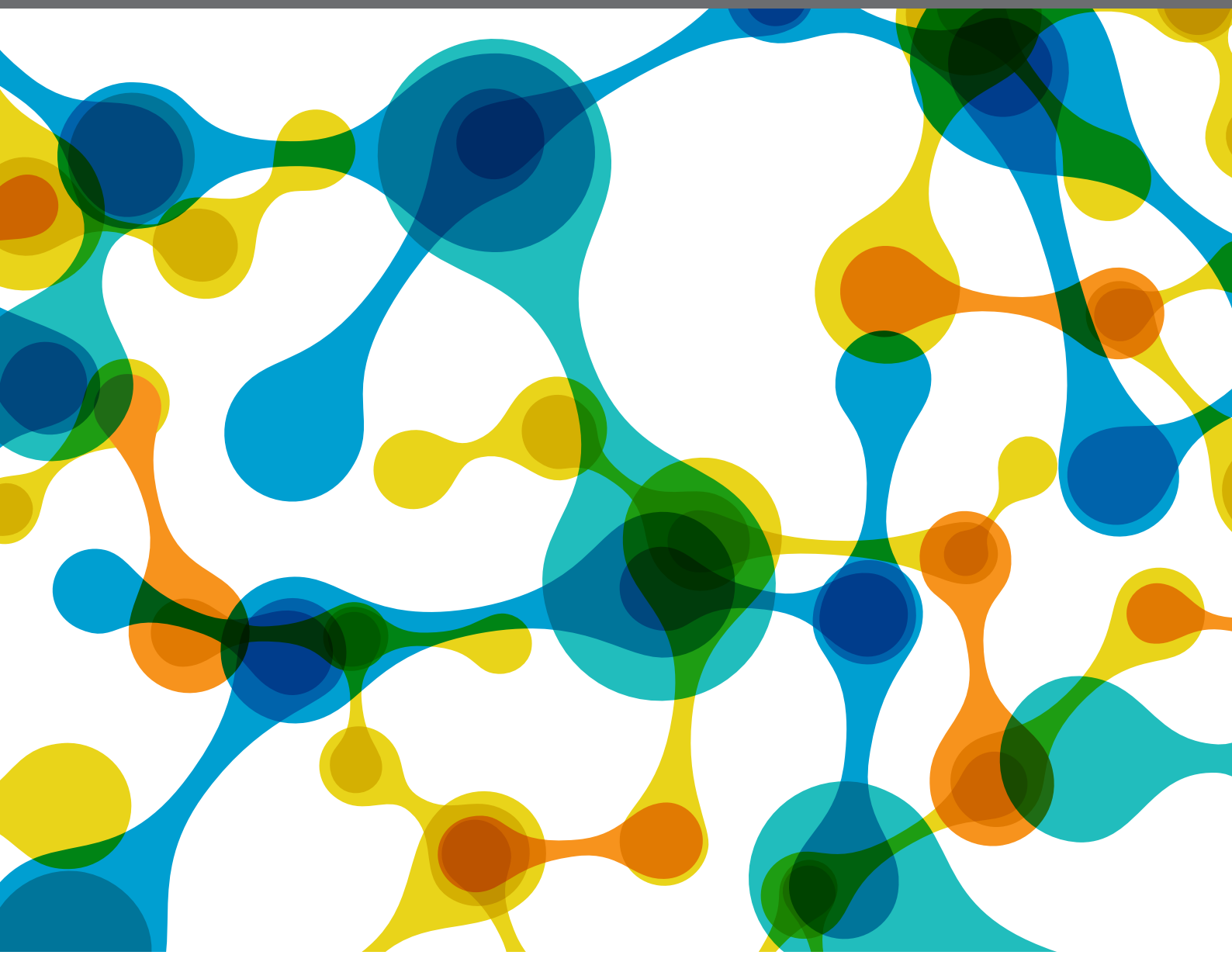

frontiers Research Topics

frontiers

ISSN 1664-8714
ISBN 978-2-83250-673-8
DOI 10.3389/978-2-83250-673-8

About Frontiers

Frontiers is more than just an open-access publisher of scholarly articles: it is a pioneering approach to the world of academia, radically improving the way scholarly research is managed. The grand vision of Frontiers is a world where all people have an equal opportunity to seek, share and generate knowledge. Frontiers provides immediate and permanent online open access to all its publications, but this alone is not enough to realize our grand goals.

Frontiers Journal Series

The Frontiers Journal Series is a multi-tier and interdisciplinary set of open-access, online journals, promising a paradigm shift from the current review, selection and dissemination processes in academic publishing. All Frontiers journals are driven by researchers for researchers; therefore, they constitute a service to the scholarly community. At the same time, the Frontiers Journal Series operates on a revolutionary invention, the tiered publishing system, initially addressing specific communities of scholars, and gradually climbing up to broader public understanding, thus serving the interests of the lay society, too.

Dedication to Quality

Each Frontiers article is a landmark of the highest quality, thanks to genuinely collaborative interactions between authors and review editors, who include some of the world's best academicians. Research must be certified by peers before entering a stream of knowledge that may eventually reach the public - and shape society; therefore, Frontiers only applies the most rigorous and unbiased reviews.
Frontiers revolutionizes research publishing by freely delivering the most outstanding research, evaluated with no bias from both the academic and social point of view. By applying the most advanced information technologies, Frontiers is catapulting scholarly publishing into a new generation.

What are Frontiers Research Topics?

Frontiers Research Topics are very popular trademarks of the Frontiers Journals Series: they are collections of at least ten articles, all centered on a particular subject. With their unique mix of varied contributions from Original Research to Review Articles, Frontiers Research Topics unify the most influential researchers, the latest key findings and historical advances in a hot research area! Find out more on how to host your own Frontiers Research Topic or contribute to one as an author by contacting the Frontiers Editorial Office: frontiersin.org/about/contact

WOMEN IN GASTROINTESTINAL SCIENCES: 2021

Topic Editors:
Kathleen E. DelGiorno, Vanderbilt University, United States
Natalie Luhtala, Salk Institute for Biological Studies, United States

Citation: DelGiorno, K. E., Luhtala, N., eds. (2022). Women in Gastrointestinal Sciences: 2021. Lausanne: Frontiers Media SA. doi: 10.3389/978-2-83250-673-8

Table of Contents

frontiers | Frontiers in Physiology

TYPE Editorial
PUBLISHED 19 October 2022
DOI 10.3389/fphys.2022.1048724

OPEN ACCESS

EDITED AND REVIEWED BY
Stephen J. Pandol,
Cedars Sinai Medical Center,
United States

*CORRESPONDENCE
Kathleen E. DelGiorno,
kathleen.delgiorno@vanderbilt.edu

SPECIALTY SECTION
This article was submitted to Gastrointestinal Sciences, a section of the journal Frontiers in Physiology

RECEIVED 19 September 2022
ACCEPTED 22 September 2022
PUBLISHED 19 October 2022

CITATION
Luhtala N and DelGiorno KE (2022), Editorial: Women in Gastrointestinal Sciences: 2021.
Front. Physiol. 13:1048724.
doi: 10.3389/fphys.2022.1048724

Editorial: Women in Gastrointestinal Sciences: 2021

Natalie Luhtala[1] and Kathleen E. DelGiorno[2]*

[1]Molecular and Cell Biology Laboratory, Salk Institute for Biological Studies, La Jolla, CA, United States, [2]Department of Cell and Developmental Biology, Vanderbilt University School of Medicine, Nashville, TN, United States

KEYWORDS

women, gastrointestinal, spotlight, Cancer, female

Editorial on the Research Topic
Women in gastrointestinal sciences: 2021

In this Research Topic, we feature the accomplishments of gastrointestinal (GI) tract researchers who identify as female. Women account for less than 30% of scientists worldwide. Gender biases and stereotyping may prevent women from pursuing careers in science. Women who choose scientific careers may experience discrimination through lower pay, fewer resources, and decreased recognition and advancement as compared to their male colleagues.

The GI tract, which includes the pancreas, liver, gallbladder, intestines, and colon, consists of multiple organs that form a continuous tract from the mouth to the anus, coordinating food intake and digestion. Herein, we highlight the work of female scientists, covering multiple areas of GI research. Reviews address advancements in the diagnosis of pancreatic intraductal neoplasms (Assarzadegan et al.), detail the relevance of purinergic and adenosinergic signaling in pancreatobiliary diseases (Faraoni et al.), and examine the role of a cystine/glutamate antiporter in GI cancer (Jyotsana et al.). Clinical questions were explored in research articles analyzing how pancreas fat contributes to metabolic risk of type 2 diabetes (Sequeira et al.) and in a study probing the use of CT scans for osteoporosis screening in pancreatitis (McNabb-Baltar et al.). In two cancer research articles, immunofluorescent techniques were developed to define the emergence of enteroendocrine cells early in pancreatic tumorigenesis (Caplan et al.) and to characterize a unique tumor microenvironment in inflammation-induced colon cancer (Vega et al.). Studies of *Acinetobacter calcoaceticus* revealed its adaptation to GI stressors and its proposed influence on the gut epithelium through pro-inflammatory signaling pathways (Glover et al.).

Bailey-Lundberg (Figure 1) studies the interplay between the epithelium and immune system in chronic inflammation and cancer with a major focus on pancreatic diseases. Her lab uses genetically engineered mouse models to evaluate plasticity in acinar and ductal cells as well as how signaling from the epithelium alters the immune and stromal microenvironment. Most recently her lab has been focused on studying purinergic and adenosine signaling with therapeutic implications for immunoprevention in pancreatic cancer.

Caplan (Figure 2) is a PhD candidate in the laboratory of Dr. Kathleen DelGiorno at Vanderbilt University. Pancreatic cancer is set to become the second leading cause of cancer-

FIGURE 1
Dr. Jennifer Bailey-Lundberg.

related deaths by 2030, however how it develops is still poorly understood. Acinar-to-ductal metaplasia (ADM), a process in which acinar cells transdifferentiate into ductal-like cells in response to injury, is an early event in tumorigenesis. ADM yields a heterogeneous population of cells including hormone-producing enteroendocrine cells rarely present in the normal pancreas. Leah Caplan is studying the role of enteroendocrine cells in pancreatic injury, repair, and tumorigenesis.

Dr. Mindy (Melinda) Engevik (Figure 3) is an Assistant Professor at the Medical University of South Carolina. Her lab focuses on the interaction between the gut microbiota and the intestinal epithelium, with an emphasis on mucus-associated microbes. Mindy complements her microbiology work with intestinal organoids, which provides a novel reductionist model of microbe-host interactions.

Jyotsana (Figure 4) is a Research Assistant Professor in the DelGiorno Laboratory at Vanderbilt University. Applying her skills as a bioengineer, she is utilizing clinically advanced lipid nanoparticles as vehicles to package and deliver RNA molecules to pancreatic tissue *in vivo* in models of intraductal papillary neoplasms (IPMN) and pancreatic

FIGURE 2
Leah Caplan.

FIGURE 3
Dr. Melinda Engevik.

cancer. Dr. Jyotsana aims to understand the molecular mechanisms of IPMN and pancreatic cancer pathogenesis, to identify novel therapeutic targets, and to efficiently and safely target IPMN and pancreatic cancer. Dr. Jyotsana is a recent recipient of a Department of Defense Partnering PI Award in Pancreatic Cancer.

Shi (Figure 5) is an Associate Professor of Pathology at the University of Michigan. She is a fellowship-trained and board-certified Gastrointestinal, Pancreas, and Hepatobiliary Pathologist and an NIH-funded physician-scientist. Her research interests are epigenetic regulation and tumor microenvironment in pancreatic cancer development and pancreas pathology. Dr. Shi has won the Benjamin Castleman Award from the United States and Canadian Academy of Pathology (USCAP) and is the recipient of an NCI Mentored Clinical Scientist Research Career Development Award (K08) and MERIT (Method to Extend Research in Time) award (R37).

Sequeira (Figure 6) explored the use of a non-invasive test of gut permeability during her doctorate and postdoctoral studies. This test was investigated as a diagnostic and used to assess how breakdown/digestion of food in the gut liberates soluble nutrients (Digesta Group at Massey University). This

FIGURE 4
Dr. Nidhi Jyotsana.

FIGURE 5
Dr. Jiaqi Shi.

test was endorsed in an editorial, with funding awarded for this work (Return on Science Fund, Massey University). Recently, Dr. Sequeira led a project as a Research Fellow (University of Auckland, PANaMAH), investigating the use of MRI and Spectroscopy to quantify fat storage in key metabolic organs such as the liver and pancreas.

Shah (Figure 7) is an Associate Professor of Radiology at The Ohio State University. Her career has focused on abdominal imaging, specifically in hepato-biliary and pancreatic disorders, and MRI imaging of the prostate and bladder. Dr. Shah advocates for diversity and equity, serving as Vice Chair for Diversity, Equity, and Inclusion, Associate Director of the Women in Medicine and Science committee, Chair-elect of the President and Provost's Council on Women, and acting as interim Director of Women's Academic Advancement. She also contributes her time by providing faculty training as part of the President and Provost's Leadership Institute.

Vega (Figure 8) is a PhD candidate in Dr. Ken Lau's laboratory within the Department of Cell and Developmental Biology and the Epithelial Biology Center at Vanderbilt

FIGURE 6
Dr. Ivana Sequeira.

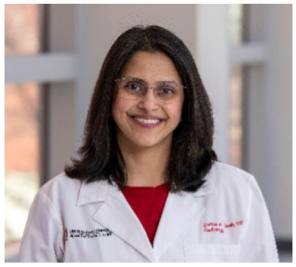

FIGURE 7
Dr. Zarine Shah.

University. Her work leverages both experimental and computational approaches to investigate epithelial-stromal cell-cell interactions in intestinal inflammation. In her publication featured in this Research Topic, she used single-cell RNA-sequencing, multiplex immunofluorescence imaging, and computational approaches to explore the colonic tumor microenvironment in mouse models of advanced adenoma and pre-invasive inflammation-induced cancer. Her goal is to gain the independence, additional training, and expertise required to launch her own laboratory as an independent academic investigator in biomedical research.

FIGURE 8
Paige Vega.

Author contributions

Both NL and KD came up with the concept of this article. NL wrote the first draft and KD edited the final draft.

Conflict of interest

The authors declare that the research was conducted in the absence of any commercial or financial relationships that could be construed as a potential conflict of interest.

Publisher's note

frontiers in Oncology

REVIEW
published: 23 February 2022
doi: 10.3389/fonc.2022.858462

The Role of Cystine/Glutamate Antiporter SLC7A11/xCT in the Pathophysiology of Cancer

Nidhi Jyotsana[1], *Kenny T. Ta*[1] *and Kathleen E. DelGiorno*[1,2,3,4]*

[1] Department of Cell and Developmental Biology, Vanderbilt University, Nashville, TN, United States, [2] Vanderbilt-Ingram Cancer Center, Vanderbilt University Medical Center, Nashville, TN, United States, [3] Vanderbilt Digestive Disease Research Center, Vanderbilt University Medical Center, Nashville, TN, United States, [4] Epithelial Biology Center, Vanderbilt University Medical Center, Nashville, TN, United States

SLC7A11/xCT is an antiporter that mediates the uptake of extracellular cystine in exchange for glutamate. Cystine is reduced to cysteine, which is a rate-limiting precursor in glutathione synthesis; a process that protects cells from oxidative stress and is, therefore, critical to cell growth, proliferation, and metabolism. SLC7A11 is expressed in different tissues and plays diverse functional roles in the pathophysiology of various diseases, including cancer, by regulating the processes of redox homeostasis, metabolic flexibility/nutrient dependency, immune system function, and ferroptosis. SLC7A11 expression is associated with poor prognosis and drug resistance in cancer and, therefore, represents an important therapeutic target. In this review, we discuss the molecular functions of SLC7A11 in normal *versus* diseased tissues, with a special focus on how it regulates gastrointestinal cancers. Further, we summarize current therapeutic strategies targeting SLC7A11 as well as novel avenues for treatment.

Keywords: SLC7A11 (xCT), metabolism, cysteine (Cys), gastrointestinal tract, ferroptosis, oxidative stress, Cancer therapy

OPEN ACCESS

Edited by:
Puttur Devi Prasad, Augusta University, United States

Reviewed by:
Wolfgang Sadee, The Ohio State University, United States
Chunming Cheng, The Ohio State University, United States

***Correspondence:**
Kathleen E. DelGiorno
kathleen.delgiorno@vanderbilt.edu

Specialty section:
This article was submitted to Cancer Metabolism, a section of the journal Frontiers in Oncology

Received: *21 January 2022*
Accepted: *04 February 2022*
Published: *23 February 2022*

Citation:
Jyotsana N, Ta KT and DelGiorno KE (2022) The Role of Cystine/Glutamate Antiporter SLC7A11/xCT in the Pathophysiology of Cancer. Front. Oncol. 12:858462. doi: 10.3389/fonc.2022.858462

INTRODUCTION

Amino acid metabolism is altered in many cancers, reflecting cancer cell uptake and altered metabolic needs, and targeting these pathways is becoming an attractive approach to patient therapy (1). The amino acid cysteine plays important roles in protein synthesis and in maintaining redox balance (2–4). Intracellular cysteine can be produced *de novo* or recycled through protein degradation (5, 6). However, under conditions of oxidative stress, such as in cancer, *de novo* biosynthesis or a catabolic supply of cysteine is not sufficient to meet the high demand for antioxidant synthesis. Therefore, most cancer cells rely on nutrient transporters that can import extracellular cystine (the oxidized dimer form of cysteine) (7, 8). Solute Carrier Family 7 Member 11 (SLC7A11) or xCT is the functional light chain subunit of system x_c^-, which is a sodium-independent, chloride-dependent, anionic L-cystine/L-glutamate antiporter on the cell surface (9, 10). The SLC7A11 protein requires either of the two heavy chain subunits of SLC3A2 to import extracellular cystine in exchange for intracellular glutamate, at a molar ratio of 1:1 (11, 12). The *SLC7A11* gene in humans is located on chromosome 4 and the SLC7A11 protein has orthologs in all vertebrates (4, 11). With 12 transmembrane domains, the N- and C- termini of the SLC7A11

protein reside in the cytoplasm (4). Unlike SLC3A2, which is a chaperone protein for many other light subunits of heterotrimeric amino acid transporter systems, SLC7A11 is specific for system x_c^- and, therefore, serves as the primary transporter for cystine and glutamate (4, 11, 13).

Extracellular cystine is imported into the cell through SLC7A11 and is converted to cysteine through a NADPH-consuming reduction reaction in the highly reducing atmosphere of the cytosol. Cysteine is further utilized to synthesize glutathione (GSH), a tripeptide, through a two-step process (1. Formation of γ-glutamylcysteine from cysteine and glutamate catalyzed by γ-glutamylcysteine synthatase; 2. Formation of GSH from γ-glutamylcysteine catalyzed by glutathione synthetase) (**Figure 1**) (4, 14, 15). SLC7A11 is a major regulator of metabolic reprogramming in normal and cancer cells. This mainly includes effects on nutrient dependency (glucose metabolism and glutamine dependency), and intracellular redox balance. Extracellular cysteine is also imported into cells through an alanine-serine-cysteine transporter and can be synthesized *de novo via* a trans-sulfuration pathway in some tissues (for example, liver, kidney, and pancreas), however, SLC7A11 remains an important transporter for cancer cells that are largely dependent on extracellular cystine for survival (6, 16). In normal tissues, SLC7A11 is primarily expressed in the brain with low levels in most other tissues (17, 18). *Slc7a11* knockout mice are viable, fertile, healthy in appearance with no evident deleterious phenotype, and live a normal lifespan (19, 20). SLC7A11 is found upregulated in various human cancers (2, 4, 8, 21–23). It is likely that *de novo* synthesis of cysteine and/or its import *via* transporters other than SLC7A11 can fulfill the requirement of intracellular cysteine in normal cells or tissues in the absence of SLC7A11. Therefore, the dispensability of SLC7A11 in normal systems and its high expression in various cancers makes it an attractive therapeutic target for cancer treatment.

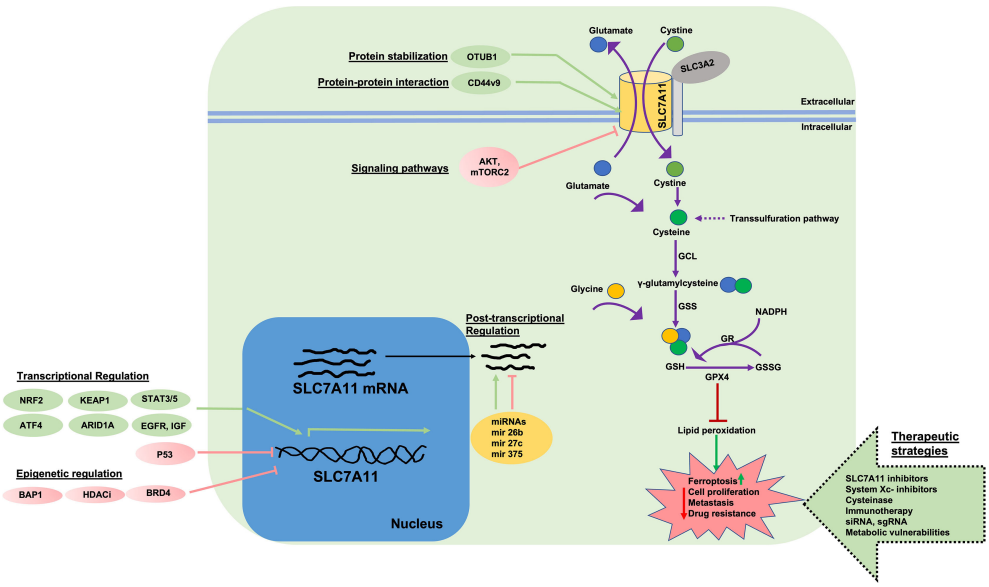

FIGURE 1 | Function, Regulation, and Targeting of SLC7A11. System x_c^- is a 1:1 cystine/glutamate exchange antiporter system comprised of light chain subunit SLC7A11 and heavy chain subunit (oligosaccharide-bound, gray circle) SLC3A2. SLC7A11 imports extracellular cystine which is reduced to cysteine through a NADPH-consuming reaction. Cysteine is utilized in conjugation with glutamate, by γ-GCL, to form γ-glutamylcysteine. In the next step, GSH tripeptide is produced *via* GS enzyme in conjugation with glycine. Intracellular cysteine can be synthesized by transsulfuration. Reduced GSH serves as a cofactor for enzymes such a GPX4 that protect cells from lipid peroxidation or ROS-induced damage. GSH is oxidized to GSSG *via* GPX4 and is recycled back to GSH at the expense of NADPH by GR enzyme. Accumulation of lipid peroxides leads to ferroptosis. In cells with high SLC7A11 levels and cystine import, GPX4 reduces lipid peroxidation and ferroptosis at the expense of GSH and protects cells from damage, allowing for cell proliferation, survival, and drug resistance. SLC7A11 is regulated at multiple levels. Transcriptional activation of SLC7A11 is induced by factors such as NRF2, ATF4, KEAP1, ARID1, STAT3/5 and is negatively regulated by p53 and ATF3. Epigenetic regulators (BAP1, BRD4 and HDAC inhibitors) negatively regulate SLC7A11 expression at the chromatin level. Post-transcriptionally, SLC7A11 is regulated by various miRNAs. Post-translationally, SLC7A11 protein is stabilized *via* protein-protein interactions (OTUB1, CD44v, CD44v9) which complex with SLC7A11 and inhibit proteasomal degradation. mTORC2 and AKT signaling inhibit SLC7A11 activity *via* phosphorylation. EGFR and IGF interact with SLC7A11 and maintain localization at the plasma membrane. SLC7A11 protein and function can be targeted *via* 1) direct inhibitors (e.g. erastin), 2) cysteinase, 3) immunotherapy, 4) targeting SLC7A11 *via* sgRNA and siRNA, 5) targeting metabolic vulnerabilities in cells with high SLC7A11 levels. ROS, Reactive oxygen species; GCL, γ-glutamylcysteine synthetase; GSS, glutathione synthetase; GPX4, glutathione peroxidase 4; GR, glutathione reductase; GSH, reduced glutathione; GSSG, oxidized glutathione; IKE, imidazole ketone erastin; GLUT, glucose transporter; sgRNA, single guide RNA; siRNA, small interfering RNA; ATF4, activating transcription factor 4; KEAP1, Kelch-like ECH associated protein-1; NRF2, nuclear factor erythroid 2-related factor 2; p53, tumor protein p53; ATF3, activating transcription factor 3; BAP1, BRCA1 associated protein-1; OTUB1, OTU deubiquitinase; ubiquitin aldehyde binding 1; mTORC2, mechanistic target of rapamaycin complex 2; miRNA, micro-RNA; HDACi, histone deacetylase inhibitors; EGFR, EGF receptor; IGF, insulin growth factor; ARID1A, AT-rich interactive domain-containing protein 1A; BRD4, bromodomain containing protein 4; NADPH, nicotinamide adenine dinucleotide phosphate.

REGULATION OF SLC7A11 AT THE MOLECULAR LEVEL

The expression of SLC7A11 can be modulated by various stress-inducing conditions (metabolic stress, amino acid starvation, genotoxic stress, hypoxia, viral infection) through transcription factors, epigenetic regulators, protein stability, interaction with other proteins, post transcriptional regulation, post-translational regulation, and transporter activity (**Figure 1**) (4). Studies have identified two transcription factors, nuclear factor erythroid 2-realted factor 2 (NRF2) and activating transcription factor 4 (ATF4), that regulate stress-induced SLC7A11 transcription (24–27). Under conditions of cell stress, the proteasomal degradation of NRF2 is impaired resulting in its stabilization and translocation to the nucleus. In the nucleus, NRF2 binds to antioxidant response elements (AREs) present in gene promoter regions and regulates the transcription of several antioxidant response-associated target genes including SLC7A11. The translation of ATF4 mRNA is enhanced under cell stress conditions but is otherwise repressed due to the presence of untranslated open reading frames (uORFs) located in the 5' untranslated region of ATF4 mRNA. Stress, including amino acid deprivation, causes phosphorylated eukaryotic initiation factor 2α (eIF2α) to inhibit the translation of many mRNAs including ATF4 uORFs, liberating ATF4 translation and increasing ATF4 protein production. ATF4 further binds to amino acid response elements (AAREs) in promoter regions of genes like *SLC7A11* which allow the cells to adapt and respond to stress (28). For example, we and others have observed that under cystine starvation conditions, pancreatic cancer cells upregulate SLC7A11 expression as a stress response (25). Under these conditions, NRF2 and ATF4 interact and cooperatively regulate SLC7A11 expression. In contrast to NRF2 and ATF4, p53 has been shown to repress SLC7A11 expression, however, the mechanism is unclear (29, 30). Recently, NRF2 and ATF4 deficiency was shown to reduce SLC7A11 levels resulting in improved cancer cell survival under low glucose conditions. Restoration of SLC7A11 in NRF2- or ATF4- deficient cells re-sensitizes them to glucose starvation. Similarly, NRF2 activation in cancer cells results in increased sensitivity towards glutamine starvation and glutaminase inhibition, potentially due to increased SLC7A11-mediated glutamate export (31).

In addition to the transcriptional regulation of SLC7A11 under conditions of cell stress, SLC7A11 is also regulated *via* post-transcriptional mechanisms (5, 32). For example, SLC7A11 mRNA can be degraded by nonsense-mediated mRNA decay or negatively regulated by microRNAs (miR-27a, miR-26b, miR-375) (33–35). Histone modifications and chromatin remodeling also control SLC7A11 expression (5). BAP1 (BRCA1 associated protein-1) deubiquitates histone 2A mono-ubiquitination (H2Aub) at lysine-119 on the *SLC7A11* gene and is associated with the transcriptional repression of SLC7A11 and ferroptosis induction. Additionally, BAP1 deficiency in cancer cells is associated with SLC7A11 upregulation and ferroptosis resistance (36–38). Polycomb repressive complex 1 (PRC1) is a ubiquitin ligase that mediates histone 2A mono-ubiquitination at the SLC7A11 promoter and represses expression (31, 38). The SWI/SNF complex is involved in chromatin remodeling. ARID1A, a component of the SWI/SNF complex binds to the SLC7A11 promoter and promotes NRF2 mediated transcriptional activation. ARID1A deficiency is associated with impaired cystine uptake and ROS induction (39, 40).

Finally, interaction with other proteins and post-translational modifications can affect the expression and activity of SLC7A11. For example, SLC3A2 is required to maintain SLC7A11 stability (13). CD44 variant (CD44v) isoforms interact with and stabilize SLC7A11 in cancer cells. CD44v maintains SLC7A11 protein stability and CD44v deficiency compromises the cell surface localization of SLC7A11, resulting in ROS induction and inhibition of tumor formation (41, 42). It was found through collaborative stable isotope labeling in cell culture (SILAC) and mass spectrometric analysis of glioblastoma cells modified to overexpress SLC7A11, that mTORC2 (mammalian target of rapamycin complex 2) binds to the N-terminal cytoplasmic tail of SLC7A11 and inhibits its transport activity *via* phosphorylation at serine 26 (43). Epidermal growth factor receptor (EGFR) was shown to interact with SLC7A11 protein to maintain its localization at the cell membrane; increased cystine uptake and enhanced glutamate export associated with tumor growth and invasiveness has been observed in EGFR-expressing glioma cells (44).

THE FUNCTIONAL ROLE OF SLC7A11 IN CELLULAR STRESS AND CARCINOGENESIS

Nutrient Dependency and Metabolic Flexibility

In comparison to normal cells, cancer cells differentially depend on certain nutrients for their survival and growth. Under certain nutrient deficient conditions, cancer cells undergo cell death whereas normal healthy cells survive because they are more metabolically flexible (45, 46). Understanding the mechanisms behind the limited metabolic flexibility, or nutrient dependency, of cancer cells may allow for targeted strategies that effectively kill cancer cells while sparing healthy cells. Glucose and glutamine are the main nutrients that provide energy for the biosynthetic machinery and various metabolic processes in most cells. Under glucose-limited conditions, for example, cells often increase their dependence on glutamine metabolism for survival (45, 47–49).

SLC7A11 mediated cystine uptake is crucial to main redox homeostasis and biomass incorporation in cells (2, 4). Cancer cells increase SLC7A11 levels to enhance cystine import and maintain ROS homeostasis (8, 50, 51) (**Figure 2**). Unlike glucose and glutamine, which are taken up by their corresponding transporters, imported cystine must first be reduced to cysteine (52, 53). Because of the 1:1 exchange of cystine and glutamate across the cell membrane, a large amount of glutamate is exported with an upregulation of SLC7A11 (53). Glutamine is

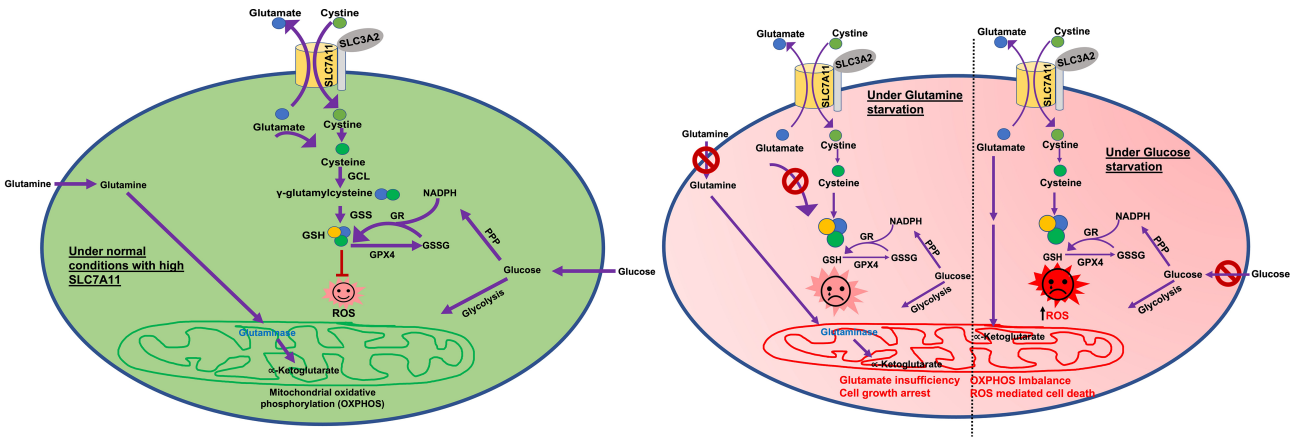

FIGURE 2 | Glucose and glutamine dependency in SLC7A11^{high} cancers. Glutamine is the major precursor for glutamate. Glucose is the main supplier of 1) carbon for the TCA cycle and 2) NADPH for GSH production. Under normal conditions (green circle) SLC7A11^{high} cells exchange higher amounts of glutamate with cystine. Large amounts of imported cystine are converted to cysteine for GSH production and ROS detoxification. However, higher export of glutamate leaves cells more dependent on glucose and/or glutamine to feed the TCA cycle and oxidative phosphorylation/mitochondrial respiration. Under glucose deprived conditions (red circle-right half), SLC7A11^{high} cells lack the required levels of carbon. Higher cystine import *via* SLC7A11 leads to higher GSH synthesis and a glucose-deficiency induced depletion in NADPH. This results in ROS induction and enhanced cell death. Under glutamine deprived conditions (red circle-left half) in SLC7A11^{high} cells, higher glutamate export results in depletion of intracellular glutamate which feeds into the TCA cycle. This drives enhanced import of glutamine and glutaminase activity to synthesize glutamate, resulting in glutamine dependency. Therefore, under glutamine starvation conditions, intracellular glutamate is inadequate to fuel the TCA cycle, leading to growth arrest. ROS, Reactive oxygen species; GSH, reduced glutathione; GSS, glutathione synthetase; GPX4, glutathione peroxidase 4; GR, glutathione reductase; GSSG, oxidized glutathione; PPP, pentose phosphate pathway; TCA cycle, tricarboxylic acid cycle; αKG, α-ketoglutarate; NADPH, nicotinamide adenine dinucleotide phosphate.

the most abundant amino acid in plasma. Once imported, glutamine is converted into glutamate *via* glutaminase and serves as a precursor for GSH synthesis, in addition to a role in the tricarboxylic acid (TCA) cycle (via conversion to α-ketoglutarate) (50, 51). Interestingly, high cystine levels in culture medium were observed to induce cystine uptake in cancer cells leading to greater glutamate export and, therefore, increased glutamine dependency (54). It has been shown that basal and claudin-low triple-negative breast cancer (TNBC) cell lines are more dependent on glutamine. These cells lines are SLC7A11-high and import more cystine than other breast cancer subtype cell lines. Treatment with sulfasalazine, a pharmacological inhibitor of SLC7A11, attenuates the growth of xenograft tumors derived from these cell lines. This suggests that SLC7A11-high cancers, like TNBCs, are more dependent on glutamine (55). This is likely because they need more glutamate to exchange for cystine due to higher SLC7A11 levels. Similarly, several pancreatic cancer cell lines (for example, PANC-1, BxPC-3 or HPAC) are glutamine dependent and results from Badgley et al. show that glutamine dependent pancreatic cancer cells are more sensitive to pharmacological and genetic inhibition of SLC7A11 (56).

Many studies indicate that several SLC7A11-high cancers are sensitive to glucose deprivation, however the exact mechanism here remains an active area of research. The loss of SLC7A11 and SLC3A2 has been shown to promote cancer cell survival under glucose starvation conditions and SLC7A11 overexpression promotes glucose starvation-induced cell death and vice versa (50, 51). Additionally, glucose deprivation was observed to induce SLC7A11 expression in cancer cells. As both glutamine and glucose are important for the TCA cycle, it has been speculated that enhanced SLC7A11 export of glutamate in cancer cells makes them more dependent on glucose to replenish the TCA cycle (5, 50, 51). However, more recent studies show that cystine deprivation can rescue cancer cell death resulting from glucose starvation. The intracellular reduction of cystine to cysteine requires NADPH. This causes SLC7A11-high cancer cells to be more dependent on the glucose pentose phosphate pathway (a major provider of NADPH in cells), which in turn is metabolically dependent on glucose (**Figure 2**). Moreover, it has been shown that glucose starvation-induced cell death in SLC7A11-high cancer cells can be prevented by restoring NADPH levels. Altogether, these data suggest that it is NADPH depletion associated with cysteine generation that causes SLC7A11-high cancer cell death under conditions of glucose starvation (**Figure 2**) (57, 58). Various lines of experimental evidence have shown that genetic or pharmacological inhibition of SLC7A11 has a pro-survival role in cancer cells under conditions of glucose starvation. Further, a loss of function screen identified SLC7A11 and SLC3A2 as the top hits for proteins where loss/inactivation provides resistance to glucose starvation (50). Collectively, these studies suggest that enhanced glutamate export and NADPH investment in cancer cells upregulate SLC7A11 levels and enhance dependency on glucose and/or glutamine, though this may be cell line and context dependent (**Figure 2**). Glucose and glutamine abundance are typically limited in the tumor microenvironment (59, 60). Therefore, SLC7A11 overexpression may promote tumor

growth/survival but once the tumor is established, SLC7A11-high tumors are more sensitive to glucose or glutamine deficiency in the tumor microenvironment (**Figure 2**).

Oxidative Stress/Redox Homeostasis

Reactive oxygen species (ROS) are free oxygen radicals such as superoxide (O_2^-), hydroxyl radical (OH^-), and hydrogen peroxide (H_2O_2) formed by reduction-oxidation (redox) reactions. ROS and their products can serve as signaling intermediates that contribute to molecular responses involved in normal biological processes, for example, in stem cell renewal, immune responses, and insulin synthesis (61). However, an unbalanced production of ROS can affect normal physiology by damaging DNA, RNA, proteins, and cellular organelles *via* lipid peroxidation and may even result in cell death (4, 61). This occurs due to an insufficiency of detoxifying mechanisms including glutathione stores and antioxidant enzymes (62). This imbalance between ROS production and the antioxidant defense has been implicated in many pathologies including cancer, pulmonary hypertension, retinal damage, and asthma (22, 63–65). SLC7A11 plays an antioxidant role by supporting GSH generation *via* cystine import (4, 9). GSH plays a vital role in many cellular functions including maintaining an intracellular redox balance, reducing hydrogen peroxide or oxygen radicals, detoxification of electrophiles, storing cysteine, and regulating multiple other cellular processes (15, 66). Cancer cells have higher levels of ROS than normal cells, which promotes tumorigenesis, however, too much intracellular ROS triggers cell death and inhibits tumor progression. These increased ROS levels can be induced by irradiation, cytotoxic compounds or inhibition of antioxidants and the antioxidant defense system (67). Oxidative stress in the tumor microenvironment is regulated by SLC7A11 *via* maintenance of the cystine/cysteine redox cycle across the cell membrane. Residual cysteine from GSH synthesis is exported and is rapidly oxidized to cystine. SLC7A11 plays a role in continuous import of this extracellular cystine. This creates a cystine/cysteine redox cycle across the membrane and creates a reducing extracellular environment that supports cancer cell growth and survival (4, 51).

Cell Death

Ferroptosis is an iron-dependent cell death which is accompanied by iron accumulation and lipid peroxidation. A ferroptosis-associated decrease in antioxidant capacity and accumulation of lipid ROS in cells leads to oxidative cell death. It differs from other forms of cell death in that those cells undergoing ferroptosis have shrunken and dense mitochondria but do not show plasma membrane blebbing, DNA fragmentation, or Caspase-3 cleavage (68). In recent years, ferroptosis has been associated with many pathologies including cancer, neurological diseases, ischemia etc. SLC7A11 overexpression confers resistance to ferroptosis in cancer cells by importing cystine for the synthesis of GSH and by relieving lipid ROS stress by activation of glutathione peroxidase 4 (GPX4) (22). GPX4 catalyzes the reduction of hydrogen and lipid peroxides and protects cells from oxidative stress. Inactivation of GPX4 leads to an accumulation of lipid peroxides and ferroptosis (68–71). Therefore, SLC7A11 prevents cells from undergoing ferroptosis by importing cystine and promoting GSH synthesis. In acute liver failure, overexpression of SLC7A11 plays a protective role in controlling the level of lipopolysaccharide-D-galactosamine-induced hepatocyte acute injury primarily through inhibiting ferroptosis (72). In contrast, SLC7A11 enhances ferroptosis in myofibroblast hepatic stellate cells, which can exacerbate liver injury (73). Escaping cell death is one of the hallmarks of cancer. In 2012, Li et al. showed that a specific mutation in p53 (3KR mutant that cannot be acetylated on certain lysine residues) causes cancer cells to lose the ability to induce cell cycle arrest or apoptosis. However, it could still prevent tumor formation *in vivo* (74). Jiang et al. later discovered that this mutation preserves the tumor suppressive effect of p53 partly by suppressing SLC7A11 expression and inducing ferroptosis (29). Additional p53 mutations also link p53 regulation of SLC7A11 and ferroptosis in cancer (75). Another tumor suppressor, BAP1, frequently found lost or mutated in cancers, has been shown to repress SLC7A11 expression thereby impairing cystine uptake and promoting ferroptosis in cancer cells. Furthermore, SLC7A11 overexpression or treatment with ferroptosis inhibitors has been shown to partly overcome the tumor growth suppression caused by BAP1 restoration in tumors (36, 76, 77). In addition to ferroptosis, SLC7A11 inhibition has been linked to apoptosis in murine melanocytes and cancer cells in a context dependent manner. Unlike erastin (**Figure 1**), SLC7A11 inhibitor HG106 mainly induces apoptosis, likely by GSH depletion (78). The exact mechanism behind the GSH depletion mediated induction of ferroptosis *vs* apoptosis remains to be understood. There may be cell and context dependent differences along with potential off-target effects of the two drugs (34, 79, 80). Therefore, studying the same cell line following treatment with erastin or HG106 may provide insight into the mechanisms underlying these cell death pathways. Studying apoptosis or ferroptosis deficient cells following SLC7A11 inhibition will address some of these unanswered questions.

Mutant-KRAS and SLC7A11

KRAS is one of the most commonly mutated oncogenes in many cancers (for example, in pancreas and lung). Mutant *KRAS* has recently been shown to promote *SLC7A11* transcription *via* its cooperation with NRF2 and/or ATF4 (**Figure 3**) (56, 78, 81). Furthermore, inhibition of SLC7A11 *via* genetic or pharmacological targeting attenuates mutant-KRAS associated tumor growth in xenograft models *via* induction of lipid peroxidation and ferroptosis (56). It has also been shown in *Slc7a11* deficient mice that oncogenic KRAS-driven pancreatic adenocarcinoma (PDAC) tumor growth is significantly impaired (56). Suppression of xCT was demonstrated to cause synthetic lethality in mutant-KRAS lung adenocarcinoma (78). This suggests that higher ROS levels in mutant-RAS driven cancers enhance dependency on GSH production for survival and that SLC7A11 associated ferroptosis suppression may support mutant-KRAS driven cancer growth. Therefore, targeting or co-targeting the SLC7A11/GSH axis will have therapeutic benefit in mutant-KRAS driven tumors.

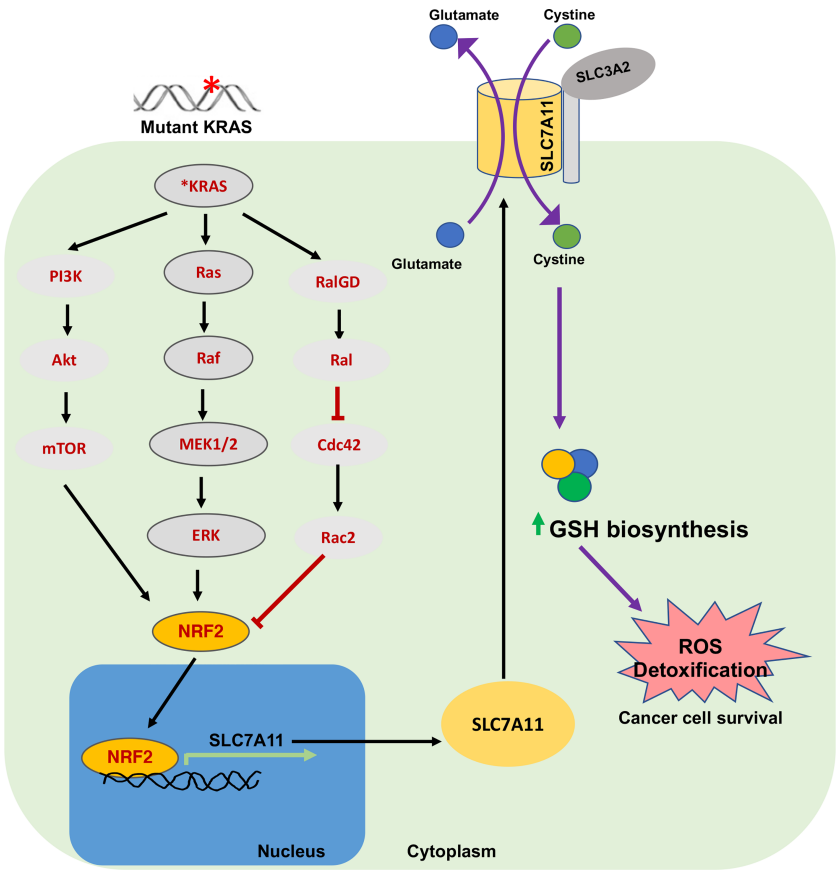

FIGURE 3 | Oncogenic KRAS and SLC7A11 in cancer. Mutations in KRAS induce SLC7A11 overexpression through activation of transcription factor NRF2 *via* downstream signaling pathways including MAPK, PI3K/AKT and RAS-related protein pathways. This regulates expression of SLC7A11 and elevates intracellular cysteine levels and GSH. This signaling plays an important role in sustaining oxidative balance in KRAS-mutant cancer cells and promotes their progression and survival. NRF2, Nuclear erythroid 2-related factor; RAL, RAS-related protein.

Cancer Immunity and SLC7A11

Several cancer immunotherapies have been shown to inhibit SLC7A11 function and, in turn, induce ferroptosis in tumor cells. For example, programmed death ligand-1 (PD-L1) blockade therapy and CD8+ T cells increase ROS levels by releasing interferon gamma (IFNγ) which promotes the binding of transcription factor STAT1 to the SLC7A11 transcriptional start site, downregulating expression. Similarly, interferon regulatory factor 1 upregulation by IFNγ reduces SLC7A11 transcription through Janus kinase (JAK) (82). Post-immunotherapy radiotherapy synergizes with IFNγ, further promoting ferroptosis *via* SLC7A11 inhibition (83). Suppression of SLC7A11 is also linked to T cell memory-associated enhanced immune responses (22). Therefore, targeting SLC7A11 in combination with immunotherapy may work as an effective treatment strategy for certain cancers.

Resistance to Cancer Therapy

SLC7A11 overexpression is associated with resistance to immunotherapy, as well as chemo- and radio-resistance, including to drugs such as gemcitabine and cisplatin (84). Enhanced GSH synthesis and inhibition of ferroptosis are believed to promote SLC7A11-associated drug and radio-resistance, respectively. For example, SLC7A11 provides resistance to BRAF and MEK inhibitors in $BRAF^{V600E}$ mutant melanoma, geldanamycin resistance in lung cancer, cisplatin resistance in gastric cancer, temozolomide resistance in glioma and gemcitabine resistance in pancreatic cancer (84–89). Multiple studies have shown that this therapeutic resistance can be reversed by direct targeting of SLC7A11 (90–92). In head and neck cancer, for example, treatment with erastin or sulfasalazine re-sensitizes cancer cells to cisplatin treatment (93).

Others

While high SLC7A11 expression may be detrimental for patient outcomes in cancer, it also plays a role in healing in many tissues. For example, low expression of SLC7A11 in cardiomyocytes results in reduced levels of GSH, increased ferroptosis, and is associated with cardiomyopathy and cardiac failure in mice (94). Overexpression of STAT3 leads to increased expression of

SLC7A11 and plays a protective role in an intestinal ischemia/reperfusion-induced acute lung injury mouse model by reducing ferroptosis (95). It was found that SLC7A11 mediated cystine uptake is crucial for gastric chief cell plasticity and ROS mitigation. CD44v9 stabilizes SLC7A11 for enhanced cystine uptake in chief cells following parietal cell loss during gastric injury (96). SLC7A11 is significantly upregulated during liver regeneration and overexpression in hepatocytes enhances repopulation and recovery following toxic liver injury (97). In contrast to these roles in healing, it was shown by Sprimont and colleagues that ablation of *Slc7a11* in the context of spinal cord injury in mice is beneficial. *Slc7a11* knockout mice have more rapid body weight and motor recovery post-injury (98).

ROLES IDENTIFIED FOR SLC7A11 IN NON-GASTROINTESTINAL TRACT CANCERS

SLC7A11 expression correlates with tumor invasion and metastasis in various non-gastrointestinal (non-GI) and gastrointestinal (GI) tract cancers (22). In prostate cancer, SLC7A11 expression is increased in the metastatic stroma and is associated with poor prognosis. *SLC7A11* knockdown leads to an increase in ROS levels, inhibiting tumor cell invasion in the context of co-culture with stromal cells (99). SLC7A11 has also been shown to be important in breast cancer stem cell maintenance and correlates with poor prognosis in patients (55, 100). Overexpression of SLC7A11 provides cancer stem cell-like properties to glioblastoma cells and is related to accelerated tumor growth and enhanced chemoresistance (88). SLC7A11 serves as an independent indicator of poor prognosis in acute myeloid leukemia (101) and an independent risk factor in ovarian cancer (102). SLC7A11 overexpression is linked to enhanced tumor proliferation and progression in melanoma and poor overall survival and advanced pathology in papillary thyroid carcinoma (103, 104). Sulforaphane (a sulfur compound found in many vegetables) induces cell death in small cell lung carcinoma *via* induction of ferroptosis. The levels of SLC7A11 were found to be significantly lower in the sulforaphane treatment group (105). Treatment with anti-SLC7A11 siRNAs induces significant cell death in KRAS-mutant lung adenocarcinoma cells (78). Likewise, SLC7A11 was found to be highly expressed in the cytoplasmic membrane in non-small-cell lung carcinoma (NSCLC) and is associated with poorer prognosis. Treatment of xenografted NSCLC mice with sulfasalazine, a potent inhibitor of SLC7A11, significantly prolonged their survival (21). Administration of SLC7A11 targeting miR-5096 induces ferroptosis in human breast cancer cells and lidocaine treatment results in ferroptosis and ROS induction in both breast and ovarian cancer cells (106). SLC7A11 has been found to be involved in approximately 50% of glioma patient tumors. Intracranially implanted SLC7A11 expressing tumor cells grow faster, produce more glutamate toxicity, induce seizures, and shorten overall survival (107). It was found that SLC7A11- and ferroptosis-related gene signatures (lipid metabolism-associated genes: ACSL4, ALOX5, ACACA, ZEB1, FADS2 and antioxidant metabolism-associated genes: NOX1, GCLM) offer prognostic value in bladder cancer and that targeting these genes is therapeutically beneficial (108).

GASTROINTESTINAL TRACT CANCERS

Esophageal Cancer

Evaluation of 127 esophageal squamous cell carcinoma patients who received radical chemoradiotherapy revealed SLC7A11 and NRF2 overexpression in the tumor tissue. Overexpression of SLC7A11 was associated with lymph node metastasis and shorter overall survival in these patients (109).

Liver Cancer

Higher levels of SLC7A11 are associated with poor differentiation and advanced disease stage in hepatocellular carcinoma (HCC) (110, 111). Analysis of clinical data from The Cancer Genome Atlas (TCGA) showed that SLC7A11 overexpression correlates with poor outcome in liver cancer (112). SLC7A11 knockdown prevents HCC growth (113). Interleukin-1β induces SLC7A11 expression in HCC cells and is associated with HIF1α levels. This αKG- HIF1α cascade upregulates PD-L1 and colony-stimulating factor-1 (CSF1), which further increase HCC metastasis *via* infiltration of tumor associated macrophages (TAMs) and myeloid derived suppressor cells (MDSCs). Either depletion of TAMs or MDSCs, treatment with a CSF1 inhibitor, an anti-PD-L1 antibody or Anakinra (an IL1β inhibitor), or SLC7A11 knockdown, all result in a reduction in HCC metastasis (114). xCT inhibition by sulfasalazine or through siRNA targeting SLC7A11 leads to reduced cell proliferation *in vitro* and *in-vivo via* reduction in GSH levels and an increase in ROS by inhibiting the CD44v9-SLC7A11 interaction (111, 113).

Gastric Cancer

Reduction of SLC7A11 expression using pharmacological inhibitors (erastin, Jiyuan Oridonin A derivative a2, levobupivacaine), miRNA (miR-375), long non-coding RNA and siRNA has been shown to inhibit tumor progression through induction of ferroptosis (115–118). Treatment with miR-375 was shown to reduce the stemness of gastric cancer stem cells (116). A local anesthetic, levobupivacaine, induces ferroptosis in gastric cancer and suppresses cell proliferation both *in vitro* and *in vivo* by elevating the levels of miR-489-3p and suppressing SLC7A11 (117). Decreased expression of long non-coding RNA SLC7A11-AS1 contributes to tumor progression and is a poor prognostic indicator in gastric cancer patients (118). Tanshione IIA, an active compound isolated from the rhizome of Chinese herb Danshen has been shown to block gastric cancer stem cells *via* ferroptosis induction and SLC7A11 downregulation (119). SLC7A11 inhibition *via* sulfasalazine

reduced colony formation, proliferation, metastasis, and invasion of gastric cancer cells *in vitro* (120).

Colorectal Cancer

Analysis of 21 different types of cancer in 7462 cancer samples showed that both SLC7A11 and GPX4 are overexpressed in colorectal cancer (CRC) (121). Elesclomol, a copper chelator, suppresses CRC both *in vitro* and *in vivo* by inducing ROS accumulation and is associated with downregulation of SLC7A11 protein levels *via* ubiquitination and degradation (122). CRC stem cells have higher levels of cysteine, GSH, and SLC7A11 and, therefore, exhibit lower levels of ROS as compared to CRCs. Genetic and pharmacological inhibition of SLC7A11 in CRC stem cells significantly attenuates their viability *in vitro* and *in vivo* in comparison to CRCs (123, 124). Using two different cell lines and a xenograft mouse model of CRC, it was shown that 2-Imino-6-methoxy-2H-chromene-3-carbothioamide (IMCA), a benzopyran derivative, downregulates SLC7A11 levels leading to increased ROS and ferroptosis in CRC cells. IMCA treatment reduces CRC cell viability *in vitro*, inhibits the growth of xenografted CRC cells *in vivo*, and is associated with a decrease in the phosphorylation of mTOR and its downstream target P70S6K (125).

Pancreatic Cancer

Pancreatic ductal adenocarcinoma (PDAC) is characterized by a poor 5-year survival rate (~10%) due to inherent chemoresistance, barriers to drug delivery, and a lack of early diagnostics. SLC7A11 expression was found to be upregulated in many pancreatic cancer cell lines (112). Recently, Badgley et al., demonstrated a role for SLC7A11 in PDAC. More than 90% of PDAC cases harbor mutations in KRAS and mutant KRAS signaling is linked to increased ROS production and, therefore, increased dependency on cystine import *via* SLC7A11. Culturing PDAC cell lines in cystine deficient conditions induces cell death in more than 80% of cells, which is rescued by the addition of antioxidant Trolox. Addition of system x_c^- inhibitor imidazole ketone erastin (IKE) has similar effects on the cell viability. Cysteine starved PDAC cells undergo plasma membrane destabilization and show significantly increased levels of lipid peroxidation, a signature of cells undergoing ferroptosis. Pharmacological or genetic inhibition of SLC7A11 induces ferroptosis and blocks PDAC growth in a genetically engineered mouse model of PDAC (56). Daher et al. showed that xCT knockout in two different PDAC cell lines (MIA PaCa-2 and CAPAN-2) induces ferroptosis and significantly affects growth and proliferation *in vitro* and *in vivo* when injected subcutaneously in nude mice (126). Gene ontology analysis of 43 different ferroptosis regulators revealed that both SLC7A11 and SLC3A2 are upregulated in pancreatic cancer samples and are associated with gemcitabine resistance (64). Bioinformatic analysis of PDAC samples from The Cancer Genome Atlas (TCGA) found that lower expression of miR-139-5p, along with higher expression of SLC7A11 is associated with poor clinical outcomes. Overexpression of miR-139-5p is associated with suppression of SLC7A11 in PDAC cells and can be exploited for inhibition of cell proliferation, invasion, and metastasis (127). One of the major contributors to PDAC progression and metastasis are cancer-associated fibroblasts (CAFs), which block drug delivery and create a hypoxic microenvironment. Sharbeen et. al., found that PDAC-associated CAFs are heavily dependent on SLC7A11 for cystine uptake and GSH synthesis to balance ROS and oxidative stress in tumors and, therefore, support PDAC tumor progression. High stromal SLC7A11 levels in human PDAC samples are predictive of poor overall survival independent of SLC7A11 expression in the tumor cells themselves. SLC7A11 knockdown in CAFs inhibited proliferation in both $SLC7A11^{low}$ and $SLC7A11^{high}$ PDAC and increased sensitivity to oxidative stress and ferroptosis. Furthermore, treatment with nanoparticle-siRNA targeting SLC7A11 significantly decreased PDAC tumor growth (23).

TARGETING SLC7A11 IN CANCER

Thus far, SLC7A11 targeting strategies include either directly inhibiting SLC7A11 transporter activity or indirectly targeting SLC7A11-associated metabolic susceptibilities and pathways in cancer. Direct targeting of SLC7A11 includes the use of inhibitors: sulfasalazine (128, 129), erastin (130, 131), imidazole ketone erastin (IKE) (132), sorafenib (133, 134), and HG106 (78). These inhibitors induce ferroptosis by blocking cystine uptake *via* SLC7A11 and fall under the category of class I ferroptosis inducers. However, each one has its pros and cons. For example, due to unfavorable pharmacological properties, sulfasalazine treatment does not result in better outcomes in PhaseI/II clinical trials. However, when delivered as a zinc oxide-sulfasalazine nanoparticle derivative, it has better tumor retention with improved cytotoxic effects and no evident damage to healthy cells (135). As a system x_c^- inhibitor and ferroptosis inducer, the therapeutic potential of erastin has been shown in multiple cancer types including breast cancer (130). However, erastin is poorly soluble and metabolically unstable *in vivo* and, therefore, cannot be used for clinical studies. An analog, IKE, is metabolically stable and was shown to be effective in genetically engineered mouse models of PDAC, however, it has not yet been tested in the clinic. Both sorafenib and sulfasalazine are FDA approved drugs that have been shown to induce ferroptosis and inhibit tumor growth, however, in addition to inhibiting SLC7A11, sorafenib acts as a multi-kinase inhibitor and sulfasalazine blocks prostaglandin production (136, 137). Because of these off target effects, both are associated with adverse clinical events (128, 138). Therefore, targeting metabolic vulnerabilities associated with SLC7A11 may prove to be a better therapeutic strategy against cancer.

As previously mentioned, $SLC7A11^{high}$ cancer cells are more vulnerable to glucose and glutamine starvation. CB-839, a glutaminase inhibitor, has been shown to potently suppress tumor progression in KEAP1-mutant *vs.* wild type patient-derived xenografts. KEAP1 mutation/inactivation leads to NRF2 stabilization and results in the upregulation of

NRF2-target genes including SLC7A11. KEAP1-mutant lung cancers are characterized by high SLC7A11 expression levels (139, 140). Similarly, KL-11743, a GLUT1/3 dual inhibitor selectively inhibits SLC7A11^{high} tumor growth in cell lines and in patient derived xenografts (141). High-throughput screening of a number of compounds that inhibit glutamate export in triple negative breast cancer cells suggests that capsazepine (CPZ) can effectively inhibit SLC7A11 and increase intracellular ROS (142). Similarly, in a screen of mutant KRAS lung adenocarcinoma cells, HG106 was found to specifically inhibit SLC7A11 function and decrease tumor burden *in vivo via* ROS induction and mitochondrial and endoplasmic reticulum dysfunction (78). Various glutamate analogues (L-Homocysteate, L-Quisqualate, 4-bromo-homoibotenate and S-4-Carboxy-phenylglycine (CPG)) have been shown to affect the exchange between L-cystine and glutamate across the cell membrane through system x_c^- (143). SLC7A11 activity can also be affected indirectly by targeting its upstream regulators. For example, MEK inhibitor AZD6244 and BAY-11-7085 inhibit NRF2, JQ-1 targets BD4, AG879 targets receptor tyrosine kinase TrkA, and all indirectly inhibit SLC7A11 expression (22). Paclitaxel enhances ferroptosis by inhibiting SLC7A11 transcription (144). Various immunotherapy approaches that reduce SLC7A11 expression *in vivo* have promise. For example, anti-SLC7A11 DNA vaccines that utilize plasmids to express full length SLC7A11 have been shown to induce regression in lung metastases in 4T1-tumor bearing mice (100). Virus-like particles (AX09-0M6) displaying the 6th extracellular loop of SLC7A11 common to both mouse and human SLC7A11 disabled the self-renewal ability of breast cancer stem cells (145). Finally, a bovine herpesvirus 4-based vector delivering full length SLC7A11 DNA protected mice from breast cancer metastases by targeting cancer stem cells (146).

FUTURE PERSPECTIVES

The redox status of cancer cells reflects many aspects of carcinogenesis including cell growth, proliferation, migration, metabolism, invasion, and metastases. Cancer progression and tissue injury are often associated with a state of redox imbalance. To survive under conditions of increased oxidative stress, cancer cells adopt various strategies to produce antioxidants, for example, upregulation of SLC7A11. SLC7A11 functions in a variety of roles in cancer including metabolic reprogramming, nutrient dependency, growth, proliferation, invasion, and drug resistance (**Figure 1**). As SLC7A11 is dispensable in normal, healthy cells and *Slc7a11* knockout mice are viable with no associated pathologies, targeting SLC7A11 poses a promising therapeutic target. In recent years, the role of SLC7A11 has been extensively studied in a variety of cancers including both GI and non-GI tract cancers. However, there are many questions that remain to be answered. A better understanding of the cell and context dependent role of SLC7A11 under different conditions of nutrient availability (for example, glucose and glutamine limiting conditions) is needed (**Figure 2**). There are multiple studies that highlight the various transcriptional and epigenetic factors that regulate SLC7A11 expression, however, further studies are required to understand whether SLC7A11 is also regulated *via* other mechanisms, especially post translational mechanisms and the existence of key interaction partners, etc. It would be interesting to elucidate the contribution of SLC7A11 to ferroptosis *versus* other forms of cell death (apoptosis, necrosis, autophagy) following inhibition in a variety of cancers. Identifying novel targets (synthetically lethal partners, metabolic vulnerabilities, immunotherapies, chemotherapies, signaling pathway inhibitors, upstream or downstream targets) that can be co-targeted with SLC7A11 inhibition in cancer may significantly improve the anti-cancer effects. For example, because of higher dependency of SLC7A11-high cancers on glucose and glutamine, combination targeting strategies including drugs/inhibitors that target/block glucose or glutamine metabolism would increase therapeutic efficacy. *Slc7a11* knockout and transgenic mouse models are ideal to study the role of SLC7A11 in tumor progression and maintenance. All currently available SLC7A11 inhibitors, including sulfasalazine and erastin, have either off-target effects or bioavailability issues. Utilizing biocompatible nanoparticles to package and deliver these drugs would enhance their efficacy, increase their bioavailability, and potentially eliminate associated side effects. Therefore, more selective SLC7A11 inhibitors and genetic targeting strategies, including small interfering RNAs (siRNA) and small guide RNAs (sgRNA), would be ideal for clinical purposes.

AUTHOR CONTRIBUTIONS

NJ conducted the research and wrote/edited the manuscript. KT researched the manuscript. KD edited the manuscript, supervised, and funded the research. All authors contributed to the article and approved the submitted version.

FUNDING

The DelGiorno laboratory is supported by the Vanderbilt-Ingram Cancer Center Support Grant (NIH/NCI 5P30 CA068485), the Vanderbilt-Ingram Cancer Center SPORE in Gastrointestinal Cancer (NIH/NCI 5P50 CA236733), a Vanderbilt Digestive Disease Research Center Pilot and Feasibility Grant (NIH/NIDDK 5P30 DK058404), an American Gastroenterological Association Research Scholar Award (AGA2021-13-02), NIH/NIGMS 1R35 GM142709, and the Sky Foundation, Inc. (AWD00000079).

ACKNOWLEDGMENTS

The authors thank Dr. Anna Means for critical reading of the manuscript.

REFERENCES

1. Wei Z, Liu X, Cheng C, Yu W, Yi P. Metabolism of Amino Acids in Cancer. *Front Cell Dev Biol* (2020) 8:603837. doi: 10.3389/fcell.2020.603837
2. Combs JA, DeNicola GM. The Non-Essential Amino Acid Cysteine Becomes Essential for Tumor Proliferation and Survival. *Cancers (Basel)* (2019) 11:678. doi: 10.3390/cancers11050678
3. Stipanuk MH, Dominy JE Jr, Lee JI, Coloso RM. Mammalian Cysteine Metabolism: New Insights Into Regulation of Cysteine Metabolism. *J Nutr* (2006) 136:1652S–9S. doi: 10.1093/jn/136.6.1652S
4. Koppula P, Zhang Y, Zhuang L, Gan B. Amino Acid Transporter SLC7A11/xCT at the Crossroads of Regulating Redox Homeostasis and Nutrient Dependency of Cancer. *Cancer Commun (Lond)* (2018) 38:12. doi: 10.1186/s40880-018-0288-x
5. Koppula P, Zhuang L, Gan B. Cystine Transporter SLC7A11/xCT in Cancer: Ferroptosis, Nutrient Dependency, and Cancer Therapy. *Protein Cell* (2021) 12:599–620. doi: 10.1007/s13238-020-00789-5
6. Zhu J, Berisa M, Schworer S, Qin W, Cross JR, Thompson CB. Transsulfuration Activity Can Support Cell Growth Upon Extracellular Cysteine Limitation. *Cell Metab* (2019) 30:865–76.e5. doi: 10.1016/j.cmet.2019.09.009
7. Trachootham D, Alexandre J, Huang P. Targeting Cancer Cells by ROS-Mediated Mechanisms: A Radical Therapeutic Approach? *Nat Rev Drug Discovery* (2009) 8:579–91. doi: 10.1038/nrd2803
8. Chio IIC, Tuveson DA. ROS in Cancer: The Burning Question. *Trends Mol Med* (2017) 23:411–29. doi: 10.1016/j.molmed.2017.03.004
9. Lewerenz J, Hewett SJ, Huang Y, Lambros M, Gout PW, Kalivas PW, et al. The Cystine/Glutamate Antiporter System X(C)(-) in Health and Disease: From Molecular Mechanisms to Novel Therapeutic Opportunities. *Antioxid Redox Signal* (2013) 18:522–55. doi: 10.1089/ars.2011.4391
10. Bannai S, Kitamura E. Transport Interaction of L-Cystine and L-Glutamate in Human Diploid Fibroblasts in Culture. *J Biol Chem* (1980) 255:2372–6. doi: 10.1016/S0021-9258(19)85901-X
11. Sato H, Tamba M, Ishii T, Bannai S. Cloning and Expression of a Plasma Membrane Cystine/Glutamate Exchange Transporter Composed of Two Distinct Proteins. *J Biol Chem* (1999) 274:11455–8. doi: 10.1074/jbc.274.17.11455
12. Kandasamy P, Gyimesi G, Kanai Y, Hediger MA. Amino Acid Transporters Revisited: New Views in Health and Disease. *Trends Biochem Sci* (2018) 43:752–89. doi: 10.1016/j.tibs.2018.05.003
13. Nakamura E, Sato M, Yang H, Miyagawa F, Harasaki M, Tomita K, et al. 4f2 (CD98) Heavy Chain is Associated Covalently With an Amino Acid Transporter and Controls Intracellular Trafficking and Membrane Topology of 4F2 Heterodimer. *J Biol Chem* (1999) 274:3009–16. doi: 10.1074/jbc.274.5.3009
14. Conrad M, Sato H. The Oxidative Stress-Inducible Cystine/Glutamate Antiporter, System X (C) (-) : Cystine Supplier and Beyond. *Amino Acids* (2012) 42:231–46. doi: 10.1007/s00726-011-0867-5
15. Lu SC. Regulation of Glutathione Synthesis. *Mol Aspects Med* (2009) 30:42–59. doi: 10.1016/j.mam.2008.05.005
16. Stipanuk MH. Sulfur Amino Acid Metabolism: Pathways for Production and Removal of Homocysteine and Cysteine. *Annu Rev Nutr* (2004) 24:539–77. doi: 10.1146/annurev.nutr.24.012003.132418
17. Bassi MT, Gasol E, Manzoni M, Pineda M, Riboni M, Martin R, et al. Identification and Characterisation of Human xCT That Co-Expresses, With 4F2 Heavy Chain, the Amino Acid Transport Activity System Xc. *Pflugers Arch* (2001) 442:286–96. doi: 10.1007/s004240100537
18. McCullagh EA, Featherstone DE. Behavioral Characterization of System Xc- Mutant Mice. *Behav Brain Res* (2014) 265:1–11. doi: 10.1016/j.bbr.2014.02.010
19. De Bundel D, Schallier A, Loyens E, Fernando R, Miyashita H, Van Liefferinge J, et al. Loss of System X(C)- Does Not Induce Oxidative Stress But Decreases Extracellular Glutamate in Hippocampus and Influences Spatial Working Memory and Limbic Seizure Susceptibility. *J Neurosci* (2011) 31:5792–803. doi: 10.1523/JNEUROSCI.5465-10.2011
20. Chintala S, Li W, Lamoreux ML, Ito S, Wakamatsu K, Sviderskaya EV, et al. Slc7a11 Gene Controls Production of Pheomelanin Pigment and Proliferation of Cultured Cells. *Proc Natl Acad Sci USA* (2005) 102:10964–9. doi: 10.1073/pnas.0502856102
21. Ji X, Qian J, Rahman SMJ, Siska PJ, Zou Y, Harris BK, et al. xCT (SLC7A11)-Mediated Metabolic Reprogramming Promotes Non-Small Cell Lung Cancer Progression. *Oncogene* (2018) 37:5007–19. doi: 10.1038/s41388-018-0307-z
22. Lin W, Wang C, Liu G, Bi C, Wang X, Zhou Q, et al. SLC7A11/xCT in Cancer: Biological Functions and Therapeutic Implications. *Am J Cancer Res* (2020) 10:3106–26.
23. Sharbeen G, McCarroll JA, Akerman A, Kopecky C, Youkhana J, Kokkinos J, et al. Cancer-Associated Fibroblasts in Pancreatic Ductal Adenocarcinoma Determine Response to SLC7A11 Inhibition. *Cancer Res* (2021) 81:3461–79. doi: 10.1101/2020.07.12.199638
24. Kilberg MS, Shan J, Su N. ATF4-Dependent Transcription Mediates Signaling of Amino Acid Limitation. *Trends Endocrinol Metab* (2009) 20:436–43. doi: 10.1016/j.tem.2009.05.008
25. Chen D, Fan Z, Rauh M, Buchfelder M, Eyupoglu IY, Savaskan N. ATF4 Promotes Angiogenesis and Neuronal Cell Death and Confers Ferroptosis in a xCT-Dependent Manner. *Oncogene* (2017) 36:5593–608. doi: 10.1038/onc.2017.146
26. Rojo de la Vega M, Chapman E, Zhang DD. NRF2 and the Hallmarks of Cancer. *Cancer Cell* (2018) 34:21–43. doi: 10.1016/j.ccell.2018.03.022
27. Anandhan A, Dodson M, Schmidlin CJ, Liu P, Zhang DD. Breakdown of an Ironclad Defense System: The Critical Role of NRF2 in Mediating Ferroptosis. *Cell Chem Biol* (2020) 27:436–47. doi: 10.1016/j.chembiol.2020.03.011
28. Pakos-Zebrucka K, Koryga I, Mnich K, Ljujic M, Samali A, Gorman AM. The Integrated Stress Response. *EMBO Rep* (2016) 17:1374–95. doi: 10.15252/embr.201642195
29. Jiang L, Kon N, Li T, Wang SJ, Su T, Hibshoosh H, et al. Ferroptosis as a P53-Mediated Activity During Tumour Suppression. *Nature* (2015) 520:57–62. doi: 10.1038/nature14344
30. Stockwell BR, Jiang X. The Chemistry and Biology of Ferroptosis. *Cell Chem Biol* (2020) 27:365–75. doi: 10.1016/j.chembiol.2020.03.013
31. Zhang Y, Koppula P, Gan B. Regulation of H2A Ubiquitination and SLC7A11 Expression by BAP1 and PRC1. *Cell Cycle* (2019) 18:773–83. doi: 10.1080/15384101.2019.1597506
32. Badeaux AI, Shi Y. Emerging Roles for Chromatin as a Signal Integration and Storage Platform. *Nat Rev Mol Cell Biol* (2013) 14:211–24. doi: 10.1038/nrm3545
33. Drayton RM, Dudziec E, Peter S, Bertz S, Hartmann A, Bryant HE, et al. Reduced Expression of miRNA-27a Modulates Cisplatin Resistance in Bladder Cancer by Targeting the Cystine/Glutamate Exchanger SLC7A11. *Clin Cancer Res* (2014) 20:1990–2000. doi: 10.1158/1078-0432.CCR-13-2805
34. Liu XX, Li XJ, Zhang B, Liang YJ, Zhou CX, Cao DX, et al. MicroRNA-26b is Underexpressed in Human Breast Cancer and Induces Cell Apoptosis by Targeting SLC7A11. *FEBS Lett* (2011) 585:1363–7. doi: 10.1016/j.febslet.2011.04.018
35. Wu Y, Sun X, Song B, Qiu X, Zhao J. MiR-375/SLC7A11 Axis Regulates Oral Squamous Cell Carcinoma Proliferation and Invasion. *Cancer Med* (2017) 6:1686–97. doi: 10.1002/cam4.1110
36. Carbone M, Yang H, Pass HI, Krausz T, Testa JR, Gaudino G. BAP1 and Cancer. *Nat Rev Cancer* (2013) 13:153–9. doi: 10.1038/nrc3459
37. Scheuermann JC, de Ayala Alonso AG, Oktaba K, Ly-Hartig N, McGinty RK, Fraterman S, et al. Histone H2A Deubiquitinase Activity of the Polycomb Repressive Complex PR-DUB. *Nature* (2010) 465:243–7. doi: 10.1038/nature08966
38. Wang H, Wang L, Erdjument-Bromage H, Vidal M, Tempst P, Jones RS, et al. Role of Histone H2A Ubiquitination in Polycomb Silencing. *Nature* (2004) 431:873–8. doi: 10.1038/nature02985
39. Kadoch C, Crabtree GR. Mammalian SWI/SNF Chromatin Remodeling Complexes and Cancer: Mechanistic Insights Gained From Human Genomics. *Sci Adv* (2015) 1:e1500447. doi: 10.1126/sciadv.1500447
40. Ogiwara H, Takahashi K, Sasaki M, Kuroda T, Yoshida H, Watanabe R, et al. Targeting the Vulnerability of Glutathione Metabolism in ARID1A-Deficient Cancers. *Cancer Cell* (2019) 35:177–90.e8. doi: 10.1016/j.ccell.2018.12.009
41. Ishimoto T, Nagano O, Yae T, Tamada M, Motohara T, Oshima H, et al. CD44 Variant Regulates Redox Status in Cancer Cells by Stabilizing the xCT Subunit of System Xc(-) and Thereby Promotes Tumor Growth. *Cancer Cell* (2011) 19:387–400. doi: 10.1016/j.ccr.2011.01.038

42. Yae T, Tsuchihashi K, Ishimoto T, Motohara T, Yoshikawa M, Yoshida GJ, et al. Alternative Splicing of CD44 mRNA by ESRP1 Enhances Lung Colonization of Metastatic Cancer Cell. *Nat Commun* (2012) 3:883. doi: 10.1038/ncomms1892
43. Gu Y, Albuquerque CP, Braas D, Zhang W, Villa GR, Bi J, et al. Mtorc2 Regulates Amino Acid Metabolism in Cancer by Phosphorylation of the Cystine-Glutamate Antiporter xCT. *Mol Cell* (2017) 67:128–38.e7. doi: 10.1016/j.molcel.2017.05.030
44. Tsuchihashi K, Okazaki S, Ohmura M, Ishikawa M, Sampetrean O, Onishi N, et al. The EGF Receptor Promotes the Malignant Potential of Glioma by Regulating Amino Acid Transport System Xc(-). *Cancer Res* (2016) 76:2954–63. doi: 10.1158/0008-5472.CAN-15-2121
45. Pavlova NN, Thompson CB. The Emerging Hallmarks of Cancer Metabolism. *Cell Metab* (2016) 23:27–47. doi: 10.1016/j.cmet.2015.12.006
46. Tian Y, Du W, Cao S, Wu Y, Dong N, Wang Y, et al. Systematic Analyses of Glutamine and Glutamate Metabolisms Across Different Cancer Types. *Chin J Cancer* (2017) 36:88. doi: 10.1186/s40880-017-0255-y
47. Hensley CT, Wasti AT, DeBerardinis RJ. Glutamine and Cancer: Cell Biology, Physiology, and Clinical Opportunities. *J Clin Invest* (2013) 123:3678–84. doi: 10.1172/JCI69600
48. Boroughs LK, DeBerardinis RJ. Metabolic Pathways Promoting Cancer Cell Survival and Growth. *Nat Cell Biol* (2015) 17:351–9. doi: 10.1038/ncb3124
49. Vander Heiden MG, Cantley LC, Thompson CB. Understanding the Warburg Effect: The Metabolic Requirements of Cell Proliferation. *Science* (2009) 324:1029–33. doi: 10.1126/science.1160809
50. Shin CS, Mishra P, Watrous JD, Carelli V, D'Aurelio M, Jain M, et al. The Glutamate/Cystine xCT Antiporter Antagonizes Glutamine Metabolism and Reduces Nutrient Flexibility. *Nat Commun* (2017) 8:15074. doi: 10.1038/ncomms15074
51. Koppula P, Zhang Y, Shi J, Li W, Gan B. The Glutamate/Cystine Antiporter SLC7A11/xCT Enhances Cancer Cell Dependency on Glucose by Exporting Glutamate. *J Biol Chem* (2017) 292:14240–9. doi: 10.1074/jbc.M117.798405
52. Bannai S. Exchange of Cystine and Glutamate Across Plasma Membrane of Human Fibroblasts. *J Biol Chem* (1986) 261:2256–63. doi: 10.1016/S0021-9258(17)35926-4
53. Bannai S, Ishii T. A Novel Function of Glutamine in Cell Culture: Utilization of Glutamine for the Uptake of Cystine in Human Fibroblasts. *J Cell Physiol* (1988) 137:360–6. doi: 10.1002/jcp.1041370221
54. Muir A, Danai LV, Gui DY, Waingarten CY, Lewis CA, Vander Heiden MG. Environmental Cystine Drives Glutamine Anaplerosis and Sensitizes Cancer Cells to Glutaminase Inhibition. *Elife 6* (2017) 6:e27713. doi: 10.7554/eLife.27713
55. Timmerman LA, Holton T, Yuneva M, Louie RJ, Padro M, Daemen A, et al. Glutamine Sensitivity Analysis Identifies the xCT Antiporter as a Common Triple-Negative Breast Tumor Therapeutic Target. *Cancer Cell* (2013) 24:450–65. doi: 10.1016/j.ccr.2013.08.020
56. Badgley MA, Kremer DM, Maurer HC, DelGiorno KE, Lee HJ, Purohit V, et al. Cysteine Depletion Induces Pancreatic Tumor Ferroptosis in Mice. *Science* (2020) 368:85–9. doi: 10.1126/science.aaw9872
57. Liu J, Xia X, Huang P. xCT: A Critical Molecule That Links Cancer Metabolism to Redox Signaling. *Mol Ther* (2020) 28:2358–66. doi: 10.1016/j.ymthe.2020.08.021
58. Joly JH, Delfarah A, Phung PS, Parrish S, Graham NA. A Synthetic Lethal Drug Combination Mimics Glucose Deprivation-Induced Cancer Cell Death in the Presence of Glucose. *J Biol Chem* (2020) 295:1350–65. doi: 10.1016/S0021-9258(17)49891-7
59. Otto AM. Metabolic Constants and Plasticity of Cancer Cells in a Limiting Glucose and Glutamine Microenvironment-A Pyruvate Perspective. *Front Oncol* (2020) 10:596197. doi: 10.3389/fonc.2020.596197
60. Sullivan MR, Danai LV, Lewis CA, Chan SH, Gui DY, Kunchok T, et al. Quantification of Microenvironmental Metabolites in Murine Cancers Reveals Determinants of Tumor Nutrient Availability. *Elife 8* (2019) 8: e44235. doi: 10.7554/eLife.44235
61. Weidinger A, Kozlov AV. Biological Activities of Reactive Oxygen and Nitrogen Species: Oxidative Stress *Versus* Signal Transduction. *Biomolecules* (2015) 5:472–84. doi: 10.3390/biom5020472
62. Auten RL, Davis JM. Oxygen Toxicity and Reactive Oxygen Species: The Devil is in the Details. *Pediatr Res* (2009) 66:121–7. doi: 10.1203/PDR.0b013e3181a9eafb
63. Gu X, El-Remessy AB, Brooks SE, Al-Shabrawey M, Tsai NT, Caldwell RB. Hyperoxia Induces Retinal Vascular Endothelial Cell Apoptosis Through Formation of Peroxynitrite. *Am J Physiol Cell Physiol* (2003) 285:C546–54. doi: 10.1152/ajpcell.00424.2002
64. Tang R, Hua J, Xu J, Liang C, Meng Q, Liu J, et al. The Role of Ferroptosis Regulators in the Prognosis, Immune Activity and Gemcitabine Resistance of Pancreatic Cancer. *Ann Transl Med* (2020) 8:1347. doi: 10.21037/atm-20-2554a
65. Qu J, Li Y, Zhong W, Gao P, Hu C. Recent Developments in the Role of Reactive Oxygen Species in Allergic Asthma. *J Thorac Dis* (2017) 9:E32–43. doi: 10.21037/jtd.2017.01.05
66. Banjac A, Perisic T, Sato H, Seiler A, Bannai S, Weiss N, et al. The Cystine/Cysteine Cycle: A Redox Cycle Regulating Susceptibility *Versus* Resistance to Cell Death. *Oncogene* (2008) 27:1618–28. doi: 10.1038/sj.onc.1210796
67. Frank NY, Schatton T, Frank MH. The Therapeutic Promise of the Cancer Stem Cell Concept. *J Clin Invest* (2010) 120:41–50. doi: 10.1172/JCI41004
68. Friedmann Angeli JP, Krysko DV, Conrad M. Ferroptosis at the Crossroads of Cancer-Acquired Drug Resistance and Immune Evasion. *Nat Rev Cancer* (2019) 19:405–14. doi: 10.1038/s41568-019-0149-1
69. Hassannia B, Vandenabeele P, Vanden Berghe T. Targeting Ferroptosis to Iron Out Cancer. *Cancer Cell* (2019) 35:830–49. doi: 10.1016/j.ccell.2019.04.002
70. Lei G, Zhang Y, Koppula P, Liu X, Zhang J, Lin SH, et al. The Role of Ferroptosis in Ionizing Radiation-Induced Cell Death and Tumor Suppression. *Cell Res* (2020) 30:146–62. doi: 10.1038/s41422-019-0263-3
71. Chu B, Kon N, Chen D, Li T, Liu T, Jiang L, et al. ALOX12 is Required for P53-Mediated Tumour Suppression Through a Distinct Ferroptosis Pathway. *Nat Cell Biol* (2019) 21:579–91. doi: 10.1038/s41556-019-0305-6
72. Liu GZ, Xu XW, Tao SH, Gao MJ, Hou ZH. HBx Facilitates Ferroptosis in Acute Liver Failure *via* EZH2 Mediated SLC7A11 Suppression. *J BioMed Sci* (2021) 28:67. doi: 10.1186/s12929-021-00762-2
73. Du K, Oh SH, Dutta RK, Sun T, Yang WH, Chi JT, et al. Inhibiting xCT/SLC7A11 Induces Ferroptosis of Myofibroblastic Hepatic Stellate Cells But Exacerbates Chronic Liver Injury. *Liver Int* (2021) 41:2214–27. doi: 10.1111/liv.14945
74. Li T, Kon N, Jiang L, Tan M, Ludwig T, Zhao Y, et al. Tumor Suppression in the Absence of P53-Mediated Cell-Cycle Arrest, Apoptosis, and Senescence. *Cell* (2012) 149:1269–83. doi: 10.1016/j.cell.2012.04.026
75. Jennis M, Kung CP, Basu S, Budina-Kolomets A, Leu JI, Khaku S, et al. An African-Specific Polymorphism in the TP53 Gene Impairs P53 Tumor Suppressor Function in a Mouse Model. *Genes Dev* (2016) 30:918–30. doi: 10.1101/gad.275891.115
76. Zhang Y, Zhuang L, Gan B. BAP1 Suppresses Tumor Development by Inducing Ferroptosis Upon SLC7A11 Repression. *Mol Cell Oncol* (2019) 6:1536845. doi: 10.1080/23723556.2018.1536845
77. Zhang Y, Shi J, Liu X, Feng L, Gong Z, Koppula P, et al. BAP1 Links Metabolic Regulation of Ferroptosis to Tumour Suppression. *Nat Cell Biol* (2018) 20:1181–92. doi: 10.1038/s41556-018-0178-0
78. Hu K, Li K, Lv J, Feng J, Chen J, Wu H, et al. Suppression of the SLC7A11/glutathione Axis Causes Synthetic Lethality in KRAS-Mutant Lung Adenocarcinoma. *J Clin Invest* (2020) 130:1752–66. doi: 10.1172/JCI124049
79. Qiao HX, Hao CJ, Li Y, He X, Chen RS, Cui J, et al. JNK Activation Mediates the Apoptosis of xCT-Deficient Cells. *Biochem Biophys Res Commun* (2008) 370:584–8. doi: 10.1016/j.bbrc.2008.03.134
80. Stockwell BR, Friedmann Angeli JP, Bayir H, Bush AI, Conrad M, Dixon SJ, et al. Ferroptosis: A Regulated Cell Death Nexus Linking Metabolism, Redox Biology, and Disease. *Cell* (2017) 171:273–85. doi: 10.1016/j.cell.2017.09.021
81. Lim JKM, Delaidelli A, Minaker SW, Zhang HF, Colovic M, Yang H, et al. Cystine/glutamate Antiporter xCT (SLC7A11) Facilitates Oncogenic RAS Transformation by Preserving Intracellular Redox Balance. *Proc Natl Acad Sci United States America* (2019) 116:9433–42. doi: 10.1073/pnas.1821323116
82. Wang W, Green M, Choi JE, Gijon M, Kennedy PD, Johnson JK, et al. CD8(+) T Cells Regulate Tumour Ferroptosis During Cancer Immunotherapy. *Nature* (2019) 569:270–4. doi: 10.1038/s41586-019-1170-y
83. Lang X, Green MD, Wang W, Yu J, Choi JE, Jiang L, et al. Radiotherapy and Immunotherapy Promote Tumoral Lipid Oxidation and Ferroptosis *via* Synergistic Repression of SLC7A11. *Cancer Discov* (2019) 9:1673–85. doi: 10.1158/2159-8290.CD-19-0338

84. Wang SF, Wung CH, Chen MS, Chen CF, Yin PH, Yeh TS, et al. Activated Integrated Stress Response Induced by Salubrinal Promotes Cisplatin Resistance in Human Gastric Cancer Cells *via* Enhanced xCT Expression and Glutathione Biosynthesis. *Int J Mol Sci* (2018) 19:3389. doi: 10.3390/ijms19113389
85. Wang L, Leite de Oliveira R, Huijberts S, Bosdriesz E, Pencheva N, Brunen D, et al. An Acquired Vulnerability of Drug-Resistant Melanoma With Therapeutic Potential. *Cell* (2018) 173:1413–25.e14. doi: 10.1016/j.cell.2018.04.012
86. Khamari R, Trinh A, Gabert PE, Corazao-Rozas P, Riveros-Cruz S, Balayssac S, et al. Glucose Metabolism and NRF2 Coordinate the Antioxidant Response in Melanoma Resistant to MAPK Inhibitors. *Cell Death Dis* (2018) 9:325. doi: 10.1038/s41419-018-0340-4
87. Liu R, Blower PE, Pham AN, Fang J, Dai Z, Wise C, et al. Cystine-Glutamate Transporter SLC7A11 Mediates Resistance to Geldanamycin But Not to 17-(Allylamino)-17-Demethoxygeldanamycin. *Mol Pharmacol* (2007) 72:1637–46. doi: 10.1124/mol.107.039644
88. Polewski MD, Reveron-Thornton RF, Cherryholmes GA, Marinov GK, Cassady K, Aboody KS. Increased Expression of System Xc- in Glioblastoma Confers an Altered Metabolic State and Temozolomide Resistance. *Mol Cancer Res* (2016) 14:1229–42. doi: 10.1158/1541-7786.MCR-16-0028
89. Lo M, Ling V, Wang YZ, Gout PW. The Xc- Cystine/Glutamate Antiporter: A Mediator of Pancreatic Cancer Growth With a Role in Drug Resistance. *Br J Cancer* (2008) 99:464–72. doi: 10.1038/sj.bjc.6604485
90. Bekeschus S, Eisenmann S, Sagwal SK, Bodnar Y, Moritz J, Poschkamp B, et al. xCT (SLC7A11) Expression Confers Intrinsic Resistance to Physical Plasma Treatment in Tumor Cells. *Redox Biol* (2020) 30:101423. doi: 10.1016/j.redox.2019.101423
91. Huang Y, Dai Z, Barbacioru C, Sadee W. Cystine-Glutamate Transporter SLC7A11 in Cancer Chemosensitivity and Chemoresistance. *Cancer Res* (2005) 65:7446–54. doi: 10.1158/0008-5472.CAN-04-4267
92. Olm E, Fernandes AP, Hebert C, Rundlof AK, Larsen EH, Danielsson O, et al. Extracellular Thiol-Assisted Selenium Uptake Dependent on the X(C)-Cystine Transporter Explains the Cancer-Specific Cytotoxicity of Selenite. *Proc Natl Acad Sci USA* (2009) 106:11400–5. doi: 10.1073/pnas.0902204106
93. Roh JL, Kim EH, Jang HJ, Park JY, Shin D. Induction of Ferroptotic Cell Death for Overcoming Cisplatin Resistance of Head and Neck Cancer. *Cancer Lett* (2016) 381:96–103. doi: 10.1016/j.canlet.2016.07.035
94. Fang X, Cai Z, Wang H, Han D, Cheng Q, Zhang P, et al. Loss of Cardiac Ferritin H Facilitates Cardiomyopathy *via* Slc7a11-Mediated Ferroptosis. *Circ Res* (2020) 127:486–501. doi: 10.1161/CIRCRESAHA.120.316509
95. Qiang Z, Dong H, Xia Y, Chai D, Hu R, Jiang H. Nrf2 and STAT3 Alleviates Ferroptosis-Mediated IIR-ALI by Regulating Slc7a11. *Oxid Med Cell Longev* (2020) 2020:5146982. doi: 10.1155/2020/5146982
96. Meyer AR, Engevik AC, Willet SG, Williams JA, Zou Y, Massion PP, et al. Cystine/Glutamate Antiporter (xCT) Is Required for Chief Cell Plasticity After Gastric Injury. *Cell Mol Gastroenterol Hepatol* (2019) 8:379–405. doi: 10.1016/j.jcmgh.2019.04.015
97. Wang AW, Wangensteen KJ, Wang YJ, Zahm AM, Moss NG, Erez N, et al. TRAP-Seq Identifies Cystine/Glutamate Antiporter as a Driver of Recovery From Liver Injury. *J Clin Invest* (2018) 128:2297–309. doi: 10.1172/JCI95120
98. Sprimont L, Janssen P, De Swert K, Van Bulck M, Rooman I, Gilloteaux J, et al. Cystine-Glutamate Antiporter Deletion Accelerates Motor Recovery and Improves Histological Outcomes Following Spinal Cord Injury in Mice. *Sci Rep* (2021) 11:12227. doi: 10.1038/s41598-021-91698-y
99. Zhong W, Weiss HL, Jayswal RD, Hensley PJ, Downes LM, St Clair DK, et al. Extracellular Redox State Shift: A Novel Approach to Target Prostate Cancer Invasion. *Free Radic Biol Med* (2018) 117:99–109. doi: 10.1016/j.freeradbiomed.2018.01.023
100. Lanzardo S, Conti L, Rooke R, Ruiu R, Accart N, Bolli E, et al. Immunotargeting of Antigen xCT Attenuates Stem-Like Cell Behavior and Metastatic Progression in Breast Cancer. *Cancer Res* (2016) 76:62–72. doi: 10.1158/0008-5472.CAN-15-1208
101. Zhao X, Li Y, Wu H. A Novel Scoring System for Acute Myeloid Leukemia Risk Assessment Based on the Expression Levels of Six Genes. *Int J Mol Med* (2018) 42:1495–507. doi: 10.3892/ijmm.2018.3739
102. Yin F, Yi S, Wei L, Zhao B, Li J, Cai X, et al. Microarray-Based Identification of Genes Associated With Prognosis and Drug Resistance in Ovarian Cancer. *J Cell Biochem* (2019) 120:6057–70. doi: 10.1002/jcb.27892
103. Shin SS, Jeong BS, Wall BA, Li J, Shan NL, Wen Y, et al. Participation of xCT in Melanoma Cell Proliferation *In Vitro* and Tumorigenesis *In Vivo*. *Oncogenesis* (2018) 7:86. doi: 10.1038/s41389-018-0098-7
104. Shen L, Qian C, Cao H, Wang Z, Luo T, Liang C. Upregulation of the Solute Carrier Family 7 Genes is Indicative of Poor Prognosis in Papillary Thyroid Carcinoma. *World J Surg Oncol* (2018) 16:235. doi: 10.1186/s12957-018-1535-y
105. Iida Y, Okamoto-Katsuyama M, Maruoka S, Mizumura K, Shimizu T, Shikano S, et al. Effective Ferroptotic Small-Cell Lung Cancer Cell Death From SLC7A11 Inhibition by Sulforaphane. *Oncol Lett* (2021) 21:71. doi: 10.3892/ol.2020.12332
106. Sun D, Li YC, Zhang XY. Lidocaine Promoted Ferroptosis by Targeting miR-382-5p /SLC7A11 Axis in Ovarian and Breast Cancer. *Front Pharmacol* (2021) 12:681223. doi: 10.3389/fphar.2021.681223
107. Robert SM, Buckingham SC, Campbell SL, Robel S, Holt KT, Ogunrinu-Babarinde T, et al. SLC7A11 Expression is Associated With Seizures and Predicts Poor Survival in Patients With Malignant Glioma. *Sci Transl Med* (2015) 7:289ra86. doi: 10.1126/scitranslmed.aaa8103
108. Liang Y, Ye F, Xu C, Zou L, Hu Y, Hu J, et al. A Novel Survival Model Based on a Ferroptosis-Related Gene Signature for Predicting Overall Survival in Bladder Cancer. *BMC Cancer* (2021) 21:943. doi: 10.1186/s12885-021-08687-7
109. Feng L, Zhao K, Sun L, Yin X, Zhang J, Liu C, et al. SLC7A11 Regulated by NRF2 Modulates Esophageal Squamous Cell Carcinoma Radiosensitivity by Inhibiting Ferroptosis. *J Transl Med* (2021) 19:367. doi: 10.1186/s12967-021-03042-7
110. Zhang L, Huang Y, Ling J, Zhuo W, Yu Z, Luo Y, et al. Overexpression of SLC7A11: A Novel Oncogene and an Indicator of Unfavorable Prognosis for Liver Carcinoma. *Future Oncol* (2018) 14:927–36. doi: 10.2217/fon-2017-0540
111. Wada F, Koga H, Akiba J, Niizeki T, Iwamoto H, Ikezono Y, et al. High Expression of CD44v9 and xCT in Chemoresistant Hepatocellular Carcinoma: Potential Targets by Sulfasalazine. *Cancer Sci* (2018) 109:2801–10. doi: 10.1111/cas.13728
112. He J, Ding H, Li H, Pan Z, Chen Q. Intra-Tumoral Expression of SLC7A11 Is Associated With Immune Microenvironment, Drug Resistance, and Prognosis in Cancers: A Pan-Cancer Analysis. *Front Genet* (2021) 12:770857. doi: 10.3389/fgene.2021.770857
113. Guo W, Zhao Y, Zhang Z, Tan N, Zhao F, Ge C, et al. Disruption of xCT Inhibits Cell Growth *via* the ROS/autophagy Pathway in Hepatocellular Carcinoma. *Cancer Lett* (2011) 312:55–61. doi: 10.1016/j.canlet.2011.07.024
114. He Q, Liu M, Huang W, Chen X, Zhang B, Zhang T, et al. IL-1beta-Induced Elevation of Solute Carrier Family 7 Member 11 Promotes Hepatocellular Carcinoma Metastasis Through Up-Regulating Programmed Death Ligand 1 and Colony-Stimulating Factor 1. *Hepatology* (2021) 74:3174–93. doi: 10.1002/hep.32062
115. Liu Y, Song Z, Liu Y, Ma X, Wang W, Ke Y, et al. Identification of Ferroptosis as a Novel Mechanism for Antitumor Activity of Natural Product Derivative A2 in Gastric Cancer. *Acta Pharm Sin B* (2021) 11:1513–25. doi: 10.1016/j.apsb.2021.05.006
116. Ni H, Qin H, Sun C, Liu Y, Ruan G, Guo Q, et al. MiR-375 Reduces the Stemness of Gastric Cancer Cells Through Triggering Ferroptosis. *Stem Cell Res Ther* (2021) 12:325. doi: 10.1186/s13287-021-02394-7
117. Mao SH, Zhu CH, Nie Y, Yu J, Wang L. Levobupivacaine Induces Ferroptosis by miR-489-3p/SLC7A11 Signaling in Gastric Cancer. *Front Pharmacol* (2021) 12:681338. doi: 10.3389/fphar.2021.681338
118. Luo Y, Wang C, Yong P, Ye P, Liu Z, Fu Z, et al. Decreased Expression of the Long Non-Coding RNA SLC7A11-AS1 Predicts Poor Prognosis and Promotes Tumor Growth in Gastric Cancer. *Oncotarget* (2017) 8:112530–49. doi: 10.18632/oncotarget.22486
119. Guan Z, Chen J, Li X, Dong N. Tanshinone IIA Induces Ferroptosis in Gastric Cancer Cells Through P53-Mediated SLC7A11 Down-Regulation. *Biosci Rep 40* (2020) 40:BSR20201807. doi: 10.1042/BSR20201807
120. Zhuang J, Liu X, Yang Y, Zhang Y, Guan G. Sulfasalazine, a Potent Suppressor of Gastric Cancer Proliferation and Metastasis by Inhibition of

xCT: Conventional Drug in New Use. *J Cell Mol Med* (2021) 25:5372–80. doi: 10.1111/jcmm.16548
121. Shi ZZ, Tao H, Fan ZW, Song SJ, Bai J. Prognostic and Immunological Role of Key Genes of Ferroptosis in Pan-Cancer. *Front Cell Dev Biol* (2021) 9:748925. doi: 10.3389/fcell.2021.748925
122. Gao W, Huang Z, Duan J, Nice EC, Lin J, Huang C. Elesclomol Induces Copper-Dependent Ferroptosis in Colorectal Cancer Cells *via* Degradation of ATP7A. *Mol Oncol* (2021) 15:3527–44. doi: 10.1002/1878-0261.13079
123. Xu X, Zhang X, Wei C, Zheng D, Lu X, Yang Y, et al. Targeting SLC7A11 Specifically Suppresses the Progression of Colorectal Cancer Stem Cells *via* Inducing Ferroptosis. *Eur J Pharm Sci* (2020) 152:105450. doi: 10.1016/j.ejps.2020.105450
124. Ju HQ, Lu YX, Chen DL, Tian T, Mo HY, Wei XL, et al. Redox Regulation of Stem-Like Cells Though the CD44v-xCT Axis in Colorectal Cancer: Mechanisms and Therapeutic Implications. *Theranostics* (2016) 6:1160–75. doi: 10.7150/thno.14848
125. Zhang L, Liu W, Liu F, Wang Q, Song M, Yu Q, et al. IMCA Induces Ferroptosis Mediated by SLC7A11 Through the AMPK/mTOR Pathway in Colorectal Cancer. *Oxid Med Cell Longev* (2020) 2020:1675613. doi: 10.1155/2020/1675613
126. Daher B, Parks SK, Durivault J, Cormerais Y, Baidarjad H, Tambutte E, et al. Genetic Ablation of the Cystine Transporter xCT in PDAC Cells Inhibits Mtorc1, Growth, Survival, and Tumor Formation *via* Nutrient and Oxidative Stresses. *Cancer Res* (2019) 79:3877–90. doi: 10.1158/0008-5472.CAN-18-3855
127. Zhu JH, De Mello RA, Yan QL, Wang JW, Chen Y, Ye QH, et al. MiR-139-5p/SLC7A11 Inhibits the Proliferation, Invasion and Metastasis of Pancreatic Carcinoma *via* PI3K/Akt Signaling Pathway. *Biochim Biophys Acta Mol Basis Dis* (2020) 1866:165747. doi: 10.1016/j.bbadis.2020.165747
128. Dixon SJ, Patel DN, Welsch M, Skouta R, Lee ED, Hayano M, et al. Pharmacological Inhibition of Cystine-Glutamate Exchange Induces Endoplasmic Reticulum Stress and Ferroptosis. *Elife* (2014) 3:e02523. doi: 10.7554/eLife.02523
129. Ogihara K, Kikuchi E, Okazaki S, Hagiwara M, Takeda T, Matsumoto K, et al. Sulfasalazine Could Modulate the CD44v9-xCT System and Enhance Cisplatin-Induced Cytotoxic Effects in Metastatic Bladder Cancer. *Cancer Sci* (2019) 110:1431–41. doi: 10.1111/cas.13960
130. Shiromizu S, Yamauchi T, Kusunose N, Matsunaga N, Koyanagi S, Ohdo S. Dosing Time-Dependent Changes in the Anti-Tumor Effect of xCT Inhibitor Erastin in Human Breast Cancer Xenograft Mice. *Biol Pharm Bull* (2019) 42:1921–5. doi: 10.1248/bpb.b19-00546
131. Dolma S, Lessnick SL, Hahn WC, Stockwell BR. Identification of Genotype-Selective Antitumor Agents Using Synthetic Lethal Chemical Screening in Engineered Human Tumor Cells. *Cancer Cell* (2003) 3:285–96. doi: 10.1016/S1535-6108(03)00050-3
132. Zhang Y, Tan H, Daniels JD, Zandkarimi F, Liu H, Brown LM, et al. Imidazole Ketone Erastin Induces Ferroptosis and Slows Tumor Growth in a Mouse Lymphoma Model. *Cell Chem Biol* (2019) 26:623–33.e9. doi: 10.1016/j.chembiol.2019.01.008
133. Louandre C, Ezzoukhry Z, Godin C, Barbare JC, Maziere JC, Chauffert B, et al. Iron-Dependent Cell Death of Hepatocellular Carcinoma Cells Exposed to Sorafenib. *Int J Cancer* (2013) 133:1732–42. doi: 10.1002/ijc.28159
134. Lachaier E, Louandre C, Godin C, Saidak Z, Baert M, Diouf M, et al. Sorafenib Induces Ferroptosis in Human Cancer Cell Lines Originating From Different Solid Tumors. *Anticancer Res* (2014) 34:6417–22.
135. Kou L, Sun R, Xiao S, Zheng Y, Chen Z, Cai A, et al. Ambidextrous Approach To Disrupt Redox Balance in Tumor Cells With Increased ROS Production and Decreased GSH Synthesis for Cancer Therapy. *ACS Appl Mater Interfaces* (2019) 11:26722–30. doi: 10.1021/acsami.9b09784
136. Wilhelm SM, Adnane L, Newell P, Villanueva A, Llovet JM, Lynch M. Preclinical Overview of Sorafenib, a Multikinase Inhibitor That Targets Both Raf and VEGF and PDGF Receptor Tyrosine Kinase Signaling. *Mol Cancer Ther* (2008) 7:3129–40. doi: 10.1158/1535-7163.MCT-08-0013
137. Stenson WF, Lobos E. Sulfasalazine Inhibits the Synthesis of Chemotactic Lipids by Neutrophils. *J Clin Invest* (1982) 69:494–7. doi: 10.1172/JCI110474
138. Robe PA, Martin DH, Nguyen-Khac MT, Artesi M, Deprez M, Albert A, et al. Early Termination of ISRCTN45828668, a Phase 1/2 Prospective, Randomized Study of Sulfasalazine for the Treatment of Progressing Malignant Gliomas in Adults. *BMC Cancer* (2009) 9:372. doi: 10.1186/1471-2407-9-372
139. Galan-Cobo A, Sitthideatphaiboon P, Qu X, Poteete A, Pisegna MA, Tong P, et al. LKB1 and KEAP1/NRF2 Pathways Cooperatively Promote Metabolic Reprogramming With Enhanced Glutamine Dependence in KRAS-Mutant Lung Adenocarcinoma. *Cancer Res* (2019) 79:3251–67. doi: 10.1158/0008-5472.CAN-18-3527
140. Romero R, Sayin VI, Davidson SM, Bauer MR, Singh SX, LeBoeuf SE, et al. Keap1 Loss Promotes Kras-Driven Lung Cancer and Results in Dependence on Glutaminolysis. *Nat Med* (2017) 23:1362–8. doi: 10.1038/nm.4407
141. Liu X, Olszewski K, Zhang Y, Lim EW, Shi J, Zhang X, et al. Cystine Transporter Regulation of Pentose Phosphate Pathway Dependency and Disulfide Stress Exposes a Targetable Metabolic Vulnerability in Cancer. *Nat Cell Biol* (2020) 22:476–86. doi: 10.1038/s41556-020-0496-x
142. Fazzari J, Balenko MD, Zacal N, Singh G. Identification of Capsazepine as a Novel Inhibitor of System Xc(-) and Cancer-Induced Bone Pain. *J Pain Res* (2017) 10:915–25. doi: 10.2147/JPR.S125045
143. Patel SA, Warren BA, Rhoderick JF, Bridges RJ. Differentiation of Substrate and Non-Substrate Inhibitors of Transport System Xc(-): An Obligate Exchanger of L-Glutamate and L-Cystine. *Neuropharmacology* (2004) 46:273–84. doi: 10.1016/j.neuropharm.2003.08.006
144. Ye J, Jiang X, Dong Z, Hu S, Xiao M. Low-Concentration PTX And RSL3 Inhibits Tumor Cell Growth Synergistically By Inducing Ferroptosis In Mutant P53 Hypopharyngeal Squamous Carcinoma. *Cancer Manag Res* (2019) 11:9783–92. doi: 10.2147/CMAR.S217944
145. Bolli E, O'Rourke JP, Conti L, Lanzardo S, Rolih V, Christen JM, et al. A Virus-Like-Particle Immunotherapy Targeting Epitope-Specific anti-xCT Expressed on Cancer Stem Cell Inhibits the Progression of Metastatic Cancer *In Vivo*. *Oncoimmunology* (2018) 7:e1408746. doi: 10.1080/2162402X.2017.1408746
146. Donofrio G, Tebaldi G, Lanzardo S, Ruiu R, Bolli E, Ballatore A, et al. Bovine Herpesvirus 4-Based Vector Delivering the Full Length xCT DNA Efficiently Protects Mice From Mammary Cancer Metastases by Targeting Cancer Stem Cells. *Oncoimmunology* (2018) 7:e1494108. doi: 10.1080/2162402X.2018.1494108

Conflict of Interest: The authors declare that the research was conducted in the absence of any commercial or financial relationships that could be construed as a potential conflict of interest.

Publisher's Note: All claims expressed in this article are solely those of the authors and do not necessarily represent those of their affiliated organizations, or those of the publisher, the editors and the reviewers. Any product that may be evaluated in this article, or claim that may be made by its manufacturer, is not guaranteed or endorsed by the publisher.

frontiers in Physiology

REVIEW
published: 04 March 2022
doi: 10.3389/fphys.2022.856803

Updates in the Diagnosis of Intraductal Neoplasms of the Pancreas

*Naziheh Assarzadegan, Sepideh Babaniamansour and Jiaqi Shi**

Department of Pathology, University of Michigan, Ann Arbor, MI, United States

Pancreatic ductal adenocarcinoma (PDAC) is one of the deadliest types of cancer worldwide. There are many reasons for this dismal prognosis, including the advanced stage at the time of diagnosis and the lack of effective therapeutic approaches. Intraductal papillary mucinous neoplasms (IPMNs) represent detectable and treatable precursor lesions of PDAC. Our understanding of the pathology of IPMNs has evolved over the past few decades, and new advances in diagnostic tools have emerged. The new World Health Organization (WHO) classification scheme now recognizes the previously considered variants of IPMNs, such as intraductal oncocytic papillary neoplasms (IOPNs) and intraductal tubulopapillary neoplasms (ITPNs), as distinct neoplasms. New imaging and molecular diagnostic tests are being developed to recognize these PDAC precursor lesions better. Here, we review the advances in diagnostic tools for IPMNs, IOPNs, and ITPNs, emphasizing the new (5th edition, 2019) WHO classification for pathological diagnosis, molecular markers, new laboratory tests, and imaging tools.

Keywords: intraductal papillary mucinous neoplasm, intraductal oncocytic papillary neoplasm, intraductal tubulopapillary neoplasm, pancreatic ductal adenocarcinoma, classification

OPEN ACCESS

Edited by:
Natalie Luhtala,
Salk Institute for Biological Studies, United States

Reviewed by:
Shin Hamada,
Tohoku University, Japan
Irene Esposito,
Heinrich Heine University of Düsseldorf, Germany

****Correspondence:***
Jiaqi Shi
jiaqis@med.umich.edu

Specialty section:
This article was submitted to Gastrointestinal Sciences, a section of the journal Frontiers in Physiology

Received: *17 January 2022*
Accepted: *17 February 2022*
Published: *04 March 2022*

Citation:
Assarzadegan N, Babaniamansour S and Shi J (2022) Updates in the Diagnosis of Intraductal Neoplasms of the Pancreas. Front. Physiol. 13:856803. doi: 10.3389/fphys.2022.856803

INTRODUCTION

All cystic tumors of the pancreas were grouped decades ago. In 1978, Compagno et al. separated mucin-producing neoplasms of the pancreas from serous cystadenomas (Compagno and Oertel, 1978a,b; Hodgkinson et al., 1978). In 1980, Ohhashi et al. (1982) first described what we now recognize as intraductal papillary mucinous neoplasms (IPMNs). A few years later, Zamboni and others separated IPMNs from mucinous cystic neoplasms (MCNs; Zamboni et al., 1999).

Intraductal papillary mucinous neoplasms are precursor lesions of pancreatic ductal adenocarcinoma (PDAC), which has a dismal prognosis. PDACs predominantly arise from two types of precursor lesions, pancreatic intraepithelial neoplasia (PanIN), and IPMNs. PanINs are considered microscopic lesions (usually <5 mm) and are not typically detected radiologically. In contrast, IPMNs lead to cystic dilatation of the pancreatic duct, which imaging studies can readily identify. IPMNs are the intraductal proliferation of mucinous epithelial cells, characterized by abundant mucinous production and papillary epithelial growth. As a result of detailed studies of the pathologic and genetic features of IPMNs in recent years, previously considered variants of IPMN, intraductal oncocytic papillary neoplasms (IOPNs), and intraductal tubulopapillary neoplasms (ITPNs) are now regarded as distinctive neoplasms as per the 2019

5th edition of World Health Organization (WHO) classification scheme (WHO Classification of Tumours Editorial Board, 2019).

Intraductal papillary mucinous neoplasms of the pancreas originate from the pancreatic ductal system. Depending on the pancreatic ductal sites affected, IPMNs can be divided into three groups: (a) main-duct IPMNs (MD-IPMN), which originate from the main pancreatic duct; (b) branch-duct IPMNs (BD-IPMN), which originate from the ductal branches of the main duct; and (c) mixed IPMNs which originate from both the main and side-branches of the ductal system (Salvia et al., 2004; Rodriguez et al., 2007). Depending on the level of epithelial dysplasia, IPMNs are further classified into low grade and high grade. IPMNs have been shown to progress from low grade to high grade and eventually to invasive carcinoma, which can be colloid or an invasive ductal adenocarcinoma (Shimizu et al., 2013; WHO Classification of Tumours Editorial Board, 2019). The overall incidence of an invasive carcinoma associated with IPMN is low; however, they are seen in association with about 60% of MD-IPMNs.

Pancreatic ductal adenocarcinoma can occur in the vicinity of IPMN lesions. The term concomitant PDAC with IPMN refers to a PDAC that is separated from the IPMN by an uninvolved segment of pancreatic duct and with no areas of transition in between. The frequency of concomitant pancreatic cancer in IPMN patients range from 2.5 to 9.2% by various studies. PDAC concomitant with IPMN are often significantly smaller, less aggressive, and are associated with longer survival compared to PDAC with no associated IPMN (Yamaguchi et al., 2011; Tanaka, 2015).

Intraductal oncocytic papillary neoplasms, previously known as an oncocytic variant of IPMNs, are rare cystic neoplasms with intraductal growth. It was recently discovered that virtually all IOPNs harbor specific fusion genes not found in any other intraductal neoplasms, which helped establish that IOPNs should be considered an entirely separate entity from the other IPMNs. Invasive adenocarcinoma is seen in about 30% of IOPNs (Basturk et al., 2016; Vyas et al., 2020).

Intraductal tubulopapillary neoplasms is another rare intraductal neoplasm distinct from IPMN due to the lack of mucin production, uniform high-grade nuclear atypia, and tubule formation. They are often less cyst forming than IPMNs. Invasive carcinoma is found in association with 70% of these lesions (Basturk et al., 2017).

In the last decade, advances in understanding IPMNs, IOPNs, and ITPNs have enabled early diagnosis and provided preoperative risk measurements to prioritize those patients who will benefit the most from surgical resection. This article will provide a brief overview of the advances of the diagnostic tools for IPMNs, IOPNs, and ITPNs, emphasizing the 5th edition of WHO classification for pathological diagnosis, molecular markers, new laboratory tests, and imaging tools.

IMAGING TOOLS

Cross-sectional and ultrasonographic imaging modalities used to diagnose and assess IPMNs have their own merits and limitations. Generally, imaging studies have two primary goals in the evaluation of IPMNs. Firstly, imaging studies aim to distinguish IPMN from other types of pancreatic cysts. Secondly, radiologic investigations aim to recognize the involvement of the main pancreatic duct to assess the risk of IPMN progressing to high-grade dysplasia or invasive carcinoma. Another marker used for the risk assessment of IPMN is the presence of mural nodules within the pancreatic cyst or adjacent to it. Preoperative radiological investigations are critical for identifying the malignancy risk in IPMNs. In 2012, the Fukuoka guidelines recommended considering the "high-risk stigmata" and "worrisome features" as criteria for the immediate surgical resection of IPMN (Tanako et al., 2012). Radiological and clinical findings in patients with IPMNs with high-risk stigmata include dilated main pancreatic duct ($\geq$10 mm), obstructive jaundice, and enhanced solid component. The worrisome features on endoscopic ultrasound (EUS) examinations include large cyst ($\geq$3 cm), thickened and enhanced cyst walls, abrupt dilatation of main pancreatic duct (5–9 mm), distal pancreatic atrophy, non-enhancing mural nodules, and lymphadenopathy (Hecht et al., 2021).

Magnetic resonance with cholangiopancreatography (MRCP) and multidetector computed tomography (MDCT) are reliable and effective imaging modalities for assessing pancreatic cyst size, morphology, and communication within the main pancreatic duct. Both MRCP and MDCT are estimated to distinguish between mucinous and non-mucinous cysts with 71–85% accuracy. MDCT, particularly dual-phase pancreatic protocol CT and gadolinium-enhanced MRI, is effective for the initial assessment of suspected IPMN. Both modalities have a 75–86% accuracy in identifying lesions with high-grade dysplasia and invasive carcinoma (Kitano et al., 2011; Morales-Oyarvide et al., 2017).

Magnetic resonance with cholangiopancreatography is believed to be more accurate than computed tomography (CT) for evaluating pancreatic cysts. It allows superior visualization of the anatomy of the ductal system and enables the detection of internal septations and mural nodules. MRCP has a 91–100% sensitivity and a specificity of 89% for assigning communication with the main pancreatic duct (Sainani et al., 2009). A CT scan is indicated in patients suspected of metastatic disease and patients who may have a postoperative recurrence of PDAC. A CT scan can assist in detecting calcifications and help assess vascular involvement.

Endoscopic ultrasound is highly accurate in evaluating the pancreatic parenchyma and the cystic component. It is an effective modality for detecting mural nodules. For the evaluation of mural nodules, contrast harmonic enhanced EUS is superior to standard EUS as it has a specificity of 80% and a sensitivity of 100% (Alvarez-Sánchez and Napoléon, 2014). Contrast-enhanced harmonic EUS allows detection of blood flow in the suspected mural nodule and can help distinguish true mural nodules from mucin plugs with a sensitivity of 89–96% and a specificity of 64–88% (Kitano et al., 2011). Furthermore, EUS-guided fine-needle aspiration (FNA) allows cytological sampling of any solid component (Kitano et al., 2011). It can also be used for aspirating cyst

fluid for subsequent protein, metabolite, molecular, and cytologic evaluation.

Different endoscopic modalities can be used to characterize suspected IPMN. Patulous "fish mouth" papilla extruding mucus is a pathognomonic feature of IPMN involving the main pancreatic duct. This classic sign can be observed *via* upper endoscopy (Salvia et al., 2004). Endoscopic retrograde cholangiopancreatography with or without pancreatoscopy can help obtain pancreatic juice and brushings for cytology. It can also assist in the visualization of villous or papillary growths along the ducts.

UPDATES IN THE 5TH EDITION OF WHO CLASSIFICATION FOR PATHOLOGICAL DIAGNOSIS OF PANCREATIC INTRADUCTAL NEOPLASMS

As mentioned earlier, because of the integrated understanding of pathological and genetic features of the pancreatic intraductal neoplasms, in the revised WHO classification scheme, IOPN and ITPN are now considered distinct neoplasms and not variants of IPMN. Also, the most recent WHO guidelines have simplified the dysplasia grading system. The dysplasia grading system has been simplified from a three- to now two-tiered grading system for these neoplasms: low-grade and high-grade dysplasia. The previously designated "intermediate-grade dysplasia" is now included in low-grade dysplasia. Low-grade neoplasms have mild to moderate atypia, well-oriented nuclei without pseudostratification, simple papillae, and rare mitoses. In contrast, high-grade neoplasms have marked atypia, complex architecture with nuclear stratification, loss of nuclear polarity, and mitoses that are brisk (WHO Classification of Tumours Editorial Board, 2019). If a neoplasm contains both low-grade and high-grade dysplasia, the highest grade is assigned to the neoplasm. The presence of high-grade dysplasia has significant clinical implications. High-grade neoplasms are at a higher risk of having an associated invasive carcinoma, and the presence of high-grade dysplasia in a surgically resected specimen is a significant risk factor for recurrence in the remnant pancreas. These updates are summarized in **Table 1**.

TABLE 1 | Summary of 5th edition of WHO updates compared to the previous edition (4th edition).

WHO 4th Edition	WHO 4th Edition
Oncocytic variant of IPMN	IOPN is now considered a separate entity
ITPN was considered a variant of IPMN	ITPN is now considered a separate entity
Three-tiered dysplasia grading system	Two-tiered dysplasia grading system
• Low-grade • Intermediate • High-grade	• Low-grade (original intermediate grade is part of the spectrum of low-grade dysplasia) • High-grade

GROSS FEATURES

Intraductal papillary mucinous neoplasms are grossly visible (>5 mm) intraductal epithelial neoplasms with excessive mucin production. MD-IPMNs are typically found in the pancreatic head but can also involve the entire main pancreatic duct. BD-IPMNs mainly occur in the uncinate process as peripheral multicystic lesions in an otherwise unremarkable pancreatic parenchyma. It has been shown by various studies that MD-IPMNs are significantly more likely to harbor high-grade dysplasia or have an associated invasive carcinoma than the BD-IPMNs (Rodriguez et al., 2007; Hirono et al., 2017; Attiyeh et al., 2018). This finding has important clinical implications as MD-IPMNs and BD-IPMNs can often be distinguished by imaging modalities, which provide a preoperative risk assessment for patients who will benefit from surgical resection. Therefore, because of the higher likelihood of high-grade dysplasia or an associated invasive carcinoma, most MD-IPMNs are treated with surgical resection, while most asymptomatic BD-IPMNs can be followed without surgical intervention. Mural nodules can also be found in some IPMNs. Compared to the flatter areas of an IPMN, mural nodules are more likely to have epithelium with high-grade dysplasia (Adsay et al., 2016). In addition, IPMNs more than 30 mm are more likely to have high-grade dysplasia and associated invasive carcinoma (WHO Classification of Tumours Editorial Board, 2019). These features are clinically significant as they can also provide preoperative risk assessments for those patients who will likely benefit from surgical resection. It is estimated that 20–40% of IPMNs are grossly multifocal. (Matthaei et al., 2012) The multifocality of IPMNs can help differentiate them from mucinous cystic neoplasms, which are often unifocal.

Intraductal oncocytic papillary neoplasms are often large (average size of 5.5 cm) intraductal solid nodules or papillary projections with pancreatic duct dilatation but less intraductal mucin accumulation (WHO Classification of Tumours Editorial Board, 2019).

Intraductal tubulopapillary neoplasms are often solid, not cystic, rubbery, or fleshy, nodular lesions in the dilated pancreatic ducts with an average size of 4.5 cm. They typically lack mucin secretion (WHO Classification of Tumours Editorial Board, 2019).

HISTOPATHOLOGY

Histologically, the neoplastic epithelium of IPMNs can have various directions of differentiation. The most seen differentiations include gastric-foveolar, intestinal, and pancreatobiliary (**Figure 1**). However, IPMNs can display a combination of different differentiation. Gastric-foveolar differentiation is the most common type and usually occurs in BD-IPMNs. The neoplastic epithelium usually forms broader and thicker papillae and is composed of columnar epithelium with basally placed nuclei and overlying mucin caps resembling gastric-foveolar epithelium (**Figure 1A**). The epithelium could be flat and typically has only low-grade dysplasia (Ban et al., 2006).

Intraductal papillary mucinous neoplasm with intestinal differentiation is the second most common type in which the

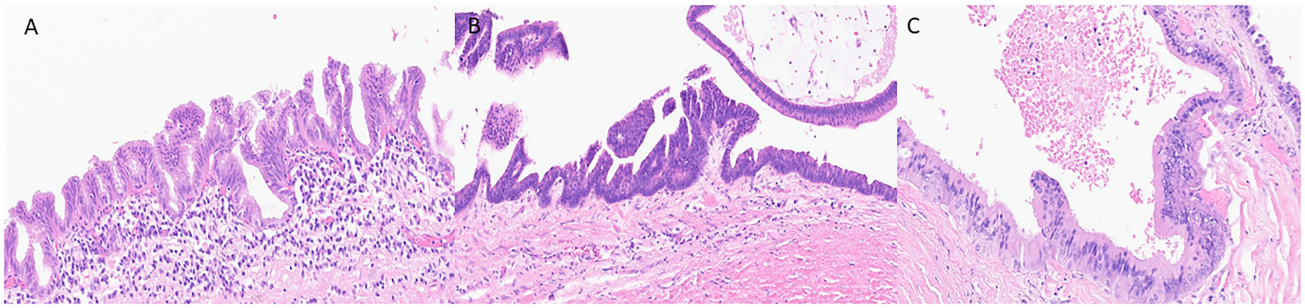

FIGURE 1 | Representative histological pictures of intraductal papillary mucinous neoplasm (IPMN). **(A)** IPMN with gastric-foveolar differentiation. The epithelium is flattened with basally placed nuclei and abundant mucin cap resembling gastric-foveolar epithelium. **(B)** An IPMN with intestinal differentiation forming villous papillae resembling villous adenoma of the colon. The cells have basophilic cytoplasm with enlarged oval and hyperchromatic nuclei and scattered goblet cells. **(C)** IPMN with pancreatobiliary differentiation. The neoplastic cells are cuboidal, have enlarged nuclei with amphophilic cytoplasm. **(A–C)** Original magnification 200×.

neoplastic epithelium forms long finger-like (villous) papillae (**Figure 1B**). The neoplastic cells show tall-columnar cells with elongated hyperchromatic nuclei. Pseudostratification with high-grade dysplasia is often seen. All colloid carcinomas of the pancreas arise from an intestinal-type IPMN (Adsay et al., 2004; Furukawa et al., 2005).

The neoplastic epithelium forms complex, thin, and branching papillae in IPMNs with pancreatobiliary differentiation, the least common form. The cytoplasm in these cells is amphophilic, and they have enlarged nuclei and often prominent nucleoli (**Figure 1C**). The neoplastic cells in IPMNs with pancreatobiliary differentiation are more cuboidal (less columnar) than those seen in other IPMN differentiation types. These often have high-grade dysplasia (Adsay et al., 2002; Furukawa et al., 2005).

As delineated earlier, a two-tiered grading system (low- vs. high grade) is now used to assign the degree of dysplasia to these neoplasms. Studies have shown that the grade of dysplasia has more clinical importance than the direction of epithelial differentiation. High-grade neoplasms are more likely to have an associated invasive carcinoma. The presence of high-grade dysplasia in surgically resected neoplasm is associated with a higher risk of progression in the remnant pancreas following surgery (Rezaee et al., 2016; Amini et al., 2020).

In IOPNs, the neoplastic epithelium forms complex, thick papillae with intraepithelial and intracellular lumina (**Figure 2**). The neoplastic cells contain abundant eosinophilic cytoplasm, and the nuclei are round with prominent nucleoli. IOPNs almost always have high-grade dysplasia and are associated with invasive carcinoma in about 30% of the cases (WHO Classification of Tumours Editorial Board, 2019). Rarely, the invasive component may show abundant mucin accumulation (Wang et al., 2019). IOPNs with a predominantly solid pattern can resemble acinar cell carcinoma or pancreatic neuroendocrine neoplasms. Immunohistochemistry for BCL-10, trypsin, and neuroendocrine markers is essential in this differential diagnosis.

Histologically, ITPNs are composed of tightly packed glands and tubules, forming large intraductal nodules with smooth contours (**Figure 3**). The neoplastic cells are cuboidal, with a moderate amount of amphophilic to eosinophilic cytoplasm, and they typically do not contain intracellular mucin. Invasive carcinoma is seen in 70% of the cases but is usually limited in extent. It is often difficult to determine the presence of an invasive carcinoma as many of the neoplastic nodules lack a peripheral rim of non-neoplastic epithelium. It is often helpful to look for invasion in areas away from the periphery of the nodules and search for individual cells and angulated small glands that are embedded in a desmoplastic stroma (Yamaguchi et al., 2009; Basturk et al., 2017). The differential diagnosis of ITPN includes acinar cell carcinoma, which may have an intraductal growth pattern. Unlike ITPNs, acinar cell carcinomas have apical acidophilic granules and intraluminal secretions. Immunohistochemistry for BCL-10 and trypsin can help in this differential.

The differential diagnosis of IPMNs includes mucinous cystic neoplasms (MCNs), other intraductal neoplasms, simple mucinous cysts, and retention cysts (**Figure 4** and **Table 2**).

Retention cysts are caused by dilatation of the pancreatic ducts due to a downstream obstructive process. They are often unilocular and lined by a flattened epithelium and lack the florid papillary projections of IPMNs (**Figure 4**). If no obstructive process is present, mucinous cysts larger than 1 cm and do not have characteristic histologic features of IPMN can be classified as simple mucinous cysts (Krasinskas et al., 2017). MCNs typically occur in women, almost always located in the tail or body, and do not communicate with the duct system. They contain ovarian-type stroma that can be demonstrated by immunohistochemistry staining of PR and ER (Wilentz et al., 2000; **Figure 4**).

IMMUNOHISTOCHEMICAL MARKERS

While immunolabeling can be used in identifying the various types of differentiation in IPMNs, this distinction is not as clinically significant as the degree of dysplasia. Most IPMNs are labeled with ductal markers, including pancytokeratin (AE1/AE3), cytokeratins-7, 8, 19, and CEA. All types of IPMN express MUC5AC. IPMNs with intestinal differentiation are labeled with antibodies to cytokeratin 20 and CDX2. IPMNs with pancreaticobiliary differentiation mark with MUC1 and IPMNs with gastric-foveolar differentiation show variable

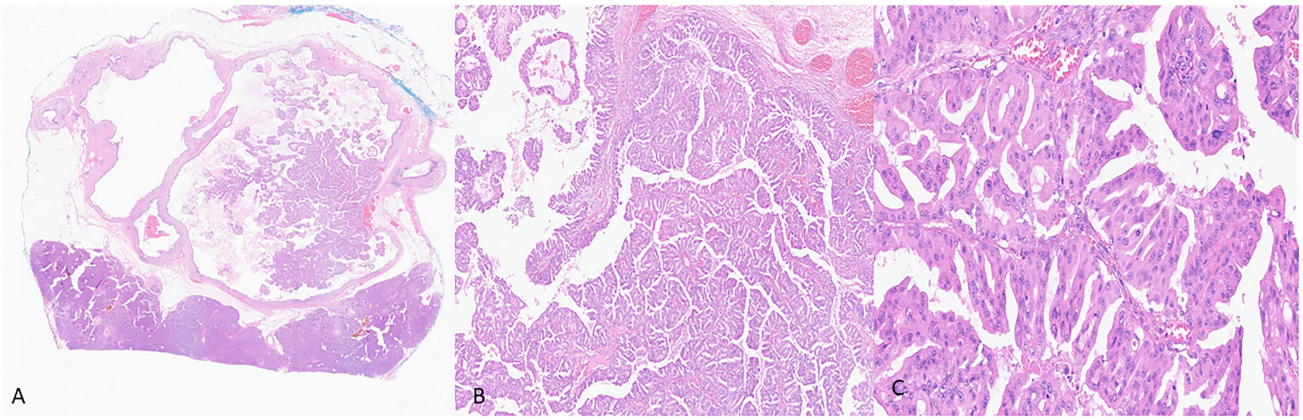

FIGURE 2 | Representative histological pictures of intraductal oncocytic papillary neoplasm (IOPN). **(A)** Low magnification shows intraductal papillary proliferation. **(B)** Intermediate magnification shows the thick, complex papillae. **(C)** Higher magnification shows that the neoplastic cells have abundant and distinctly oncocytic (eosinophilic) cytoplasm. The nuclei are round and often contain prominent nucleoli. **(A)** Original magnification 10×. **(B)** Original magnification 100×. **(C)** Original magnification 200×.

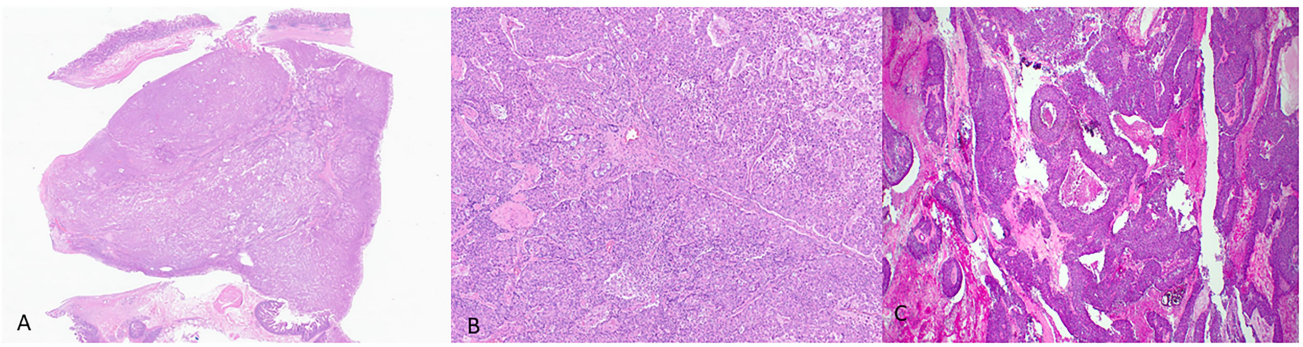

FIGURE 3 | Representative histological pictures of intraductal tubulopapillary neoplasm (ITPN). **(A)** Low magnification shows small, tightly packed glands forming intraductal nodules. **(B)** Higher magnification shows the cuboidal neoplastic cells with no significant mucin. **(C)** Another case of ITPN showing foci of comedo-type necrosis resembling intraductal carcinoma of the breast. **(A)** Original magnification 10×. **(B)** Original magnification 200×. **(C)** Original magnification 100×.

expression with MUC6. For IOPNs, the immunohistochemical markers expressed include EMA (MUC1), MUC6, hepatocyte-1 (Hep Par-1), and CD117 (Mattiolo et al., 2020). MUC2 and MUC5AC expression are limited to goblet cells. ITPNs are most commonly labeled with MUC1 and MUC6, while consistently negative for MUC5AC (WHO Classification of Tumours Editorial Board, 2019). The various immunophenotypes of these neoplasms are summarized in **Table 3**.

GENETIC ALTERATIONS

The new advances in molecular studies have revolutionized our understanding of human neoplasms, including IPMNs. Various genes have been identified as the driver genes following exome sequencing of IPMNs. Somatic activating mutations in the *KRAS* and *GNAS* genes are the most common alterations (Wu et al., 2011). Other less common alterations include *KLF4, PIK3CA, p16/CDKN2A, RNF43, SMAD4, TGFBR2, TP53,* and rarely *BRAF* mutations (Schonleben et al., 2006; Fujikura et al., 2021) Gene fusions such as *ATP1B1-PRKA*CB and *DNAJB1-PRKACA* are restricted to IOPNs (Singhi et al., 2020; Vyas et al., 2020). Germline genetic alterations have also been reported in patients with IPMNs. In a study by N. Roberts and colleagues, 23 (7.3%) of the 315 patients who had surgically resected IPMNs showed deleterious variants in *ATM, PTCH1,* and *SFU* genes (Skaro et al., 2019). Biallelic inactivation of the *STK11* gene has been reported in IPMNs in patients with Peutz-Jeghers syndrome (Sato et al., 2001). Identifying these genetic alterations can be a valuable tool in studying these lesions, and potentially, they can have diagnostic implications and increase diagnostic accuracy. For example, while studying IPMNs, Wood et al. showed that the different foci of IPMN in the same pancreas harbor different somatic alterations, which confirms the multifocality of IPMNs (Pea et al., 2017; Fischer et al., 2019).

Distinct patterns of methylation have been reported in IPMNs. Methylations of *BNIP3, CDO1, EBF3, NXPH1, PTCHD2, and SOX17* are most reported in high-grade IPMNs than low-grade IPMNs (Hong et al., 2012; Fujiyama et al., 2020). Methylation profiling is now practiced for brain tumor

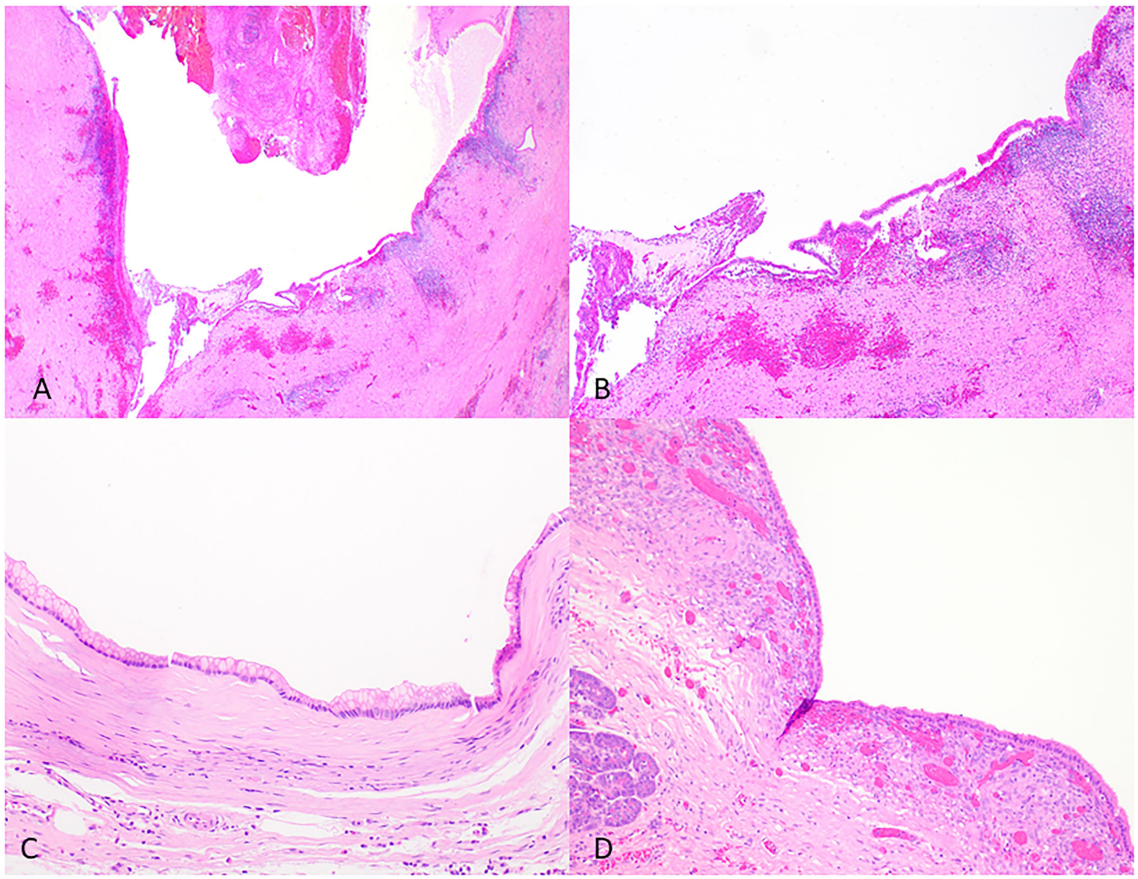

FIGURE 4 | Representative histological pictures of retention cyst, simple mucinous cyst, and mucinous cystic neoplasm. **(A)** Retention cyst. Low magnification shows a dilated pancreatic duct. **(B)** Higher magnification shows a flattened epithelium with no papillary projections. Note the background pancreas with extensive atrophy and fibrosis. No ovarian-type stroma is seen. **(C)** Simple mucinous cyst. The cyst is lined by a benign mucinous epithelium and lacks an ovarian stroma. **(D)** Mucinous cystic neoplasm. The cyst is lined by mucinous epithelium and unlike simple mucinous cyst or a retention cyst is associated with an ovarian-type stroma. **(A)** Original magnification 10×; **(B)** Original magnification 100×; and **(C,D)** Original magnification 200×.

classification and is emerging for pancreatic neuroendocrine neoplasms and has the potential to be used in EUS-FNA cyst fluid as an adjunct tool in further classifying the cyst type.

MicroRNAs are currently recognized as biomarkers and molecular targets of various diseases, including malignancies. RNA markers can also be used as a diagnostic tool in the EUS-FNA obtained cyst fluid. Approximately 80% of IPMNs show high expression for microRNAs—miR-155 and miR-21. The expression of these microRNAs is particularly noticeable in advanced IPMNs and has been investigated as a potential diagnostic approach in pancreatic cyst fluid as a marker for evaluating the malignant transformation of IPMNs (Shirakami et al., 2021).

The use of microRNAs in different types of body fluids such as urine, serum, or saliva has also been studied as biomarkers for the early detection of pancreatic cancer (Ishige et al., 2020). For example, urine miR-30e, miR-143, miR-223, and miR-204 levels and serum miR-21 and miR-34a have been proven useful as potential minimally invasive biomarkers for the diagnosis of PDAC (Debernardi et al., 2015; Alemar et al., 2016). The combination of urine miR-143 with miR-30e achieved a sensitivity of 83.3% and a specificity of 96.2% for diagnosing pancreatic cancer in one study (Debernardi et al., 2015). The sensitivity and specificity of miR-21 were 82.6 and 77.8%, and those of miR-34a were 91.3 and 77.8% for discriminating PDAC from control samples, respectively (Alemar et al., 2016). Combining both serum and urine miR-1246 levels yielded a sensitivity of 85% for the diagnosis of pancreatic cancer (Ishige et al., 2020). The expression of hsa-miR-21, hsa-miR-23a, hsa-miR-23b, and miR-29c is significantly upregulated in the saliva of pancreatic cancer patients compared to control, showing sensitivities of 71.4, 85.7, 85.7, and 57%, respectively, and 100% specificity (Humeau et al., 2015). Salivary miR-3679-5p and miR-940 also show good discriminatory power to detect respectable pancreatic cancer when compared to healthy controls, with reasonable specificity (45 and 40%) and sensitivity (82.5 and 90%; Xie et al., 2015).

CYST FLUID ANALYSIS AND CYTOPATHOLOGY

Cyst fluid can be characterized by protein analysis, metabolite analysis, cytological analysis, and molecular analysis. Cyst fluid

TABLE 2 | Differential diagnosis of IPMN.

	Intraductal papillary mucinous neoplasm	Mucinous cystic neoplasm	Retention cyst	Simple mucinous cyst
Demographics	More common in elderly men (7th–8th decade of life)	More common in women (5th decade)	F = M Any age	F = M Any age
Location	Often head of the pancreas (>80%)	Tail or body (>90%)	Anywhere in the pancreas	Anywhere in the pancreas
Imaging	Dilated main pancreatic duct or multilocular cyst Mural nodules may correspond to invasive carcinoma or high-grade dysplasia	Multilocular or unilocular thick-walled cyst No connection with the main pancreatic duct	Unilocular cyst	Unilocular cyst
Histology	Papillary projections With low-grade or high-grade dysplasia	No connection with the main duct Contain ovarian-type stroma (ER+, PR+)	Downstream obstruction Lined by flattened epithelium, and lack papillary projections	No obstructive process No papillary projections No ovarian-type stroma
Molecular	*KRAS* *GNAS* *TP53/PIK3CA/PTEN* *RNF43* *BRAF* *KLF4* *P16/CDKN2A* *SMAD4* *TGFBR2*	*KRAS* *SMAD4* *TP53*	No specific mutations	*KRAS* *KMT2C* *BRAF* *RNF43* *CDKN2A* *SMAD4* *TP53*
Cyst fluid analysis	Elevated CEA levels (of >200 ng/ml) High amylase level	Elevated CEA Low amylase	Variable CEA or amylase	Variable CEA or amylase

protein analysis includes CEA, mAB-Das 1, and amylase (Cizginer et al., 2011; Jhala et al., 2020; Das et al., 2021). Carcinoembryonic antigen (CEA) is the most studied protein marker in pancreatic cyst fluid (Cizginer et al., 2011). Although CEA cannot effectively distinguish between benign cysts and those with high-grade dysplasia or invasive carcinoma, it can effectively differentiate between mucinous and non-mucinous lesions. A cyst fluid CEA threshold value of 192 ng/ml is the most widely used cut-off value. A value of >200 ng/ml strongly supports a neoplastic mucin-producing cyst. However, it does not help differentiate IPMN from MCN or low-grade from high-grade IPMN. mAB-Das 1 is a monoclonal antibody that reacts specifically with intestinal metaplasia of the lower esophagus and normal colonic epithelium. This antibody has been found to detect high-risk IPMN with a sensitivity of 89% and specificity of 100% (Das et al., 2021). High amylase levels in cyst fluid can confirm communication with the main pancreatic duct and suggest either a pseudocyst or IPMN. CA 19.9 can be a useful biomarker for distinguishing mucinous and non-mucinous lesions when CEA values are indeterminate. The cytopathologic evaluation confirms the diagnosis and can provide the degree of dysplasia. IPMNs often show thick inspissated mucin and papillary projections, which are highly characteristic when evident. The sensitivity of the cytological analysis can be hampered because of the scant cellularity, the heterogeneity of the lesion, insufficient aspirated volume, and contamination of the fluid with gastric and duodenal mucosal cells.

Molecular analysis on EUS-FNA obtained cyst fluid is increasingly employed and can enhance the diagnostic accuracy when used in combination with protein markers such as VEGFA and CEA (Cizginer et al., 2011; Carr et al., 2017). Mutations in *KRAS* and *GNAS* are the two common gene alterations seen in IPMN (Schmitz et al., 2021). *KRAS* mutations are highly specific to mucinous lesions and are found in the cyst fluid of more than 50% of IPMN cases (Nikiforova et al., 2013; Singhi et al., 2018). Singhi et al. (2018) found that the presence of *TP53/PIK3CA/PTEN* mutations was indicative of high-grade dysplasia. Therefore, sequencing the cyst fluids can be a highly sensitive and specific tool for diagnosing the cyst type. *GNAS* gene alterations are believed to be specific to IPMNs and are observed in the fluid of approximately two-thirds of cases (Wu et al., 2011; Kadayifci et al., 2017). However, gene mutations do not indicate the risk of high-grade dysplasia or invasive carcinoma. While these molecular advances are promising when combined with clinical features, they suffer from imperfection due to the underlying heterogeneity of IPMNs.

Recently, we have reported that specific metabolites in the cyst fluid can also be used as potential diagnostic biomarkers to distinguish malignant from benign pancreatic cysts and mucinous from non-mucinous cysts (Shi et al., 2021). We found that (Iso)-butyrylcarnitine alone has a diagnostic accuracy of 89% to separate malignant from benign pancreatic cysts, and 5-oxoproline alone has a diagnostic accuracy of 90% to differentiate mucinous from non-mucinous cysts (compared

TABLE 3 | Immunohistochemical profile of IPMNs, IOPNs, and ITPNs.

IPMN	Cytokeratins	CK20	MUC1	MUC2	MUC5AC	MUC6	CDX2
Gastric	+	–	–	–	+	+/–	–
Intestinal	+	+	–	+	+	–	+
Pancreatobiliary	+	–	+	–	+	+	–
IOPN	+	+ in GCs	+	+ in GCs	+	+	+ in GCs
ITPN	+	–	+	–	–	+	–

GC, goblet cells.

to previously reported glucose which has an accuracy of 82% in our study; Park et al., 2013).

CLINICAL RELEVANCE

Advances in our understanding of the pathology and molecular features of IPMNs, IOPNs, and ITPNs have significant clinical implications. Importantly, IPMNs are heterogeneous neoplasms and can be multifocal. It is not practically possible to sample all the foci. Hence, the preoperative cyst fluid analysis and cytologic evaluation, while accurate for the sampled focus, are inherently imperfect, particularly regarding the degree of dysplasia. As a manifestation of IPMN multifocality, there is a risk of synchronous or metachronous disease in the remaining portion of a patient's pancreas in those who have undergone surgery. The risk is higher in MD-IPMNs and those with high-grade dysplasia. Therefore, careful clinical follow-up is necessary to rule out synchronous or metachronous disease in the remnant pancreas (He et al., 2013). If not initially performed, it would also be important to submit the entire lesion for histologic evaluation to exclude the presence of invasive carcinoma.

Another issue of clinical concern is whether IPMN at the resection margin is associated with the risk of progression or recurrence. However, the studies are controversial. While some data have shown that the presence of high-grade dysplastic focus of >0.5 cm at the resection margin is associated with relapse, other data have shown that the dysplastic foci at the resection margin may represent separate PanINs unrelated to the IPMN (Pflüger et al., 2020).

Understanding the genetics of precursor lesions will potentially provide helpful guidance in targeting the tumors at an earlier stage and enabling new and more effective therapeutic approaches. These could prevent malignant transformation or perhaps treat cancers arising from IPMNs. Discovering the *KRAS* mutation as a driver in most IPMNs has identified potential targeted therapies with novel inhibitors and antibodies that target mutant *KRAS* (Arbour et al., 2021; Douglass et al., 2021). Additionally, the therapies that inhibit the *Wnt* pathway may have potential in tumors with the loss of function mutation in *RNF43* (Yu et al., 2020).

CONCLUSION AND PERSPECTIVES

Despite the improved understanding of the pathophysiology underlying IPMNs, IOPNs, and ITPNs over the recent years, there are still many patients with lesions that mimic IPMNs—named by some authors "pseudo-IPMNs" (Muraki et al., 2022)—who undergo unnecessary surgeries and are overtreated. New approaches to predict the risk of progression preoperatively more accurately and risk of recurrence following surgery are needed. The 5th edition of the WHO classification scheme of IPMNs with the introduction of IOPNs and ITPNs as separate entities has created new opportunities for more nuanced future studies and more targeted strategies in the clinical management of these patients.

AUTHOR CONTRIBUTIONS

NA and SB contributed to original draft preparation of the manuscript. JS contributed to the review design, writing, and editing. All authors reviewed and approved the final version of the manuscript.

FUNDING

JS is supported in part by the National Cancer Institute of the National Institutes of Health under award number K08CA234222.

REFERENCES

Adsay, N. V., Merati, K., Andea, A., Sarkar, F., Hruban, R. H., Wilentz, R. E., et al. (2002). The dichotomy in the preinvasive neoplasia to invasive carcinoma sequence in the pancreas: differential expression of MUC1 and MUC2 supports the existence of two separate pathways of carcinogenesis. *Mod. Pathol.* 15, 1087–1095. doi: 10.1097/01.MP.0000028647.98725.8B

Adsay, N. V., Merati, K., Basturk, O., Iacobuzio-Donahue, C., Levi, E., Cheng, J. D., et al. (2004). Pathologically and biologically distinct types of epithelium in intraductal papillary mucinous neoplasms: delineation of an "intestinal" pathway of carcinogenesis in the pancreas. *Am. J. Surg. Pathol.* 28, 839–848. doi: 10.1097/00000478-200407000-00001

Adsay, V., Mino-Kenudson, M., Furukawa, T., Basturk, O., Zamboni, G., Marchegiani, G., et al. (2016). Pathologic evaluation and reporting of intraductal papillary mucinous neoplasms of the pancreas and other tumoral intraepithelial neoplasms of pancreatobiliary tract: recommendations of Verona Consensus Meeting. *Ann. Surg.* 263, 162–177. doi: 10.1097/SLA.0000000000001173

Alemar, B., Izetti, P., Gregório, C., Macedo, G. S., Castro, M. A., Osvaldt, A. B., et al. (2016). miRNA-21 and miRNA-34a are potential minimally invasive

biomarkers for the diagnosis of pancreatic ductal adenocarcinoma. *Pancreas* 45, 84–92. doi: 10.1097/MPA.0000000000000383

Alvarez-Sánchez, M.-V., and Napoléon, B. (2014). Contrast-enhanced harmonic endoscopic ultrasound imaging: basic principles, present situation and future perspectives. *World J. Gastroenterol.* 20, 15549–15563. doi: 10.3748/wjg.v20.i42.15549

Amini, N., Habib, J. R., Blair, A., Rezaee, N., Kinny-Koster, B., Cameron, J. L., et al. (2020). Invasive and non-invasive progression after resection of non-invasive intraductal papillary mucinous neoplasms. *Ann. Surg.* doi: 10.1097/SLA.0000000000004488 [Epub ahead of print]

Arbour, K. C., Rizvi, H., Plodkowski, A. J., Hellmann, M. D., Knezevic, A., Heller, G., et al. (2021). Treatment outcomes and clinical characteristics of patients with KRAS-G12C-mutant non-small cell lung cancer. *Clin. Cancer Res.* 27, 2209–2215. doi: 10.1158/1078-0432.CCR-20-4023

Attiyeh, M. A., Fernandez-Del Castillo, C., Al Efishat, M., Eaton, A. A., Gonen, M., Batts, R., et al. (2018). Development and validation of a multi-institutional preoperative nomogram for predicting grade of dysplasia in intraductal papillary mucinous neoplasms (IPMNs) of the pancreas: a report from the Pancreatic Surgery Consortium. *Ann. Surg.* 267, 157–163. doi: 10.1097/SLA.0000000000002015

Ban, S., Naitoh, Y., Mino-Kenudson, M., Sakurai, T., Kuroda, M., Koyama, I., et al. (2006). Intraductal papillary mucinous neoplasm (IPMN) of the pancreas: its histopathologic difference between 2 major types. *Am. J. Surg. Pathol.* 30, 1561–1569. doi: 10.1097/01.pas.0000213305.98187.d4

Basturk, O., Adsay, V., Askan, G., Dhall, D., Zamboni, G., Shimizu, M., et al. (2017). Intraductal tubulopapillary neoplasm of the pancreas: a clinicopathologic and immunohistochemical analysis of 33 cases. *Am. J. Surg. Pathol.* 41, 313–325. doi: 10.1097/PAS.0000000000000782

Basturk, O., Chung, S. M., Hruban, R. H., Adsay, N. V., Askan, G., Iacobuzio-Donahue, C., et al. (2016). Distinct pathways of pathogenesis of intraductal oncocytic papillary neoplasms and intraductal papillary mucinous neoplasms of the pancreas. *Virchows Arch.* 469, 523–532. doi: 10.1007/s00428-016-2014-x

Carr, R., Yip-Schneider, M., Dolejs, S., Hancock, B., Wu, H., Radovich, M., et al. (2017). Pancreatic cyst fluid vascular endothelial growth factor A and carcinoembryonic antigen: a highly accurate test for the diagnosis of serous cystic neoplasm. *J. Am. Coll. Surg.* 225, 93–100. doi: 10.1016/j.jamcollsurg.2017.05.003

Cizginer, S., Turner, B. G., Bilge, A. R., Karaca, C., Pitman, M. B., and Brugge, W. R. (2011). Cyst fluid carcinoembryonic antigen is an accurate diagnostic marker of pancreatic mucinous cysts. *Pancreas* 40, 1024–1028. doi: 10.1097/MPA.0b013e31821bd62f

Compagno, J., and Oertel, J. E. (1978a). Microcystic adenomas of the pancreas (glycogen-rich cystadenomas): a clinicopathologic study of 34 cases. *Am. J. Clin. Pathol.* 69, 289–298. doi: 10.1093/ajcp/69.1.289

Compagno, J., and Oertel, J. E. (1978b). Mucinous cystic neoplasms of the pancreas with overt and latent malignancy (cystadenocarcinoma and cystadenoma). A clinicopathologic study of 41 cases. *Am. J. Clin. Pathol.* 69, 573–580. doi: 10.1093/ajcp/69.6.573

Das, K. K., Brown, J. W., Fernandez Del-Castillo, C., Huynh, T., Mills, J. C., Matsuda, Y., et al. (2021). mAb Das-1 identifies pancreatic ductal adenocarcinoma and high-grade pancreatic intraepithelial neoplasia with high accuracy. *Hum. Pathol.* 111, 36–44. doi: 10.1016/j.humpath.2021.01.003

Debernardi, S., Massat, N. J., Radon, T. P., Sangaralingam, A., Banissi, A., Ennis, D. P., et al. (2015). Noninvasive urinary miRNA biomarkers for early detection of pancreatic adenocarcinoma. *Am. J. Cancer Res.* 5, 3455–3466.

Douglass, J., Hsiue, E., Mog, B., Hwang, M., DiNapoli, S., Pearlman, A., et al. (2021). Bispecific antibodies targeting mutant RAS neoantigens. *Sci. Immunol.* 6. doi: 10.1126/sciimmunol.abd5515

Fischer, C. G., Beleva Guthrie, V., Braxton, A. M., Zheng, L., Wang, P., Song, Q., et al. (2019). Intraductal papillary mucinous neoplasms arise from multiple independent clones, each with distinct mutations. *Gastroenterology* 157, 1123.e22–1137.e22. doi: 10.1053/j.gastro.2019.06.001

Fujikura, K., Hosoda, W., Felsenstein, M., Song, Q., Reiter, J. G., Zheng, L., et al. (2021). Multiregion whole-exome sequencing of intraductal papillary mucinous neoplasms reveals frequent somatic KLF4 mutations predominantly in low-grade regions. *Gut* 70, 928–939. doi: 10.1136/gutjnl-2020-321217

Fujiyama, Y., Kumamoto, Y., Nishizawa, N., Nakamoto, S., Harada, H., Yokota, K., et al. (2020). Promoter DNA hypermethylation of the cysteine dioxygenase 1 (CDO1) gene in intraductal papillary mucinous neoplasm (IPMN). *Ann. Surg. Oncol.* 27, 4007–4016. doi: 10.1245/s10434-020-08291-2

Furukawa, T., Kloppel, G., Volkan Adsay, N., Albores-Saavedra, J., Fukushima, N., Horii, A., et al. (2005). Classification of types of intraductal papillary-mucinous neoplasm of the pancreas: a consensus study. *Virchows Arch.* 447, 794–799. doi: 10.1007/s00428-005-0039-7

He, J., Cameron, J. L., Ahuja, N., Makary, M. A., Hirose, K., Choti, M. A., et al. (2013). Is it necessary to follow patients after resection of a benign pancreatic intraductal papillary mucinous neoplasm? *J. Am. Coll. Surg.* 216, 657–665. doi: 10.1016/j.jamcollsurg.2012.12.026

Hecht, E. M., Khatri, G., Morgan, D., Kang, S., Bhosale, P. R., Francis, I. R., et al. (2021). Intraductal papillary mucinous neoplasm (IPMN) of the pancreas: recommendations for standardized imaging and reporting from the Society of Abdominal Radiology IPMN disease focused panel. *Abdom. Radiol.* 46, 1586–1606. doi: 10.1007/s00261-020-02853-4

Hirono, S., Kawai, M., Okada, K. I., Miyazawa, M., Shimizu, A., Kitahata, Y., et al. (2017). Factors associated with invasive intraductal papillary mucinous carcinoma of the pancreas. *JAMA Surg.* 152:e165054. doi: 10.1001/jamasurg.2016.5054

Hodgkinson, D. J., ReMine, W. H., and Weiland, L. H. (1978). A clinicopathologic study of 21 cases of pancreatic cystadenocarcinoma. *Ann. Surg.* 188, 679–684. doi: 10.1097/00000658-197811000-00017

Hong, S. M., Omura, N., Vincent, A., Li, A., Knight, S., Yu, J., et al. (2012). Genome-wide CpG island profiling of intraductal papillary mucinous neoplasms of the pancreas. *Clin. Cancer Res.* 18, 700–712. doi: 10.1158/1078-0432.CCR-11-1718

Humeau, M., Vignolle-Vidoni, A., Sicard, F., Martins, F., Bournet, B., Buscail, L., et al. (2015). Salivary microRNA in pancreatic cancer patients. *PLoS One* 10:e0130996. doi: 10.1371/journal.pone.0130996

Ishige, F., Hoshino, I., Iwatate, Y., Chiba, S., Arimitsu, H., Yanagibashi, H., et al. (2020). MIR1246 in body fluids as a biomarker for pancreatic cancer. *Sci. Rep.* 10:8723. doi: 10.1038/s41598-020-65695-6

Jhala, N., Srimunta, P., and Jhala, D. (2020). Role of ancillary testing on endoscopic US-guided fine needle aspiration samples from cystic pancreatic neoplasms. *Acta Cytol.* 64, 124–135. doi: 10.1159/000502372

Kadayifci, A., Atar, M., Wang, J. L., Forcione, D. G., Casey, B. W., Pitman, M. B., et al. (2017). Value of adding GNAS testing to pancreatic cyst fluid KRAS and carcinoembryonic antigen analysis for the diagnosis of intraductal papillary mucinous neoplasms. *Dig. Endosc.* 29, 111–117. doi: 10.1111/den.12710

Kitano, M., Sakamoto, H., Komaki, T., and Kudo, M. (2011). New techniques and future perspective of EUS for the differential diagnosis of pancreatic malignancies: contrast harmonic imaging. *Dig. Endosc.* 23, 46–50. doi: 10.1111/j.1443-1661.2011.01146.x

Krasinskas, A. M., Oakley, G. J., Bagci, P., Jang, K. T., Kuan, S. F., Reid, M. D., et al. (2017). "Simple mucinous cyst" of the pancreas: a clinicopathologic analysis of 39 examples of a diagnostically challenging entity distinct From intraductal papillary mucinous neoplasms and mucinous cystic neoplasms. *Am. J. Surg. Pathol.* 41, 121–127. doi: 10.1097/PAS.0000000000000750

Matthaei, H., Norris, A. L., Tsiatis, A. C., Olino, K., Hong, S. M., dal Molin, M., et al. (2012). Clinicopathological characteristics and molecular analyses of multifocal intraductal papillary mucinous neoplasms of the pancreas. *Ann. Surg.* 255, 326–333. doi: 10.1097/SLA.0b013e3182378a18

Mattiolo, P., Hong, S. M., Paolino, G., Rusev, B. C., Marchegiani, G., Salvia, R., et al. (2020). CD117 is a specific marker of Intraductal papillary mucinous neoplasms (IPMN) of the pancreas, oncocytic subtype. *Int. J. Mol. Sci.* 21. doi: 10.3390/ijms21165794

Morales-Oyarvide, V., Fong, Z. V., Fernandez-Del Castillo, C., and Warshaw, A. L. (2017). Intraductal papillary mucinous neoplasms of the pancreas: strategic considerations. *Visc. Med.* 33, 466–476. doi: 10.1159/000485014

Muraki, T., Jang, K. T., Reid, M. D., Pehlivanoglu, B., Memis, B., Basturk, O., et al. (2022). Pancreatic ductal adenocarcinomas associated with intraductal papillary mucinous neoplasms (IPMNs) versus pseudo-IPMNs: relative frequency, clinicopathologic characteristics and differential diagnosis. *Mod. Pathol.* 35, 96–105. doi: 10.1038/s41379-021-00902-x

Nikiforova, M. N., Khalid, A., Fasanella, K. E., McGrath, K. M., Brand, R. E., Chennat, J. S., et al. (2013). Integration of KRAS testing in the diagnosis

of pancreatic cystic lesions: a clinical experience of 618 pancreatic cysts. *Mod. Pathol.* 26, 1478–1487. doi: 10.1038/modpathol.2013.91

Ohhashi, K. M. F., Maruyama, M., Takekoshi, T., Ohta, H., Ohhashi, I., Takagi, K., et al. (1982). Four cases of mucous secreting pancreatic cancer. *Prog. Dig. Endosc.* 20, 348–351.

Park, W. G., Wu, M., Bowen, R., Zheng, M., Fitch, W. L., Pai, R. K., et al. (2013). Metabolomic-derived novel cyst fluid biomarkers for pancreatic cysts: glucose and kynurenine. *Gastrointest. Endosc.* 78, 295–302.e2. doi: 10.1016/j.gie.2013.02.037

Pea, A., Yu, J., Rezaee, N., Luchini, C., He, J., Dal Molin, M., et al. (2017). Targeted DNA sequencing reveals patterns of local progression in the pancreatic remnant following resection of intraductal papillary mucinous neoplasm (IPMN) of the pancreas. *Ann. Surg.* 266, 133–141. doi: 10.1097/SLA.0000000000001817

Pflüger, M., Griffin, J., Hackeng, W., Kawamoto, S., Yu, J., Chianchiano, P., et al. (2020). The impact of clinical and pathological features on intraductal papillary mucinous neoplasm recurrence after surgical resection: long-term follow-up analysis. *Ann. Surg.* doi: 10.1097/SLA.0000000000004427 [Epub ahead of print].

Rezaee, N., Barbon, C., Zaki, A., He, J., Salman, B., Hruban, R. H., et al. (2016). Intraductal papillary mucinous neoplasm (IPMN) with high-grade dysplasia is a risk factor for the subsequent development of pancreatic ductal adenocarcinoma. *HPB* 18, 236–246. doi: 10.1016/j.hpb.2015.10.010

Rodriguez, J. R., Salvia, R., Crippa, S., Warshaw, A. L., Bassi, C., Falconi, M., et al. (2007). Branch-duct intraductal papillary mucinous neoplasms: observations in 145 patients who underwent resection. *Gastroenterology* 133, 72–79. doi: 10.1053/j.gastro.2007.05.010

Sainani, N. I., Saokar, A., Deshpande, V., Fernandez-del Castillo, C., Hahn, P., and Sahani, D. V. (2009). Comparative performance of MDCT and MRI with MR cholangiopancreatography in characterizing small pancreatic cysts. *AJR Am. J. Roentgenol.* 193, 722–731. doi: 10.2214/AJR.08.1253

Salvia, R., Fernandez-del Castillo, C., Bassi, C., Thayer, S. P., Falconi, M., Mantovani, W., et al. (2004). Main-duct intraductal papillary mucinous neoplasms of the pancreas: clinical predictors of malignancy and long-term survival following resection. *Ann. Surg.* 239, 678–687. doi: 10.1097/01.sla.0000124386.54496.15

Sato, N., Rosty, C., Jansen, M., Fukushima, N., Ueki, T., Yeo, C. J., et al. (2001). STK11/LKB1 Peutz-Jeghers gene inactivation in intraductal papillary-mucinous neoplasms of the pancreas. *Am. J. Pathol.* 159, 2017–2022. doi: 10.1016/S0002-9440(10)63053-2

Schmitz, D., Kazdal, D., Allgauer, M., Trunk, M., Vornhusen, S., Nahm, A. M., et al. (2021). KRAS/GNAS-testing by highly sensitive deep targeted next generation sequencing improves the endoscopic ultrasound-guided workup of suspected mucinous neoplasms of the pancreas. *Genes Chromosom. Cancer* 60, 489–497. doi: 10.1002/gcc.22946

Schonleben, F., Qiu, W., Ciau, N. T., Ho, D. J., Li, X., Allendorf, J. D., et al. (2006). PIK3CA mutations in intraductal papillary mucinous neoplasm/carcinoma of the pancreas. *Clin. Cancer Res.* 12, 3851–3855. doi: 10.1158/1078-0432.CCR-06-0292

Shi, J., Yi, Z., Jin, L., Zhao, L., Raskind, A., Yeomans, L., et al. (2021). Cyst fluid metabolites distinguish malignant from benign pancreatic cysts. *Neoplasia* 23, 1078–1088. doi: 10.1016/j.neo.2021.09.004

Shimizu, Y., Yamaue, H., Maguchi, H., Yamao, K., Hirono, S., Osanai, M., et al. (2013). Predictors of malignancy in intraductal papillary mucinous neoplasm of the pancreas: analysis of 310 pancreatic resection patients at multiple high-volume centers. *Pancreas* 42, 883–888. doi: 10.1097/MPA.0b013e31827a7b84

Shirakami, Y., Iwashita, T., Uemura, S., Imai, H., Murase, K., and Shimizu, M. (2021). Micro-RNA analysis of pancreatic cyst fluid for diagnosing malignant transformation of Intraductal papillary mucinous neoplasm by comparing Intraductal papillary mucinous adenoma and carcinoma. *J. Clin. Med.* 10. doi: 10.3390/jcm10112249

Singhi, A. D., McGrath, K., Brand, R. E., Khalid, A., Zeh, H. J., Chennat, J. S., et al. (2018). Preoperative next-generation sequencing of pancreatic cyst fluid is highly accurate in cyst classification and detection of advanced neoplasia. *Gut* 67, 2131–2141. doi: 10.1136/gutjnl-2016-313586

Singhi, A. D., Wood, L. D., Parks, E., Torbenson, M. S., Felsenstein, M., Hruban, R. H., et al. (2020). Recurrent rearrangements in PRKACA and PRKACB in intraductal oncocytic papillary neoplasms of the pancreas and bile duct. *Gastroenterology* 158, 573.e2–582.e2. doi: 10.1053/j.gastro.2019.10.028

Skaro, M., Nanda, N., Gauthier, C., Felsenstein, M., Jiang, Z., Qiu, M., et al. (2019). Prevalence of germline mutations associated with cancer risk in patients with intraductal papillary mucinous neoplasms. *Gastroenterology* 156, 1905–1913. doi: 10.1053/j.gastro.2019.01.254

Tanaka, M. (2015). International consensus on the management of intraductal papillary mucinous neoplasm of the pancreas. *Ann. Transl. Med.* 3:8. doi: 10.3978/ j.issn.2305-5839.2015.11.09

Tanako, M., Fernández-del Castillo, C., Adsay, V., Chari, S., Falconi, M., Jang, J. Y., et al. (2012). International consensus guidelines 2012 for the management of IPMN and MCN of the pancreas. *Pancreatology* 12, 183–197. doi: 10.1016/j.pan.2012.04.004

Vyas, M., Hechtman, J. F., Zhang, Y., Benayed, R., Yavas, A., Askan, G., et al. (2020). DNAJB1-PRKACA fusions occur in oncocytic pancreatic and biliary neoplasms and are not specific for fibrolamellar hepatocellular carcinoma. *Mod. Pathol.* 33, 648–656. doi: 10.1038/s41379-019-0398-2

Wang, T., Askan, G., Adsay, V., Allen, P., Jarnagin, W. R., Memis, B., et al. (2019). Intraductal oncocytic papillary neoplasms: clinical-pathologic characterization of 24 cases, with an emphasis on associated invasive carcinomas. *Am. J. Surg. Pathol.* 43, 656–661. doi: 10.1097/PAS.0000000000001226

WHO Classification of Tumours Editorial Board (2019). *Digestive System Tumours. 5th Edn*. Lyon (France): International Agency for Research on Cancer.

Wilentz, R. E., Albores-Saavedra, J., and Hruban, R. H. (2000). Mucinous cystic neoplasms of the pancreas. *Semin. Diagn. Pathol.* 17, 31–42.

Wu, J., Jiao, Y., Dal Molin, M., Maitra, A., de Wilde, R. F., Wood, L. D., et al. (2011). Whole-exome sequencing of neoplastic cysts of the pancreas reveals recurrent mutations in components of ubiquitin-dependent pathways. *Proc. Natl. Acad. Sci. U. S. A.* 108, 21188–21193. doi: 10.1073/pnas.1118046108

Wu, J., Matthaei, H., Maitra, A., Dal Molin, M., Wood, L. D., Eshleman, J. R., et al. (2011). Recurrent GNAS mutations define an unexpected pathway for pancreatic cyst development. *Sci. Transl. Med.* 3:ra66. doi: 10.1126/scitranslmed.3002543

Xie, Z., Yin, X., Gong, B., Nie, W., Wu, B., Zhang, X., et al. (2015). Salivary microRNAs show potential as a noninvasive biomarker for detecting resectable pancreatic cancer. *Cancer Prev. Res.* 8, 165–173. doi: 10.1158/1940-6207.CAPR-14-0192

Yamaguchi, K., Kanemitsu, S., Hatori, T., Maguchi, H., Shimizu, Y., Tada, M., et al. (2011). Pancreatic ductal adenocarcinoma derived from IPMN and pancreatic ductal adenocarcinoma concomitant with IPMN. *Pancreas* 40, 571–580. doi: 10.1097/MPA.0b013e318215010c

Yamaguchi, H., Shimizu, M., Ban, S., Koyama, I., Hatori, T., Fujita, I., et al. (2009). Intraductal tubulopapillary neoplasms of the pancreas distinct from pancreatic intraepithelial neoplasia and intraductal papillary mucinous neoplasms. *Am. J. Surg. Pathol.* 33, 1164–1172. doi: 10.1097/PAS.0b013e3181a162e5

Yu, J., Yusoff, P. A. M., Woutersen, D. T. J., Goh, P., Harmston, N., Smits, R., et al. (2020). The functional landscape of patient-derived RNF43 mutations predicts sensitivity to Wnt inhibition. *Cancer Res.* 80, 5619–5632. doi: 10.1158/0008-5472.CAN-20-0957

Zamboni, G., Scarpa, A., Bogina, G., Iacono, C., Bassi, C., Talamini, G., et al. (1999). Mucinous cystic tumors of the pancreas: clinicopathological features, prognosis, and relationship to other mucinous cystic tumors. *Am. J. Surg. Pathol.* 23, 410–422. doi: 10.1097/00000478-199904000-00005

Conflict of Interest: The authors declare that the research was conducted in the absence of any commercial or financial relationships that could be construed as a potential conflict of interest.

Publisher's Note: All claims expressed in this article are solely those of the authors and do not necessarily represent those of their affiliated organizations, or those of the publisher, the editors and the reviewers. Any product that may be evaluated in this article, or claim that may be made by its manufacturer, is not guaranteed or endorsed by the publisher.

frontiers | Frontiers in Physiology

CORRECTION
published: 13 May 2022
doi: 10.3389/fphys.2022.923917

Corrigendum: Updates in the Diagnosis of Intraductal Neoplasms of the Pancreas

*Naziheh Assarzadegan, Sepideh Babaniamansour and Jiaqi Shi**

Department of Pathology, University of Michigan, Ann Arbor, MI, United States

Keywords: intraductal papillary mucinous neoplasm, intraductal oncocytic papillary neoplasm, intraductal tubulopapillary neoplasm, pancreatic ductal adenocarcinoma, classification

OPEN ACCESS

Approved by:
Frontiers Editorial Office, Frontiers Media SA, Switzerland

****Correspondence:***
Jiaqi Shi
jiaqis@med.umich.edu

Specialty section:
This article was submitted to Gastrointestinal Sciences, a section of the journal Frontiers in Physiology

Received: *19 April 2022*
Accepted: *21 April 2022*
Published: *13 May 2022*

Citation:
Assarzadegan N, Babaniamansour S and Shi J (2022) Corrigendum: Updates in the Diagnosis of Intraductal Neoplasms of the Pancreas. Front. Physiol. 13:923917. doi: 10.3389/fphys.2022.923917

A Corrigendum on

Updates in the Diagnosis of Intraductal Neoplasms of the Pancreas
by Assarzadegan, N., Babaniamansour, S. and Shi, J. (2022). Front. Physiol. 13:856803. doi: 10.3389/fphys.2022.856803

An author name was incorrectly spelled as "Sepideh Babanianmansour". The correct spelling is "Sepideh Babaniamansour".

The authors apologize for this error and state that this does not change the scientific conclusions of the article in any way. The original article has been updated.

frontiers in Physiology

REVIEW
published: 14 March 2022
doi: 10.3389/fphys.2022.849258

Purinergic and Adenosinergic Signaling in Pancreatobiliary Diseases

*Erika Y. Faraoni[1], Cynthia Ju[1], Simon C. Robson[2], Holger K. Eltzschig[1] and Jennifer M. Bailey-Lundberg[1]**

[1]Department of Anesthesiology, Center for Perioperative Medicine, McGovern Medical School, The University of Texas Health Science Center at Houston, Houston, TX, United States, [2]Departments of Internal Medicine and Anesthesiology, Center for Inflammation Research, Beth Israel Deaconess Medical Center and Harvard Medical School, Boston, MA, United States

OPEN ACCESS

Edited by:
Natalie Luhtala,
Salk Institute for Biological Studies,
United States

Reviewed by:
Francesco Di Virgilio,
University of Ferrara, Italy
Francisco Westermeier,
FH Joanneum, Austria

***Correspondence:**
Jennifer M. Bailey-Lundberg
jennifer.m.bailey@uth.tmc.edu

Specialty section:
This article was submitted to Gastrointestinal Sciences, a section of the journal Frontiers in Physiology

Received: 05 January 2022
Accepted: 03 February 2022
Published: 14 March 2022

Citation:
Faraoni EY, Ju C, Robson SC, Eltzschig HK and Bailey-Lundberg JM (2022) Purinergic and Adenosinergic Signaling in Pancreatobiliary Diseases.
Front. Physiol. 13:849258.
doi: 10.3389/fphys.2022.849258

Adenosine 5'-triphosphate (ATP), other nucleotides, and the nucleoside analogue, adenosine, all have the capacity to modulate cellular signaling pathways. The cellular processes linked to extracellular purinergic signaling are crucial in the initiation, evolution, and resolution of inflammation. Injured or dying cells in the pancreatobiliary tract secrete or release ATP, which results in sustained purinergic signaling mediated through ATP type-2 purinergic receptors (P2R). This process can result in chronic inflammation, fibrosis, and tumor development. In contrast, signaling *via* the extracellular nucleoside derivative adenosine *via* type-1 purinergic receptors (P1R) is largely anti-inflammatory, promoting healing. Failure to resolve inflammation, as in the context of primary sclerosing cholangitis or chronic pancreatitis, is a risk factor for parenchymal and end-organ scarring with the associated risk of pancreatobiliary malignancies. Emerging immunotherapeutic strategies suggest that targeting purinergic and adenosinergic signaling can impact the growth and invasive properties of cancer cells, potentiate anti-tumor immunity, and also block angiogenesis. In this review, we dissect out implications of disordered purinergic responses in scar formation, end-organ injury, and in tumor development. We conclude by addressing promising opportunities for modulation of purinergic/adenosinergic signaling in the prevention and treatment of pancreatobiliary diseases, inclusive of cancer.

Keywords: biliary cancer, pancreatic cancer, immune suppression, hypoxia, CD73, CD39

INTRODUCTION

Relationships between inflammation, wound-healing, scarring, and cancer were first proposed in the middle of the 19th century by Virchow (Dvorak, 1986). Currently, inflammation is recognized as a canonical hallmark of cancer given roles linked to the various stages of tumor development and in impacting responses to therapy (Greten and Grivennikov, 2019).

Inflammation appears tightly regulated by the release of inflammatory mediators inclusive of extracellular purines, heterocyclic aromatic organic compounds, and fundamental biochemical constituents of purinergic signaling (Miller and Urey, 1959). ATP is the vital purine nucleotide generated by glycolysis and oxidative phosphorylation and provides the intracellular energy currency fundamental for biological processes. Typical intracellular stores of ATP are in the range of 5–8 mM; however, several stimuli trigger heightened levels of ATP release by various cell types. This process increases local extracellular ATP concentrations to tens or even hundreds of micromoles per liter in inflamed or hypoxic tissues, such as in the tumor microenvironment (Di Virgilio et al., 2018a). Elevated extracellular ATP levels during pathophysiological conditions, such as tissue stress, necrosis, hypoxia, platelet activation, and vascular thrombosis, directly modulate recruitment and function of innate immune cells by exerting signals through purinergic receptors (Di Virgilio et al., 2018a). In this review, we consider the implications of dysregulated purinergic signaling in the evolution of pancreatobiliary diseases and in cancer.

DELETERIOUS VS. BENEFICIAL ELEMENTS OF PURINERGIC AND ADENOSINE SIGNALING

Decades of research have indicated extracellular ATP is pro-inflammatory, whereas the primary metabolite, adenosine, is largely anti-inflammatory. Integrated ATP-directed purinergic and adenosine-mediated signaling pathways appear imperative for appropriate responses to injury, healing, and subsequent tissue repair (**Figure 1A**).

Seminal work by Dr. Burnstock described novel ATP receptors, which were denoted Purinergic-type 2 receptors (P2R; Burnstock, 2006). In the extracellular environment, ATP-mediated purinergic signaling is initiated when ATP binds and activates P2R resulting in context and cell type-dependent responses. To date, eight P2YR ($P2Y_{1/2/4/6/11/12/13/14}$) and seven P2XR (P2X1-7) members have been identified in this family (**Figure 1B**).

P2YRs are metabotropic receptors that act as G protein-coupled receptors (GPCR), while P2XRs are nucleotide-gated ion channels and are more commonly known as ionotropic receptors (Idzko et al., 2014). Unlike P2YR that can bind several nucleoside tri- and di-phosphates, P2XR are ATP-selective. P2XR affinity is generally in the low micromolar range and highly sensitive to sudden changes in local ATP concentrations. P2X7R is the exception and has a remarkably high tetrabasic ATP activation threshold in the millimolar range (North and Surprenant, 2000; Magistroni et al., 2019). Active release of ATP to the extracellular compartment is tightly mediated by connexins, pannexins, and exocytosis, which are predominantly regulated by P2XR-dependent feedback loops (Di Virgilio et al., 2020; Li et al., 2020). Heightened ATP stimulation of P2X7 triggers opening of a non-selective plasma membrane pore, known as a macropore, which promotes the release of large hydrophilic molecules (Di Virgilio et al., 2018b). Macropore activation and conductance occur as a pathophysiological function of P2X7 (Pippel et al., 2017) and can result in membrane depolarization and cell death (Harkat et al., 2017). Isoforms of P2X7R have been described that impact macropore formation including nfP2X7, an isoform with conformational changes resulting in loss of the capacity for macropore formation (Pegoraro et al., 2021). This isoform is localized to the cytosol but can be translocated to the plasma membrane after cellular exposure to high ATP concentrations (Barden et al., 2003). Strategies to rescue macropore formation are promising therapeutic avenues as these adaptations are proposed to occur in tumor microenvironments (Lara et al., 2020).

Adenosine, once available in the extracellular space, signals through the Purinergic-type 1 receptor (P1R) family, which consists of four GPCR: ADORA (A_1R, $A_{2A}R$, $A_{2B}R$, and A_3R; **Figure 1A**; Borea et al., 2018). P1 receptor activation on epithelial or immune cells modulates intracellular cAMP levels and contributes to anti-inflammatory and immunosuppressive responses, dampening ATP-triggered responses by P2 receptors and contributing to resolution of injury (**Figure 1B**; Colgan, 2015).

Under homeostatic conditions, low levels of extracellular ATP are rapidly converted through the catalytic actions of ectonucleotidases. Tandem-linked enzymatic activities of ectonucleoside triphosphate diphosphohydrolase 1 (ENTPD1/CD39) decrease extracellular ATP and ADP levels through conversion to AMP, followed by ecto-5′-nucleotidase (CD73) catalyzed adenosine generation. Under hypoxic conditions, adenosine signaling elicits tissue-protective effects and coordinates reparative mechanisms through inhibition of leukocyte cell recruitment and reduced production of pro-inflammatory cytokines. Adenosine levels are in turn regulated by cellular uptake by equilibrative nucleoside transporters (ENTs; Eltzschig et al., 2005; Rose et al., 2011; Wang et al., 2021a). In humans, nucleoside transporters are encoded by *SLC28* and *SLC29*. The *SLC28* family includes three human Concentrative Nucleoside Transporters (hCNT1, hCNT2, and hCNT3) which have characteristic transporter properties, whereas the *SLC29* family comprises four human Equilibrative Nucleoside Transporters (hENT1, hENT2, hENT3, and hENT4) which are regulators of nucleoside pools and purinergic signaling (Pastor-Anglada and Pérez-Torras, 2018). In addition to cellular uptake, adenosine levels are regulated by the catalytic activity of adenosine deaminase (ADA) that terminates extracellular and intracellular adenosine signaling by irreversibly degrading adenosine to inosine (Wiginton et al., 1981; Idzko et al., 2014). However, when these processes are overwhelmed, sustained adenosine-mediated signaling exacerbates immunosuppressive states, resulting in immune exhaustion. Tumors arising in the pancreatobiliary tract have elevated CD39 and CD73, placing CD39 or CD73 inhibitors as high priority candidates for reversing immune suppression in these lethal malignancies (Sciarra et al., 2019).

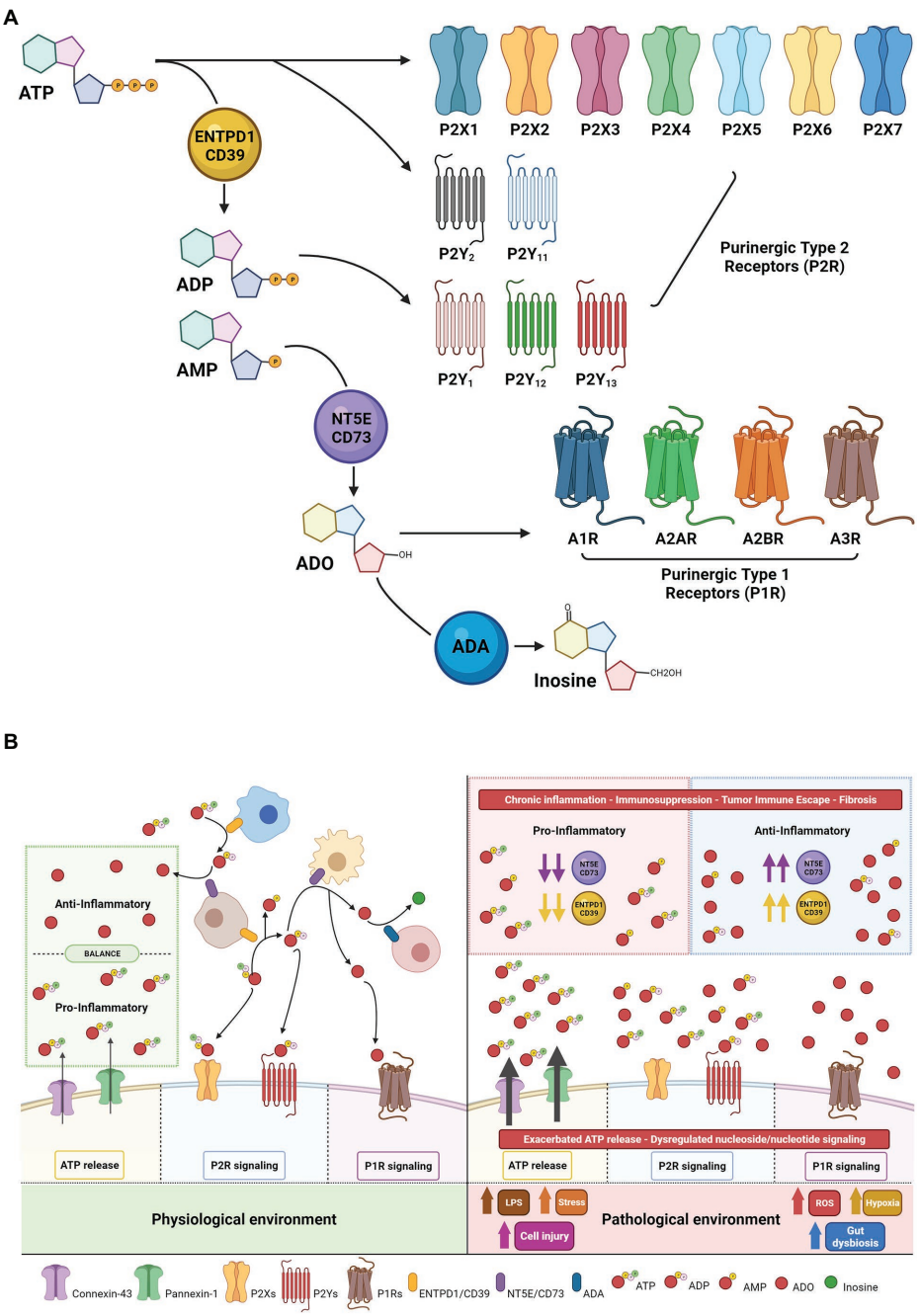

FIGURE 1 | Purinergic signaling mechanisms—receptors and ecto-enzymes. **(A)** Extracellular nucleotides, nucleosides and specific receptors. Extracellular ATP initiates vascular and immune cellular signaling through purinergic-type 2 receptors (classified as P2X ligand-gated channels and P2Y—G protein-coupled receptors). Enzymatic conversion of extracellular ATP to ADP/AMP by ENTPD1/CD39 modulates nucleotide/nucleoside signaling *via* ADP generation with binding and activation of selective P2Ys receptors and/or followed by AMP conversion to adenosine (ADO) by NT5E/CD73. ADO initiates adenosinergic/nucleoside-mediated signaling through purinergic-type 1 receptors P1R or can be degraded by ADA to inosine, resulting in termination of adenosine signaling. **(B)** Beneficial vs. Deleterious Purinergic Signaling Responses in Physiological and Pathological States. With physiological quiescent conditions, low-level nanomolar concentrations of extracellular ATP in the microenvironment are essential to fine-tune and preserve cell functionality. Tightly controlled ATP conversion and purinergic signaling enable co-ordination of signals in the extracellular compartment allowing tissue-specific homeostatic functions (Left). In the setting of inflammation and other pathological states, injured cells increase ATP release, which then achieve millimolar concentrations in the extracellular compartment, promoting cellular activation and strong pro-inflammatory responses. Sustained inflammation alters the nature of purinergic signaling through P2 and P1 receptors and may promote chronic injury. In this context, ADO generation can at first exhibit beneficial cytoprotective and anti-inflammatory functions through P1 receptors to help mitigate ATP exacerbated signaling; however, in the presence of high CD39/CD73 expression and high substrate levels of extracellular nucleotides, consequent ADO signaling triggers tumor immune escape, angiogenesis, excessive fibrosis and detrimental immunosuppression (Right).

HYPOXIA-DRIVEN ADENOSINERGIC SIGNALING

Pancreatobiliary malignancies including cholangiocarcinoma and pancreatic ductal adenocarcinoma have profoundly hypoxic and immunosuppressive tumor microenvironments. Hypoxia has been shown to enhance the invasive and malignant properties of these malignant cells (Lee et al., 2016; Yu et al., 2020). Their hypoxic microenvironments are important in the context of nucleoside signaling as hypoxia-mediated adenosine signaling is central for immunosuppression and immune escape (Bastid et al., 2015; Hayes et al., 2015). Under hypoxic conditions, P1-mediated adenosine signaling is boosted by the concerted and upregulated ecto-enzymatic activity of CD39 and CD73 on epithelial cells. CD73 transcriptional activity is regulated by a Hypoxia Response Element (HRE) located in the promoter region of *NT5E* (CD73). This HRE element allows HIF-1α to directly regulate CD73 in epithelial cells under hypoxic conditions (Synnestvedt et al., 2002). In addition, under hypoxic conditions in epithelial cells, HIF-1α cooperates with Sp1 to elevate expression of CD39 (Hart et al., 2010), which is also regulated by HIF-1β/ARNT and AhR receptor responses (Mascanfroni et al., 2015).

Hypoxia-dependent adenosine signaling also promotes angiogenesis, which has implications for invasion and metastasis. In human endothelial cells, hypoxic conditions enable HIF-2α to directly regulate adenosine $A_{2A}R$, and HIF-1α to regulate $A_{2B}R$, ENTs, and associated receptors. This mechanism promotes autonomous adenosine signaling and increased tissue vascularization (Li et al., 2020). In addition, adenosine impacts barrier-protective functions and RhoA activation in endothelial cells (Hassanian et al., 2014). Hence, in pancreatobiliary tumors, the adenosine rich stromal environment generated by elevated CD39 and CD73 enables neoplastic cells to escape $CD8^+$ T-cell and NK cell immune surveillance (Ohta et al., 2006) and may facilitate cell invasion and metastatic dissemination by transiently increasing tumor vascularity (Ohta et al., 2006; Sun et al., 2010; Chiu et al., 2017; Kjaergaard et al., 2018).

Controversial roles of tumor-derived extracellular adenosine are emphasized at the interface of inflammation and cancer where transient or chronic hypoxic events play key roles in both inflamed areas of normal tissue and solid tumors. In this regard, the $A_{2A}R$ has been shown to protect normal tissues by promoting termination of inflammation but also support tumor promotion by protecting cancerous tissues from anti-tumor T cells. Tissue-protective mechanisms involve the hypoxia-driven accumulation of adenosine which, *via* cAMP, enhances $A_{2A}R$ expression downregulating the inflammatory response and preventing exacerbated tissue damage after injury. An important characteristic of this beneficial hypoxia-adenosinergic downregulation of activated immune cells is that it acts in a delayed-negative feedback manner, which is crucial for avoiding damaging ischemic events and for the protection of normal tissues from overactive immune cells (Ohta and Sitkovsky, 2001; Sitkovsky, 2009). Conversely, deleterious effects of $A_{2A}R$ signaling have been described that rely on diminished TCR signaling and IFN-gamma production (Ohta et al., 2006). Both events are triggered by hypoxic-driven elevated intracellular levels of cAMP which ends up misguiding anti-tumor T cells (Ohta et al., 2006).

Hypoxic conditions haves remarkable influences in the purinergic system by regulating CD39, CD73, and both the P1 and P2 receptors; thus, it is important to highlight potential therapeutic implications of weakening the hypoxia-A2-adenosinergic immunosuppressive pathway in the TME (Hatfield and Sitkovsky, 2020). Studies have shown that modulating hypoxic conditions improves anti-tumor effects in a metastatic model of orthotopically grown breast tumors (Hatfield et al., 2015). Moreover, increased oxygenation decreases levels of tumor-protecting extracellular adenosine and reduces expression of HIF-1α dependent tumor-protecting proteins (Hatfield et al., 2014).

INFLAMMATORY BILE DUCT DISEASES

Primary Sclerosing Cholangitis (PSC) is a cholestatic form of liver disease, characterized by inflammation, thickening, and abnormal fibrosis of the intrahepatic and extrahepatic bile ducts. Risk factors for PSC include gut dysbiosis and inflammatory bowel disease. PSC has the potential to evolve into biliary cirrhosis and is a preneoplastic condition, predisposing to cholangiocarcinoma, and colorectal cancer (Razumilava et al., 2011).

The role of CD39 in PSC was recently highlighted in a murine model of biliary injury and sclerosing cholangitis induced by multidrug resistance protein 2 (Mdr2) deficiency (Peng et al., 2017). Here, genetic deletion of CD39 resulted in higher levels of hepatic $CD8^+$ T cells, liver injury, ductular reaction, and scarring. Loss of CD39 resulted in elevated ATP release in the gut, which activated DC and $CD8^+$ T cells. Activated DC and $CD8^+$ T cells then trafficked to the liver to target biliary epithelia, resulting in cholangitis and periductular fibrosis (**Figure 2**; Peng et al., 2017). These data are consistent with the complex mechanisms linking intestinal inflammation and PSC. Notably, the role of CD39 in limiting inflammation in this model is complicated by discordant impacts on ATP- and adenosine-mediated effects. As an example, subsets of bacterial species in dysbiosis activate immune cells, which upregulate CD39 and traffic to the liver. This mechanism increases intrahepatic levels of adenosine, perhaps resulting in aberrant immunosuppression, predisposing to cancers in cholestatic liver disease (Longhi et al., 2017; Tripathi et al., 2018; Vuerich et al., 2020).

To address this in the myeloid lineage, the role of CD39 in liver fibrosis has been studied in myeloid-specific CD39-deficient mice. After exposure to 3,5-diethoxycarbonyl-1.4-dihydrocollidine (DDC), myeloid-specific $CD39^{-/-}$ mice manifested worse liver fibrosis compared to wild-type mice, indicating CD39 myeloid expression is protective in sclerosing

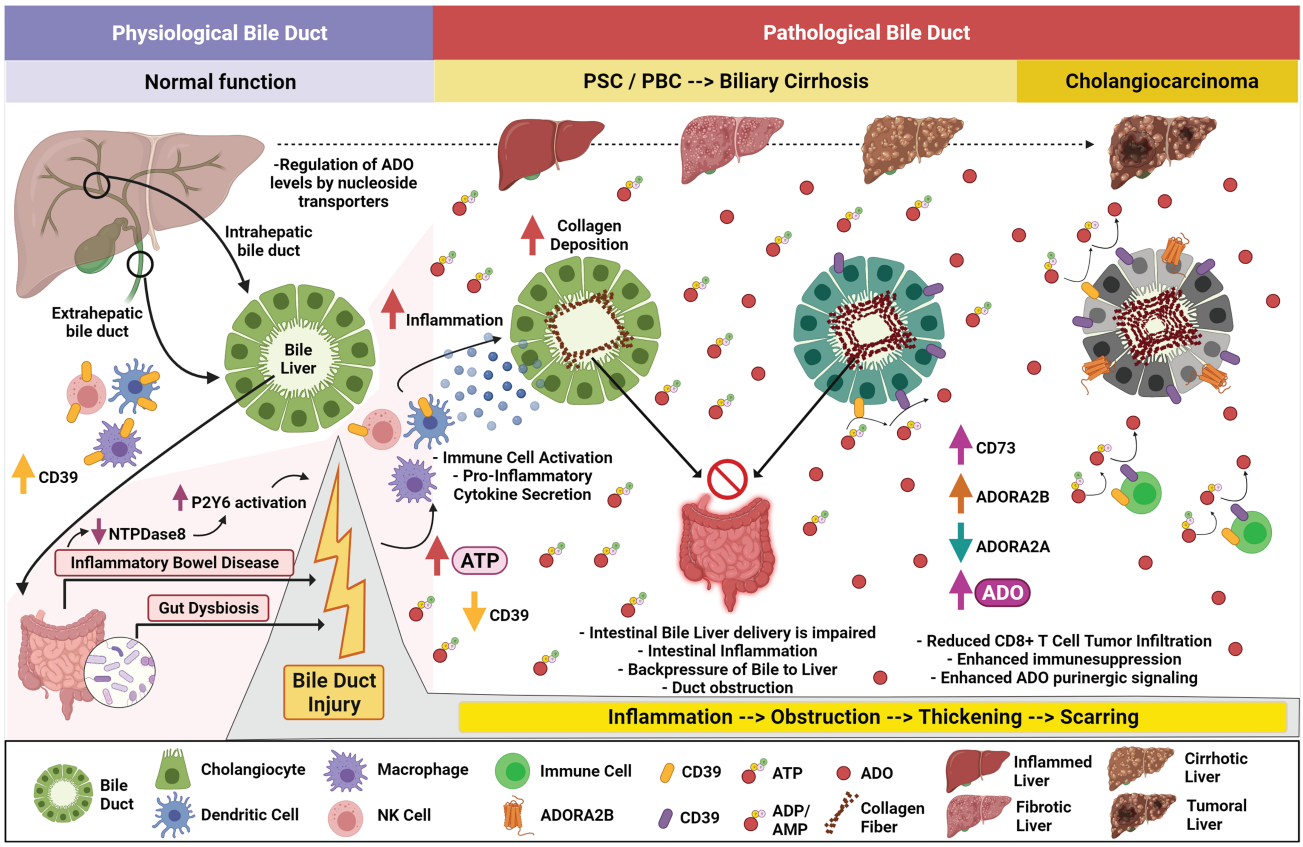

FIGURE 2 | Purinergic signaling in cholestatic liver disease, biliary cirrhosis, and development of cholangiocarcinoma. Ectonucleotidase-expressing immune cells, pancreatic acinar cells, and cholangiocytes help balance gut-derived ATP levels arising within the hepatopancreatobiliary tract. During Inflammatory Bowel Disease (IBD) with associated gut dysbiosis, increased levels of ATP are secreted impacting physiological bile duct function and provoking further cholestasis. Decreased intestinal ENTPDase8 promotes enhanced $P2Y_6$ activation and exacerbates the inflammatory phenotype. Immune cells may lose CD39 expression, allowing systemic ATP accumulation with activation of dendritic cells, macrophages, and NK cells. This effect is pronounced when in presence of CD39-deprived macrophages. The activated immune cells secrete pro-inflammatory signals when these cells arrive within the pancreatobiliary tract promoting cholangiocyte inflammation. Primary Sclerosing Cholangitis (PSC) and Primary Biliary Cholangitis (PBC) are associated with chronic ductular injury, impairing intestinal bile liver delivery, promoting backpressure to the liver, and exacerbating intestinal inflammation. Chronic inflammation and intra bile duct fibrosis trigger duct obstruction, thickening, and scarring which leads to biliary cirrhosis. Decreased $A_{2A}R$ and elevated CD73 and $A_{2B}R$ expression amplify adenosine signaling which reduces $CD8^+$ T-cell tumor infiltration and enhances immune suppression, priming Cholangiocarcinoma initiation and development.

cholangitis (Rothweiler et al., 2019). These data indicate at early stages of biliary fibrosis, CD39 may be important for scavenging nucleotides and decreasing extracellular ATP levels to protect from sustained or chronic inflammatory signaling, but the consequences of sustained elevated CD39 in mediating long-term aberrant adenosinergic effects are to be still determined.

Primary Biliary Cholangitis (PBC) is an autoimmune cholestatic liver disease, which is characterized by damage to the intrahepatic bile ducts resulting in cirrhosis in some patients. PBC is slow progressing and associated with a number of malignancies including pancreatic, breast, and hepatocellular carcinoma. PBC is manifested by accumulation of bile in the liver, portal inflammation, and antimitochondrial antibodies (Ide et al., 2017). PBC can be managed with ursodeoxycholic acid (UDCA), a hydrophilic bile salt metabolized by the microbiome (Guarino et al., 2013). The proportions of $CD4^+CD39^+$ and $CD8^+$ T regulatory cells, important for preventing autoimmune disease, are decreased in these patients (Lan et al., 2006; Bernuzzi et al., 2010) and CD4 + CD39+ cells are significantly reduced in the PBMCs of these patients compared to healthy controls. A mouse model for PBC has been described using 16-week chronic exposure to polyinosinic–polycytidylic acid (poly I:C). In these mice, similar to observed findings in human patients, $CD39^+CD4^+$ and $CD39^+$ T regulatory cells are decreased in spleens and livers and $CD39^+$ cells were decreased in PBMC. However, $CD73^+$ cell numbers were not altered. In addition to loss of CD39, the $A_{2A}R$, but not any other adenosine receptor, was decreased in the livers of poly I:C treated mice, indicating loss of hepatic $A_{2A}R$ and reduced anti-inflammatory adenosine signaling may be associated with early progression of PBC (**Figure 2**; Gong et al., 2021).

BILE DUCT CANCER

Tumors arising in the bile ducts are considered rare, yet highly lethal. Cholangiocarcinoma is considered aggressive and highly invasive with poor prognosis. This malignancy arises in the biliary tract and consists of two major subtypes: intra- vs. extrahepatic cholangiocarcinoma. HIF-1α levels are significantly elevated in cholangiocarcinoma cell lines compared to normal biliary cells and HIF-1α is important for cholangiocarcinoma cell line proliferation, migration, and invasion (Yu et al., 2020). ATP and adenosine have been shown to have anti-proliferative and anti-motility effects (Lertsuwan and Ruchirawat, 2017) in experiments conducted using cholangiocarcinoma cell (CCA) lines. Purinergic receptor expression levels in CCA cell lines were analyzed using qPCR and P2 receptors were expressed in CCA cell lines and in immortalized cholangiocytes, but in this study, adenosine receptors were not identified. Further elucidation of these mechanisms is needed, especially in the context of hypoxia, to evaluate the mechanistic consequences of elevated purinergic receptors in cholangiocarcinoma.

In contrast to *in vitro* studies, correlative immunohistochemical analysis of patients with cholangiocarcinoma in two separate cohorts has shown CD73 is elevated in cholangiocarcinoma and has prognostic implications. Immunohistochemistry in the first cohort showed CD73 staining in the majority of intra- and extrahepatic cholangiocarcinoma tissues. Notably, in normal hepatobiliary tissue, CD73 was expressed in the apical region of cholangiocytes and pancreatic ducts, and in the canalicular of hepatocytes (Sciarra et al., 2019). In the second cohort of 140 patients, elevated CD73 was highly correlated to lymphatic metastasis, tumor size and negatively associated with tumor-infiltrating $CD8^+$ T cells. These data suggest that inhibition of CD73 is a promising modality for immunotherapy in patients diagnosed with intra- or extrahepatic cholangiocarcinoma (Xu et al., 2021).

In homeostatic biliary epithelia, the expression of hCNT3 is well represented and appears to be the major player in the extracellular regulation of adenosine levels. Moreover, as this receptor is regulated by $A_{2A}R$, it contributes to complete purinergic control of bile flow which was started by ATP secretion into the bile (Godoy et al., 2014). On the other hand, in a subgroup of patients with biliary tract cancer, hENT1 expression correlated with overall survival, suggesting its participation in the intracellular transport of gemcitabine may play a role in predicting the subpopulation of patients who could benefit from this therapy (Santini et al., 2011).

INFLAMMATORY PANCREATIC DISEASES

Under normal physiologic conditions, pancreatic acinar cells express P2X1, P2X4, $P2Y_2$, and $P2Y_4$. The role of these P2R is thought to be related to signaling responses driven by secretion of ATP at the luminal side. In addition, intercalated pancreatic ducts expressing functional P2Rs, such as $P2Y_2$, $P2Y_4$, $P2Y_6$, $P2Y_{11}$, P2X4, and P2X7, respond and mediate ductal secretion of bicarbonate-rich fluid (Hayashi et al., 2016; Sciarra et al., 2019). ATP released by acini is hydrolyzed to ADP/AMP and adenosine by ectonucleotidase expression on ducts and both ADP and adenosine regulate ion channels on pancreatic ducts (Burnstock and Novak, 2012; Novak et al., 2020).

In acute pancreatitis, injured acinar cells undergo autophagy or uncontrolled cellular death promoting the release of trypsinogen, cytokines, and ATP to the extracellular space allowing the activation and infiltration of several immune cells to the injured site (Sendler et al., 2018; Mayerle et al., 2019; Saluja et al., 2019). Heightened trypsinogen and ATP release elevates induction of acinar cell p38 MAPK and NF-κB pathways, which further contribute to pancreatic inflammation (Dixit et al., 2019). Elevated purinergic or adenosine signaling in pancreatic ducts results in dysregulation of bicarbonate secretion which alters the pH of pancreatic secretions provoking pancreatitis (**Figure 3**). In addition, purinergic receptors expressed on infiltrating neutrophils exacerbate pancreatitis. In a mouse model of acute pancreatitis, P2X1 expressed on neutrophils contributes to the inflammatory response and severity of pancreatitis (Wang et al., 2020). Expression of purinergic receptors and ectonucleotidases play an important role in mediating the physiological and pathological function of the pancreas, given their broad expression in epithelial, immune, and stromal cells (Novak et al., 2020).

Chronic pancreatitis is an important risk factor for development of pancreatic ductal adenocarcinoma and is characterized by acinar injury, damage of the gland, sustained inflammation, fibrosis, and loss of islet cells. Chronic pancreatitis manifests in unrelenting abdominal pain, malnutrition, pancreatogenic diabetes (type 3c diabetes), and exocrine and endocrine insufficiency (Bhattamisra et al., 2019; Singh et al., 2019; Illés et al., 2020; Wei et al., 2020; Cruz-Monserrate et al., 2021). Risk factors include heavy alcohol abuse, tobacco smoking, and genetic predispositions (Majumder and Chari, 2016; Singh et al., 2019). Events that promote sustained pancreatic injury, like chronic pancreatitis, result in excessive accumulation of ATP which dysregulates the physiological state of the gland and may be a key driver of neoplasia.

In vitro cultures of ethanol-induced toxicity on pancreatic ductal epithelial cells exposed to micromolar concentrations of ATP/ADP resulted in a protective effect *via* the $P2Y_1$ receptor. ATP/ADP activation of the $P2Y_1$ receptor increased intracellular levels of cAMP which is an important mechanism for maintenance of ductal epithelial integrity in the presence of ethanol (Seo et al., 2016). While a protective mechanism through P2R purinergic signaling has been studied in pancreatic ducts, the role of adenosine signaling in alcohol-associated pancreatitis has not been described.

In addition, the role of purinergic signaling in the development of pancreatogenic or secondary type 3C diabetes has not been established (Hart et al., 2016). Experiments evaluating the function of islets in models of insulin resistance, diabetes, and obesity have shown increased production of ATP in diabetic and obese mice. This has been shown to reduce anti-inflammatory

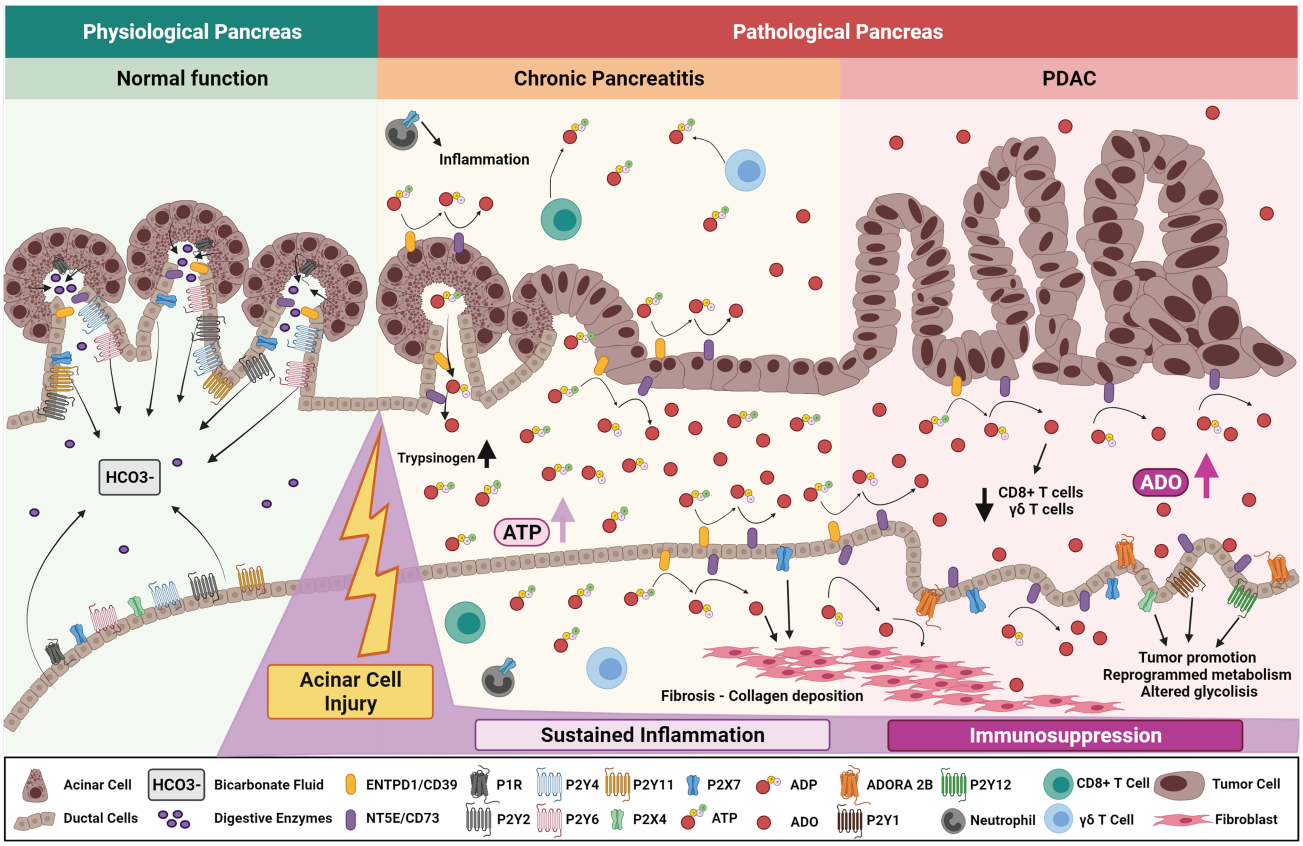

FIGURE 3 | Purinergic signaling mechanisms in chronic pancreatitis and development of pancreatic cancer. Purinergic signaling mediates normal pancreatic function by regulating ductal P2Rs-dependent bicarbonate fluid release and acinar CFTR-dependent exocrine pancreatic secretion. After acinar cell injury, increased levels of ATP are secreted into the extracellular compartment primarily from acinar cells, increasing pancreatic trypsinogen levels and affecting normal pancreatic function. In time, sustained ATP-derived inflammation and adenosine generation stabilizes pancreatic chronic injury and/or ongoing pancreatitis. Increased expression of ductal CD73 elevates adenosinergic signaling triggering collagen deposition and further fibrotic development. Altered ductal cells undergo aberrant purinergic signaling though P2Rs affecting glycolytic metabolism and cumulative pancreatic ADO signaling promotes $CD8^+$ T cell and ϒδ T-cell depletion. These factors promote an immunosuppressive environment ultimately priming the organ to malignant transformation, PDAC initiation, and progression.

secretion of IL-10 from islet-associated macrophages indicating increased ATP may have a pathogenic role in development of type 3C diabetes (Weitz et al., 2020). Adenosine signaling also regulates ß-cell survival and regeneration in inflammatory microenvironments as well as regulates insulin secretion and lipid homeostasis through P1 receptors (Antonioli et al., 2015).

Global deletion of CD39L (*Entpd3*$^{-/-}$) and islet-specific deletion of CD39L using *Entpd3*$^{flox/flox;InsCre}$ mice have been studied as this ENTPD is the dominant islet and β cell ectonucleotidase. *Entpd3*$^{-/-}$ mice are resistant to high fat diet-induced obesity and have elevated basal metabolic rates, when fed a high fat diet associated with improved glucose tolerance. This phenotype was associated with higher uncoupling protein 1 (UCP-1) in brown adipose tissue. Studies on *Entpd3*$^{flox/flox;InsCre}$ mice show a similar phenotype indicating Entpd3 in β cells is not protective against diet-induced obesity and insulin resistance (Sandhu et al., 2021). The potential role of purinergic and adenosine signaling in pancreatogenic diabetes has a number of therapeutic implications and should be further explored.

DUCTAL ADENOCARCINOMA OF THE PANCREAS

Pancreatic ductal adenocarcinoma (PDAC) is one of the world's most lethal malignancies. Risk factors include age, smoking, inherited predisposition due to a germline mutation, obesity, long-standing diabetes, chronic pancreatitis, and type 3 C diabetes (Xiao et al., 2016; Saluja and Maitra, 2019; Hart and Conwell, 2020).

Several purinergic P2Rs are widely expressed in pancreatic cancer cell lines (Hansen et al., 2008). Among these, P2X5, was found elevated in human PDAC and associated with malignant behavior of cancer cells; however, the role of P2X5 in pancreatitis and tumor development is not yet well stablished (Zaccagnino et al., 2016) and there remains uncertainty regarding the role of P2X7 in pancreatitis and PDAC initiation.

An *in vivo* study using P2X7 inhibitors revealed a tumor-promoting function for this receptor and highlighted its participation in stellate cell fibrosis and collagen deposition (Giannuzzo et al., 2016). Other P2 receptors including $P2Y_1$,

$P2Y_6$, and $P2Y_{12}$ were identified as increased in PDAC cell lines and exerted tumor-promoting functions in the presence of ATP (Qadir et al., 2018; Novak et al., 2020). Studies show that $P2Y_2$ is associated with poor prognosis and its activation promotes PDAC cancer progression by reprogramming cancer cell metabolism and glycolysis (Hu et al., 2019). $P2Y_2$ effects were prevented when genetically or pharmacologically inhibited, providing enhanced evidence regarding mechanisms of ATP-mediated PDAC progression through $P2Y_2$ receptor on malignant epithelium (Choi et al., 2013; Hu et al., 2019).

Adenosine signaling is emerging as a critical mediator of PDAC. Evaluation of adenosine P1 receptors from gene expression analysis of PDAC tissues based on The Cancer Genome Atlas (TCGA) show that both *ADORA2A* and *ADORA2B* expression are increased in PDAC compared to normal tissues. Of interest, *ADORA2B* is a marker of poor prognosis and *ADORA2A* has better overall survival prognostic impact (Hayashi, 2019). Another well-studied receptor in this disease is A_3R, which promotes the tumorigenic phenotype *via* ERK1/2 signaling pathway (Gorzalczany et al., 2017).

In addition to P1 receptors, CD73 is elevated in pancreatic cancer (Chen et al., 2020; Zhao et al., 2021). In pancreatic cancer, adenosine generation mediated by the concerted activity of CD39 and CD73 is correlated with lower infiltration of $CD8^+$ T cells and $\gamma\delta^+$ T cells, as well as stellate cell proliferation and collagen production (Künzli et al., 2008; Chen et al., 2020; Shevchenko et al., 2020). While correlative, these data indicate that adenosine signaling promotes pancreas fibrotic development by modulating ECM remodeling and immunosuppression (Blocking CD73 Can Shrink Pancreatic Tumors, 2021).

High expression of CD73 has been described in tumor cells in two independent cohorts of PDAC patients (Chen et al., 2020; Zhao et al., 2021). Elevated CD73 is associated with a decrease in $CD4^+$, $CD8^+$, and $CD21^+$ tumor-infiltrating lymphocytes and is associated with aggressive clinical behavior (Zhao et al., 2021). Histologic evaluation of CD73 in pancreatic and PDAC tissues has shown CD73 is expressed in pancreatic ducts and in PDAC tissue, but not acinar cell carcinoma (Sciarra et al., 2019). In genetically engineered mouse models of PDAC, CD73 is highly expressed on neoplastic and invasive lesions arising in pancreatic ducts and high CD73 is associated with high adenosine levels in pancreata from these mice. Inhibition of adenosine generation decreased tumor growth in spontaneous and established models and is correlated with increased activated $CD8^+$, $CD4^+$ T cells and macrophages, implicating anti-CD73 immunotherapy in PDAC patients with high CD73 expression (Singh et al., 2021). Further studies are needed to fully comprehend the molecular mechanisms underlying CD73 function and adenosine generation in pancreatitis and PDAC microenvironment modulation. CD39 and CD39L transcripts are both increased in chronic pancreatitis and pancreatic cancer. Pathologic analysis reveals both are localized in vascular and stromal elements. In contrast to CD73, high expression of CD39 is significantly associated with better long-term survival in PDAC (Künzli et al., 2007).

Nucleoside transporter expression was found altered during the progression from normal pancreatic epithelia to a malignant state. Evidence suggests that functional hENTs may result in increased gemcitabine uptake by pancreatic cells. Hence, reduced expression of hENT1 implicates a link between protein expression levels and chemoresistance (Nakano et al., 2007; Carter et al., 2021). Moreover, in PDAC patients, its low expression correlates with a significant reduction in progression-free survival and disease-free survival when compared to patients with medium to high levels of hENT1 expression (Farrell et al., 2009). Aberrant expression of hENT2 was also observed in pancreatic cancer cells and suggested to contribute to chemoresistance; however, its participation is not yet fully elucidated (Alvarellos et al., 2014). On the contrary, hCNT3 expression in pancreatic tumors correlates with overall patient survival, with an increased expression of the transporter usually associated with a longer overall patient survival. The aberrant expression of hCNT3 was observed in pancreatic tumors and pancreatic cancer cell lines and is of high relevance for pancreatic cancer patients given its ability to transport a large variety of nucleoside-derived drugs and, more importantly, gemcitabine for solid tumors (Stecula et al., 2017).

THERAPEUTIC CONSIDERATIONS IN PANCREATOBILIARY CANCERS

Therapeutic intervention has been proposed to correct the pathophysiological levels of extracellular nucleotides and nucleosides to restore CD39 or P2 receptor functionality in chronic inflammatory states. Given space constraints and the important recent developments in purinergic immunotherapy and check point inhibition in cancer, may we refer the interested reader to several reviews that cover the topics of augmenting adenosinergic pathways and blocking ATP-mediated pathways in the liver, pancreas, and GI tract in several inflammatory disease states in order to limit cancer development (Eltzschig et al., 2012; Burnstock et al., 2014; Longhi et al., 2017, 2021; Vuerich et al., 2020).

Given the complex expression of purinergic mediators in epithelial, stromal, and immune compartments, receptor blockade may not only impair the specific signaling pathway but also modulate the tumor microenvironment impacting other purinergic receptors. Preclinical studies targeting the purinergic system suggest that combined inhibition of more than one member of the pathway may enhance anti-tumor immune responses (Young et al., 2016; Moesta et al., 2020).

Firstly, metastatic dissemination and colonization are complex processes linked to spread of tumor cells. *In vivo* lineage tracing experiments indicate circulating pancreatic neoplastic epithelial cells disseminate prior to establishment of a primary tumor. In these *in vivo* experiments, inflammation appears as a potent driver of epithelial dissemination or delamination (Rhim et al., 2012, 2014; Hendley et al., 2016). Defining the role of purinergic signaling coordinated between neoplastic epithelial cells, innate or adaptive immune cells and the foreign parenchymal microenvironment will be crucial to determining whether immune mechanisms prevail and eliminate tumor cells before these cells spread.

Secondly, ectonucleotidases, P2 and P1 receptors are predicted to play central roles in shaping the foreign microenvironment by boosting ATP/AMP/adenosine conversion, favoring an immunosuppressive niche. P2X1 negative neutrophils are key players in the invasion of foreign liver tissues. After being mobilized and recruited to metastatic sites, P2X1 negative neutrophils exert immunosuppressive activities *via* Nrf2-supported mitochondrial metabolism and predispose the foreign tissue as a suitable site to successful metastatic colonization (Wang et al., 2021b). In addition, purinergic signaling impacts T-cell memory and exhaustion. These prior findings indicate that targeting CD39 has merit for augmenting checkpoint therapies for treating cancer and chronic infections (Sun et al., 2010; Deaglio and Robson, 2011). These observations suggest that specific mechanisms operate to modulate purinergic responses in memory T cells. The response of memory T cells to adenosine and specific receptor agonists might be modulated at the level of intracellular cyclic-AMP and the signaling pathways it controls (Peter et al., 2007). Furthermore, given the recent discovery of $CD39^+CD8^+$ T cells in regulating metastatic dormancy, understanding the mechanisms of purinergic signaling in metastasis is critical especially given the predicted duration of time from primary tumor to metastatic disease in pancreatic cancer (Yachida et al., 2010). These experiments also infer major implications for CD39 inhibitors, which may block metastatic spread of cancer cells in experimental models (Sun et al., 2010).

In the context of checkpoint inhibitors, targeting CD39 is likely to be more effective than single agents targeting CD73 (Beavis et al., 2012), due to reduced generation of immunosuppressive adenosine, and also promoting the accumulation of immunostimulatory ATP (Martins et al., 2009; Vieira et al., 2014). ATP in the tumor microenvironment amplifies TCR signaling in lymphocytes triggering anti-tumor $CD8^+$ infiltration and activation (Boison and Yegutkin, 2019). In addition, sustained ATP promotes long-term memory $CD8^+$ T cells critical for adaptive immunity. CD39 blockade has been shown to reduce tumor growth not only because of the diminished generation of downstream adenosine (see below) but also by enhanced P2X7-mediated NRLP3 inflammasome due to extracellular accumulation of ATP (Li et al., 2019; Baeza-Raja et al., 2020). In models of melanoma metastasis, tumor growth in the liver is substantively inhibited in mice with CD39 null vasculature or CD39 null bone marrow-derived cells. $CD4^+FoxP3^+$ Tregs expressing CD39 repressed anti-tumor immunity by NK cells and pharmacologic inhibition of CD39 significantly limited melanoma tumor growth. Thus, CD39 expression on Tregs promotes metastatic growth and targeting this may provide a strategy for secondary hepatic malignancies (Sun et al., 2010).

In contrast, adenosine is generated by CD39-CD73 expression on Treg and memory T cells and inhibits effector T-cell immunity, which opposes effects of ATP. Adenosine receptor stimulation ($A_{2A}R$ or $A_{2B}R$) on macrophages restrains production of nitric oxide and pro-inflammatory cytokines. Thus, adenosine receptors resolve inflammation and promote tissue repair, yet in chronic inflammation and neoplasia, cumulative adenosine signaling promotes transformation and immunosuppression (Boison and Yegutkin, 2019).

When targeting adenosine receptors, it is important to consider that A_1R and A_2R have the capacity to form heteromers, which implies a cross-communication between Gi and Gs proteins (Navarro et al., 2018). These structures were shown to act as sensors of adenosine concentration and modulate adenosine signaling in such a way that there is either A_1R or A_2R-mediated effects. Similar properties were described for heteromers formed between $A_{2A}R$ and $A_{2B}R$ (Franco et al., 2021). Thus, these recent findings highlight the need to elucidate whether heteromer formation is found in pancreatobiliary cancers, as studying its peculiar signaling dynamic will be essential to understand adenosine-mediated effects and potentially propose them as targetable structures.

A challenging aspect when targeting purinergic or adenosinergic receptors is most physiological and preclinical studies to unravel receptor function and therapeutic effects have been carried out in rodents, which, do not necessarily represent the affinity and functioning of human receptors. Hence, several compounds in preclinical platforms were selected based on their affinity to human receptors, which do not necessarily represent similar rodent receptor interaction. Indeed, this aspect was analyzed for adenosine receptors and determined that for some ligands the potency and selectivity are species-dependent and proposed that a comprehensive characterization of compounds and species-specific affinities are key to understand whether they may be suitable ligands to pursue drug therapy in the clinic (Alnouri et al., 2015).

Beneficial effects were observed when targeting CD73 and $A_{2A}R$ alone or in combination with PD-1/PD-L1 inhibitors (Allard et al., 2013; Mittal et al., 2014; Beavis et al., 2015; Hay et al., 2016). Moreover, preliminary results of the first phase 1/2a study of a CD73 inhibitor in combination with the PD-1 inhibitor nivolumab induced partial responses or stable disease in 28% of patients with various malignancies (NCT02754141). Another phase 1 clinical trial recently evaluated simultaneously inhibiting CD73 and PD-L1 in subjects with select advanced solid tumors (NCT02503774), however, results remain to be published.

Currently, several phase I/II studies are evaluating CD39 (NCT04336098) and $A_{2A}R$ blockade in combination with PD-1 (NCT03884556, NCT03207867), PD-L1 (NCT02655822) inhibitors, or with standard chemo- or immunotherapy (NCT04306900). Besides, in locally advanced or recurrent/metastatic PDAC, several phase I clinical trials are being conducted by targeting CD73 alone (NCT04148937) or in combination with PD-1 (NCT04104672) and $A_{2A}AR$ inhibitors (NCT03549000, NCT03454451; **Table 1**).

Lastly, the role of microbiome in regulating systemic ATP or adenosine signaling in metastasis warrants further analysis. Inosine derived from the microbiome was recently described as a key mediator of immunosuppression and response to checkpoint inhibitor immunotherapy (Mager et al., 2020) and analysis of human PDAC microbiome has revealed certain bacterial species are correlated with overall survival (Riquelme et al., 2019). However, the role of gut bacteria in altering local and systemic purinergic and adenosine signaling in pancreatic diseases has not been well defined.

TABLE 1 | Clinical trials evaluating the potential use of purinergic mediators as targets for hepatopancreatobiliary tumors.

Target	Drug +/– combination therapy or Outcome	Tumor	Identifier	Study phase	Sponsor company
A2AAR	NIR178 (A2AAR antagonist) in combination with PDR001 (anti-PD-1 Ab)	Patients with solid tumors (including pancreatic cancer) and Non-Hodgkin Lymphoma	NCT03207867	Phase II	Novartis Pharmaceuticals
A2AAR	Ciforadenant (A2AAR inhibitor) in combination with Atezolizumab (PD-L1 inhibitor)	Patients with selected incurable tumors	NCT02655822	Phase I/Ib	Corvus Pharmaceuticals
CD39	TTX-030 (anti-CD39 Ab) in combination with standard chemo- or immunotherapy	Patients with advanced tumors	NCT04306900	Phase I/Ib	Trishula Therapeutics
CD39	SRF617(anti-CD39 Ab)	Patients with advanced solid tumors	NCT04336098	Phase I	Surface Oncology
CD39	TTX-030 (anti-CD39 Ab) +/– anti-PD-1 immunotherapy	Patients with Lymphoma or solid tumors	NCT03884556	Phase I	Trishula Therapeutics
CD39	Monotherapy	Patients with advanced solid tumors	NCT05234853	Phase I	Purinomia Biotech, Inc
CD73	LY3475070 (CD73 inhibitor) +/– Pembrolizumab	Patients with advanced solid tumors including PDAC	NCT04148937	Phase I	Eli Lilly and Company
CD73 +/– A2AAR	NZV930 (anti-CD73 Ab) +/– PDR001 (anti-PD-1 Ab) +/– NIR178 (A2A antagonist)	Patients with advanced solid tumors including PDAC	NCT03549000	Phase I/Ib	Novartis Pharmaceuticals
CD73 +/– A2AAR	CPI-006 (anti-CD73 Ab) +/– ciforadenant (oral A2A inhibitor) +/– pembrolizumab (anti-PD1 Ab)	Patients with selected advanced solid tumors including PDAC	NCT03454451	Phase I/Ib	Corvus Pharmaceuticals
CD73 +/– PD-1	AB680 in combination with Zimberelimab (AB122), nab-paclitaxel and gemcitabine	Patients with advanced PDAC	NCT04104672	Phase I	Arcus Biosciences

CONCLUSION

Purinergic signaling pathways have important roles in initiation, progression and resolution of inflammation, yet sustained activation appears to disrupt normal tissue homeostasis and promote chronic inflammatory conditions and scar formation. These factors elevate the risk of end-organ failure and development of pancreatobiliary cancer. Beneficial ATP inflammatory P2R-mediated effects might be overshadowed in chronically inflamed tissues or neoplastic environments, where enzymatic conversion of nucleotides through elevated CD39 and CD73 may lead to excessive adenosine accumulation. Instead of promoting resolution of inflammation and tissue repair, this rather promotes A_{2B}R-mediated or other aberrant pathways important for cellular transformation and immune suppression. In this context, it should be kept in mind that outcomes are not only determined by extracellular bioavailability of ATP and its nucleoside derivatives, but also by the expression of other purinergic mediators and P1 or P2 receptor functionality.

Therapeutic strategies targeting CD39 or CD73 as well as A_{2B}R antagonism have the potential to reverse adenosine-mediated immunosuppression, albeit only CD39 blockade will boost ATP-mediated anti-tumor immunity. However, the widespread expression of CD39, CD73, and purinergic receptors on immune cells, myofibroblasts, and epithelial cells complicates understanding of the mechanistic basis for purinergic and adenosine signaling during chronic inflammation, fibrosis, and tumor formation.

We propose that modulation of purinergic signaling represents novel avenues for reversing inflammation, and by virtue of limiting scar formation and cell transformation, decreasing the risk of cancer. Once cancer has developed, then immunotherapy strategies for treatment of pancreatobiliary malignancies show great promise. Dissecting out the implications of these propositions and determining the clinical timing of these divergent approaches will require further study, attention to personalized medicine, and innovative clinical trials.

AUTHOR CONTRIBUTIONS

EF and JMB-L wrote the main manuscript file. CJ, SCR, and HKE edited the manuscript file. All authors contributed to the article and approved the submitted version.

FUNDING

NIH R21CA249924 and DK056338-18 (Pilot) to JMB-L. NIH grants R01HL154720, R01DK122796, R01HL133900 and Department of Defense W18XWH2110032 to HKE. NIH R01DK122708, R01DK121330 and R01DK122796 to CJ. NIH R01DK108894; R21CA221702, Emerson Collective Cancer Research Fund Award and Department of Defense Award W81XWH-16-0464 to SCR.

ACKNOWLEDGMENTS

The figures for this review were created using BioRender Software.

REFERENCES

Allard, B., Pommey, S., Smyth, M. J., and Stagg, J. (2013). Targeting CD73 enhances the antitumor activity of anti-PD-1 and anti-CTLA-4 mAbs. *Clin. Cancer Res.* 19, 5626–5635. doi: 10.1158/1078-0432.CCR-13-0545

Alnouri, M. W., Jepards, S., Casari, A., Schiedel, A. C., Hinz, S., and Müller, C. E. (2015). Selectivity is species-dependent: characterization of standard agonists and antagonists at human, rat, and mouse adenosine receptors. *Purinergic Signal* 11, 389–407. doi: 10.1007/s11302-015-9460-9

Alvarellos, M. L., Lamba, J., Sangkuhl, K., Thorn, C. F., Wang, L., Klein, D. J., et al. (2014). PharmGKB summary: gemcitabine pathway. *Pharmacogenet. Genomics* 24, 564–574. doi: 10.1097/FPC.0000000000000086

Antonioli, L., Blandizzi, C., Csóka, B., Pacher, P., and Haskó, G. (2015). Adenosine signalling in diabetes mellitus--pathophysiology and therapeutic considerations. *Nat. Rev. Endocrinol.* 11, 228–241. doi: 10.1038/nrendo.2015.10

Baeza-Raja, B., Goodyear, A., Liu, X., Lam, K., Yamamoto, L., Li, Y., et al. (2020). Pharmacological inhibition of P2RX7 ameliorates liver injury by reducing inflammation and fibrosis. *PLoS One* 15:e0234038. doi: 10.1371/journal.pone.0234038

Barden, J. A., Sluyter, R., Gu, B. J., and Wiley, J. S. (2003). Specific detection of non-functional human P2X(7) receptors in HEK293 cells and B-lymphocytes. *FEBS Lett.* 538, 159–162. doi: 10.1016/S0014-5793(03)00172-8

Bastid, J., Regairaz, A., Bonnefoy, N., Déjou, C., Giustiniani, J., Laheurte, C., et al. (2015). Inhibition of CD39 enzymatic function at the surface of tumor cells alleviates their immunosuppressive activity. *Cancer Immunol. Res.* 3, 254–265. doi: 10.1158/2326-6066.CIR-14-0018

Beavis, P. A., Milenkovski, N., Henderson, M. A., John, L. B., Allard, B., Loi, S., et al. (2015). Adenosine receptor 2A blockade increases the efficacy of anti-PD-1 through enhanced antitumor T-cell responses. *Cancer Immunol. Res.* 3, 506–517. doi: 10.1158/2326-6066.CIR-14-0211

Beavis, P. A., Stagg, J., Darcy, P. K., and Smyth, M. J. (2012). CD73: a potent suppressor of antitumor immune responses. *Trends Immunol.* 33, 231–237. doi: 10.1016/j.it.2012.02.009

Bernuzzi, F., Fenoglio, D., Battaglia, F., Fravega, M., Gershwin, M. E., Indiveri, F., et al. (2010). Phenotypical and functional alterations of CD8 regulatory T cells in primary biliary cirrhosis. *J. Autoimmun.* 35, 176–180. doi: 10.1016/j.jaut.2010.06.004

Bhattamisra, S. K., Siang, T. C., Rong, C. Y., Annan, N. C., Sean, E. H. Y., Xi, L. W., et al. (2019). Type-3c diabetes mellitus, diabetes of exocrine pancreas - an update. *Curr. Diabetes Rev.* 15, 382–394. doi: 10.2174/1573399815666190115145702

Blocking CD73 Can Shrink Pancreatic Tumors (2021). American Association for Cancer Research.

Boison, D., and Yegutkin, G. G. (2019). Adenosine metabolism: emerging concepts for cancer therapy. *Cancer Cell* 36, 582–596. doi: 10.1016/j.ccell.2019.10.007

Borea, P. A., Gessi, S., Merighi, S., Vincenzi, F., and Varani, K. (2018). Pharmacology of adenosine receptors: the state of the art. *Physiol. Rev.* 98, 1591–1625. doi: 10.1152/physrev.00049.2017

Burnstock, G. (2006). Pathophysiology and therapeutic potential of purinergic signaling. *Pharmacol. Rev.* 58, 58–86. doi: 10.1124/pr.58.1.5

Burnstock, G., and Novak, I. (2012). Purinergic signalling in the pancreas in health and disease. *J. Endocrinol.* 213, 123–141. doi: 10.1530/JOE-11-0434

Burnstock, G., Vaughn, B., and Robson, S. C. (2014). Purinergic signalling in the liver in health and disease. *Purinergic Signal* 10, 51–70. doi: 10.1007/s11302-013-9398-8

Carter, C. J., Mekkawy, A. H., and Morris, D. L. (2021). Role of human nucleoside transporters in pancreatic cancer and chemoresistance. *World J. Gastroenterol.* 27, 6844–6860. doi: 10.3748/wjg.v27.i40.6844

Chen, Q., Pu, N., Yin, H., Zhang, J., Zhao, G., Lou, W., et al. (2020). CD73 acts as a prognostic biomarker and promotes progression and immune escape in pancreatic cancer. *J. Cell. Mol. Med.* 24, 8674–8686. doi: 10.1111/jcmm.15500

Chiu, D. K., Tse, A. P., Xu, I. M., Di Cui, J., Lai, R. K., Li, L. L., et al. (2017). Hypoxia inducible factor HIF-1 promotes myeloid-derived suppressor cells accumulation through ENTPD2/CD39L1 in hepatocellular carcinoma. *Nat. Commun.* 8:517. doi: 10.1038/s41467-017-00530-7

Choi, J. H., Ji, Y. G., and Lee, D. H. (2013). Uridine triphosphate increases proliferation of human cancerous pancreatic duct epithelial cells by activating P2Y2 receptor. *Pancreas* 42, 680–686. doi: 10.1097/MPA.0b013e318271bb4b

Colgan, S. P. (2015). Neutrophils and inflammatory resolution in the mucosa. *Semin. Immunol.* 27, 177–183. doi: 10.1016/j.smim.2015.03.007

Cruz-Monserrate, Z., Gumpper, K., Pita, V., Hart, P. A., Forsmark, C., Whitcomb, D. C., et al. (2021). Biomarkers of chronic pancreatitis: a systematic literature review. *Pancreatology* 21, 323–333. doi: 10.1016/j.pan.2021.01.006

Deaglio, S., and Robson, S. C. (2011). Ectonucleotidases as regulators of purinergic signaling in thrombosis, inflammation, and immunity. *Adv. Pharmacol.* 61, 301–332. doi: 10.1016/B978-0-12-385526-8.00010-2

Di Virgilio, F., Sarti, A. C., and Coutinho-Silva, R. (2020). Purinergic signaling, DAMPs, and inflammation. *Am. J. Phys. Cell Physiol.* 318, C832–C835. doi: 10.1152/ajpcell.00053.2020

Di Virgilio, F., Sarti, A. C., Falzoni, S., De Marchi, E., and Adinolfi, E. (2018a). Extracellular ATP and P2 purinergic signalling in the tumour microenvironment. *Nat. Rev. Cancer* 18, 601–618. doi: 10.1038/s41568-018-0037-0

Di Virgilio, F., Schmalzing, G., and Markwardt, F. (2018b). The elusive P2X7 macropore. *Trends Cell Biol.* 28, 392–404. doi: 10.1016/j.tcb.2018.01.005

Dixit, A., Cheema, H., George, J., Iyer, S., Dudeja, V., Dawra, R., et al. (2019). Extracellular release of ATP promotes systemic inflammation during acute pancreatitis. *Am. J. Physiol. Gastrointest. Liver Physiol.* 317, G463–G475. doi: 10.1152/ajpgi.00395.2018

Dvorak, H. F. (1986). Tumors: wounds that do not heal. Similarities between tumor stroma generation and wound healing. *N. Engl. J. Med.* 315, 1650–1659. doi: 10.1056/NEJM198612253152606

Eltzschig, H. K., Abdulla, P., Hoffman, E., Hamilton, K. E., Daniels, D., Schönfeld, C., et al. (2005). HIF-1-dependent repression of equilibrative nucleoside transporter (ENT) in hypoxia. *J. Exp. Med.* 202, 1493–1505. doi: 10.1084/jem.20050177

Eltzschig, H. K., Sitkovsky, M. V., and Robson, S. C. (2012). Purinergic signaling during inflammation. *N. Engl. J. Med.* 367, 2322–2333. doi: 10.1056/NEJMra1205750

Farrell, J. J., Elsaleh, H., Garcia, M., Lai, R., Ammar, A., Regine, W. F., et al. (2009). Human equilibrative nucleoside transporter 1 levels predict response to gemcitabine in patients with pancreatic cancer. *Gastroenterology* 136, 187–195. doi: 10.1053/j.gastro.2008.09.067

Franco, R., Cordomí, A., Llinas Del Torrent, C., Lillo, A., Serrano-Marín, J., Navarro, G., et al. (2021). Structure and function of adenosine receptor heteromers. *Cell. Mol. Life Sci.* 78, 3957–3968. doi: 10.1007/s00018-021-03761-6

Giannuzzo, A., Saccomano, M., Napp, J., Ellegaard, M., Alves, F., and Novak, I. (2016). Targeting of the P2X7 receptor in pancreatic cancer and stellate cells. *Int. J. Cancer* 139, 2540–2552. doi: 10.1002/ijc.30380

Godoy, V., Banales, J. M., Medina, J. F., and Pastor-Anglada, M. (2014). Functional crosstalk between the adenosine transporter CNT3 and purinergic receptors in the biliary epithelia. *J. Hepatol.* 61, 1337–1343. doi: 10.1016/j.jhep.2014.06.036

Gong, Y., Xue, J., Yang, Z., Zhu, W., Lu, F., Yan, C., et al. (2021). Reduced proportion of CD39+ treg cells correlates with the development of primary biliary cholangitis in patients and a murine model. *J. Alter. Complement. Integr. Med.* 7. doi: 10.24966/ACIM-7562/100180

Gorzalczany, Y., Akiva, E., Klein, O., Merimsky, O., and Sagi-Eisenberg, R. (2017). Mast cells are directly activated by contact with cancer cells by a mechanism involving autocrine formation of adenosine and autocrine/paracrine signaling of the adenosine A3 receptor. *Cancer Lett.* 397, 23–32. doi: 10.1016/j.canlet.2017.03.026

Greten, F. R., and Grivennikov, S. I. (2019). Inflammation and cancer: triggers, mechanisms, and consequences. *Immunity* 51, 27–41. doi: 10.1016/j.immuni.2019.06.025

Guarino, M. P., Cocca, S., Altomare, A., Emerenziani, S., and Cicala, M. (2013). Ursodeoxycholic acid therapy in gallbladder disease, a story not yet completed. *World J. Gastroenterol.* 19, 5029–5034. doi: 10.3748/wjg.v19.i31.5029

Hansen, M. R., Krabbe, S., and Novak, I. (2008). Purinergic receptors and calcium signalling in human pancreatic duct cell lines. *Cell. Physiol. Biochem.* 22, 157–168. doi: 10.1159/000149793

Harkat, M., Peverini, L., Cerdan, A. H., Dunning, K., Beudez, J., Martz, A., et al. (2017). On the permeation of large organic cations through the pore

of ATP-gated P2X receptors. *Proc. Natl. Acad. Sci. U. S. A.* 114, E3786–E3795. doi: 10.1073/pnas.1701379114

Hart, P. A., Bellin, M. D., Andersen, D. K., Bradley, D., Cruz-Monserrate, Z., Forsmark, C. E., et al. (2016). Type 3c (pancreatogenic) diabetes mellitus secondary to chronic pancreatitis and pancreatic cancer. *Lancet Gastroenterol. Hepatol.* 1, 226–237. doi: 10.1016/S2468-1253(16)30106-6

Hart, P. A., and Conwell, D. L. (2020). Chronic pancreatitis: managing a difficult disease. *Am. J. Gastroenterol.* 115, 49–55. doi: 10.14309/ajg.0000000000000421

Hart, M. L., Gorzolla, I. C., Schittenhelm, J., Robson, S. C., and Eltzschig, H. K. (2010). SP1-dependent induction of CD39 facilitates hepatic ischemic preconditioning. *J. Immunol.* 184, 4017–4024. doi: 10.4049/jimmunol.0901851

Hassanian, S. M., Dinarvand, P., and Rezaie, A. R. (2014). Adenosine regulates the proinflammatory signaling function of thrombin in endothelial cells. *J. Cell. Physiol.* 229, 1292–1300. doi: 10.1002/jcp.24568

Hatfield, S. M., Kjaergaard, J., Lukashev, D., Belikoff, B., Schreiber, T. H., Sethumadhavan, S., et al. (2014). Systemic oxygenation weakens the hypoxia and hypoxia inducible factor 1α-dependent and extracellular adenosine-mediated tumor protection. *J. Mol. Med.* 92, 1283–1292. doi: 10.1007/s00109-014-1189-3

Hatfield, S. M., Kjaergaard, J., Lukashev, D., Schreiber, T. H., Belikoff, B., Abbott, R., et al. (2015). Immunological mechanisms of the antitumor effects of supplemental oxygenation. *Sci. Transl. Med.* 7:277ra30. doi: 10.1126/scitranslmed.aaa1260

Hatfield, S. M., and Sitkovsky, M. V. (2020). Antihypoxic oxygenation agents with respiratory hyperoxia to improve cancer immunotherapy. *J. Clin. Invest.* 130, 5629–5637. doi: 10.1172/JCI137554

Hay, C. M., Sult, E., Huang, Q., Mulgrew, K., Fuhrmann, S. R., McGlinchey, K. A., et al. (2016). Targeting CD73 in the tumor microenvironment with MEDI9447. *Oncoimmunology* 5:e1208875. doi: 10.1080/2162402X.2016.1208875

Hayashi, M. (2019). Expression of adenosine receptors in rodent pancreas. *Int. J. Mol. Sci.* 20:5329. doi: 10.3390/ijms20215329

Hayashi, M., Inagaki, A., Novak, I., and Matsuda, H. (2016). The adenosine A2B receptor is involved in anion secretion in human pancreatic duct Capan-1 epithelial cells. *Pflugers Arch.* 468, 1171–1181. doi: 10.1007/s00424-016-1806-9

Hayes, G. M., Cairns, B., Levashova, Z., Chinn, L., Perez, M., Theunissen, J. W., et al. (2015). CD39 is a promising therapeutic antibody target for the treatment of soft tissue sarcoma. *Am. J. Transl. Res.* 7, 1181–1188.

Hendley, A. M., Wang, Y. J., Polireddy, K., Alsina, J., Ahmed, I., Lafaro, K. J., et al. (2016). p120 catenin suppresses basal epithelial cell extrusion in invasive pancreatic neoplasia. *Cancer Res.* 76, 3351–3363. doi: 10.1158/0008-5472.CAN-15-2268

Hu, L. P., Zhang, X. X., Jiang, S. H., Tao, L. Y., Li, Q., Zhu, L. L., et al. (2019). Targeting purinergic receptor P2Y2 prevents the growth of pancreatic ductal adenocarcinoma by inhibiting cancer cell glycolysis. *Clin. Cancer Res.* 25, 1318–1330. doi: 10.1158/1078-0432.CCR-18-2297

Ide, R., Oshita, A., Nishisaka, T., Nakahara, H., Aimitsu, S., and Itamoto, T. (2017). Primary biliary cholangitis metachronously complicated with combined hepatocellular carcinoma-cholangiocellular carcinoma and hepatocellular carcinoma. *World J. Hepatol.* 9, 1378–1384. doi: 10.4254/wjh.v9.i36.1378

Idzko, M., Ferrari, D., and Eltzschig, H. K. (2014). Nucleotide signalling during inflammation. *Nature* 509, 310–317. doi: 10.1038/nature13085

Illés, D., Iványi, E., Holzinger, G., Kosár, K., Adam, M. G., Kamlage, B., et al. (2020). New onset of DiabetEs in aSsociation with pancreatic ductal adenocarcinoma (NODES trial): protocol of a prospective, multicentre observational trial. *BMJ Open* 10:e037267. doi: 10.1136/bmjopen-2020-037267

Kjaergaard, J., Hatfield, S., Jones, G., Ohta, A., and Sitkovsky, M. (2018). A. *J. Immunol.* 201, 782–791. doi: 10.4049/jimmunol.1700850

Künzli, B. M., Berberat, P. O., Giese, T., Csizmadia, E., Kaczmarek, E., Baker, C., et al. (2007). Upregulation of CD39/NTPDases and P2 receptors in human pancreatic disease. *Am. J. Physiol. Gastrointest. Liver Physiol.* 292, G223–G230. doi: 10.1152/ajpgi.00259.2006

Künzli, B. M., Nuhn, P., Enjyoji, K., Banz, Y., Smith, R. N., Csizmadia, E., et al. (2008). Disordered pancreatic inflammatory responses and inhibition of fibrosis in CD39-null mice. *Gastroenterology* 134, 292–305. doi: 10.1053/j.gastro.2007.10.030

Lan, R. Y., Cheng, C., Lian, Z. X., Tsuneyama, K., Yang, G. X., Moritoki, Y., et al. (2006). Liver-targeted and peripheral blood alterations of regulatory T cells in primary biliary cirrhosis. *Hepatology* 43, 729–737. doi: 10.1002/hep.21123

Lara, R., Adinolfi, E., Harwood, C. A., Philpott, M., Barden, J. A., Di Virgilio, F., et al. (2020). P2X7 in cancer: from molecular mechanisms to therapeutics. *Front. Pharmacol.* 11:793. doi: 10.3389/fphar.2020.00793

Lee, K. E., Spata, M., Bayne, L. J., Buza, E. L., Durham, A. C., Allman, D., et al. (2016). Hif1a deletion reveals pro-neoplastic function of B cells in pancreatic neoplasia. *Cancer Discov.* 6, 256–269. doi: 10.1158/2159-8290.CD-15-0822

Lertsuwan, J., and Ruchirawat, M. (2017). Inhibitory effects of ATP and adenosine on cholangiocarcinoma cell proliferation and motility. *Anticancer Res.* 37, 3553–3561. doi: 10.21873/anticanres.11725

Li, X., Berg, N. K., Mills, T., Zhang, K., Eltzschig, H. K., and Yuan, X. (2020). Adenosine at the interphase of hypoxia and inflammation in lung injury. *Front. Immunol.* 11:604944. doi: 10.3389/fimmu.2020.604944

Li, X. Y., Moesta, A. K., Xiao, C., Nakamura, K., Casey, M., Zhang, H., et al. (2019). Targeting CD39 in cancer reveals an extracellular ATP- and inflammasome-driven tumor immunity. *Cancer Discov.* 9, 1754–1773. doi: 10.1158/2159-8290.CD-19-0541

Longhi, M. S., Feng, L., and Robson, S. C. (2021). Targeting ectonucleotidases to treat inflammation and halt cancer development in the gut. *Biochem. Pharmacol.* 187:114417. doi: 10.1016/j.bcp.2021.114417

Longhi, M. S., Moss, A., Jiang, Z. G., and Robson, S. C. (2017). Purinergic signaling during intestinal inflammation. *J. Mol. Med.* 95, 915–925. doi: 10.1007/s00109-017-1545-1

Mager, L. F., Burkhard, R., Pett, N., Cooke, N. C. A., Brown, K., Ramay, H., et al. (2020). Microbiome-derived inosine modulates response to checkpoint inhibitor immunotherapy. *Science* 369, 1481–1489. doi: 10.1126/science.abc3421

Magistroni, R., Mangolini, A., Guzzo, S., Testa, F., Rapanà, M. R., Mignani, R., et al. (2019). TRPP2 dysfunction decreases ATP-evoked calcium, induces cell aggregation and stimulates proliferation in T lymphocytes. *BMC Nephrol.* 20:355. doi: 10.1186/s12882-019-1540-6

Majumder, S., and Chari, S. T. (2016). Chronic pancreatitis. *Lancet* 387, 1957–1966. doi: 10.1016/S0140-6736(16)00097-0

Martins, I., Tesniere, A., Kepp, O., Michaud, M., Schlemmer, F., Senovilla, L., et al. (2009). Chemotherapy induces ATP release from tumor cells. *Cell Cycle* 8, 3723–3728. doi: 10.4161/cc.8.22.10026

Mascanfroni, I. D., Takenaka, M. C., Yeste, A., Patel, B., Wu, Y., Kenison, J. E., et al. (2015). Metabolic control of type 1 regulatory T cell differentiation by AHR and HIF1-α. *Nat. Med.* 21, 638–646. doi: 10.1038/nm.3868

Mayerle, J., Sendler, M., Hegyi, E., Beyer, G., Lerch, M. M., and Sahin-Tóth, M. (2019). Genetics, cell biology, and pathophysiology of pancreatitis. *Gastroenterology* 156, 1951.e1–1968.e1. doi: 10.1053/j.gastro.2018.11.081

Miller, S. L., and Urey, H. C. (1959). Organic compound synthesis on the primitive earth. *Science* 130, 245–251.

Mittal, D., Young, A., Stannard, K., Yong, M., Teng, M. W., Allard, B., et al. (2014). Antimetastatic effects of blocking PD-1 and the adenosine A2A receptor. *Cancer Res.* 74, 3652–3658. doi: 10.1158/0008-5472.CAN-14-0957

Moesta, A. K., Li, X. Y., and Smyth, M. J. (2020). Targeting CD39 in cancer. *Nat. Rev. Immunol.* 20, 739–755. doi: 10.1038/s41577-020-0376-4

Nakano, Y., Tanno, S., Koizumi, K., Nishikawa, T., Nakamura, K., Minoguchi, M., et al. (2007). Gemcitabine chemoresistance and molecular markers associated with gemcitabine transport and metabolism in human pancreatic cancer cells. *Br. J. Cancer* 96, 457–463. doi: 10.1038/sj.bjc.6603559

Navarro, G., Cordomí, A., Brugarolas, M., Moreno, E., Aguinaga, D., Pérez-Benito, L., et al. (2018). Cross-communication between G i and G s in a G-protein-coupled receptor heterotetramer guided by a receptor C-terminal domain. *BMC Biol.* 16:24. doi: 10.1186/s12915-018-0491-x

North, R. A., and Surprenant, A. (2000). Pharmacology of cloned P2X receptors. *Annu. Rev. Pharmacol. Toxicol.* 40, 563–580. doi: 10.1146/annurev.pharmtox.40.1.563

Novak, I., Yu, H., Magni, L., and Deshar, G. (2020). Purinergic signaling in pancreas-from physiology to therapeutic strategies in pancreatic cancer. *Int. J. Mol. Sci.* 21:8781. doi: 10.3390/ijms21228781

Ohta, A., Gorelik, E., Prasad, S. J., Ronchese, F., Lukashev, D., Wong, M. K., et al. (2006). A2A adenosine receptor protects tumors from antitumor T

cells. *Proc. Natl. Acad. Sci. U. S. A.* 103, 13132–13137. doi: 10.1073/pnas.0605251103

Ohta, A., and Sitkovsky, M. (2001). Role of G-protein-coupled adenosine receptors in downregulation of inflammation and protection from tissue damage. *Nature* 414, 916–920. doi: 10.1038/414916a

Pastor-Anglada, M., and Pérez-Torras, S. (2018). Emerging roles of nucleoside transporters. *Front. Pharmacol.* 9:606. doi: 10.3389/fphar.2018.00606

Pegoraro, A., De Marchi, E., and Adinolfi, E. (2021). P2X7 variants in Oncogenesis. *Cell* 10:189. doi: 10.3390/cells10010189

Peng, Z. W., Rothweiler, S., Wei, G., Ikenaga, N., Liu, S. B., Sverdlov, D. Y., et al. (2017). The ectonucleotidase ENTPD1/CD39 limits biliary injury and fibrosis in mouse models of sclerosing cholangitis. *Hepatol. Commun.* 1, 957–972. doi: 10.1002/hep4.1084

Peter, D., Jin, S. L., Conti, M., Hatzelmann, A., and Zitt, C. (2007). Differential expression and function of phosphodiesterase 4 (PDE4) subtypes in human primary CD4+ T cells: predominant role of PDE4D. *J. Immunol.* 178, 4820–4831. doi: 10.4049/jimmunol.178.8.4820

Pippel, A., Stolz, M., Woltersdorf, R., Kless, A., Schmalzing, G., and Markwardt, F. (2017). Localization of the gate and selectivity filter of the full-length P2X7 receptor. *Proc. Natl. Acad. Sci. U. S. A.* 114, E2156–E2165. doi: 10.1073/pnas.1610414114

Qadir, M. M. F., Álvarez-Cubela, S., Klein, D., Lanzoni, G., García-Santana, C., Montalvo, A., et al. (2018). P2RY1/ALK3-expressing cells within the adult human exocrine pancreas are BMP-7 expandable and exhibit progenitor-like characteristics. *Cell Rep.* 22, 2408–2420. doi: 10.1016/j.celrep.2018.02.006

Razumilava, N., Gores, G. J., and Lindor, K. D. (2011). Cancer surveillance in patients with primary sclerosing cholangitis. *Hepatology* 54, 1842–1852. doi: 10.1002/hep.24570

Rhim, A. D., Mirek, E. T., Aiello, N. M., Maitra, A., Bailey, J. M., McAllister, F., et al. (2012). EMT and dissemination precede pancreatic tumor formation. *Cell* 148, 349–361. doi: 10.1016/j.cell.2011.11.025

Rhim, A. D., Thege, F. I., Santana, S. M., Lannin, T. B., Saha, T. N., Tsai, S., et al. (2014). Detection of circulating pancreas epithelial cells in patients with pancreatic cystic lesions. *Gastroenterology* 146, 647–651. doi: 10.1053/j.gastro.2013.12.007

Riquelme, E., Zhang, Y., Zhang, L., Montiel, M., Zoltan, M., Dong, W., et al. (2019). Tumor microbiome diversity and composition influence pancreatic cancer outcomes. *Cell* 178, 795.e12–806.e12. doi: 10.1016/j.cell.2019.07.008

Rose, J. B., Naydenova, Z., Bang, A., Ramadan, A., Klawitter, J., Schram, K., et al. (2011). Absence of equilibrative nucleoside transporter 1 in ENT1 knockout mice leads to altered nucleoside levels following hypoxic challenge. *Life Sci.* 89, 621–630. doi: 10.1016/j.lfs.2011.08.007

Rothweiler, S., Feldbrügge, L., Jiang, Z. G., Csizmadia, E., Longhi, M. S., Vaid, K., et al. (2019). Selective deletion of ENTPD1/CD39 in macrophages exacerbates biliary fibrosis in a mouse model of sclerosing cholangitis. *Purinergic Signal* 15, 375–385. doi: 10.1007/s11302-019-09664-3

Saluja, A., Dudeja, V., Dawra, R., and Sah, R. P. (2019). Early intra-acinar events in pathogenesis of pancreatitis. *Gastroenterology* 156, 1979–1993. doi: 10.1053/j.gastro.2019.01.268

Saluja, A., and Maitra, A. (2019). Pancreatitis and pancreatic cancer. *Gastroenterology* 156, 1937–1940. doi: 10.1053/j.gastro.2019.03.050

Sandhu, B., Perez-Matos, M. C., Tran, S., Singhal, G., Syed, I., Feldbrügge, L., et al. (2021). Global deletion of NTPDase3 protects against diet-induced obesity by increasing basal energy metabolism. *Metabolism* 118:154731. doi: 10.1016/j.metabol.2021.154731

Santini, D., Schiavon, G., Vincenzi, B., Cass, C. E., Vasile, E., Manazza, A. D., et al. (2011). Human equilibrative nucleoside transporter 1 (hENT1) levels predict response to gemcitabine in patients with biliary tract cancer (BTC). *Curr. Cancer Drug Targets* 11, 123–129. doi: 10.2174/156800911793743600

Sciarra, A., Monteiro, I., Ménétrier-Caux, C., Caux, C., Gilbert, B., Halkic, N., et al. (2019). CD73 expression in normal and pathological human hepatobiliopancreatic tissues. *Cancer Immunol. Immunother.* 68, 467–478. doi: 10.1007/s00262-018-2290-1

Sendler, M., Weiss, F. U., Golchert, J., Homuth, G., van den Brandt, C., Mahajan, U. M., et al. (2018). Cathepsin B-mediated activation of trypsinogen in endocytosing macrophages increases severity of pancreatitis in mice. *Gastroenterology* 154, 704.e10–718.e10. doi: 10.1053/j.gastro.2017.10.018

Seo, J. B., Jung, S. R., Hille, B., and Koh, D. S. (2016). Extracellular ATP protects pancreatic duct epithelial cells from alcohol-induced damage through P2Y1 receptor-cAMP signal pathway. *Cell Biol. Toxicol.* 32, 229–247. doi: 10.1007/s10565-016-9331-3

Shevchenko, I., Mathes, A., Groth, C., Karakhanova, S., Müller, V., Utikal, J., et al. (2020). Enhanced expression of CD39 and CD73 on T cells in the regulation of anti-tumor immune responses. *Oncoimmunology* 9:1744946. doi: 10.1080/2162402X.2020.1744946

Singh, K., Faraoni, E. Y., Dai, Y., Vidhi, C., Vucic, E., Mills, T., et al. (2021). Pancreatic cancer ductal cell of origin drives CD73-dependent generation of immunosuppressive adenosine. *bioRxiv* [preprint]. doi: 10.1101/2021.11.29.470415

Singh, V. K., Yadav, D., and Garg, P. K. (2019). Diagnosis and management of chronic pancreatitis: a review. *JAMA* 322, 2422–2434. doi: 10.1001/jama.2019.19411

Sitkovsky, M. V. (2009). T regulatory cells: hypoxia-adenosinergic suppression and re-direction of the immune response. *Trends Immunol.* 30, 102–108. doi: 10.1016/j.it.2008.12.002

Stecula, A., Schlessinger, A., Giacomini, K. M., and Sali, A. (2017). Human concentrative nucleoside transporter 3 (hCNT3, SLC28A3) forms a cyclic homotrimer. *Biochemistry* 56, 3475–3483. doi: 10.1021/acs.biochem.7b00339

Sun, X., Wu, Y., Gao, W., Enjyoji, K., Csizmadia, E., Müller, C. E., et al. (2010). CD39/ENTPD1 expression by CD4+Foxp3+ regulatory T cells promotes hepatic metastatic tumor growth in mice. *Gastroenterology* 139, 1030–1040. doi: 10.1053/j.gastro.2010.05.007

Synnestvedt, K., Furuta, G. T., Comerford, K. M., Louis, N., Karhausen, J., Eltzschig, H. K., et al. (2002). Ecto-5′-nucleotidase (CD73) regulation by hypoxia-inducible factor-1 mediates permeability changes in intestinal epithelia. *J. Clin. Invest.* 110, 993–1002. doi: 10.1172/JCI0215337

Tripathi, A., Debelius, J., Brenner, D. A., Karin, M., Loomba, R., Schnabl, B., et al. (2018). The gut-liver axis and the intersection with the microbiome. *Nat. Rev. Gastroenterol. Hepatol.* 15, 397–411. doi: 10.1038/s41575-018-0011-z

Vieira, C., Magalhães-Cardoso, M. T., Ferreirinha, F., Silva, I., Dias, A. S., Pelletier, J., et al. (2014). Feed-forward inhibition of CD73 and upregulation of adenosine deaminase contribute to the loss of adenosine neuromodulation in postinflammatory ileitis. *Mediat. Inflamm.* 2014:254640. doi: 10.1155/2014/254640

Vuerich, M., Mukherjee, S., Robson, S. C., and Longhi, M. S. (2020). Control of gut inflammation by modulation of purinergic signaling. *Front. Immunol.* 11:1882. doi: 10.3389/fimmu.2020.01882

Wang, W., Chen, N. Y., Ren, D., Davies, J., Philip, K., Eltzschig, H. K., et al. (2021a). Enhancing extracellular adenosine levels restores barrier function in acute lung injury through expression of focal adhesion proteins. *Front. Mol. Biosci.* 8:636678. doi: 10.3389/fmolb.2021.636678

Wang, X., Hu, L. P., Qin, W. T., Yang, Q., Chen, D. Y., Li, Q., et al. (2021b). Identification of a subset of immunosuppressive P2RX1-negative neutrophils in pancreatic cancer liver metastasis. *Nat. Commun.* 12:174. doi: 10.1038/s41467-020-20447-y

Wang, X., Liu, D., Qin, W., Liu, Y., Yuan, X., Zhang, X., et al. (2020). P2RX1-involved glycolytic metabolism supports neutrophil activation in acute pancreatitis. *Front. Immunol.* 11:549179. doi: 10.3389/fimmu.2020.549179

Wei, Q., Qi, L., Lin, H., Liu, D., Zhu, X., Dai, Y., et al. (2020). Pathological mechanisms in diabetes of the exocrine pancreas: what's known and what's to know. *Front. Physiol.* 11:570276. doi: 10.3389/fphys.2020.570276

Weitz, J. R., Jacques-Silva, C., Qadir, M. M. F., Umland, O., Pereira, E., Qureshi, F., et al. (2020). Secretory functions of macrophages in the human pancreatic islet are regulated by endogenous purinergic signaling. *Diabetes* 69, 1206–1218. doi: 10.2337/db19-0687

Wiginton, D. A., Coleman, M. S., and Hutton, J. J. (1981). Purification, characterization and radioimmunoassay of adenosine deaminase from human leukaemic granulocytes. *Biochem. J.* 195, 389–397. doi: 10.1042/bj1950389

Xiao, A. Y., Tan, M. L., Wu, L. M., Asrani, V. M., Windsor, J. A., Yadav, D., et al. (2016). Global incidence and mortality of pancreatic diseases: a systematic review, meta-analysis, and meta-regression of population-based cohort studies. *Lancet Gastroenterol. Hepatol.* 1, 45–55. doi: 10.1016/S2468-1253(16)30004-8

Xu, Y. P., Zhou, Y. Q., Zhao, Y. J., Zhao, Y., Wang, F., Huang, X. Y., et al. (2021). High level of CD73 predicts poor prognosis of intrahepatic cholangiocarcinoma. *J. Cancer* 12, 4655–4660. doi: 10.7150/jca.51038

Yachida, S., Jones, S., Bozic, I., Antal, T., Leary, R., Fu, B., et al. (2010). Distant metastasis occurs late during the genetic evolution of pancreatic cancer. *Nature* 467, 1114–1117. doi: 10.1038/nature09515

Young, A., Ngiow, S. F., Barkauskas, D. S., Sult, E., Hay, C., Blake, S. J., et al. (2016). Co-inhibition of CD73 and A2AR adenosine signaling improves anti-tumor immune responses. *Cancer Cell* 30, 391–403. doi: 10.1016/j.ccell.2016.06.025

Yu, A., Zhao, L., Kang, Q., Li, J., Chen, K., and Fu, H. (2020). Transcription factor HIF1α promotes proliferation, migration, and invasion of cholangiocarcinoma via long noncoding RNA H19/microRNA-612/Bcl-2 axis. *Transl. Res.* 224, 26–39. doi: 10.1016/j.trsl.2020.05.010

Zaccagnino, A., Pilarsky, C., Tawfik, D., Sebens, S., Trauzold, A., Novak, I., et al. (2016). In silico analysis of the transportome in human pancreatic ductal adenocarcinoma. *Eur. Biophys. J.* 45, 749–763. doi: 10.1007/s00249-016-1171-9

Zhao, J., Soto, L. M. S., Wang, H., Katz, M. H., Prakash, L. R., Kim, M., et al. (2021). Overexpression of CD73 in pancreatic ductal adenocarcinoma is associated with immunosuppressive tumor microenvironment and poor survival. *Pancreatology* 21, 942–949. doi: 10.1016/j.pan.2021.03.018

Conflict of Interest: SCR is a scientific founder of Purinomia Biotech Inc and has consulted for eGenesis. AbbVie and SynLogic Inc; his interests are reviewed and managed by HMFP and Beth Israel Deaconess Medical Center in accordance with the conflict-of-interest policies.

The remaining authors declare that the research was conducted in the absence of any commercial or financial relationships that could be construed as a potential conflict of interest.

Publisher's Note: All claims expressed in this article are solely those of the authors and do not necessarily represent those of their affiliated organizations, or those of the publisher, the editors and the reviewers. Any product that may be evaluated in this article, or claim that may be made by its manufacturer, is not guaranteed or endorsed by the publisher.

frontiers in Physiology

ORIGINAL RESEARCH
published: 31 March 2022
doi: 10.3389/fphys.2022.819606

Pancreas Fat, an Early Marker of Metabolic Risk? A Magnetic Resonance Study of Chinese and Caucasian Women: TOFI_Asia Study

Ivana R. Sequeira[1,2], Wilson C. Yip[1,2], Louise W. W. Lu[1,2], Yannan Jiang[3], Rinki Murphy[2,4,5,6], Lindsay D. Plank[7], Garth J. S. Cooper[4,8,9,10], Carl N. Peters[4,11], Jun Lu[12], Kieren G. Hollingsworth[13] and Sally D. Poppitt[1,2,4,9,14]*

[1] Human Nutrition Unit, Faculty of Science, School of Biological Sciences, University of Auckland, Auckland, New Zealand, [2] High Value Nutrition National Science Challenge, Auckland, New Zealand, [3] Department of Statistics, Faculty of Science, University of Auckland, Auckland, New Zealand, [4] Department of Medicine, Faculty of Medical and Health Sciences, University of Auckland, Auckland, New Zealand, [5] Auckland District Health Board, Auckland, New Zealand, [6] Maurice Wilkins Centre for Molecular Biodiscovery, University of Auckland, Auckland, New Zealand, [7] Department of Surgery, Faculty of Medical and Health Sciences, University of Auckland, Auckland, New Zealand, [8] Centre for Advanced Discovery and Experimental Therapeutics (CADET), Division of Cardiovascular Sciences, Faculty of Biology, Medicine and Health, University of Manchester, Manchester, United Kingdom, [9] Faculty of Science, School of Biological Sciences, University of Auckland, Auckland, New Zealand, [10] Division of Medical Sciences, Department of Pharmacology, University of Oxford, Oxford, United Kingdom, [11] Waitemata District Health Board, Auckland, New Zealand, [12] Faculty of Health and Environmental Sciences, Auckland University of Technology, Auckland, New Zealand, [13] Translational and Clinical Research Institute, Faculty of Medical Sciences, Newcastle University, Newcastle upon Tyne, United Kingdom, [14] Riddet Centre of Research Excellence for Food and Nutrition, Palmerston North, New Zealand

OPEN ACCESS

Edited by:
Natalie Luhtala,
Salk Institute for Biological Studies,
United States

Reviewed by:
Dominik H. Pesta,
German Aerospace Center (DLR),
Germany
Albrecht Ingo Schmid,
Medical University of Vienna, Austria

***Correspondence:**
Ivana R. Sequeira
i.sequeira@auckland.ac.nz
orcid.org/0000-0001-5414-9925

Specialty section:
This article was submitted to Gastrointestinal Sciences, a section of the journal Frontiers in Physiology

Received: 21 November 2021
Accepted: 17 February 2022
Published: 31 March 2022

Citation:
Sequeira IR, Yip WC, Lu LWW, Jiang Y, Murphy R, Plank LD, Cooper GJS, Peters CN, Lu J, Hollingsworth KG and Poppitt SD (2022) Pancreas Fat, an Early Marker of Metabolic Risk? A Magnetic Resonance Study of Chinese and Caucasian Women: TOFI_Asia Study. Front. Physiol. 13:819606. doi: 10.3389/fphys.2022.819606

Objective: Prevalence of type 2 diabetes (T2D) is disproportionately higher in younger outwardly lean Asian Chinese compared to matched Caucasians. Susceptibility to T2D is hypothesised due to dysfunctional adipose tissue expansion resulting in adverse abdominal visceral and organ fat accumulation. Impact on early risk, particularly in individuals characterised by the thin-on-the-outside-fat-on-the-inside (TOFI) phenotype, is undetermined.

Methods: Sixty-eight women [34 Chinese, 34 Caucasian; 18–70 years; body mass index (BMI), 20–45 kg/m^2] from the TOFI_Asia study underwent magnetic resonance imaging and spectroscopy to quantify visceral, pancreas, and liver fat. Total body fat was (TBF) assessed by dual-energy x-ray absorptiometry, and fasting blood biomarkers were measured. Ethnic comparisons, conducted using two-sample tests and multivariate regressions adjusted for age, % TBF and ethnicity, identified relationships between abdominal ectopic fat depots with fasting plasma glucose (FPG), insulin resistance (HOMA2-IR), and related metabolic clinical risk markers in all, and within ethnic groups.

Results: Despite being younger and of lower bodyweight, Chinese women in the cohort had similar BMI and % TBF compared to their Caucasian counterparts. Protective high-density lipoprotein cholesterol, total- and high-molecular weight adiponectin

were significantly lower, while glucoregulatory glucagon-like peptide-1 and glucagon significantly higher, in Chinese. There were no ethnic differences between % pancreas fat and % liver fat. However, at low BMI, % pancreas and % liver fat were ∼1 and ∼2% higher in Chinese compared to Caucasian women. In all women, % pancreas and visceral adipose tissue had the strongest correlation with FPG, independent of age and % TBF. Percentage (%) pancreas fat and age positively contributed to variance in FPG, whereas % TBF, amylin and C-peptide contributed to IR which was 0.3 units higher in Chinese.

Conclusion: Pancreas fat accumulation may be an early adverse event, in TOFI individuals, with peptides highlighting pancreatic dysfunction as drivers of T2D susceptibility. Follow-up is warranted to explore causality.

Keywords: liver fat, pancreas fat, visceral adipose tissue, type 2 diabetes, magnetic resonance imaging and spectroscopy

INTRODUCTION

Individuals with obesity have a 50- to 80-fold increased risk of type 2 diabetes (T2D) compared to those with lean bodyweight (Colditz et al., 1995). A decline in lean body mass and consequent increase in body fat often increases with age (Alva et al., 2017), accompanied by altered beta-cell function and insulin resistance (IR). Using body mass index (BMI) as a predictor, however, is shown to potentially misclassify both low BMI (Reilly et al., 2018) and, on occasion, younger (Ramachandran et al., 2012) individuals. Ethnicity is shown to be of importance since, at a fixed BMI, Chinese individuals are shown to have 3–5% higher total body fat (TBF) than Caucasians (Haldar et al., 2015).

Highlighted in large cohort studies (Lear et al., 2007; Nazare et al., 2012; Chen et al., 2018; Jo and Mainous, 2018), including in our recently published TOFI_Asia study (Sequeira et al., 2020), visceral adipose tissue (VAT) is an important factor that differs between these groups. In Chinese, typified by the thin-on-the-outside-fat-on-the-inside (TOFI) phenotype, even modest weight gain may differentially promote lipid deposition into VAT (Hocking et al., 2013) which is associated with increased hepatic IR (Tchernof and Després, 2013), and further promotes ectopic fat infiltration into key metabolic non-adipose tissue organs such as liver and pancreas (Rossi et al., 2011).

The need for phenotypic characterisation based on non-adipose ectopic fat is now recognised to be vital to understanding susceptibility to developing T2D (Neeland et al., 2019), particularly in TOFI individuals (Sequeira et al., 2020). Decreased levels of liver fat are associated with the normalisation of blood glucose (Lim et al., 2011; Nazare et al., 2012; Zhyzhneuskaya et al., 2018) with emerging evidence for the role of pancreas fat (Lim et al., 2011; Taylor et al., 2018). Some studies have reported increased pancreas fat in dysglycaemic individuals (Lingvay et al., 2009; Ou et al., 2013; Gaborit et al., 2014; Kim et al., 2014; Lim et al., 2014; Wang et al., 2014; Macauley et al., 2015; Steven et al., 2016) while others showed a negative correlation with beta-cell function (Tushuizen et al., 2007; Heni et al., 2010; Lim et al., 2011; Szczepaniak et al., 2012; Yokota et al., 2012; Nowotny et al., 2018) albeit as yet inconsistent in cohorts with prediabetes and diabetes (Tushuizen et al., 2007; Lê et al., 2011; van der Zijl et al., 2011). Discrepancies between pancreatic fat and beta-cell dysfunction may be in part due to methodological differences in pancreas fat assessment, in addition to variable glycaemic status in these early studies. A recent meta-analysis attempted to define an upper limit for pancreatic fat percentage, as weighted mean + 2 standard deviations (SDs), determined from pooled data from nine studies in 1,209 healthy individuals who underwent magnetic resonance imaging and spectroscopy (MRI/S) (Singh et al., 2017). A limitation of the recommended normal upper limit of 6.2% pancreas fat, as acknowledged by the authors, are the different methods and quantitative approaches used in the various MR studies which preclude comparisons.

An absence of published data on ectopic fat, particularly pancreatic fat, in different ethnicities, and its contribution to early dysglycaemia led us to undertake the current TOFI_Asia MR study. We hypothesised that fat deposition in non-adipose ectopic sites may be associated with the dysregulation of glucose, and IR, with Chinese participants potentially more susceptible to ectopic lipid infiltration when younger and at lower bodyweight than Caucasians. Furthermore, to identify clinical risk markers, and ectopic fat depots, that are associated with and predictive of fasting plasma glucose (FPG) and IR. Notably, while haemoglobin A1c (HbA1c) is a reliable marker of frank T2D, it has limited sensitivity and specificity for identifying prediabetes (Barry et al., 2017) and hence was not considered an outcome measure.

MATERIALS AND METHODS

Ethical approval was received from the New Zealand Health and Disabilities Ethics Committee (16/STH/23) and all research, and study protocols, performed in accordance with Committee guidelines. The study is registered with the Australian New Zealand Clinical Trials Registry ACTRN12616000362493.

MR Study Population

To avoid potential confounding due to gender differences in body composition, women (202; 108 Asian Chinese, 94 European

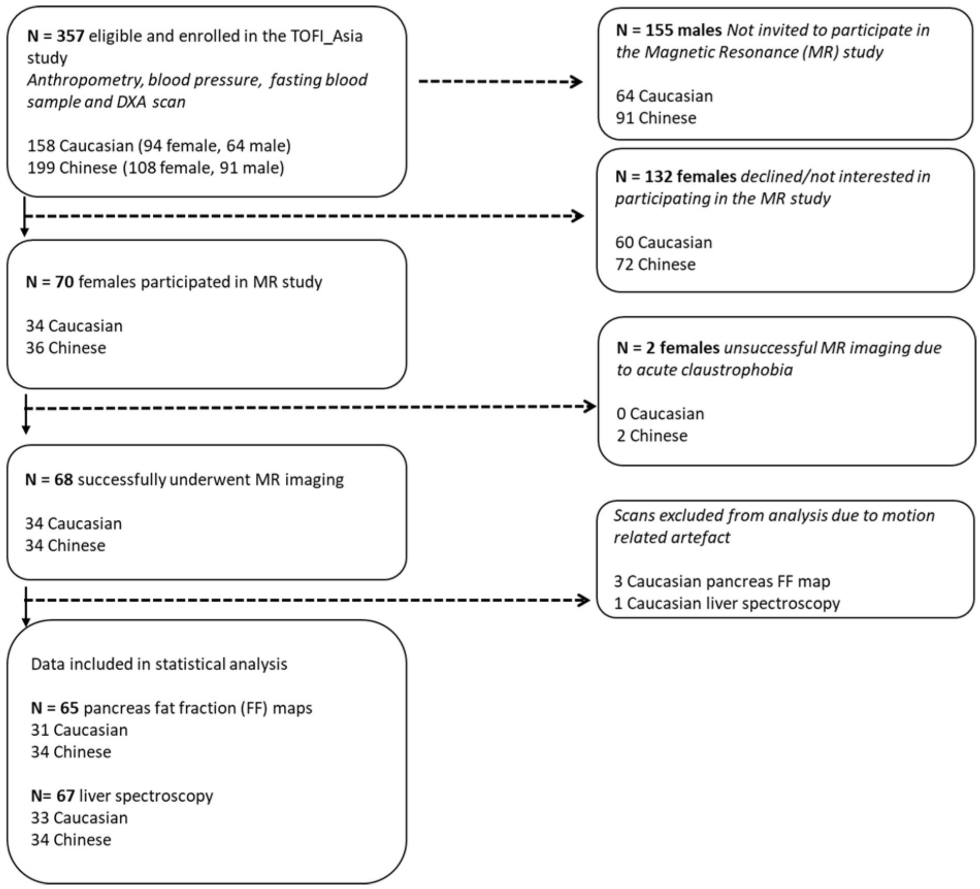

FIGURE 1 | Flowchart illustrating enrolment and eligibility of 202 female participants from the TOFI_Asia study into the MR study. DXA, dual-energy X-ray absorptiometry.

Caucasian) from a larger mixed gender cohort the TOFI_Asia study (Sequeira et al., 2020), recruited in our clinic, were additionally invited for a MRI/S assessment of ectopic visceral, pancreas, and liver fat respectively. The TOFI_Asia cohort consisted of participants over a wide age and BMI range, of which a random cohort of 70 women (20–70 years, BMI 20–45 kg/m^2) provided informed written consent to participate in the current MR sub-study (**Figure 1**). Women were normoglycaemic or had impaired fasting glucose (IFG), as defined by the American Diabetes Association (2018), self-reported healthy with no significant disease, no significant weight gain or loss (>10%) in previous 3 months, and no contraindications for MRI/S procedures. Imaging was successfully completed in 68 women (34 Chinese, 34 Caucasian). Two women were excluded due to acute claustrophobic episodes during MRI.

Experimental Protocol

All women attended the Human Nutrition Unit following an overnight fast. Bodyweight, height, waist/hip circumference, and blood pressure were recorded and fasted blood samples obtained as previously described (Sequeira et al., 2020). TBF was determined by dual-energy X-ray absorptiometry (DXA) (iDXA, GE Healthcare, Madison, WI, United States). MRI/S scans were conducted fasted within 1 week of clinical assessments using a 3T Magnetom Skyra scanner, VE 11A (Siemens, Germany). Instruction for adherence to scan protocol and imaging requirements, e.g., breath hold sequences, were given to minimise motion-related artefact.

Analyses of Blood Biochemistry

Venous samples were centrifuged (Eppendorf, HH, Germany) at 1,300 × *g* for 10 min at 4°C with plasma and serum stored at −80°C until batch analyses. HbA1c was determined by capillary electrophoresis (Cap2FP, IDF, France), FPG by the hexokinase method, alanine amino transferase (ALT), aspartate amino transferase (AST), and alkaline phosphatase (ALP) by the International Federation of Clinical Chemistry methods, and gamma glutamyl transferase (GGT) by the Szasz method. Total cholesterol (TC) was analysed by cholesterol esterase/cholesterol oxidase/peroxidase method, triacylglycerol (TAG) by lipase/glycerol kinase method, high-density lipoprotein cholesterol (HDL-C) by detergent/cholesterol esterase/cholesterol oxidase/peroxidase method. Low-density lipoprotein cholesterol (LDL-C) was calculated using the Friedewald formula. Plasma insulin, C-peptide, glucagon, (total)

amylin, gastric inhibitory peptide (GIP), and (total) glucagon-like peptide-1 (GLP-1) were analysed using MILLIPLEX MAP Human Metabolic Hormone Magnetic Bead Panel (Merck, HE, Germany). Intra- and inter-assay coefficients of variation (CV) for all analytes were <10 and <15%, respectively. Serum total- and high-molecular weight (HMW) adiponectin was measured by enzyme-linked immunosorbent assay (R&D Systems Quantikine kit, Bio-Techne, Minneapolis, MN, United States). IR, using the updated homeostasis model assessment of insulin resistance (HOMA2-IR), was determined by using the online HOMA Calculator (The University of Oxford 2013, Version 2.2.3).

Assessment of Body Composition by Dual-Energy X-Ray Absorptiometry

Total body fat and lean (fat-free soft tissue) masses were obtained from a full body DXA scan with participants measured according to manufacturer's standard protocols. DXA-percentage (%) TBF was calculated as 100 × TBF mass/(total body lean mass + TBF mass).

Assessment of Ectopic Fat by MRI/Magnetic Resonance Spectroscopy

Fast sagittal localising images were acquired from diaphragm to pelvis, using respiratory gating to reduce motion artefacts. A 3D dual gradient-echo sequence (VIBE) was acquired to separate fat and water signals using a 2-point Dixon technique: repetition time/echo times/flip angle = 3.85 ms/1.27, 2.50 ms/9°. Three blocks (11 s breath hold each) of forty 5 mm axial slices using a field of view of 500 mm × 400 mm, matrix 320 × 256, were acquired to cover the abdominal cavity using partial Fourier and parallel imaging with total acceleration factor of 3.1. Following the abdominal scan, the pancreas was located and imaged using a higher resolution sequence, requiring a 11 s breath hold, to acquire fourteen 5 mm axial slices with repetition time/echo times/flip angle/signal averages = 5.82 ms/2.46, 3.69 ms/9°/1 with a field of view of 500 mm × 400 mm, matrix 512 × 410, using partial Fourier and parallel imaging with total acceleration factor of 2.8. MRS with respiratory-gated sequence determined liver fat content. Localiser images were obtained in the transverse, coronal, and sagittal planes and a voxel (2 × 2 × 2 cm^3) placed in the right lobe of the liver, avoiding blood vessels and the biliary tree. MRS of the selected voxel was acquired using the stimulated-echo acquisition mode sequence with respiratory triggering; echo time: 20 ms, repetition time: 3,000 ms and mixing time: 33 ms, 1,024 data points collected with 50 averages. A water-suppressed spectrum with 50 averages was also recorded to detect weak lipid signals.

Magnetic Resonance Imaging and Spectroscopy Image Analysis

Custom Matlab R2017a software (The MathWorks, Inc., Natick, MA, United States) was used to separate the fat and water contributions of the abdominal MRI and construct a fat fraction (FF) map with noise bias correction at the L4–L5 intervertebral disc space. The single FF map was separated into MR-VAT and MR-subcutaneous adipose tissue (SAT) with Image J (Schneider et al., 2012), using the polygon tool to manually circumscribe contours around each region. The single slice MR abdominal adipose tissue (MR-AAT) measurement at the L4–L5 anatomical location is shown to be concordant with fat mass measured at all intervertebral spaces (Schweitzer et al., 2015; Linder et al., 2016). MRI analysis was conducted independently by two trained investigators, IS and WY. The intra-observer repeatability CV for MR-VAT and MR-SAT, conducted by IS calculated from 10% of total scans was 0.2 and 0.1%, respectively, while the inter-observer CV of all scans, between IS and WY, was 0.02 and 0.1%. Percentage (%) pancreas fat was determined by MR-opsy (Al-Mrabeh et al., 2017) with thresholding applied to eliminate potential inclusion of non-parenchymal tissue. Briefly, two candidate pancreas (5 mm each) FF maps were created from images in which the head, body, and tail of the pancreas were clearly visualised. Three regions of interest (ROIs) were placed in the head, body, and tail of each image, respectively, to estimate pancreas fat; thresholding (1–20%) was also applied to eliminate potential inclusion of non-parenchymal tissue within the selected ROI. Percentage pancreas fat was calculated as the average fat of both candidate pancreas FF images [39]. FF maps obtained from three Caucasian women contained artefact and were unable to be analysed, hence % pancreas fat was measured in 65 women. As conducted for MR-AAT compartments, the intra-observer repeatability % pancreas fat CV, from 10% of total scans, was 3.4% and the inter-observer CV was 2.4%. Pancreas volume (cm^3) was determined as previously described (Macauley et al., 2015), and volume divided by body surface area, using the Dubois and Dubois method, to obtain pancreas volume index (PVI) which accounts for potential effect of anthropometry on measurements. Liver fat was calculated, using the SIVIC software (Crane et al., 2013), from area under the curve of water and fat peaks from non-water-suppressed spectra, corrected for T2-weighting according to previous literature values (Hamilton et al., 2011) and presented as percentage volume/volume from 67 women; the spectroscopy signal obtained from one Caucasian woman could not be analysed. Liver fat ≥5.6% was considered elevated, this cut off reported as the upper 95 percentile in healthy subjects that corresponds to ∼15% histological liver fat (Petäjä and Yki-Järvinen, 2016). There is no global comparable cut off for % pancreas fat, particularly since our pancreas imaging in this study has T1 weighting and will overestimate FF by a factor of approximately 1.4 (de Bazelaire et al., 2004). To internally compare % pancreas fat in our cohort of women we used an arbitrary 4.5% cut off.

Statistical Analyses

Continuous variables are expressed as mean ± SD in the descriptive summary. Group comparisons were performed using two-sample tests with level of significance set at $P < 0.05$. The distribution of outcome measures (FPG and HOMA2-IR) was assessed and log-transformation was applied to non-normally distributed data if applicable. Relationships between the two outcome measures with MR-VAT (cm^2), % pancreas and % liver fat were assessed using multiple linear regression models in all women and for each ethnic group separately. The models were adjusted for age and % TBF, as well as ethnicity in the total cohort. The interaction effect between ethnicity and the predictor

TABLE 1 | Summary of metabolic risk factors of women enrolled in the TOFI_Asia MR study.

	All (*n* = 68)	Chinese (*n* = 34)	Caucasian (*n* = 34)	*P* value
Age (year)	44.4 ± 14.5	41.0 ± 13.0	47.8 ± 15.4	0.05
Anthropometry				
Bodyweight (kg)	73.7 ± 13.9	68.5 ± 11.5	79.0 ± 14.2	0.001
Height (m)	1.64 ± 0.08	1.60 ± 0.05	1.68 ± 0.08	<0.0001
BMI (kg/m^2)	27.3 ± 4.4	26.7 ± 4.2	28.0 ± 4.5	0.24
Waist circumference (cm)	88.6 ± 12.9	85.6 ± 11.1	91.7 ± 13.9	0.05
Hip circumference (cm)	101.0 ± 11.8	96.8 ± 9.0	105.3 ± 12.8	0.002
Systolic blood pressure, SBP (mmHg)	120 ± 21	120 ± 22	120 ± 19	0.93
Diastolic blood pressure, DBP (mmHg)	64 ± 10	65 ± 12	64 ± 8	0.61
Body composition – DXA				
Total body fat, DXA-TBF (kg)	29.0 ± 10.0	26.2 ± 7.2	31.8 ± 11.7	0.02
Total body fat, DXA-TBF (%)	39.8 ± 7.6	39.2 ± 4.9	40.4 ± 9.6	0.51
Body composition – MRI/S				
Visceral adipose tissue, MR-VAT (cm^2)	73.2 ± 38.8	70.2 ± 31.2	76.3 ± 45.4	0.52
Subcutaneous adipose tissue, MR-SAT (cm^2)	165.3 ± 65.1	138.7 ± 30.6	191.9 ± 78.8	0.001
Abdominal adipose tissue, MR-AAT (cm^2)	238.5 ± 87.4	208.9 ± 48.7	268.2 ± 106.5	0.004
VAT:SAT ratio	0.445 ± 0.3	0.51 ± 0.2	0.398 ± 0.3	0.46
Pancreas fat (%)[a]	4.2 ± 1.9	4.3 ± 2.0	4.1 ± 1.9	0.69
Liver fat (%)[b]	4.2 ± 4.8	4.6 ± 4.7	3.7 ± 4.8	0.47
Pancreas volume (cm^3)[a]	74.0 ± 19.6	72.9 ± 22.3	75.2 ± 16.4	0.63
Pancreas volume index, PVI[a]	41.5 ± 10.7	42.4 ± 12.0	40.6 ± 9.1	0.49
Blood biochemistry				
HbA1c (mmol/mol)	34.7 ± 3.9	35.5 ± 3.8	33.9 ± 3.9	0.09
Fasting plasma glucose, FPG (mmol/L)	5.1 ± 0.6	5.2 ± 0.5	5.1 ± 0.7	0.52
Fasting plasma insulin (pg/ml)	537.7 ± 363.1	578.1 ± 350.3	497.4 ± 376.4	0.36
HOMA2-IR	1.7 ± 1.1	1.8 ± 1.0	1.6 ± 1.2	0.37
HOMA2-β	129.9 ± 68.3	138.4 ± 78.3	121.4 ± 56.3	0.31
Total cholesterol, TC (mmol/L)	4.8 ± 0.9	4.5 ± 0.9	5.2 ± 0.9	0.004
Triglycerides, TAG (mmol/L)	1.1 ± 0.6	1.3 ± 0.7	1.0 ± 0.5	0.09
HDL-cholesterol (mmol/L)	1.6 ± 0.4	1.4 ± 0.4	1.8 ± 0.4	0.001
LDL-cholesterol (mmol/L)	2.7 ± 0.8	2.5 ± 0.7	2.9 ± 0.9	0.02
TC:HDL-C ratio	3.2 ± 0.8	3.3 ± 0.8	3.0 ± 0.8	0.38
Alanine amino transferase, ALT (U/L)	14.9 ± 10.1	14.7 ± 10.7	15.1 ± 9.6	0.88
Aspartate amino transferase, AST (U/L)	18.8 ± 7.4	17.8 ± 5.4	19.9 ± 90	0.24
Alkaline phosphatase, ALP (U/L)	96.6 ± 27.4	92.9 ± 26.0	100.4 ± 28.6	0.27
Gamma glutamyl transferase, GGT (U/L)	23.1 ± 20.7	26.3 ± 27.1	20.0 ± 10.5	0.21
Amylin (pg/mL)	29.1 ± 13.7	29.9 ± 13.8	28.3 ± 13.8	0.63
C-peptide (pg/mL)	950.9 ± 502.6	918.5 ± 400.0	983.4 ± 592.2	0.60
Gastric inhibitory peptide, GIP (pg/mL)	68.7 ± 37.9	71.5 ± 40.8	66.0 ± 35.2	0.55
Glucagon like peptide-1, GLP-1 (pg/mL)	136.2 ± 45.5	147.6 ± 46.2	124.9 ± 42.4	0.04
Glucagon (pg/mL)	57.9 ± 32.0	65.6 ± 33.1	50.1 ± 29.5	0.05
Total adiponectin (mg/L)	8.5 ± 5.2	6.8 ± 4.9	10.2 ± 5.0	0.006
HMW adiponectin (mg/L)	6.1 ± 3.9	4.8 ± 3.6	7.5 ± 3.9	0.005

Results are mean ± SD. Statistical significance P < 0.05. Numbers as stated above each column except for superscripted values.
[a] *Pancreas fat assessed in 31 Caucasian women.*
[b] *Liver fat assessed in 33 Caucasian women.*
DXA, dual-energy x-ray absorptiometry; MRI/S, magnetic resonance imaging and spectroscopy; HbA1c, haemoglobin A1c; HOMA2-IR, homeostasis model assessment of insulin resistance; HOMA2-β, homeostasis model assessment of β-cell function; HMW, high-molecular weight.

of interest was tested in the models to assess ethnicity as a potential effect modifier. All MR quantified non-adipose tissue organ fat measurements were included in statistical analyses, as no outliers were detected. Of the two outcome variables, analyses were conducted on raw FPG data while HOMA2-IR was normalised using log-transformation due to skewed distribution. Univariate and multivariate regression analyses were conducted to identify clinical risk markers that predicted the difference in FPG and log HOMA2-IR. Associations between the clinical risk markers and FPG, and log HOMA2-IR, were each assessed using single predictor linear regression models, adjusted for ethnicity. Those clinical risk markers that showed statistical

significance at $P < 0.1$ were included in stepwise multiple linear regression analyses using SAS version 9.4 (SAS Institute Inc., Cary, NC, United States). The software utilises a combination of backward and forward selection techniques to retain independent predictors that showed a significant effect ($P < 0.05$) to give a final prediction model with risk markers that predicted FPG, and log HOMA2-IR. Additionally, we also performed stepwise multiple linear regression and the least angle regression (LAR) models treating ethnicity as a potential predictor same as the clinical markers that showed statistical significance at $P < 0.1$ in the models. The results were cross-validated with the main analysis using ethnicity-adjusted stepwise regression models.

RESULTS

Participant Characteristics

Mean age and BMI of the full cohort was 44.4 ± 14.5 years and 27.3 ± 4.4 kg/m^2. The women were predominantly healthy and normoglycaemic, with 19% ($n = 13$) with IFG with an equal division of prediabetes between ethnicities ($n = 7$ Caucasian, $n = 6$ Chinese). Although significantly younger ($P = 0.05$), the Chinese women were of similar mean BMI to Caucasian ($P > 0.05$, **Table 1**) with lower mean bodyweight, height (both $P < 0.001$), waist ($P = 0.05$), and hip circumference ($P = 0.002$).

Body Composition—Adipose Tissue Compartments

Mean DXA-% TBF was 39.8 ± 7.6% in the full cohort of women. In accordance with lower bodyweight and stature, DXA-assessed TBF mass (kg) was also significantly lower in Chinese ($P = 0.02$) but when normalised as % of total soft tissue mass there were no ethnic-specific differences in DXA-% TBF between the Chinese and Caucasian women (**Table 1**). While MR-assessed SAT (cm^2) and MR-VAT (cm^2) were again both numerically lower in these smaller stature Chinese women, notably this difference was highly significant for MR-SAT ($P = 0.001$, **Figure 1**) but not for MR-VAT ($P > 0.05$) which was not significantly different from the Caucasian subcohort. In turn, while mean MR-AAT (cm^2) was again significantly lower ($P = 0.004$) in smaller stature Chinese than Caucasian women, there was greater contribution of VAT (34 vs. 28%) than SAT (66 vs. 72%) to the abdominal fat compartment in the Chinese subcohort (**Figure 2**).

Non-adipose Tissue Organ Fat—Pancreas and Liver

Mean MRI-assessed % pancreas fat (determined in 65 of 68 women) was 4.2 ± 1.9% (**Table 1**). Mean pancreas volume was 74.0 ± 19.6 cm^3, and PVI was 41.5 ± 10.7. Notably, 39% ($n = 25$; mean age: 49 ± 12 years; BMI: 28.7 ± 4.4 kg/m^2) of women were identified with pancreas fat above our chosen threshold of 4.5% with mean pancreas volume and PVI of 77.3 ± 18.6 cm^3 and 41.5 ± 9.6, respectively. Similarly, mean MRS-assessed % liver fat (measured in 67 of 68 women) was lower than the 5.6% threshold (mean: 4.2 ± 4.8%, **Table 1**) with 22% ($n = 15$; mean age: 50.1 ± 13.0 years; BMI: 28.9 ± 3.6 kg/m^2) of women identified with elevated liver fat.13% of women ($n = 9$, mean age: 52.8 ± 12.2 years; BMI: 29.4 ± 3.9 kg/m^2) had both fatty liver and pancreatic fat above the chosen cut offs.

Comparisons of organ fat between the two ethnic groups showed no significant difference in mean % pancreas fat ($P > 0.05$, **Table 1**). However, linear regression (**Supplementary Figure 1**) revealed that at a fixed BMI in the lean range between 20 and 25 kg/m^2 Chinese women had ∼1% higher predicted pancreas fat than their Caucasian counterparts (range: 3–3.5 vs. 1.8–2.7%). Notably, there were similar numbers of Chinese ($n = 13$) and Caucasian ($n = 12$) women with % pancreas fat above the chosen threshold, despite the Chinese subcohort being 2 BMI units lower (mean BMI: 27.9 ± 5.2 vs. 30.0 ± 3.3 kg/m^2; $P = 0.35$) and 10 years younger (mean age: 44 ± 11 vs. 54 ± 12 years; $P = 0.06$) than Caucasian. Mean pancreas volume and mean PVI were not significantly different between ethnicities in the full cohort (**Table 1**). Also similarly, no difference in either pancreas volume (Chinese: 68.1 ± 20.5 cm^3; Caucasian: 77.3 ± 18.6 cm^3) or PVI (Chinese: 38.4 ± 9.6; Caucasian: 41.5 ± 9.6) was observed in Chinese and Caucasian women with pancreas fat above the chosen 4.5% threshold.

Again, while there was no significant difference in mean % liver fat between the two ethnicities, linear regression analysis showed, as for % pancreas fat, that at a fixed BMI in the lean range of between 20 and 25 kg/m^2 (**Supplementary Figure 1**) Chinese women had ∼2% higher predicted liver fat than their Caucasian counterparts (range: 3–3.5 vs. 1.3–1.5%). Twice as many Chinese ($n = 10$) had elevated liver fat (Caucasian, $n = 5$), despite the Chinese subcohort being 3 BMI units lower (mean BMI: 27.9 ± 4.9 vs. 30.8 ± 3.5 kg/m^2; $P = 0.10$) and 10 years younger (mean age: 44 ± 12 vs. 55 ± 12 years; $P = 0.03$) than their Caucasian counterparts.

Blood Biochemistry

Mean concentrations of all blood biochemical markers were within the normal range in the full cohort. However, TC ($P = 0.004$), LDL-C ($P = 0.02$), HDL-C ($P = 0.001$), total- ($P = 0.006$), and HMW adiponectin ($P = 0.005$) were significantly lower, while GLP-1 ($P = 0.04$) and glucagon ($P = 0.05$) were significantly higher, in Chinese compared to Caucasian women.

Relationship Between Metabolic Risk Factors

Associations between MR-VAT, % pancreas and % liver fat depots with FPG and log HOMA2-IR were strengthened by age and % TBF, and independent of ethnicity. The adjusted models showed that despite significant improvement in the relationships with addition of these covariates, the variance, i.e., beta coefficient, attributed to the depots themselves weakened to non-significance in the overall relationships (**Table 2** and **Supplementary Table 1**). FPG was significantly and positively associated with MR-VAT ($r = 0.47$, $P < 0.0001$) and notably % pancreas fat ($r = 0.46$, $P < 0.0001$) in the full cohort, unlike % liver fat ($r = 0.21$, $P = 0.09$) (**Supplementary Figure 2**). While both MRI measurements had the strongest correlation with FPG, these relationships were strengthened when linear models were adjusted for age, % TBF

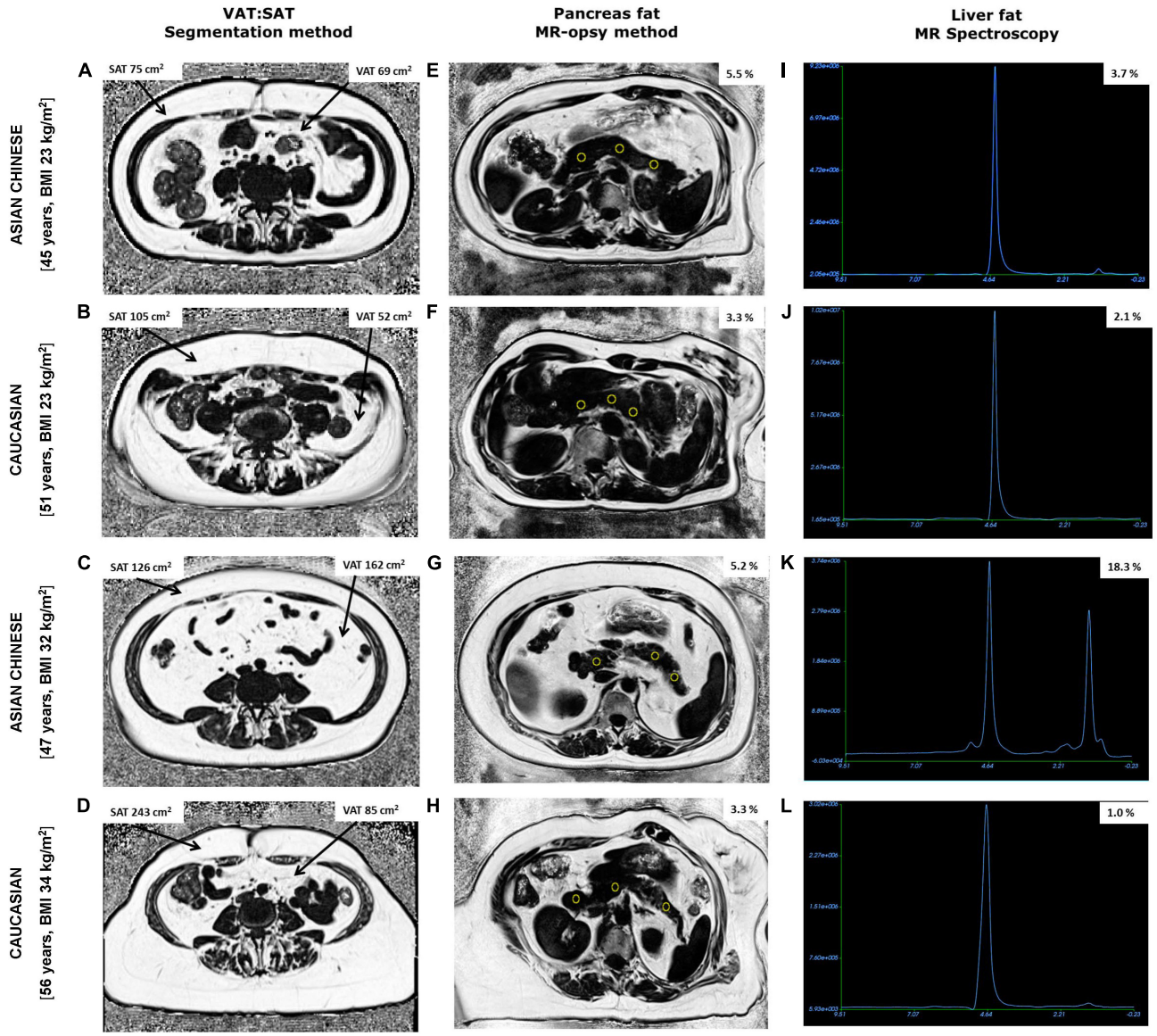

FIGURE 2 | Fat fraction maps obtained from abdominal MRI scans showing subcutaneous (SAT), visceral adipose tissue (VAT), and pancreas fat along with MR spectroscopy of liver fat from two Chinese and two Caucasian women. Chinese women aged 45 years, BMI 23 kg/m^2 **(A,E,I)** and 47 years, BMI 32 kg/m^2 **(C,G,K)** had lower SAT and higher pancreas fat compared to older BMI matched Caucasian women aged 51 years, BMI 23 kg/m^2 **(B,F,J)** and 56 years, BMI 34 kg/m^2 **(D,H,L)**, respectively. Notably, VAT, % pancreas and % liver fat were higher in both Chinese women compared with BMI matched Caucasian counterparts exhibiting the TOFI profile.

and ethnicity (both, r = 0.54, P < 0.0001). Interestingly, it was age that explained the most significant variance in FPG in both the adjusted models. Although non-significant for MR-VAT (**Table 2**) the beta coefficient between % pancreas fat and FPG (**Table 2**) remained statistically significant in all women. The adjusted model improved the relationship between % liver fat with FPG (r = 0.54, P = 0.009) with the most significant independent predictors being age and % TBF in the full cohort (**Supplementary Table 1**). Again, the only significant positive relationship with log HOMA2-IR was observed in the full cohort with MR-VAT (r = 0.24, P = 0.05). Adjusted models, however, significantly improved relationships with IR and expectedly were mainly driven by % TBF (**Supplementary Table 1**).

Independent Predictors of Fasting Plasma Glucose and Insulin Resistance

Of the clinical risk markers, age and % pancreas fat positively, while liver enzyme AST negatively, contributed to the variance in the model for predicting FPG (P < 0.0001) (**Table 3**, with all significant independent predictors **Table 4**). Notably, ethnicity did not contribute to the model (P = 0.20). On the contrary,

ethnicity explained the greatest variance in the model for IR (log HOMA2-IR), which was higher in Chinese, followed by % TBF, amylin and C-peptide concentrations ($P < 0.0001$) (**Table 3**).

DISCUSSION

In the TOFI_Asia MR cohort, comprising healthy and dysglycaemic Chinese and Caucasian women with similar BMI and % TBF, we show the importance of phenotypic characterisation of MRI/S quantified ectopic fat and highlight the need for early markers of T2D risk, aligning with and in accordance to the recent joint position statement from the International Atherosclerosis Society and the International Chair on Cardiometabolic Risk Working Group on Visceral Adiposity (Neeland et al., 2019). Multivariate analysis revealed MRI-assessed % pancreas fat as a positive predictor of increased FPG, and pancreatic glucoregulatory peptides amylin, that is involved in muscle glycogenolysis (Young et al., 1993), and C-peptide, a component of proinsulin, as predictors of IR. Additional linear relationships with non-adipose % pancreas fat suggest that it may be an early T2D risk marker, particularly in Chinese characterised by TOFI, which contributes to increased IR and/or declining beta-cell function to alter glucose metabolism and requires further investigation.

Recent studies have demonstrated ethnic variability in abdominal and visceral adiposity (Lear et al., 2007; Nazare et al., 2012; Chen et al., 2018), including the wider TOFI_Asia study

TABLE 2 | Relationships between fasting plasma glucose, and insulin resistance (log HOMA2-IR) with visceral adipose tissue, pancreas, and liver fat in the MR cohort.

	FPG (mmol/L)					log HOMA2-IR				
	β	SE	*t*	*P* value	Interaction with ethnicity, *P* value	β	SE	*t*	*P* value	Interaction with ethnicity, *P* value
Visceral adipose tissue, MR-VAT (cm^2)					0.30					0.28
All	0.003	0.003	1.15	0.25		0.002	0.003	0.73	0.47	
Chinese	−0.001	0.004	−0.14	0.89		0.002	0.004	0.49	0.63	
Caucasian	0.006	0.004	1.40	0.17		0.001	0.005	0.15	0.88	
Pancreas fat (%)					0.76					0.19
All	0.08	0.04	1.99	0.05		0.008	0.05	0.16	0.87	
Chinese	0.07	0.04	1.64	0.11		−0.01	0.05	−0.30	0.77	
Caucasian	0.10	0.09	1.15	0.26		0.03	0.11	0.30	0.77	
Liver fat (%)					0.25					0.09
All	−0.005	0.015	−0.295	0.77		−0.006	0.02	−0.35	0.72	
Chinese	−0.02	0.02	−1.05	0.30		−0.03	0.02	−1.14	0.26	
Caucasian	0.01	0.02	0.42	0.68		0.01	0.03	0.40	0.69	

Data are presented as beta coefficients for each metabolic risk factor with FPG and log HOMA2-IR. All models are adjusted for age and % total body fat. The models for all women also additionally adjusted for ethnicity. The interaction effect between ethnicity and the predictor of interest was tested. Statistical significance at $P < 0.05$. Pancreas fat determined from MRI scans in 65 women (31 Caucasian and 34 Chinese); liver fat determined from MRS scans in 67 women (33 Caucasian and 34 Chinese).

TABLE 3 | Stepwise linear regression models, adjusted for ethnicity, with significant independent metabolic risk factors that predict (i) fasting plasma glucose and (ii) insulin resistance (log HOMA2-IR) in women ($n = 68$) from the MR study.

	β coefficient	SE	*t*	*P* value
FPG (mmol/L)				
Intercept	4.42	0.27	16.44	<0.001
Chinese	0.16	0.13	1.28	0.20
Age	0.01	0.005	2.58	0.01
Pancreas fat (%)	0.09	0.04	2.60	0.01
AST (U/L)	−0.02	0.008	−2.35	0.02
log HOMA2-IR				
Intercept	−1.45	0.31	−4.75	<0.001
Chinese	0.30	0.11	2.71	0.009
DXA-%TBF	0.02	0.008	2.49	0.02
Amylin (pg/ml)	0.01	0.006	2.14	0.04
C-peptide (pg/ml)	0.001	0.0001	3.57	0.001

*Summary of the Stepwise models are as follows (i) FPG: $R^2 = 0.33$, $P < 0.0001$ and (ii) log HOMA2-IR: $R^2 = 0.56$, $P < 0.0001$. Models for each outcome include all independent significant predictors ($P < 0.10$); details available in **Table 4**. Statistical significance was set at $P < 0.05$.*

TABLE 4 | Association between (i) fasting plasma glucose (FPG) and (ii) insulin resistance (calculated using HOMA2-IR) with individual metabolic risk factors in $n = 68$ women that underwent MR imaging using single predictor regression models.

	FPG (mmol/L)			log HOMA2-IR		
	Beta coefficients (±95% CI)	R^2	***P* value**	**Beta coefficients (±95% CI)**	R^2	***P* value**
Age (year)	0.02 (0.01, 0.03)	0.20	0.0002	−0.003 (−0.01, 0.01)	0.04	0.66
BMI (kg/m^2)	0.04 (0.003, 0.07)	0.07	0.03	0.06 (0.03, 010)	0.21	0.001
Waist circumference (cm)	0.01 (0.003, 0.03)	0.09	0.02	0.02 (0.001, 0.03)	0.15	0.006
Systolic blood pressure, SBP (mmHg)	0.01 (0.004, 0.02)	0.14	0.002	0.01 (−0.003, 0.01)	0.06	0.20
Diastolic blood pressure, DBP (mmHg)	0.01 (−0.002, 0.03)	0.05	0.09	0.01 (−0.01, 0.02)	0.06	0.28
Total body fat, DXA-TBF (kg)	0.01 (−0.002, 0.03)	0.05	0.09	0.03 (0.01, 0.04)	0.21	0.0003
Total body fat, DXA-TBF (%)	0.03 (0.008, 0.05)	0.12	0.006	0.04 (0.02, 0.06)	0.23	0.0002
Visceral adipose tissue, MR-VAT (cm^2)	0.007 (0.004, 0.01)	0.23	0.001	0.004 (0.0003, 0.008)	0.10	0.03
Pancreas fat (%)	0.14 (0.07, 0.20)	0.22	0.0002	0.05 (−0.03, 0.13)	0.07	0.27
Liver fat (%)	0.01 (−0.002, 0.03)	0.05	0.09	0.01 (−0.01, 0.02)	0.07	0.41
Fasting plasma insulin (pg/mL)	0.0003 (−0.0001, 0.001)	0.03	0.18	0.002 (0.001, 0.002)	0.82	<0.0001
Total cholesterol (mmol/L)	0.02 (−0.15, 0.19)	0.01	0.83	−0.05 (−0.23, 0.13)	0.04	0.56
Triglycerides, TAG (mmol/L)	0.25 (0.01, 0.50)	0.07	0.04	0.24 (−0.02, 0.50)	0.09	0.07
HDL-cholesterol (mmol/L)	−0.27 (−0.64, 0.10)	0.04	0.14	−0.52 (−0.90, −0.14)	0.14	0.001
LDL-cholesterol (mmol/L)	0.03 (−0.17, 0.23)	0.01	0.76	0.01 (−0.20, 0.22)	0.04	0.94
Alanine amino transferase, ALT (U/L)	0.001 (−0.01, 0.02)	0.01	0.91	0.001 (−0.02, 0.02)	0.04	0.94
Aspartate amino transferase, AST (U/L)	−0.02 (−0.04, 0.001)	0.06	0.06	−0.02 (−0.04, 0.002)	0.09	0.07
Alkaline phosphatase, ALP (U/L)	0.002 (−0.003, 0.008)	0.02	0.40	0.001 (−0.005, 0.007)	0.04	0.65
Gamma glutamyl transferase, GGT (U/L)	0.000 (−0.007, 0.007)	0.01	0.99	0.0002 (−0.008, 0.008)	0.04	0.95
Amylin (pg/mL)	0.01 (−0.001, 0.02)	0.05	0.07	0.03 (0.02, 0.04)	0.40	<0.0001
C-peptide (pg/mL)	0.001 (0.0002, 0.001)	0.15	0.001	0.001 (0.001, 0.001)	0.47	<0.0001
Gastric inhibitory peptide, GIP (pg/mL)	−0.001 (−0.005, 0.003)	0.01	0.71	0.004 (0.0003, 0.01)	0.10	0.03
Glucagon like peptide-1, GLP-1 (pg/mL)	−0.001 (−0.005, 0.002)	0.02	0.43	0.01 (0.003, 0.01)	0.23	0.0001
Glucagon (pg/mL)	−0.002 (−0.01, 0.003)	0.01	0.50	0.007 (0.002, 0.01)	0.14	0.007
Total adiponectin (mg/L)	0.0001 (−0.03, 0.03)	0.006	0.99	−0.02 (−0.05, 0.02)	0.06	0.30
High-molecular weight adiponectin (mg/L)	0.005 (−0.04, 0.05)	0.007	0.81	−0.03 (−0.07, 0.02)	0.06	0.21

Data are presented as beta coefficients (±95% confidence intervals) for each metabolic risk factor with (i) FPG and (ii) log HOMA2-IR. Statistical significance at $P < 0.10$. Each model is adjusted for Ethnicity

(Sequeira et al., 2020), and shown increased risk of dysglycaemia associated with these compartments. Although accumulation of pancreas fat is postulated to result in damage to the beta-cell in preclinical studies (Lee et al., 2009), causal associations with beta-cell dysfunction, and glucose intolerance in humans remains to be established. The pancreas plays a key role in T2D, characterised by chronic hyperglycaemia in the context of IR and/or beta-cell dysfunction. Insulin secretion (IS) in response to a glucose challenge is complex and dependent not only on co-existing plasma glucose concentration but also beta-cell responsiveness to changing glucose levels and the rate of insulin clearance, both modulated by the prevailing IR (Del Prato et al., 2002). In IR, increased beta-cell response to glucose and reduced insulin clearance are adaptive mechanisms to maintenance normal glucose tolerance.

Previous work in dysglycaemic individuals, including Chinese and Caucasians, has reported increased pancreas fat (Lingvay et al., 2009; Ou et al., 2013; Gaborit et al., 2014; Kim et al., 2014; Lim et al., 2014; Wang et al., 2014; Macauley et al., 2015; Steven et al., 2016) and decreased beta-cell function (Tushuizen et al., 2007; Heni et al., 2010; Lim et al., 2011; Szczepaniak et al., 2012; Yokota et al., 2012). There are, however, inconsistent findings regarding the association between pancreatic fat and glucose metabolism (Tushuizen et al., 2007; Lê et al., 2011; van der Zijl et al., 2011), possibly due to varied methodologies in determination of pancreas fat and/or the heterogeneity in distribution of fat within the pancreas itself (Schwenzer et al., 2008; Lee et al., 2009; Smits and van Geenen, 2011) which often precludes comparisons between studies. In our current study we adopted the MR-opsy method (Al-Mrabeh et al., 2017), and though mean % pancreas fat was below the threshold adopted for internal comparisons between ethnicities in our cohort, a wide range was observed with pancreas fat an important predictor of FPG compared to the other adipose tissue compartments and liver. There were no ethnic differences observed in mean pancreas volume or index; however, the mean levels observed were concordant to those previously reported (Macauley et al., 2015) in healthy normoglycaemic individuals.

Furthermore, a significant association between FPG with pancreas and liver fat in the cohort was observed, notably with some participants with raised FPG (≥5.6 mmol/L) even when fat infiltration in these organs was low to possibly demonstrate that even small amounts of ectopic fat, likely representative of early stage deposition, may increase T2D susceptibility. Intrahepatic fat inhibits insulin suppression of hepatic glucose output to consequently result in increased basal IS, which exacerbates liver fat content and increases circulating plasma TAG concentration. Exposure of pancreatic beta-cells to excess fatty acids, derived from circulating and locally deposited TAG, inhibits glucose-mediated IS with consequent increase in plasma glucose. The

degree of beta-cell decompensation is thought to occur based on a personal fat threshold which when exceeded exacerbates T2D risk (Taylor and Holman Rury, 2015).

Alongside % pancreas fat and age, lower concentration of AST predicted higher FPG in this MR study. Elevated liver function enzymes ALT and GGT, but not AST, have previously been associated with increased risk of T2D in meta-analyses (Fraser et al., 2009; Kunutsor et al., 2013). However, AST, like ALT, catalyses the transfer of amino groups to generate by-products during gluconeogenesis and amino acid metabolism, so it is not unexpected that lower concentrations may be associated with variable FPG. The concordance of findings reiterated in LAR and Stepwise regression analyses without ethnicity included in the model (**Supplementary Tables 2A,B**) additionally emphasises that % pancreas fat is indeed a strong predictor of FPG. Furthermore, significant variability in IR in the multiple regression models (also concordant with results from **Supplementary Tables 2A,B**) was explained by % TBF, pancreatic glucose regulating peptides amylin and C-peptide. While amylin decreases glucagon-stimulated hepatic glucose output, and shown to regulate muscle glycogenolysis, this does not occur during insulin-induced hypoglycaemic states (Aronoff et al., 2004). It is notable that the most significant contribution to variation in IR was ethnicity, with HOMA2 assessed IR greater by 0.3 units in the Chinese.

Phenotypic characterisation also revealed that Chinese women in the cohort although younger, and of lower bodyweight and stature, had similar BMI, % TBF, MR-VAT (cm^2) and non-adipose tissue % pancreas and % liver fat than the Caucasian women. Conversely, abdominal SAT (cm^2) was lower. Outwardly lean, low BMI Chinese women were also observed with greater propensity to TOFI than their lean Caucasian counterparts, with fixed BMI cut-points of 20 and 25 kg/m^2 associated with greater pancreas fat and greater liver fat content in the Chinese subcohort. Also, lower protective circulating HDL-C and glucose regulating total- and HMW adiponectin were observed in Chinese than Caucasian women. Circulating peptides GLP-1 and glucagon, also involved in glucose regulation, were also higher. Although not possible to draw conclusions from this smaller cohort, it is important to highlight that some of the observed differences are in line with previous reports, in larger cohort studies, showing that Asians are at a greater risk of T2D than Caucasians due to differential fat partitioning (Lear et al., 2007; Lê et al., 2011; Nazare et al., 2012; Chen et al., 2018).

Strengths of our study include a healthy, primarily normoglycaemic, cohort from both ethnicities, in which we evaluated relationships between body fat compartments and ectopic lipid deposition in the absence of significant comorbidities. Pancreas fat determined by the MR-opsy method was averaged from the head, body, and tail of the pancreas to account for potential heterogeneity in fat distribution and was the most significant independent predictor of FPG in this cohort of women. In the absence of gold standard clamp technique to assess IR, the preferred HOMA2-IR method was used. Limitations include T1-weighting of the pancreas fat acquisition, which will overestimate the pancreatic fat, precluding direct comparison with other studies, however, they are internally consistent in comparing ethnicities. Causality cannot be confirmed from associations observed in this cross-sectional study and hence the authors are conducting longitudinal assessments in this cohort of women. Also, that these observations are from a single gender and may not be generalised to both genders due to likely gender-specific differences in energy substrate-utilisation patterns with dimorphism in glucose and fatty acid metabolism. Nonetheless, methodologies used for data collection and analyses are robust and validated.

DATA AVAILABILITY STATEMENT

De-identified data will be shared and made available upon reasonable request to the corresponding author and subject to an approved proposal and data access agreement.

ETHICS STATEMENT

The study was reviewed and approved by the New Zealand Health and Disabilities Ethics Committee (16/STH/23). The study is registered with the Australian New Zealand Clinical Trials Registry ACTRN12616000362493. All participants provided written informed consent to participate in this study.

AUTHOR CONTRIBUTIONS

IS: study design and supervision, participant recruitment, data analyses and interpretation, manuscript preparation, and corresponding author. WY and LL: study design, participant recruitment, and data collection. YJ: senior statistician and advisor, data curation, and formal analysis. RM: study design, study advisor, and critical revision of manuscript. LP: study design, supervision of body composition (DXA), and critical revision of manuscript. GC: study design and methodology and critical revision of manuscript. CP: advisor MR methodology, software, and supervision. JL: development of MRI/S scan protocols and MRS processing methods. KH: supervised and reviewed MRI post-scan analysis and critical revision of manuscript. SP: funding, PI on project, study design and supervision, critical revision of manuscript, and senior author. All authors approved of the final version of the manuscript.

FUNDING

This study was funded by the New Zealand National Science Challenge High Value Nutrition (NSC-HVN) Program, Ministry for Business, Innovation and Employment (MBIE, grant nos. 3710040 and 3716382).

ACKNOWLEDGMENTS

We thank Hong Liu, Shaoping Zhang, Greeshma Amarsingh, and James Chuang, from the School of Biological Sciences,

The University of Auckland, for their analytical expertise in adiponectin and peptide assays, study participants for their involvement and the clinical research staff at the Human Nutrition Unit, Body Composition Unit and Centre for Advanced MRI for their care of the participants.

SUPPLEMENTARY MATERIAL

The Supplementary Material for this article can be found online at: https://www.frontiersin.org/articles/10.3389/fphys.2022.819606/full#supplementary-material

REFERENCES

Al-Mrabeh, A., Hollingsworth, K. G., Steven, S., Tiniakos, D., and Taylor, R. (2017). Quantification of intrapancreatic fat in type 2 diabetes by MRI. *PLoS one* 12:e0174660. doi: 10.1371/journal.pone.0174660

Alva, M. L., Hoerger, T. J., Zhang, P., and Gregg, E. W. (2017). Identifying risk for type 2 diabetes in different age cohorts: does one size fit all? *BMJ Open Diabetes Res. Care* 5:e000447. doi: 10.1136/bmjdrc-2017-000447

American Diabetes Association (2018). Classification and diagnosis of diabetes: standards of medical care in diabetes – 2018. *Diabetes Care* 41, S13–S27. doi: 10.2337/dc18-S002

Aronoff, S. L., Berkowitz, K., Shreiner, B., and Want, L. (2004). Glucose metabolism and regulation: beyond insulin and glucagon. *Diabetes Spectr.* 17, 183–190.

Barry, E., Roberts, S., Oke, J., Vijayaraghavan, S., Normansell, R., and Greenhalgh, T. (2017). Efficacy and effectiveness of screen and treat policies in prevention of type 2 diabetes: systematic review and meta-analysis of screening tests and interventions. *BMJ* 356:6538. doi: 10.1136/bmj.i6538

Chen, P., Hou, X., Hu, G., Wei, L., Jiao, L., Wang, H., et al. (2018). Abdominal subcutaneous adipose tissue: a favorable adipose depot for diabetes? *Cardiovasc. Diabetol.* 17:93. doi: 10.1186/s12933-018-0734-8

Colditz, G. A., Willett, W. C., Rotnitzky, A., and Manson, J. E. (1995). Weight gain as a risk factor for clinical diabetes mellitus in women. *Ann. Intern. Med.* 122, 481–486. doi: 10.7326/0003-4819-122-7-199504010-00001

Crane, J. C., Olson, M. P., and Nelson, S. J. (2013). SIVIC: open-source, standards-based software for DICOM MR Spectroscopy workflows. *Int. J. Biomed. Imaging* 2013:12. doi: 10.1155/2013/169526

de Bazelaire, C. M., Duhamel, G. D., Rofsky, N. M., and Alsop, D. C. (2004). MR imaging relaxation times of abdominal and pelvic tissues measured in vivo at 3.0 T: preliminary results. *Radiology* 230, 652–659. doi: 10.1148/radiol.2303021331

Del Prato, S., Marchetti, P., and Bonadonna, R. C. (2002). Phasic insulin release and metabolic regulation in type 2 diabetes. *Diabetes* 51, S109–S116. doi: 10.2337/diabetes.51.2007.s109

Fraser, A., Harris, R., Sattar, N., Ebrahim, S., Davey Smith, G., and Lawlor, D. A. (2009). Alanine aminotransferase, gamma-glutamyltransferase, and incident diabetes: the British Women's Heart and Health Study and meta-analysis. *Diabetes Care* 32, 741–750. doi: 10.2337/dc08-1870

Gaborit, B., Abdesselam, I., Kober, F., Jacquier, A., Ronsin, O., Emungania, O., et al. (2014). Ectopic fat storage in the pancreas using 1H-MRS: importance of diabetic status and modulation with bariatric surgery-induced weight loss. *Int. J. Obesity* 39:480. doi: 10.1038/ijo.2014.126

Haldar, S., Chia, S. C., and Henry, C. J. (2015). "Body composition in asians and caucasians: comparative analyses and influences on cardiometabolic outcomes," in *Advances in Food and Nutrition Research*, ed. J. Henry (Cambridge, MA: Academic Press), 97–154. doi: 10.1016/bs.afnr.2015.07.001

Hamilton, G., Yokoo, T., Bydder, M., Cruite, I., Schroeder, M. E., Sirlin, C. B., et al. (2011). In vivo characterization of the liver fat 1H MR spectrum. *NMR Biomed.* 24, 784–790. doi: 10.1002/nbm.1622

Heni, M., Machann, J., Staiger, H., Schwenzer, N. F., Peter, A., Schick, F., et al. (2010). Pancreatic fat is negatively associated with insulin secretion in individuals with impaired fasting glucose and/or impaired glucose tolerance: a nuclear magnetic resonance study. *Diabetes/Metab. Res. Rev.* 26, 200–205. doi: 10.1002/dmrr.1073

Hocking, S., Samocha-Bonet, D., Milner, K.-L., Greenfield, J. R., and Chisholm, D. J. (2013). Adiposity and insulin resistance in humans: the role of the different tissue and cellular lipid depots. *Endocrine Rev.* 34, 463–500. doi: 10.1210/er.2012-1041

Jo, A., and Mainous, A. G. III (2018). Informational value of percent body fat with body mass index for the risk of abnormal blood glucose: a nationally representative cross-sectional study. *BMJ Open* 8:e019200. doi: 10.1136/bmjopen-2017-019200

Kim, S. Y., Kim, H., Cho, J. Y., Lim, S., Cha, K., Lee, K. H., et al. (2014). Quantitative assessment of pancreatic fat by using unenhanced CT: pathologic correlation and clinical implications. *Radiology* 271, 104–112. doi: 10.1148/radiol.13122883

Kunutsor, S. K., Apekey, T. A., and Walley, J. (2013). Liver aminotransferases and risk of incident type 2 diabetes: a systematic review and meta-analysis. *Am. J. Epidemiol.* 178, 159–171. doi: 10.1093/aje/kws469

Lê, K.-A., Ventura, E. E., Fisher, J. Q., Davis, J. N., Weigensberg, M. J., Punyanitya, M., et al. (2011). Ethnic differences in pancreatic fat accumulation and its relationship with other fat depots and inflammatory markers. *Diabetes Care* 34, 485–490. doi: 10.2337/dc10-0760

Lear, S. A., Humphries, K. H., Kohli, S., Chockalingam, A., Frohlich, J. J., and Birmingham, C. L. (2007). Visceral adipose tissue accumulation differs according to ethnic background: results of the Multicultural Community Health Assessment Trial (M-CHAT). *Am. J. Clin. Nutr.* 86, 353–359. doi: 10.1093/ajcn/86.2.353

Lee, Y., Lingvay, I., Szczepaniak, L. S., Ravazzola, M., Orci, L., and Unger, R. H. (2009). Pancreatic steatosis: harbinger of type 2 diabetes in obese rodents. *Int. J. Obesity* 34, 396–400. doi: 10.1038/ijo.2009.245

Lim, E. L., Hollingsworth, K. G., Aribisala, B. S., Chen, M. J., Mathers, J. C., and Taylor, R. (2011). Reversal of type 2 diabetes: normalisation of beta cell function in association with decreased pancreas and liver triacylglycerol. *Diabetologia* 54, 2506–2514. doi: 10.1007/s00125-011-2204-7

Lim, S., Bae, J. H., Chun, E. J., Kim, H., Kim, S. Y., Kim, K. M., et al. (2014). Differences in pancreatic volume, fat content, and fat density measured by multidetector-row computed tomography according to the duration of diabetes. *Acta Diabetol.* 51, 739–748. doi: 10.1007/s00592-014-0581-3

Linder, N., Schaudinn, A., Garnov, N., Blüher, M., Dietrich, A., Schütz, T., et al. (2016). Age and gender specific estimation of visceral adipose tissue amounts from radiological images in morbidly obese patients. *Sci. Rep.* 6:22261. doi: 10.1038/srep22261

Lingvay, I., Esser, V., Legendre, J. L., Price, A. L., Wertz, K. M., Adams-Huet, B., et al. (2009). Noninvasive quantification of pancreatic fat in humans. *J. Clin. Endocrinol. Metab.* 94, 4070–4076. doi: 10.1210/jc.2009-0584

Macauley, M., Percival, K., Thelwall, P. E., Hollingsworth, K. G., and Taylor, R. (2015). Altered volume, morphology and composition of the pancreas in type 2 diabetes. *PLoS One* 10:e0126825. doi: 10.1371/journal.pone.0126825

Nazare, J.-A., Smith, J. D., Borel, A.-L., Haffner, S. M., Balkau, B., Ross, R., et al. (2012). Ethnic influences on the relations between abdominal subcutaneous and visceral adiposity, liver fat, and cardiometabolic risk profile: the international Study of Prediction of Intra-Abdominal Adiposity and Its Relationship With Cardiometabolic Risk/Intra-Abdominal Adiposity. *Am. J. Clin. Nutr.* 96, 714–726. doi: 10.3945/ajcn.112.035758

Neeland, I. J., Ross, R., Després, J.-P., Matsuzawa, Y., Yamashita, S., Shai, I., et al. (2019). Visceral and ectopic fat, atherosclerosis, and cardiometabolic disease: a position statement. *Lancet Diabetes Endocrinol.* 7, 715–725. doi: 10.1016/S2213-8587(19)30084-1

Nowotny, B., Kahl, S., Klüppelholz, B., Hoffmann, B., Giani, G., Livingstone, R., et al. (2018). Circulating triacylglycerols but not pancreatic fat associate with insulin secretion in healthy humans. *Metabolism* 81, 113–125. doi: 10.1016/j.metabol.2017.12.005

Ou, H.-Y., Wang, C.-Y., Yang, Y.-C., Chen, M.-F., and Chang, C.-J. (2013). The association between nonalcoholic fatty pancreas disease and diabetes. *PLoS One* 8:e62561. doi: 10.1371/journal.pone.0062561

Petäjä, E. M., and Yki-Järvinen, H. (2016). Definitions of normal liver fat and the association of insulin sensitivity with acquired and genetic NAFLD – a systematic review. *Int. J. Mol. Sci.* 17:633. doi: 10.3390/ijms17050633

Ramachandran, A., Chamukuttan, S., Shetty, S. A., Arun, N., and Susairaj, P. (2012). Obesity in Asia – is it different from rest of the world. *Diabetes Metab. Res. Rev.* 28, 47–51. doi: 10.1002/dmrr.2353

Reilly, J. J., El-Hamdouchi, A., Diouf, A., Monyeki, A., and Somda, S. A. (2018). Determining the worldwide prevalence of obesity. *Lancet* 391, 1773–1774.

Rossi, A. P., Fantin, F., Zamboni, G. A., Mazzali, G., Rinaldi, C. A., Del Giglio, M., et al. (2011). Predictors of ectopic fat accumulation in liver and pancreas in obese men and women. *Obesity* 19, 1747–1754. doi: 10.1038/oby.2011.114

Schneider, C. A., Rasband, W. S., and Eliceiri, K. W. (2012). NIH Image to ImageJ: 25 years of image analysis. *Nat. Methods* 9, 671–675. doi: 10.1038/nmeth.2089

Schweitzer, L., Geisler, C., Pourhassan, M., Braun, W., Glüer, C.-C., Bosy-Westphal, A., et al. (2015). What is the best reference site for a single MRI slice to assess whole-body skeletal muscle and adipose tissue volumes in healthy adults? *Am. J. Clin. Nutr.* 102, 58–65. doi: 10.3945/ajcn.115.111203

Schwenzer, N. F., Machann, J., Martirosian, P., Stefan, N., Schraml, C., Fritsche, A., et al. (2008). Quantification of pancreatic lipomatosis and liver steatosis by MRI: comparison of in/opposed-phase and spectral-spatial excitation techniques. *Invest. Radiol.* 43, 330–337. doi: 10.1097/RLI.0b013e31816a88c6

Sequeira, I. R., Yip, W., Lu, L., Jiang, Y., Murphy, R., Plank, L., et al. (2020). Visceral adiposity and glucoregulatory peptides are associated with susceptibility to type 2 diabetes: the TOFI_Asia study. *Obesity* 28, 2368–2378.

Singh, R. G., Yoon, H. D., Wu, L. M., Lu, J., Plank, L. D., and Petrov, M. S. (2017). Ectopic fat accumulation in the pancreas and its clinical relevance: a systematic review, meta-analysis, and meta-regression. *Metab. Clin. Exp.* 69, 1–13. doi: 10.1016/j.metabol.2016.12.012

Smits, M. M., and van Geenen, E. J. M. (2011). The clinical significance of pancreatic steatosis. *Nat. Rev. Gastroenterol. Hepatol.* 8, 169–177. doi: 10.1038/nrgastro.2011.4

Steven, S., Hollingsworth, K. G., Small, P. K., Woodcock, S. A., Pucci, A., Aribisala, B., et al. (2016). Weight loss decreases excess pancreatic triacylglycerol specifically in type 2 diabetes. *Diabetes Care* 39, 158–165. doi: 10.2337/dc15-0750

Szczepaniak, L. S., Victor, R. G., Mathur, R., Nelson, M. D., Szczepaniak, E. W., Tyer, N., et al. (2012). Pancreatic steatosis and its relationship to β-cell dysfunction in humans: racial and ethnic variations. *Diabetes care* 35, 2377–2383. doi: 10.2337/dc12-0701

Taylor, R., Al-Mrabeh, A., Zhyzhneuskaya, S., Peters, C., Barnes, A. C., Aribisala, B. S., et al. (2018). Remission of human type 2 diabetes requires decrease in liver and pancreas fat content but is dependent upon capacity for β cell recovery. *Cell Metab.* 28, 547–556.e543.

Taylor, R., and Holman Rury, R. (2015). Normal weight individuals who develop type 2 diabetes: the personal fat threshold. *Clin. Sci.* 128, 405–410. doi: 10.1042/CS20140553

Tchernof, A., and Després, J.-P. (2013). Pathophysiology of human visceral obesity: an update. *Physiol. Rev.* 93, 359–404. doi: 10.1152/physrev.00033.2011

Tushuizen, M. E., Bunck, M. C., Pouwels, P. J., Bontemps, S., van Waesberghe, J. H. T., Schindhelm, R. K., et al. (2007). Pancreatic fat content and β-cell function in men with and without type 2 diabetes. *Diabetes Care* 30, 2916–2921. doi: 10.2337/dc07-0326

van der Zijl, N. J., Goossens, G. H., Moors, C. C. M., van Raalte, D. H., Muskiet, M. H. A., Pouwels, P. J. W., et al. (2011). Ectopic fat storage in the pancreas, liver, and abdominal fat depots: impact on β-cell function in individuals with impaired glucose metabolism. *J. Clin. Endocrinol. Metab.* 96, 459–467. doi: 10.1210/jc.2010-1722

Wang, C.-Y., Ou, H.-Y., Chen, M.-F., Chang, T.-C., and Chang, C.-J. (2014). Enigmatic ectopic fat: prevalence of nonalcoholic fatty pancreas disease and its associated factors in a Chinese population. *J. Am. Heart Assoc.* 3:e000297. doi: 10.1161/JAHA.113.000297

Yokota, K., Fukushima, M., Takahashi, Y., Igaki, N., and Seino, S. (2012). Insulin secretion and computed tomography values of the pancreas in the early stage of the development of diabetes. *J. Diabetes Invest.* 3, 371–376. doi: 10.1111/j.2040-1124.2012.00212.x

Young, A. A., Cooper, G. J., Carlo, P., Rink, T. J., and Wang, M. W. (1993). Response to intravenous injections of amylin and glucagon in fasted, fed, and hypoglycemic rats. *Am. J. Physiol. Endocrinol. Metab.* 264, E943–E950. doi: 10.1152/ajpendo.1993.264.6.E943

Zhyzhneuskaya, S. V., Al-Mrabeh, A., Peters, C., Barnes, A. C., Hollingsworth, K. G., Pilkington, H., et al. (2018). Diabetes remission clinical trial (DiRECT)—plasma liver function tests reflect change in liver fat content in early type 2 diabetes. *Diabetes* 67:1834.

Conflict of Interest: The authors declare that the research was conducted in the absence of any commercial or financial relationships that could be construed as a potential conflict of interest.

Publisher's Note: All claims expressed in this article are solely those of the authors and do not necessarily represent those of their affiliated organizations, or those of the publisher, the editors and the reviewers. Any product that may be evaluated in this article, or claim that may be made by its manufacturer, is not guaranteed or endorsed by the publisher.

frontiers | Frontiers in Physiology

ORIGINAL RESEARCH
published: 27 April 2022
doi: 10.3389/fphys.2022.865452

Enteroendocrine Cell Formation Is an Early Event in Pancreatic Tumorigenesis

*Leah R. Caplan[1†], Vera Vavinskaya[2†], David G. Gelikman[1,3], Nidhi Jyotsana[1], Vincent Q. Trinh[4], Kenneth P. Olive[5], Marcus C. B. Tan[4,6,7] and Kathleen E. DelGiorno[1,6,7,8]**

[1]Department of Cell and Developmental Biology, Vanderbilt University, Nashville, TN, United States, [2]Department of Pathology, University of California, San Diego, San Diego, CA, United States, [3]College of Medicine, University of Central Florida, Orlando, FL, United States, [4]Department of Surgery, Vanderbilt University Medical Center, Nashville, TN, United States, [5]Department of Medicine, Herbert Irving Comprehensive Cancer Center, Columbia University Irving Medical Center, New York, NY, United States, [6]Vanderbilt Digestive Disease Research Center, Vanderbilt University Medical Center, Nashville, TN, United States, [7]Vanderbilt Ingram Cancer Center, Nashville, TN, United States, [8]Epithelial Biology Center, Vanderbilt University School of Medicine, Nashville, TN, United States

Pancreatic ductal adenocarcinoma (PDAC) is a devastating disease with a 5-year survival rate of only 11%, due, in part, to late diagnosis, making the need to understand early events in tumorigenesis critical. Acinar-to-ductal metaplasia (ADM), when not resolved, is a PDAC precursor. Recently, we showed that ADM is constituted by a heterogenous population of cells, including hormone-producing enteroendocrine cells (EECs: gamma, delta, epsilon, and enterochromaffin cells). In this study, we employed histopathological techniques to identify and quantify the abundance of EEC subtypes throughout pancreatic tumorigenesis in mouse models and human disease. We found that EECs are most abundant in ADM and significantly decrease with lesion progression. Co-immunofluorescence identifies distinct lineages and bihormonal populations. Evaluation of EEC abundance in mice lacking *Pou2f3* demonstrates that the tuft cell master regulator transcription factor is not required for EEC formation. We compared these data to human neoplasia and PDAC and observed similar trends. Lastly, we confirm that EECs are a normal cellular compartment within the murine and human pancreatic ductal trees. Altogether, these data identify EECs as a cellular compartment of the normal pancreas, which expands early in tumorigenesis and is largely lost with disease progression.

Keywords: enteroendocrine cells, pancreas, pancreatic polypeptide (PP), serotonin, ghrelin, somatostatin

OPEN ACCESS

Edited by:
Richard T. Waldron, Cedars Sinai Medical Center, United States

Reviewed by:
Charles Murtaugh, The University of Utah, United States
Christopher Pin, Western University, Canada

***Correspondence:**
Kathleen E. DelGiorno
kathleen.delgiorno@vanderbilt.edu

[†]These authors have contributed equally to this work

Specialty section:
This article was submitted to Gastrointestinal Sciences, a section of the journal Frontiers in Physiology

Received: *29 January 2022*
Accepted: *22 March 2022*
Published: *27 April 2022*

Citation:
Caplan LR, Vavinskaya V, Gelikman DG, Jyotsana N, Trinh VQ, Olive KP, Tan MCB and DelGiorno KE (2022) Enteroendocrine Cell Formation Is an Early Event in Pancreatic Tumorigenesis. Front. Physiol. 13:865452. doi: 10.3389/fphys.2022.865452

INTRODUCTION

Pancreatic ductal adenocarcinoma (PDAC) is a devastating disease and is predicted to become the second leading cause of cancer-related deaths by the year 2030 (Rahib et al., 2014). While the 5-year survival rate recently increased to 11%, progress is slow. This is due, in part, to late diagnosis and a lack of knowledge of early events in tumorigenesis. Acinar-to-ductal metaplasia (ADM) is a reparative program in which pancreatic acinar cells transdifferentiate into ductal cells in response to injury or oncogenic mutation (Giroux and Rustgi, 2017). Recently, we combined acinar cell lineage tracing in murine models and single cell RNA sequencing (scRNA-seq) and revealed that ADM does not result in the formation of homogeneous ductal cells but seeds a

heterogeneous population that includes tuft cells and enteroendocrine cell (EEC) subtypes, identified by hormone expression (DelGiorno et al., 2020a; Ma et al., 2021). These ADM-derived EEC subtypes include gamma cells (pancreatic polypeptide, PP), delta cells (somatostatin, SST), epsilon cells (ghrelin, GHRL), and enterochromaffin cells (serotonin, 5-HT) (Ma et al., 2021). While these hormones are present in murine islet development and in normal human islets (to varying degrees), we define ADM populations as EECs due to incorporation into ducts and their similarity to analogous populations throughout the gut (Wierup et al., 2002; Ohta et al., 2011; Ma et al., 2021).

Under conditions of unresolved injury, ADM can serve as a precursor for PDAC. Progression is a response to oncogenic mutation(s), such as in *KRAS*, the most common mutation in human pancreatic cancer, which is sufficient to drive the formation of precancerous lesions like pancreatic intraepithelial neoplasia (PanIN) (Hingorani et al., 2003). Previous studies have documented endocrine-like cell formation in murine and human PanIN and PDAC, however these studies did not address the formation, abundance, and dynamics of EEC subtypes throughout pancreatic tumorigenesis (Chen et al., 1988; Farrell et al., 2017; Sinha et al., 2017). Here, we identified and quantified the abundance of each EEC subtype present in multiple autochthonous models of pancreatic tumorigenesis and compared these findings to EEC abundance in patient samples encompassing normal pancreas, ADM, PanIN, and PDAC. We found that EEC subtype abundance in mouse models is highest in ADM and significantly decreases with disease progression. This trend holds true in human disease, with divergence between mouse and human observed primarily in invasive adenocarcinoma. Further, we evaluated EEC subtype-specific hormone expression and found it to be largely subtype-restricted, apart from several bihormonal populations which have not previously been described in pancreatic tumorigenesis. We demonstrate that tuft cell master regulator transcription factor, POU2F3, is not required for EEC formation (Yamaguchi et al., 2014; Gerbe et al., 2016). Recently, we found that tuft cell formation inhibits pancreatic tumorigenesis by modulating the microenvironment with anti-inflammatory prostaglandins (DelGiorno et al., 2020b). These data demonstrate that ADM-derived populations can have a significant effect on disease progression, suggesting that EEC subtype formation and abundance could have a significant impact on tumor formation and severity. Therefore, studying disease-associated EEC subtypes may identify pathways to target or co-opt for patient benefit.

MATERIALS AND METHODS

Mice

Mice were housed in accordance with NIH guidelines in AAALAC-accredited facilities at the Salk Institute for Biological Studies or Columbia University. The IACUC committees at the Salk Institute or Columbia University approved all animal studies. *LSL-Kras$^{G12D/+}$; Ptf1a$^{Cre/+}$* (*KC*), *LSL-Kras$^{G12D/+}$;Pou2f3$^{fl/fl}$; Ptf1a$^{Cre/+}$* (*KPouC*), and *LSL-Kras$^{G12D/+}$;Trp53^{R17H};Pdx1Cre* (*KPC*) mice have been described previously (Hingorani et al., 2003; Hingorani et al., 2005; DelGiorno et al., 2020b).

Human Samples

Distribution and use of all human samples was approved by the Institutional Review Boards at Vanderbilt University and Vanderbilt University Medical Center.

Histological Staining

Tissues were fixed overnight in zinc-containing, neutral-buffered formalin (Fisher Scientific), embedded in paraffin, cut in 5 µm sections, mounted, and stained. Sections were deparaffinized in xylene, rehydrated in a graded series of ethanols, and then washed in PBST and PBS. Endogenous peroxidase activity was blocked with a 1:50 solution of 30% H_2O_2:PBS followed by microwave antigen retrieval in 100 mM sodium citrate, pH 6.0. Sections were blocked with 1% bovine serum albumin (BSA) and 5% normal goat or rabbit serum in 10 mM Tris (pH 7.4), 100 mM $MgCl_2$, and 0.5% Tween-20 for 1 h at room temperature. Primary antibodies were diluted in blocking solution and incubated overnight. Information on primary antibodies is provided in **Supplementary Table S1**. Slides were then washed, incubated in streptavidin-conjugated secondaries (for rabbit or mouse antibodies, Abcam, for rat or goat antibodies, Vector) and developed with DAB substrate (Vector). Immunofluorescence on paraffin-embedded tissues followed the immunohistochemistry protocol until the blocking step. Instead, tissues were blocked with 5% normal donkey serum and 1% BSA in 10 mM PBS for 1 h at room temperature. Tissue sections were stained with primary antibodies in 10 mM PBS supplemented with 1% BSA and 0.1% Triton X-100 overnight (**Supplementary Table S1**). Sections were then washed 3 × 15 min in PBS with 1% Triton X-100, incubated in Alexa Fluor secondary antibodies, washed again for 3 × 5 min, rinsed with distilled water, and mounted with Prolong Gold containing Dapi (Invitrogen). All slides were scanned and imaged on an Olympus VS-200 Virtual Slide Scanning microscope.

Murine Co-Immunofluorescence Quantification

Slides from normal C57 BL/6 and CD1 mice were stained with antibody panels to quantify the presence of hormone+ cells in normal murine ducts. Due to their rare occurrence, only the number of intra- and interlobular ducts harboring a hormone+ cell were quantified, as opposed calculating the percentage of hormone+ cell(s) relative to the total number of cells per duct. Only ductal structures with clear lumens were counted. Intercalated ducts were excluded due to their variability in 2D appearance. The common bile duct was excluded due to its different morphology, function, and similarity to the small intestine.

Slides from 6-month-old *KC* mice were stained with antibody panels to determine if single EECs express multiple hormones or if hormones are EEC subtype restricted. Stained slides were imaged using identical imaging parameters to compare results

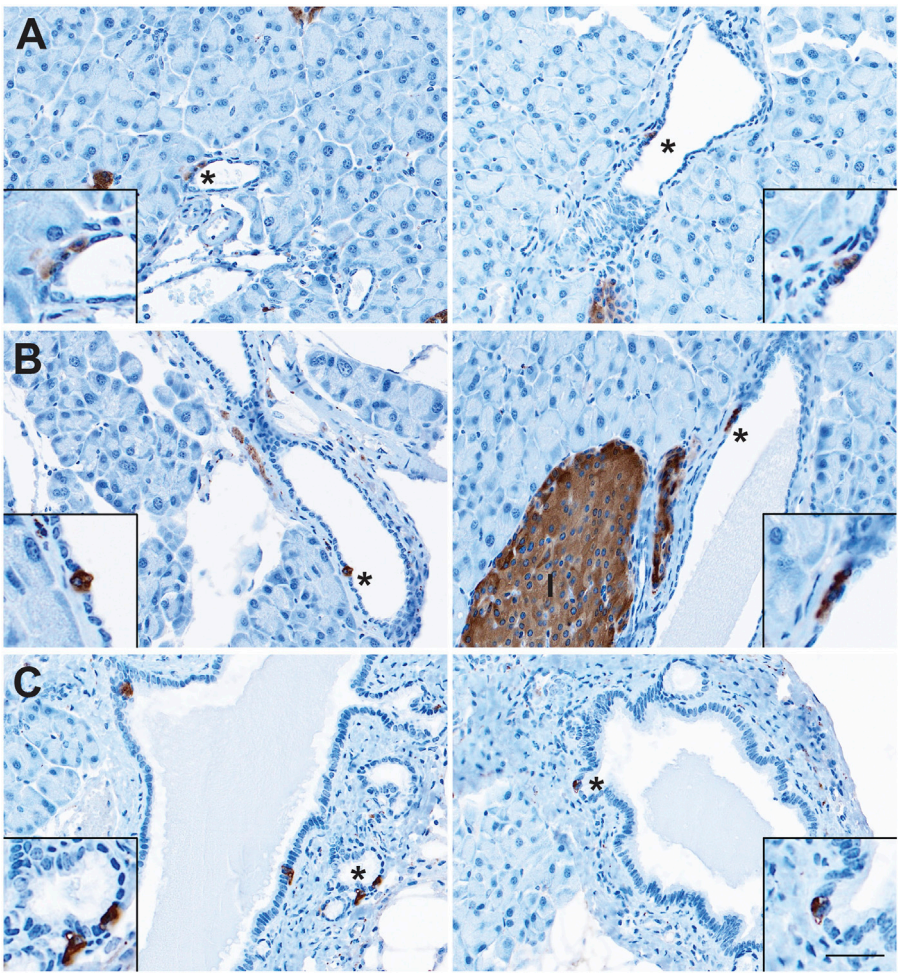

FIGURE 1 | Enteroendocrine cells as a cellular compartment of the normal murine pancreas. Immunohistochemistry for synaptophysin (brown) in the **(A)** small and **(B)** large ducts of the normal pancreas, as well as in **(C)** the pancreatobiliary duct. I, islet. Scale bar, 50 μm.

between samples. To control for autofluorescence or channel bleed through, a minimum intensity threshold was determined for each antibody for each staining combination. Positive cells were identified in luminal and PanIN structures, excluding islets or islets closely adjacent to ductal lesions. For hormone co-expression analysis, 100 positive cells were identified for each hormone per mouse (n = 3) independent of the co-stained hormone. Of note, only 236 gastrin+ cells were identified (per mouse = 100, 100, 36 gastrin+ cells). Next, the cells positive for each hormone were individually assessed for co-positivity based on the previously set minimum thresholding. The number of co-positive cells were combined, and the percentage of co-positivity was calculated.

Pathological Scoring of Murine Samples

Stained slides from *KC*, *KPouC*, or *KPC* mice were scanned on an Olympus VS-200 Virtual Slide Scanning microscope and approximately 10, 10× images were captured per mouse per stain (synaptophysin, somatostatin, pancreatic polypeptide, serotonin, and ghrelin). Lesions with or without staining (1–6 per image depending on abundance) were randomly chosen and were then graded by a pathologist (VV). The number of positively stained cells and nuclei in each lesion was then counted and the percentage of positive cells in that lesion determined.

A second pathologist subspecialized in liver and pancreas diseases (VQT) blindly scored 114 previously scored regions of interest. Concordance was noted for 72% of ROIs, and discordances never surpassed one grade. Interobserver agreement was tested in SPSS version 26 by transforming ADM, PanIN-1A, PanIN-1B, PanIN-2, PanIN-3, and invasive cancer into 1-2-3-4-5-6. Cohen's κ coefficient was 0.633 (ASD = 0.053), interpreted as substantial interobserver agreement. This suggests that the first pathologist's scoring is reliable and constant, as prior studies have noted κ coefficients ranging from 0.13 to 0.43 in prior studies of PanIN interobserver variability (Hruban et al., 2001; Longnecker et al., 2005).

Pathological Scoring of Patient Samples

Multiple samples from 11 patients with PDAC (n = 21 total slides) were stained for EEC hormones and analyzed individually.

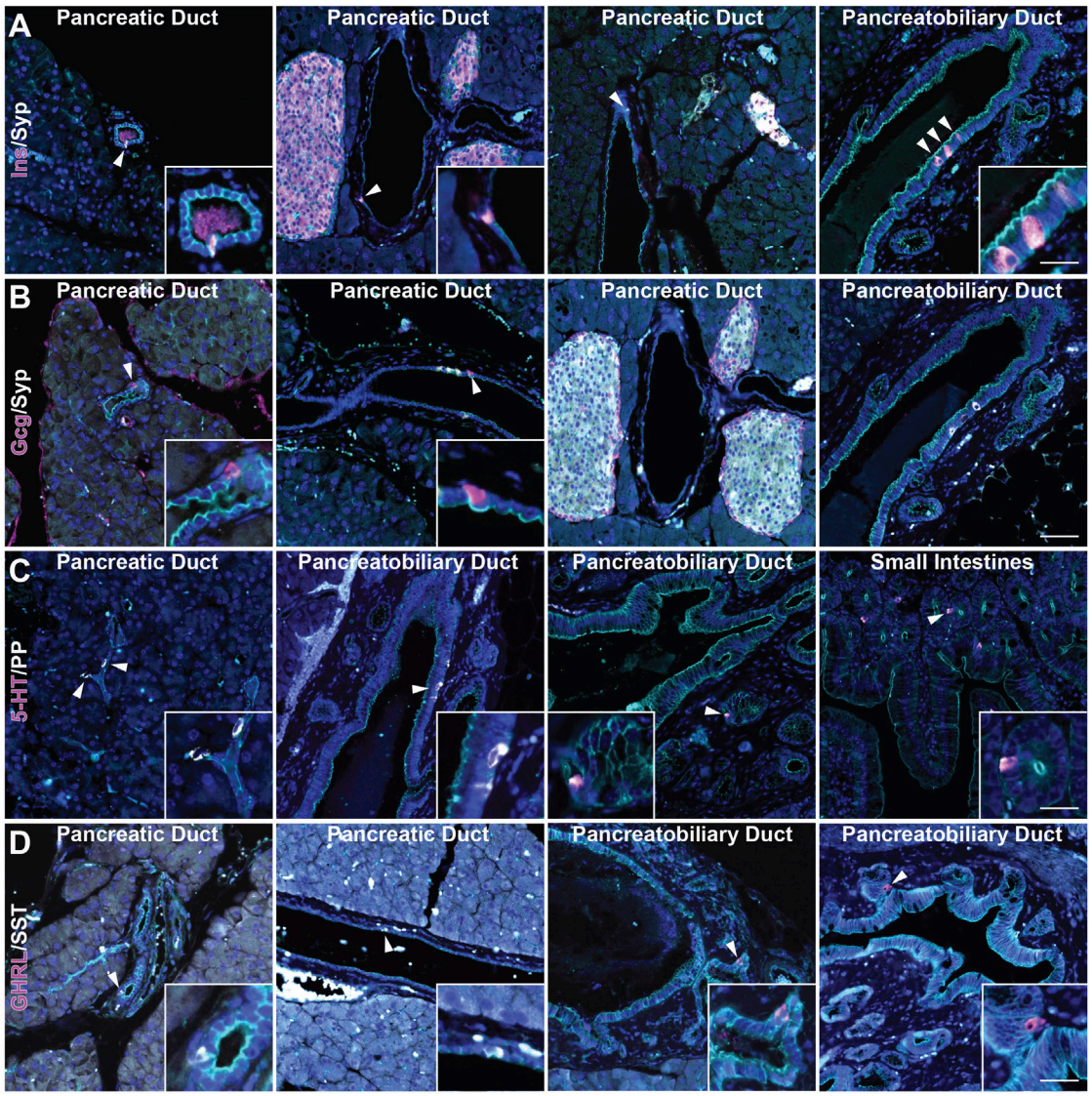

FIGURE 2 | Characterization of enteroendocrine cell subtypes in the normal murine pancreas. Co-immunofluorescence for DAPI (blue), γ Actin (cyan) and **(A)** insulin (Ins, magenta) and synaptophysin (Syp, white), **(B)** glucagon (Gcg, magenta) and synaptophysin (Syp, white), **(C)** serotonin (5-HT, magenta) and PP (white), and **(D)** ghrelin (GHRL, magenta) and SST (white) in ducts of pancreas, including the pancreatobiliary duct, or small intestines. Scale bar, 50 μm.

Hormone+ cells (GHRL, SST, 5-HT, and PP) were identified in lesions with ductal morphology; acinar and islet-associated hormone+ cells were excluded from analysis. Lesions harboring hormone+ cell(s) were then graded by a pathologist (VQT) using both the stained slide and an H&E stain from the same block. The lesion and the surrounding area were graded and recorded. Morphologically normal pancreatic ducts were graded and recorded as either normal or reactive. Lesions were classified as ADM, PanIN1a, PanIN1b, PanIN2, PanIN3, or invasive adenocarcinoma. The total number of lesions harboring at least one hormone+ cell was calculated (e.g. 268 SST+ lesions were identified in 21 slides). The percentage of each lesion grade relative to the total number of lesions was calculated (e.g. 76 of the 268 SST+ cells are found in ADM which is 28.4% of SST+ lesions).

Statistical Analysis

Statistical analyses were performed in Prism (GraphPad). Statistical significance was calculated by either two-tailed unpaired t-tests assuming equal variance or one-way ANOVA. Data are expressed as mean ± standard deviation.

Image Processing

Images were captured with an Olympus VS-200 Virtual Slide Scanning microscope and processed using ImageJ or Fiji. Figures were made using Adobe Photoshop and Illustrator.

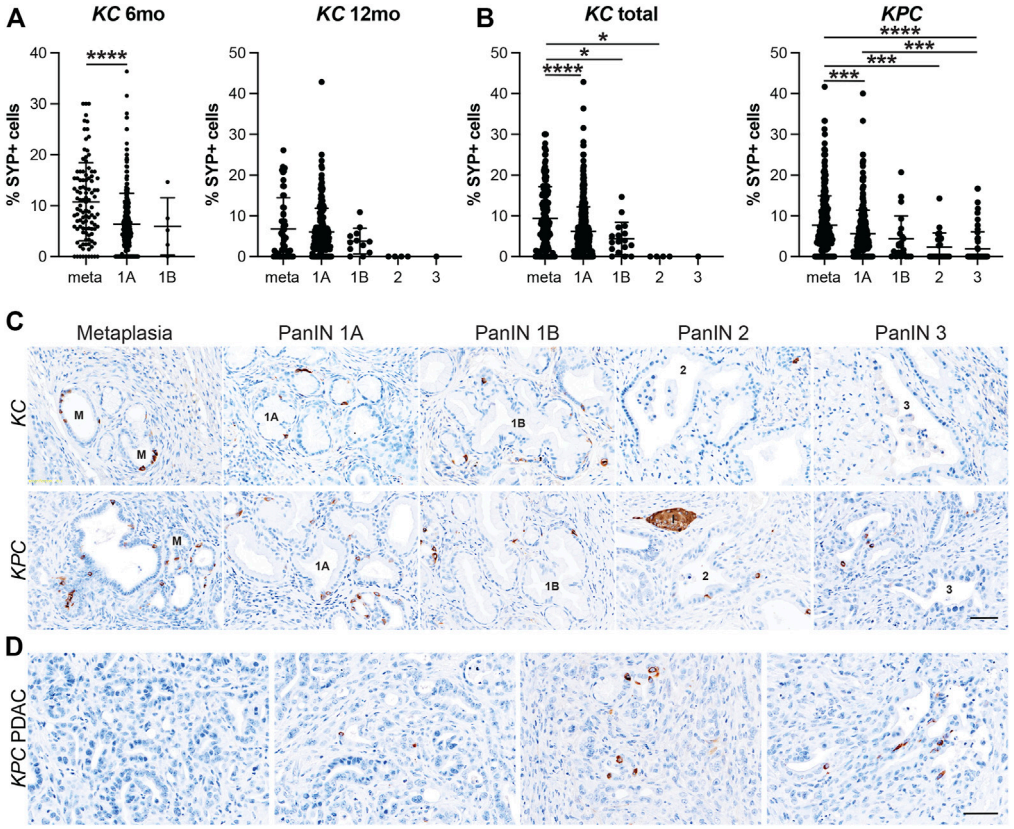

FIGURE 3 | Enteroendocrine cell abundance decreases throughout pancreatic tumorigenesis. Quantification of EECs as the percentage of synaptophysin (SYP) positive cells per lesion in metaplastic ducts (meta) through increasing grades of PanIN (1A-3) in **(A)** 6- or 12-month old *KC* mice or **(B)** *KPC* mice in various stages of disease progression. *$p < 0.05$; ***$p < 0.005$; ****$p < 0.001$. **(C)** Representative SYP IHC of lesions of increasing grade from either *KC* or *KPC* mice. I, islet. **(D)** IHC for SYP+ or SYP-adenocarcinoma in *KPC* mice. Scale bar, 50 μm.

RESULTS

Enteroendocrine Cells Are a Cellular Compartment of the Normal Pancreas

The presence of sporadic cells expressing islet-associated hormones (insulin [INS], glucagon [GCG], SST, and PP) within the normal pancreatic and pancreatobiliary ducts of rats and humans has been reported on for decades (Chen et al., 1988; Park and Bendayan, 1992; Bouwens and Pipeleers, 1998; Li et al., 2016). However, some of these populations may represent ductal-like enteroendocrine cells (EECs) similar to those found throughout the gut rather than solitary islet cells. To confirm the presence of solitary islet cells or EECs in the murine pancreatic ductal tree, we conducted immunohistochemistry (IHC) for pan-endocrine marker, synaptophysin (SYP), on normal pancreata from CD1 (n = 5) and C57 BL/6 (n = 5) mice and examined expression throughout the ducts (**Figure 1**). We observed solitary SYP+ cells within the epithelial lining of small and large ducts, as well as in the pancreatobiliary duct, which forms from the convergence of the main pancreatic duct and the common bile duct and empties into the duodenum (**Figure 1**).

Recently, we reported the formation of multiple EEC subtypes arising in injury-induced ADM (Ma et al., 2021). These EECs include archetypal islet cell types (gamma and delta cells expressing pancreatic polypeptide (PP) and somatostatin (SST), respectively), as well as EECs found in the epithelial lining of the stomach and intestines (delta cells, enterochromaffin cells expressing (5-HT), and epsilon cells expressing ghrelin (GHRL)) (Andersson-Rolf et al., 2000). While the presence of gamma, delta, and enterochromaffin cells in the normal rat pancreatic ductal epithelium has been described, epsilon cell formation has not and studies in the murine ductal tree are lacking (Park and Bendayan, 1992). To assay for these cell types in normal murine pancreatic ducts, we performed co-immunofluorescence (co-IF) for the previously listed archetypal islet cell types including insulin (INS), glucagon (GCG), SST, and PP, as well as serotonin (5-HT) and ghrelin (GHRL)+ EECs, and cell membrane marker γ-actin, to confirm the localization of these cells within the ducts (**Figure 2**). Consistent with previous reports, we observed INS+ and GCG+ cells in intra- and interlobular ducts (**Figures 2A,B**). INS+ cells were also observed in the pancreatobiliary duct, however GCG+ cells were not (**Figures 2A,B**). Additionally, INS+ cells, but not GCG+ cells, were co-positive for SYP (**Figure 2B** and **Supplementary Figure S1**). PP+ and SST+ cells were observed in intercalated, intra- and

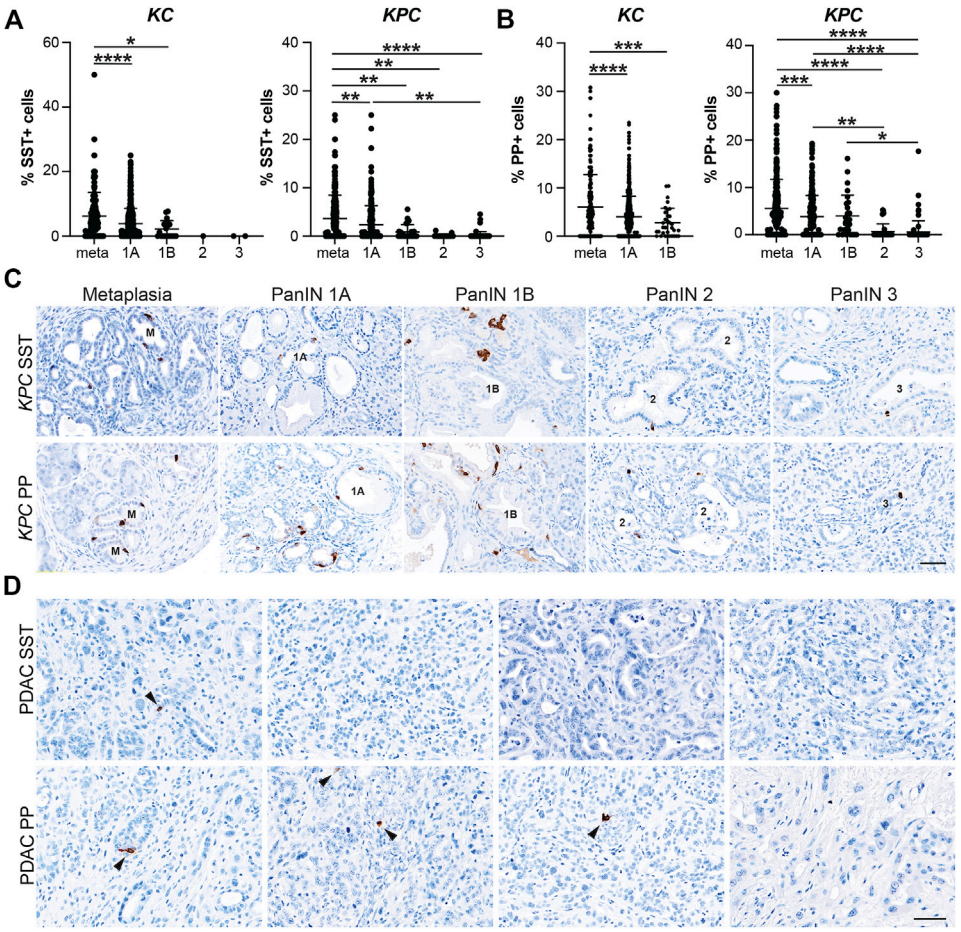

FIGURE 4 | Delta and gamma cell abundance throughout pancreatic tumorigenesis. Quantification of **(A)** delta cells (SST+) or **(B)** gamma cells (PP+) in lesions from *KC* or *KPC* mice. *$p < 0.05$; **$p < 0.01$, ***$p < 0.005$; ****$p < 0.001$. **(C)** Representative SST or PP IHC of lesions of increasing grade in *KPC* mice. **(D)** IHC for SST or PP in adenocarcinoma in *KPC* mice. Arrows, positive cells. Scale bar, 50 μm.

interlobular, and pancreatobiliary ducts consistent with previous reports (**Figures 2C,D**) (Park and Bendayan, 1992; Bertelli et al., 1994). Interestingly, 5-HT+ and GHRL+ cells were mainly observed in the pancreatobiliary duct and associated peribiliary glands, terminal structures that bud from the main ducts located in the head of the pancreas (**Figures 2C,D**). To assess the proportion of normal murine pancreatic ducts containing hormone-expressing cells, we calculated the percentage of intra- and interlobular ducts harboring at least one SST+, PP+, 5-HT+ or GHRL+ cell. SST+ cells were found in 2.34% of ducts (n = 683), and PP+ cells were found in 2.86% of normal ducts (n = 593) (**Supplementary File S1**). Alternatively, 5-HT+ and GHRL+ cells were not observed in any of the analyzed inter- and intralobular ducts (n = 593 and 683, respectively) (**Supplementary File S1**). These observations are consistent with previous studies of the pancreatic ductal tree in humans and other model systems, but also confirm the presence of EECs in the murine ductal tree and describe the presence of GHRL+ and 5-HT+ cells as largely restricted to the pancreatobiliary duct in mice.

Synaptophysin Expression Is Most Abundant in Early Stages of Tumorigenesis

We have recently shown that EECs arise in the injured pancreas during ADM (Ma et al., 2021). To determine when EEC formation occurs in pancreatic tumorigenesis, we conducted IHC on pancreas tissue from 6 or 12-month old *Kras*^{G12D};*Ptf1a*$^{Cre/+}$ (*KC*) mice and *Kras*^{G12D};*Trp53*^{R172H};*Pdx1-Cre* (*KPC*) mice with or without PDAC for pan-EEC marker SYP. Multiple regions of interest were chosen and lesions spanning pancreatic tumorigenesis (metaplasia, PanIN1a, PanIN1b, PanIN2, PanIN3, and PDAC) were graded by a pathologist. The proportion of SYP-positive cells was then calculated as well as the total number of nuclei (hematoxylin) in each lesion to determine the relative abundance of EECs. In total, 690 and 689 lesions from *KC* and *KPC* mice, respectively, were analyzed. In 6-month-old *KC*

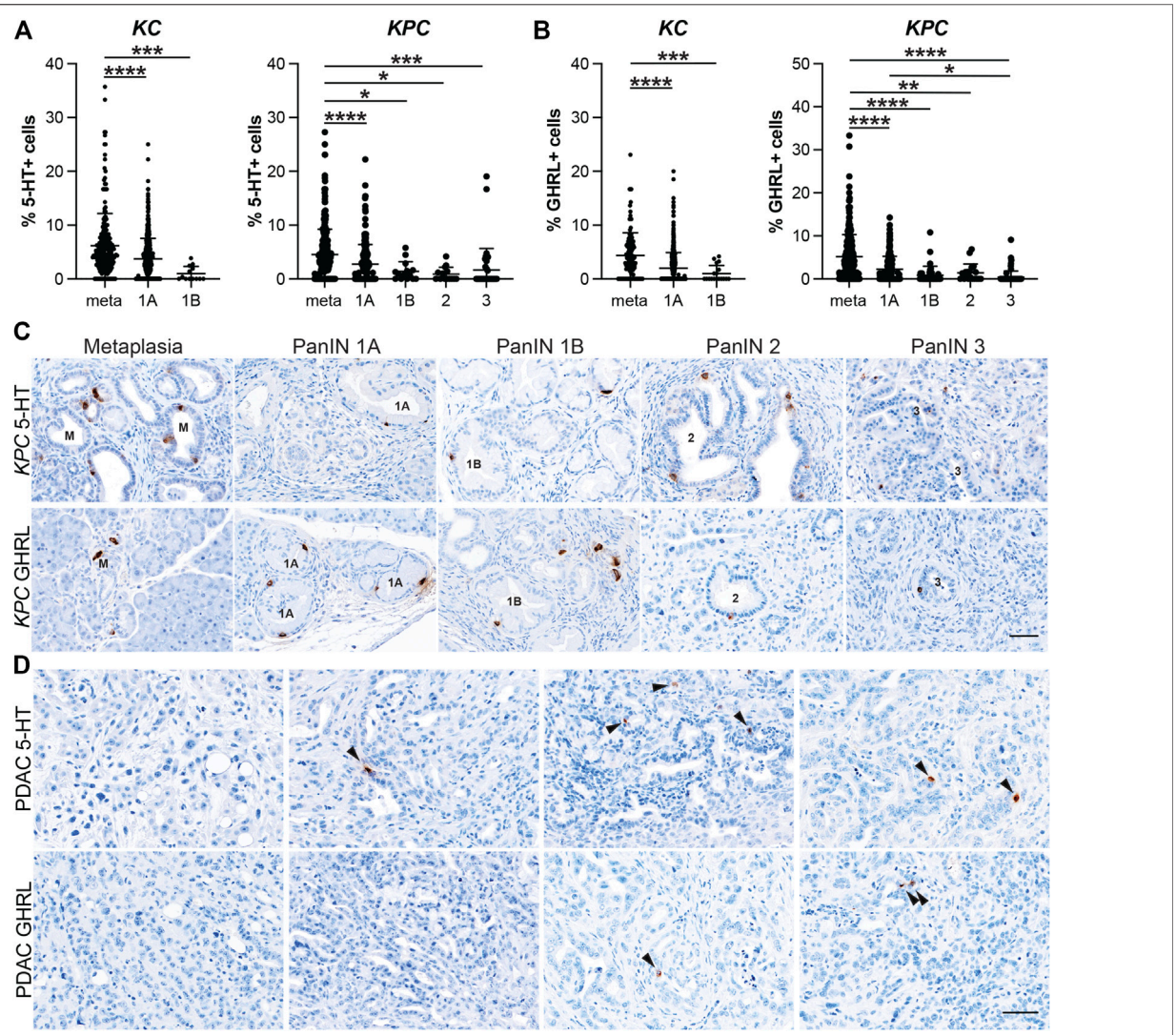

FIGURE 5 | Enterochromaffin and epsilon cell abundance throughout pancreatic tumorigenesis. Quantification of **(A)** enterochromaffin cells (5-HT+) or **(B)** epsilon cells (GHRL+) in lesions from *KC* or *KPC* mice. *$p < 0.05$; **$p < 0.01$, ***$p < 0.005$; ****$p < 0.001$. **(C)** Representative 5-HT or GHRL IHC of lesions of increasing grade in *KPC* mice. **(D)** IHC for 5-HT or GHRL in adenocarcinoma in *KPC* mice. Arrows, positive cells. Scale bar, 50 μm.

pancreata ($n = 7$ mice), metaplastic ducts were found to contain a significantly higher proportion of SYP+ cells as compared to PanIN1a lesions (10.76%, $n = 105$ vs 6.35%, $n = 302$; $p < 0.001$) (**Figures 3A,C** and **Supplementary File S1**). As 6-month-old *KC* mice typically do not develop high-grade lesions, we next examined pancreata from mice aged 12 months ($n = 5$) where more PanIN1b and PanIN2 lesions were observed. Consistent with patterns identified in 6-month-old *KC* mice, we found SYP+ cells to be most abundant in metaplasia (6.82%, $n = 58$), decreasing with increasing PanIN grade (PanIN1a, 6.00%, $n = 203$; PanIN1b, 3.79%, $n = 12$; PanIN2, 0%, $n = 4$; PanIN3, 0%, $n = 1$) (**Figures 3A,C** and **Supplementary File S1**). SYP+ cells are more abundant in 6-month-old than in 12-month-old *KC* pancreata in lesions of equivalent grade (**Supplementary Figure S2A**). To examine more high-grade lesions and PDAC specimens, we next extended our analysis to pancreata from *KPC* mice ($n = 19$).

Similar to the *KC* dataset, the *KPC* dataset is also composed primarily of metaplasia and PanIN1a, but additionally harbors more high-grade lesions and PDAC, presenting a more complete distribution of lesion grades throughout pancreatic tumorigenesis. In total, pancreata from 19 *KPC* mice were analyzed including 10 mice with cancer. As shown in **Figures 3B–C**, SYP+ cells are most abundant in metaplasia (7.72%, $n = 301$) and decrease with increasing lesion grade (PanIN1a, 5.59%, $n = 281$; PanIN1b, 4.39%, $n = 22$; PanIN2, 2.32%, $n = 24$; PanIN3, 1.89%, $n = 61$). Of the 10 mice with cancer, only three pancreata had SYP+ cells associated with PDAC. Whether these cells are cancerous or are associated low grade lesions enveloped by the cancerous tissue is unclear

(**Figure 3D**). Interestingly, we found that SYP+ cells are significantly more abundant in metaplasia in *KC* mice than in *KPC* mice (9.36%, n = 163 vs 7.72%, n = 301; $p < 0.05$), although SYP+ cells are more abundant in *KPC* pancreata later in disease progression (**Supplementary Figure S2B**). Altogether, analysis of SYP expression in the *KC* and *KPC* datasets demonstrates that EECs are significantly more prevalent in low-grade lesions consistent with EEC formation as an early event in tumorigenesis.

EEC Subtype Dynamics Throughout Pancreatic Tumorigenesis

After confirming that injury-induced EEC subtypes are present in neoplasia, we sought to determine the relative abundance of these subtypes and their temporal dynamics throughout tumorigenesis. Using the same IHC lesion assessment and quantification methods described for SYP quantification (**Figure 3**), we stained pancreata from 6 and 12-month-old *KC* mice and *KPC* mice with and without PDAC for each EEC subtype specific hormone. As anticipated, the proportion of each hormone-expressing population per lesion grade followed similar dynamics observed for SYP, with EEC subtype abundance decreasing with increasing lesion grade (**Supplementary File S1**). For SST expression, 442 and 344 lesions from 6 and 12-month-old *KC* pancreata (n = 8 and n = 6, respectively) were combined and analyzed as well as 661 lesions from *KPC* (n = 19) mice. The percentage of SST+ lesions in *KC* pancreata was significantly higher in metaplastic lesions as compared to PanIN1a (5.49%, n = 155 vs 3.91%, n = 607; $p < 0.001$) and PanIN1b (2.21%, n = 20; $p < 0.05$) (**Figure 4A** and **Supplementary File S1**). Only 1 PanIN2 and 2 PanIN3 lesions were captured in the *KC* data set, all of which were negative for SST. For *KPC* (n = 19), the percentage of SST+ cells in metaplastic lesions (3.64%, n = 329) was significantly higher than PanIN1a (2.35%, n = 220; $p < 0.01$), PanIN1b (0.89%, n = 28; $p < 0.01$), PanIN2 (0.11%, n = 17; $p < 0.01$), and PanIN3 (0.18%, n = 67; $p < 0.001$) (**Figures 4A,C** and **Supplementary File S1**). Additionally, the percentage of SST+ cells was significantly higher in PanIN1a lesions versus PanIN3 ($p < 0.01$) further supporting the observed downward trend. PDAC-associated SST+ cells were identified in only two PDAC regions of interest (ROIs, out of 67) from only two *KPC* mice (**Figure 4D**). These analyses demonstrate that SST+ cells are most abundant in the metaplastic lesions of *KC* and *KPC* pancreata, and that incidence decreases throughout pancreatic tumorigenesis.

In our analyses we also found that the proportion of PP+ cells follow a similar trajectory to SST+ cells throughout pancreatic tumorigenesis where abundance decreases as lesion grade progresses. Lesions totaling 538 and 472 from 6 and 12-month-old *KC* mice (n = 9 and n = 8, respectively) were assessed. The highest proportion of PP+ cells was observed in the metaplastic lesions (6.07%, n = 220), which was significantly higher than PanIN1a (4.01%, n = 717; $p < 0.001$) and PanIN1b (2.78%, n = 33; $p < 0.005$) (**Figure 4B** and **Supplementary File S1**). No PanIN2 or PanIN3 lesions were identified in the *KC* data set. In the *KPC* pancreata (n = 19), the proportion of PP+ cells in metaplastic lesions (5.57%, n = 336) were significantly higher than PanIN1a (3.85%, n = 236; $p < 0.005$), PanIN2 (0.67%, n = 37; $p < 0.001$), and PanIN3 (0.59%, n = 84; $p = 0.001$) (**Figures 4B,C** and **Supplementary File S1**). Additionally, the proportion of PP+ cells was significantly higher in PanIN1a versus PanIN2 ($p < 0.01$) and PanIN3 ($p < 0.001$) lesions further supporting the observed downward trend of PP+ cells as lesion grade progresses. Lastly, four PDAC ROIs (out of 51) from four different *KPC* mice contained PP+ cells (**Figure 4D**).

5-HT+ cells exhibited similar dynamics to SST+ and PP+ cells throughout tumorigenesis. Lesions from 6 and 12-month-old *KC* mice (n = 8 and n = 7, respectively) totaled 457 and 351. The percentage of 5-HT+ cells per lesion was significantly higher in metaplastic lesions (6.18%, n = 233) compared to PanIN1a (3.73%, n = 562; $p < 0.001$) and PanIN1b (0.98%, n = 13; $p < 0.005$) (**Figure 5A** and **Supplementary File S1**). No PanIN2 or -3 lesions were identified in this *KC* data set. 572 total lesions were analyzed from *KPC* pancreata with or without PDAC (n = 19) and displayed a similar trend to the *KC* data. Metaplastic *KPC* lesions contained a significantly higher percentage of 5-HT+ cells per lesion (4.54%, n = 290) compared to PanIN1a (2.75%, n = 213; $p < 0.001$), PanIN1b (1.42%, n = 14; $p < 0.05$), PanIN2 (0.89%, n = 14; $p < 0.05$), and PanIN3 (1.65%, n = 41; $p < 0.005$) (**Figures 5A,C** and **Supplementary File S1**). Interestingly, 34/88 5-HT+ PDAC ROIs were identified in seven of nine tumor bearing *KPC* mice compared to SST (n = 2), PP (n = 4), and GHRL (n = 5) (**Figure 5D**). This observation suggests differing roles for each hormone throughout different stages of tumorigenesis.

Lastly, the dynamics of GHRL+ cells followed a similar course as the previously described hormones. 374 and 296 lesions from 6 and 12-month-old *KC* mice (n = 7 and n = 5, respectively) were analyzed, and metaplastic ducts contained a significantly higher proportion of GHRL+ positive cells (4.34%, n = 122) as compared to PanIN1a (2.00%, n = 517; $p < 0.001$) and PanIN1b (1.00%, n = 18; $p < 0.005$) (**Figure 5B** and **Supplementary File S1**). There were no PanIN2 or -3 lesions identified in this *KC* dataset. The *KPC* (n = 19) dataset exhibited the same trend where the percentage of GHRL+ cells significantly decrease as lesion grade increases. Metaplastic *KPC* lesions contained a significantly higher percentage of GHRL+ cells (5.19%, n = 337) as compared to PanIN1a (2.25%, n = 168; $p < 0.001$), PanIN1b (0.87%, n = 38; $p < 0.001$), PanIN2 (1.45%, n = 19; $p < 0.01$), and PanIN3 (0.41%, n = 70; $p < 0.001$) (**Figures 5B,C** and **Supplementary File S1**). Additionally, the percentage of GHRL+ cells was significantly higher in PanIN1a versus PanIN3 ($p < 0.05$) further supporting the observed downward trend. GHRL+ cells were identified in 5 PDAC ROIs (n = 64) from two different *KPC* mice (**Figure 5D**). Altogether, the expression of each EEC subtype hormone is most abundant in metaplasia and significantly decreases with tumor progression. EEC subtype abundance in 6- vs 12-month-old *KC* mice and

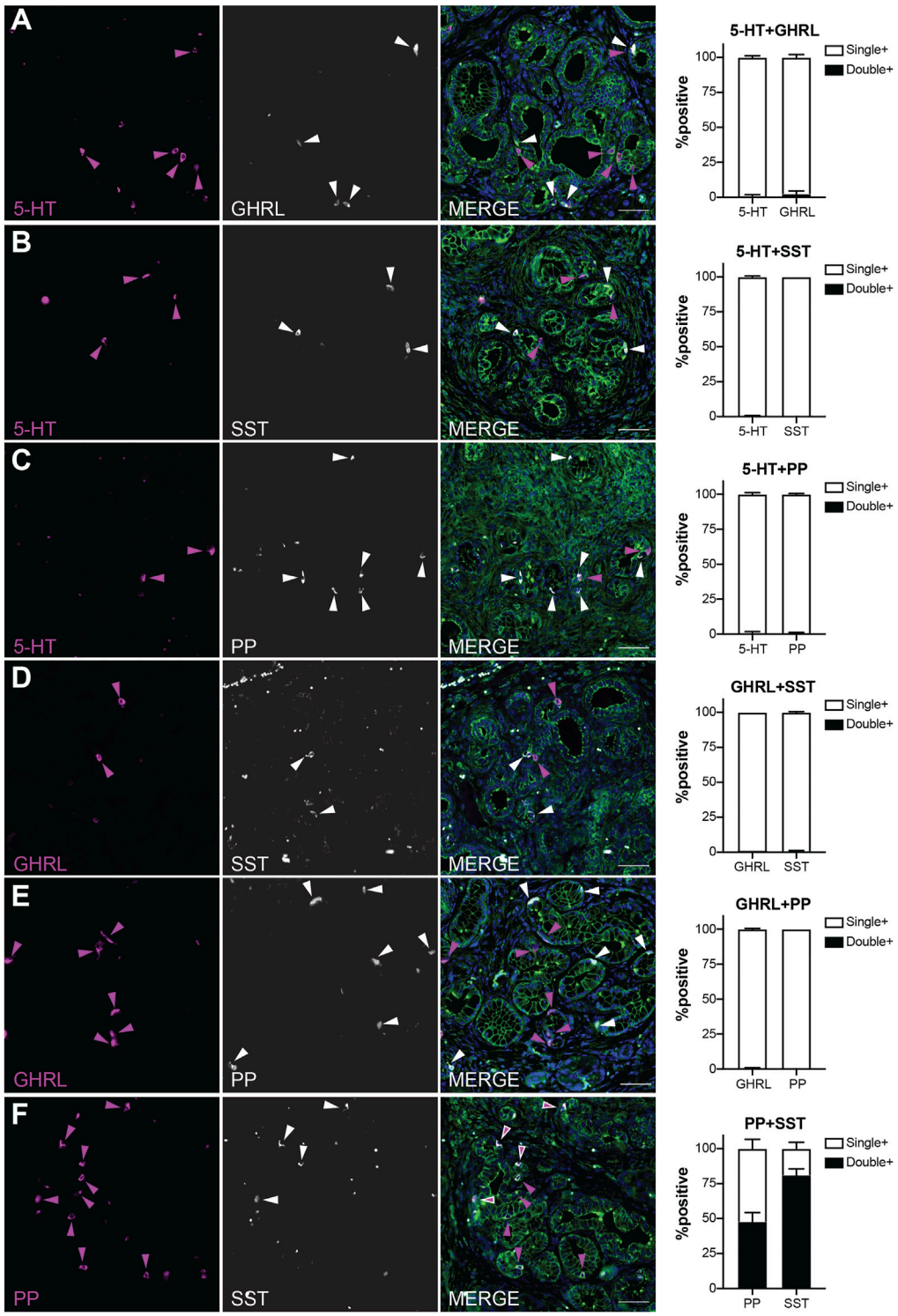

FIGURE 6 | EEC subtypes identified by distinct and overlapping hormone signatures. Co-immunofluorescence and quantification of **(A)** 5-HT and ghrelin (0.67 and 2.33% co-expression, respectively), **(B)** 5-HT and SST (0.33 and 0% co-expression, respectively), **(C)** 5-HT and PP (0.67 and 0.67% co-expression, respectively), **(D)** ghrelin and SST (1 and 0.67% co-expression, respectively), **(E)** PP and ghrelin (0 and 0.33% co-expression, respectively), and **(F)** PP and SST (47.7 and 81% co-expression, respectively). Scale bar, 50 μm.

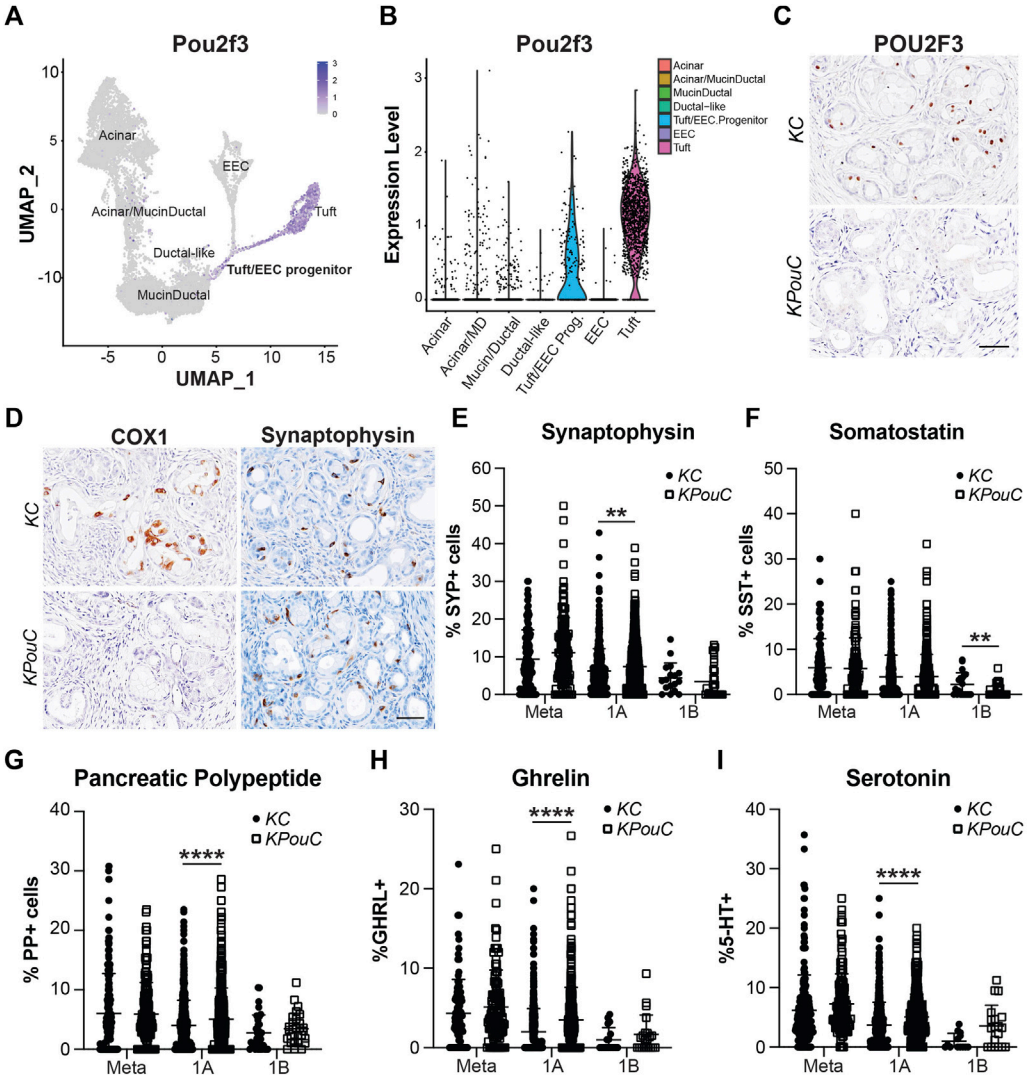

FIGURE 7 | POU2F3 is not required for EEC formation but affects abundance. **(A)** UMAP and **(B)** Violin plot of *Pou2f3* expression in an injury-induced pancreatic metaplasia dataset demonstrating expression in tuft cells as well as the predicted tuft/EEC common progenitor population. Modified from Ma et al. **(C)** IHC for POU2F3 or **(D)** COX1 or SYP in 6-month-old *KC* or *KPouC* pancreata. Scale bar, 50 μm. **(E)** Quantification of pan-EEC marker synaptophysin (SYP) and EEC subtype markers **(F)** SST, delta cells, **(G)** PP, gamma cells, **(H)** GHRL, epsilon cells, and **(I)** 5-HT, enterochromaffin cells, in the pancreata of 6- and 12-month-old *KC* or *KPouC* mice. $^{**}p < 0.01$; $^{****}p < 0.001$.

between *KC* and *KPC* mice varies by subtype (**Supplementary Figure S3**).

PanIN Are Constituted by Distinct Enteroendocrine Cell Subtypes

Our recently published scRNA-seq study of injury-induced pancreatic ADM identified multiple EEC subtypes based on individual hormone expression (Ma et al., 2021). Based on these results, we hypothesized that hormone expression in pancreatic tumorigenesis is largely EEC subtype restricted. To test this hypothesis, we performed co-IF on 6-month-old *KC* pancreata (n = 3 mice) for the previously described EEC hormones to determine if the EECs arising in tumorigenesis represent distinct lineages. Pancreata in this analysis harbored primarily ADM and PanIN1a lesions and were co-stained with 2-hormone combinations and γ-actin which served as a membranous marker. 100 non-islet associated, hormone positive cells were identified for each staining panel per mouse (300 total cells), then dual-hormone expression was identified and quantified (*see* **methods**). Most hormone expression in 6-month-old *KC* pancreata is subtype-restricted, with a co-positivity rate of 2.3% or less (**Figure 6**). Only 0.67% of 5-HT+ cells were co-positive for GHRL, and 2.33% GHRL+

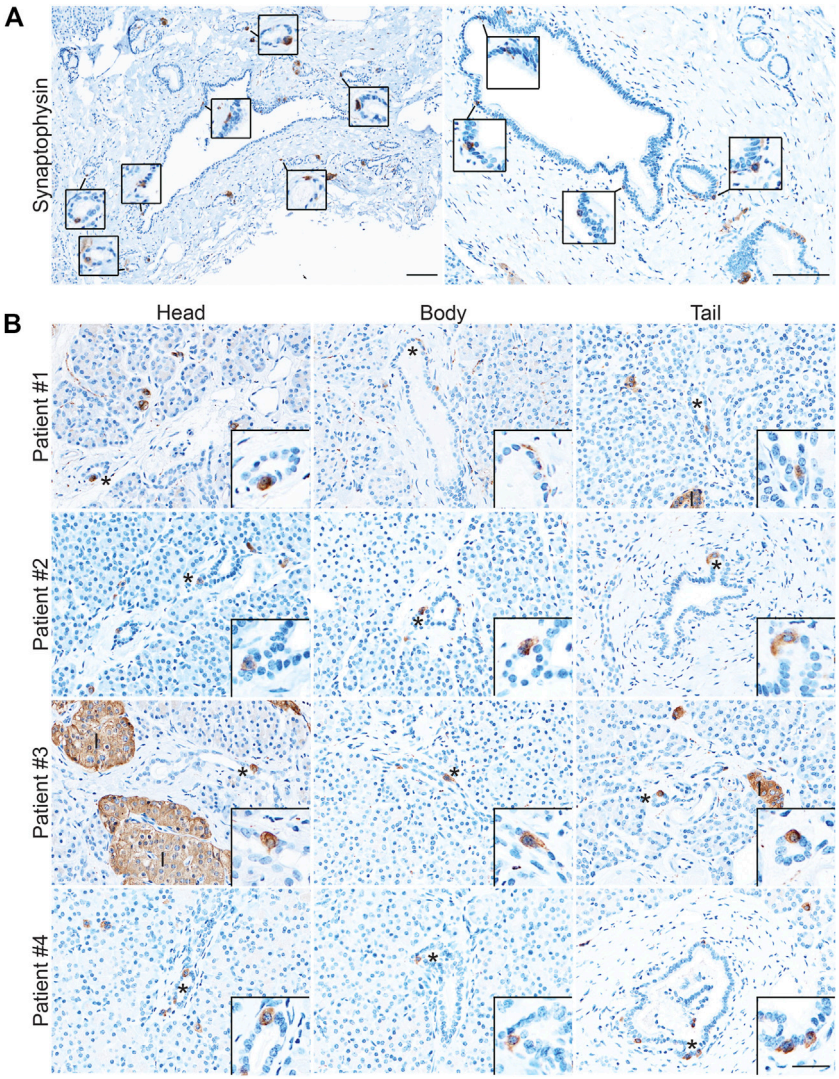

FIGURE 8 | Enteroendocrine cells as a cellular compartment of the normal human pancreas. Synaptophysin IHC of **(A)** large, pathologically normal ducts in human pancreata. Scale bar, 100 μm. **(B)** Synaptophysin IHC of pancreata from four human donors determined to have normal islet function. Images are representative of the head, body, and tail of the same pancreata. Scale bars, 50 μm for main images, 25 μm for inserts.

were co-positive for 5-HT (**Figure 6A**). Similar results were observed between 5-HT and SST, with 0.33% of 5-HT+ cells co-positive for SST, and 0% of SST+ cells co-positive for 5-HT (**Figure 6B**). 0.67% of 5-HT+ and PP+ cells were co-positive (**Figure 6C**). 1% of GHRL+ cells were co-positive for SST, and 0.67% of SST+ cells were co-positive for GHRL (**Figure 6D**). 0% of PP+ cells were co-positive for GHRL, and 0.33% of GHRL+ cells were co-positive for PP (**Figure 6E**). This confirms our hypothesis that hormone expression is largely EEC subtype restricted.

In contrast, PP and SST showed a high degree of co-expression with 81% of SST+ cells co-positive for PP, and 47.7% of PP+ cells co-positive for SST (**Figure 6F**). This high degree of overlap could be due to the common lineage trajectory identified for these two EEC subtypes in our previous work or could be the formation of bihormonal ADM-derived gamma cells similar to those in islets recently reported by Perez-Frances et al. (Ma et al., 2021; Perez-Frances et al., 2021). Additionally, our scRNA-seq data predicts that a subset of enterochromaffin cells co-express gastrin, a hormone secreted by G cells located in the antrum of the stomach and duodenum (Yacoub et al., 1996; Ma et al., 2021). Co-IF analysis of 5-HT and gastrin identified 15% of 236 gastrin+ cells positive for 5-HT, and 9.33% of 300 5-HT+ cells as co-expressing gastrin (**Supplementary Figure S4**). Together, these observations support the hypothesis that EEC hormone expression is

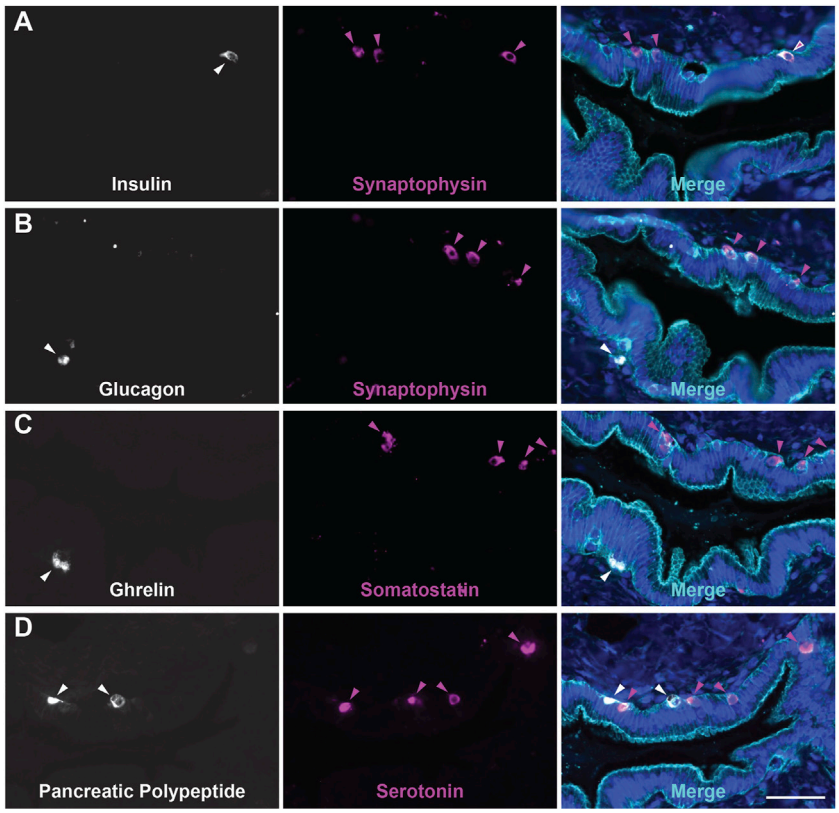

FIGURE 9 | Endocrine/Enteroendocrine cell subtypes in the ducts of the human pancreas. Co-immunofluorescence for hormones **(A)** INS (white) and SYP (magenta), **(B)** GCG (white) and SYP (magenta), **(C)** GHRL (white) and SST (magenta), or **(D)** PP (white) and 5-HT (magenta), and γ Actin (cyan) and DAPI (blue). Scale bar, 50 μm.

primarily restricted to its respective subtype, but also identifies dual PP-SST and 5-HT-gastrin expressing EECs in pancreatic tumorigenesis.

POU2F3 Is Not Required for EEC Formation

Transcription factor POU2F3 is the master regulator of tuft cell formation in normal organs and in pancreatic tumorigenesis (Gerbe et al., 2016; DelGiorno et al., 2020b). Our scRNA-seq study of pancreatic ADM identified *Pou2f3* expression in a progenitor cell population predicted to seed both tuft cells and EECs (**Figures 7A,B**) (Ma et al., 2021). Comparison of our dataset with a scRNA-seq study of $Kras^{G12D}$-induced ADM suggests this population is present in pancreatic tumorigenesis as well (**Supplementary Figure S5A**) (Ma et al., 2021; Schlesinger et al., 2020). To determine if POU2F3 is required for EEC formation in pancreatic tumorigenesis, we examined EEC abundance in the pancreata of $Kras^{G12D}$; $Pou2f3^{fl/fl}$;$Ptf1a^{Cre/+}$ (*KPouC*, tuft cell knockout) mice aged to 6 or 12-months (DelGiorno et al., 2020b). IHC staining for POU2F3 demonstrates a lack of expression in *KPouC* pancreata (**Figure 7C**). Additionally, COX1, a marker of mature tuft cells, is absent from the epithelium of *KPouC* pancreata, consistent with a lack of tuft cell formation (**Figure 7D**) (Grunddal et al., 2021; Ma et al., 2021; Manco et al., 2021). Interestingly, SYP+ cells were identified in both *KC* and *KPouC* pancreata indicating that EEC formation is not prevented by the loss of POU2F3 (**Figure 7D**). Further, all EEC subtype-specific hormones are also present in *KPouC* pancreata and display the same general downward trend in abundance as lesion grade increases (**Supplementary Figure S5**). These data demonstrate that ablating *Pou2f3* in the context of an activating $Kras^{G12D}$ mutation does not prevent EEC formation.

Loss of POU2F3 Impacts EEC Subtype Abundance

To determine if loss of POU2F3 affects the dynamics of EEC subtype formation and abundance, we executed the same IHC quantification strategy used for *KC* and *KPC* mice (**Figures 3–5**). SYP IHC staining of combined 6 and 12-month *KPouC* pancreata ($n = 13$) exhibited the same trend as in the *KC* and *KPC* models, with metaplastic lesions containing a significantly higher percentage of SYP+ cells (11.10%, $n = 139$) as compared to PanIN1a (7.44%, $n = 562$; $p < 0.001$), PanIN1b (3.47%, $n = 28$; $p < 0.001$), PanIN2 (0%, $n = 15$; $p < 0.001$), and PanIN3 (0%, $n = 12$; $p < 0.001$) (**Supplementary Figure S5B** and **Supplementary File S1**). As compared to *KC*,

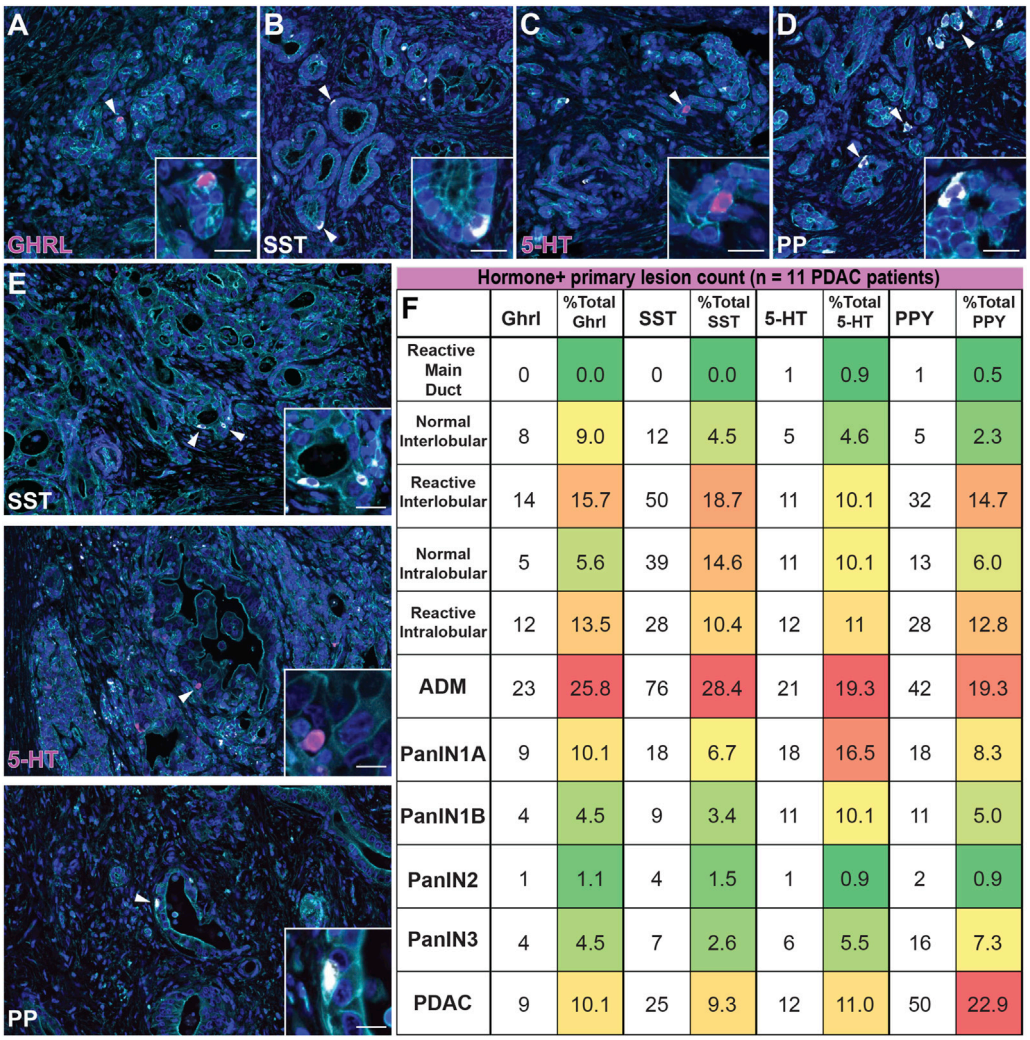

F

Hormone+ primary lesion count (n = 11 PDAC patients)								
	Ghrl	%Total Ghrl	SST	%Total SST	5-HT	%Total 5-HT	PPY	%Total PPY
Reactive Main Duct	0	0.0	0	0.0	1	0.9	1	0.5
Normal Interlobular	8	9.0	12	4.5	5	4.6	5	2.3
Reactive Interlobular	14	15.7	50	18.7	11	10.1	32	14.7
Normal Intralobular	5	5.6	39	14.6	11	10.1	13	6.0
Reactive Intralobular	12	13.5	28	10.4	12	11	28	12.8
ADM	23	25.8	76	28.4	21	19.3	42	19.3
PanIN1A	9	10.1	18	6.7	18	16.5	18	8.3
PanIN1B	4	4.5	9	3.4	11	10.1	11	5.0
PanIN2	1	1.1	4	1.5	1	0.9	2	0.9
PanIN3	4	4.5	7	2.6	6	5.5	16	7.3
PDAC	9	10.1	25	9.3	12	11.0	50	22.9

FIGURE 10 | Enteroendocrine cell subtype dynamics throughout human pancreatic tumorigenesis. Co-immunofluorescence for **(A)** GHRL (magenta), **(B)** SST (white), **(C)** 5-HT (magenta), or **(D)** PP (white) and γactin (cyan), and DAPI (blue) in human ADM lesions. **(E)** Co-immunofluorescence for SST (white), 5-HT (magenta), or PP (white) and γactin (cyan), and DAPI (blue) in human adenocarcinoma. Scale bar, 50 μm. **(F)** Table depicting the number of human lesions harboring at least one hormone+ cell for each EEC subtype and organized by lesion grade. The number of EEC-containing lesions were totaled per hormone, and the relative distribution (%) of EEC-containing graded lesions are displayed (11 patients); red = highest % of total; green = lowest % of total.

KPouC PanIN1a lesions contain a significantly higher percentage of SYP+ cells (7.44%, n = 562 vs 6.21%, n = 505; $p < 0.01$), while SYP+ cells are similarly abundant in metaplasia and PanIN1b (**Figure 7E**). Differences were also identified in EEC subtype abundance between the tuft cell+ (*KC*) and tuft cell knockout (*KPouC*) mice. Delta/SST+ cell abundance is significantly lower in *KPouC* vs *KC* PanIN1b lesions (0.68%, n = 37 vs 2.12%, n = 20; $p < 0.01$) (**Figure 7F** and **Supplementary File S1**). In terms of PanIN1a, *KPouC* mice have a significantly higher abundance of PP (5.07%, n = 617 vs 4.01%, n = 717; $p < 0.001$), GHRL (3.48%, n = 460 vs 2.00%, n = 517; $p < 0.001$), and 5-HT (5.09%, n = 420 vs 3.73%, n = 562; $p < 0.001$) cells (**Figures 7G–I** and **Supplementary File S1**). These differences may be attributed to the faster rate of tumorigenesis in *KPouC* versus *KC* mice which is supported by the identification of more PanIN2 and PanIN3 lesions in *KPouC* pancreata (**Supplementary File S1**) (DelGiorno et al., 2020b). Alternatively, POU2F3 or tuft cells may play a role, directly or indirectly, in specifying EEC subtype formation.

Enteroendocrine Cells as a Cellular Compartment of the Normal Human Pancreas

While the presence of solitary hormone secreting cells has been described in the normal pancreas, injured pancreas, Type 1 diabetes, and cystic fibrosis, the characterization of EECs in

the normal pancreas is incomplete (Chen et al., 1988; Brissova et al., 2018; Hart et al., 2018; Ma et al., 2021). To determine if normal human ducts are populated by EECs, we assessed three distinct regions (head, body, tail) of normal human donor pancreata (n = 4) for the presence of SYP and EEC subtype markers. As shown in **Figure 8A**, we identified SYP+ cells within the epithelial layer of pathologically normal large ducts, as well as in surrounding basal glands. Additionally, SYP+ cells were identified in smaller, intra- and interlobular ducts throughout the head, body, and tail of all pancreata, supporting the observation that EECs are a cellular compartment of the normal human pancreas (**Figure 8B**). To determine if human pancreata are populated by the EEC subtypes described in this study, we performed co-IF for GHRL, SST, PP, and 5-HT, as well as INS (beta cells) and GCG (alpha cells) (**Figure 9**). Interestingly, we identified solitary INS+ and GCG+ cells within ducts in the head (INS, ¾ pancreata; GCG ²⁄₄ pancreata), body (INS, ¼ pancreata; GCG ¼ pancreata), and tail (INS, ¼ pancreata; GCG ²⁄₄ pancreata) (**Figures 9A,B**). Whether these cells are associated with islets in another plane could not be determined, however, these solitary cells are part of the single layer epithelium of these ducts. Next, we assayed pancreata for EEC subtype hormones and could identify expression in the head (SST, ¾; PP, ¼; 5-HT, ¼), body (GHRL, ¼; SST, ²⁄₄; PP, ¾; 5-HT, ¼), and tail (GHRL, ¾; SST, ¼; PP, ²⁄₄; 5-HT, ²⁄₄) (**Figures 9C,D**). Altogether all EEC subtype hormones were identified in the ducts of normal human pancreata, supporting the identification of EECs as a cellular compartment of the normal human pancreas. Whether or not these cells have a distinct origin from islets remains to be determined.

Dynamics of EEC Subtype Abundance in Human Pancreatic Tumorigenesis

Expression of endocrine hormones has been reported in human PanIN and PDAC, however the formation and dynamics of EEC subtypes throughout tumorigenesis has not been assessed (Farrell et al., 2017; Sinha et al., 2017; Chen et al., 1988; Sakaki et al., 2002). Here, we performed co-IF for SST/γ-actin/GHRL (n = 21 slides) and 5-HT/γ-actin/PP (n = 20 slides) on human PanIN and PDAC samples (n = 11 patients), as well as adjacent normal, and identified ductal lesions containing hormone+ cells. These lesions were then graded by a pathologist. Ducts were classified as normal or reactive (**Supplementary Figure S6A**) and lesions were classified by grade (ADM, PanIN1a, PanIN1b, PanIN2, PanIN3, invasive adenocarcinoma). Additionally, ADM-like ductal structures residing within a lobule harboring a higher graded lesion were termed a "basal gland" of that lesion. These glands are similar to the glands associated with the pancreatic and common bile ducts, and therefore may be considered an extension of the larger lesion (*see* **Supplementary File S2** for classification definitions) (Yamaguchi et al., 2015). As we cannot confirm the origin of basal glands in our 2D analysis, these structures were analyzed separately from their associated ductal lesion (**Supplementary Figure S6B** and **Supplementary File S2**).

The percentage of each hormone+ lesion class (e.g. normal, PanIN, etc.) relative to the total number of positive lesions for that hormone were calculated and analyzed. Consistent with our mouse data set, we observed similar dynamics throughout tumorigenesis for each hormone analyzed. ADM lesions represented the highest percentage of GHRL+ (25.8%), SST+ (28.4%), 5-HT+ (19.3%), and PP+ (19.3%) lesions relative to the average of combined normal inter- and intralobular ducts (7.3, 9.6, 7.4, and 4.2%, respectively) and high grade (PanIN3, 4.5, 2.6, 5.5, and 7.3%, respectively) for each hormone (**Figures 10A–D,F**). In general, the relative proportion of hormone+ lesions decreased as lesion grade increased. Overall, *KC* and *KPC* mouse data recapitulate EEC dynamics observed in human tumorigenesis.

Upon further analysis of each individual hormone, we observed notable differences in EEC dynamics within the human data set as compared to mouse models. Of the non-lesion ducts (normal and reactive main, inter-, and intralobular), reactive interlobular ducts harbored the highest percentage GHRL+ (15.7%), SST+ (18.7%), and PPY+ (14.7%) lesions (**Supplementary Figure S6A**). Additionally, we observed more hormone+ reactive inter- and intralobular ducts as compared to their normal counterparts (**Figure 10F**). Interestingly, we observed that the percentage of 5-HT+ lesions is largely represented by ADM and PanIN1a, with a notable, but less pronounced increase in invasive adenocarcinoma (**Figures 10E,F**). Lastly, the abundance of PP+ lesions most notably fluctuates over the course of tumorigenesis, as compared to the other hormone+ lesions. While the proportion of hormone+ invasive adenocarcinoma lesions is relatively high for each individual hormone (10.1% of total GHRL+, 9.3% of total SST+, and 11.0% of total 5-HT+ lesions) we observed a more exaggerated second peak of PP-harboring invasive adenocarcinoma lesions (22.9% of total PP+ lesions) (**Figures 10E,F**). These observations demonstrate the dynamic nature of EECs throughout human tumorigenesis.

DISCUSSION

Early events in pancreatic tumorigenesis are poorly understood. Here, we used histological methods to describe and quantify the dynamics of EEC subtype (gamma, delta, epsilon, and enterochromaffin cell) formation and abundance throughout tumorigenesis in murine models and human disease (Ma et al., 2021). We found, in both murine and human pancreata, that EEC subtypes are most abundant in ADM and PanIN1a lesions and that these cells decrease in frequency with disease progression. In human disease we observed a moderate resurgence of EEC subtype abundance in invasive adenocarcinoma relative to pre-invasive lesions suggesting that these cells may have different functional roles in different stages of tumorigenesis. Additionally, we quantified previously undescribed bihormonal EECs (gastrin and 5-HT, SST and PP) in 6-month-old *KC* pancreata, the latter of which has been described only in

islets (Perez-Frances et al., 2021). This bihormonal expression reflects either the maturation state of this population, or a functional subclass of these EECs. We also show that tuft cell master regulator transcription factor POU2F3 is not required for EEC formation in *KC* mice but does affect the abundance of EEC subtypes in early lesions. This could be due to the direct actions(s) of tuft cell secretory products on EEC formation or could be an indirect response to the stromal changes that result from tuft cell loss (DelGiorno et al., 2020b). Collectively, these data demonstrate that EEC subtype formation within $Kras^{G12D}$-induced epithelial lesions is an early event in pancreatic tumorigenesis and that these cells likely play different functional roles throughout tumor progression.

Interestingly, we also observed differences in the abundance of each EEC population throughout tumorigenesis and between mouse models and human disease. In mice, 34 of 88 PDAC ROIs contain 5-HT+ cells, the highest of all subtypes analyzed. In human disease, ADM, PanIN1a, and PanIN1b contain the highest proportion of 5-HT+ lesions while other hormone+ lesions decrease in PanIN1b. Additionally, the proportion of 5-HT+ lesions moderately increase again in invasive adenocarcinoma. Previous studies have shown that 5-HT supports pancreatic tumor growth and modulates inflammation (Jiang et al., 2017; Schneider et al., 2021; Wang et al., 2021). In the context of our findings, we predict that the increase in 5-HT+ enterochromaffin cells in ADM and early PanIN is a reaction to metaplasia and initially inhibits tumorigenesis, but in later stages supports the formation of more aggressive lesions (Soll et al., 2010; Sarrouilhe and Mesnil, 2019). Further studies are required to elucidate the function of 5-HT in tumorigenesis and may also identify therapeutic routes for early intervention.

In our analyses, we observed a relatively high proportion of PP+ and SST+ EECs in normal and reactive pancreatic ducts in the human data set, consistent with prior studies of the normal human pancreatic ductal tree (Li et al., 2016). We also observed an increase in PP+ gamma cells in invasive adenocarcinoma relative to both pre-invasive PP+ lesions and other hormone+ lesions. PP regulates endocrine and exocrine secretion in the normal pancreas and can stimulate certain neuronal pathways (Whitcomb et al., 1990). In pancreatic tumorigenesis, PP may control the function of other secretory cells, such as tuft cells and the EECs described here. However, the function of PP in cancer in unknown and warrants further investigation. In contrast, SST is known to inhibit secretory processes and other cellular processes. SST analogs such as Octreotide and Lanreotide are currently used for the treatment of multiple diseases, including certain cancers (particularly neuroendocrine tumors), which supports a role for SST in downregulating pro-tumorigenic processes in the pancreas (Enzler and Fojo, 2017).

Finally, we report the presence of GHRL+ epsilon cells within the peribiliary glands of the pancreatobiliary duct, a glandular structure reported to serve as a possible progenitor niche, as well as expansion of this population in $Kras^{G12D}$-induced tumorigenesis (Yamaguchi et al., 2015). While considered a differentiated cell type in the stomach and intestines, functioning in glucose metabolism (among other roles), GHRL+ cells have also been shown to be a progenitor population in the developing islet (Wren et al., 2001; Tong et al., 2010; Arnes et al., 2012; Poher et al., 2018). Recently, ghrelin was shown to downregulate ductal and fibrotic markers in a genetic model of cholestasis, consistent with an anti-inflammatory role in disease progression (Petrescu et al., 2020). Our data demonstrate that GHRL+ cells are more abundant early in disease progression in both mouse and human, and when coupled with these studies are consistent with a role for ghrelin in mitigating tumorigenesis.

While the number of lesions included in this analysis is extensive, we recognize that 2D histological methods may have captured a single islet cell adjacent to the basement membrane of the ductal epithelium. To limit this possibility, we took care to exclude hormone+ cells not within the epithelial sheet in our analyses. Additionally, without lineage tracing we recognize that we cannot confirm the origin of these EECs (e.g. from acinar cells), however we expect that inclusion into ADM and PanIN would lead to similar functional effects despite cell of origin. Furthermore, despite positive stains for various hormones, evidence of hormone secretion has not yet been demonstrated, and the physiological function of these EEC subtypes remains be investigated.

Altogether, our study identifies and quantifies the dynamics of EEC subtype formation throughout murine and human pancreatic tumorigenesis. In contrast to the endocrine-islet compartment of the pancreas, this enteroendocrine compartment represents an understudied population with a potentially huge impact on pancreas function and disease progression. Further studies are required to determine the individual and combined role(s) of these EEC subtypes and their respective hormones. Manipulation of these pathways alone or in combination with standard chemotherapy may provide more efficacious treatments for PDAC.

DATA AVAILABILITY STATEMENT

The original contributions presented in the study are included in the article/**Supplementary Material**, further inquiries can be directed to the corresponding author.

ETHICS STATEMENT

The studies involving human participants were reviewed and approved by The IRB committee of Vanderbilt University Medical Center. Written informed consent for participation was not required for this study in accordance with the national legislation and the institutional requirements. The animal study was reviewed and approved by The IACUC committees at the Salk Institute and Columbia University.

AUTHOR CONTRIBUTIONS

Author contributions: Conceptualization: KD. Formal analysis: LC, VV, NJ, DG, VT, and KD. Funding acquisition: KD. Investigation: LC and KD. Administration: KD. Resources: KO. Supervision: MT and KD. Visualization: LC and KD. Writing: LC and KD.

FUNDING

LC is supported by the Integrated Biological Systems Training in Oncology Grant (NIH/NCI T32 CA119925). DG was supported by the Vanderbilt Short Term Research Training Program for Medical Students (NIH/NIDDK T35 DK007383). Work in the Olive laboratory is supported by the Herbert Irving Comprehensive Cancer Center Support Grant (P30CA013696) and the Pancreas Center of New York Presbyterian Hospital. MT is supported by a Vanderbilt Digestive Disease Research Center Pilot and Feasibility Grant (NIH/NIDDK P30 DK058404) and a Nikki Mitchell Foundation Pancreas Club Seed Grant. The DelGiorno laboratory is supported by the Vanderbilt-Ingram Cancer Center Support Grant (NIH/NCI P30 CA068485), NIH/NCI T32 CA119925, a Vanderbilt Digestive Disease Research Center Pilot and Feasibility Grant (NIH/NIDDK P30 DK058404), an American Gastroenterological Association Research Scholar Award (AGA 2021-13-02), and NIH/NIGMS R35 GM142709.

ACKNOWLEDGMENTS

The authors thank Anna Means for critical reading of the manuscript. Normal human pancreatic sections were graciously provided by Alvin Powers and Marcela Brissova at Vanderbilt University Medical Center, who organized the collection of deidentified human pancreatic samples as part of NIH-funded grants (DK106755 and DK104211).

SUPPLEMENTARY MATERIAL

The Supplementary Material for this article can be found online at: https://www.frontiersin.org/articles/10.3389/fphys.2022.865452/full#supplementary-material

REFERENCES

Andersson-Rolf, A., Clevers, H., and Dayton, T. L. (2000). "Diffuse Hormonal Systems," in *Endotext*. Editors K. R. Feingold, B. Anawalt, A. Boyce, G. Chrousos, W. W. de Herder, K. Dhatariya, et al. (South Dartmouth (MA)).

Arnes, L., Hill, J. T., Gross, S., Magnuson, M. A., and Sussel, L. (2012). Ghrelin Expression in the Mouse Pancreas Defines a Unique Multipotent Progenitor Population. *PLoS One* 7, e52026. doi:10.1371/journal.pone.0052026

Bertelli, E., Regoli, M., and Bastianini, A. (1994). Endocrine Tissue Associated with the Pancreatic Ductal System: A Light and Electron Microscopic Study of the Adult Rat Pancreas with Special Reference to a New Endocrine Arrangement. *Anat. Rec.* 239, 371–378. doi:10.1002/ar.1092390404

Bouwens, L., and Pipeleers, D. G. (1998). Extra-insular Beta Cells Associated with Ductules Are Frequent in Adult Human Pancreas. *Diabetologia* 41, 629–633. doi:10.1007/s001250050960

Brissova, M., Haliyur, R., Saunders, D., Shrestha, S., Dai, C., Blodgett, D. M., et al. (2018). α Cell Function and Gene Expression Are Compromised in Type 1 Diabetes. *Cell Rep.* 22, 2667–2676. doi:10.1016/j.celrep.2018.02.032

Chen, J., Baithun, S. I., Pollock, D. J., and Berry, C. L. (1988). Argyrophilic and Hormone Immunoreactive Cells in Normal and Hyperplastic Pancreatic Ducts and Exocrine Pancreatic Carcinoma. *Vichows Archiv A. Pathol. Anat.* 413, 399–405. doi:10.1007/bf00716988

DelGiorno, K. E., Chung, C. Y., Vavinskaya, V., Maurer, H. C., Novak, S. W., Lytle, N. K., et al. (2020). Tuft Cells Inhibit Pancreatic Tumorigenesis in Mice by Producing Prostaglandin D2. *Gastroenterology* 159, 1866–1881. doi:10.1053/j.gastro.2020.07.037

DelGiorno, K. E., Naeem, R. F., Fang, L., Chung, C.-Y., Ramos, C., Luhtala, N., et al. (2020). Tuft Cell Formation Reflects Epithelial Plasticity in Pancreatic Injury: Implications for Modeling Human Pancreatitis. *Front. Physiol.* 11, 88. doi:10.3389/fphys.2020.00088

Enzler, T., and Fojo, T. (2017). Long-Acting Somatostatin Analogues in the Treatment of Unresectable/Metastatic Neuroendocrine Tumors. *Semin. Oncol.* 44, 141–156. doi:10.1053/j.seminoncol.2017.07.001

Farrell, A. S., Joly, M. M., Allen-Petersen, B. L., Worth, P. J., Lanciault, C., Sauer, D., et al. (2017). MYC Regulates Ductal-Neuroendocrine Lineage Plasticity in Pancreatic Ductal Adenocarcinoma Associated with Poor Outcome and Chemoresistance. *Nat. Commun.* 8, 1728. doi:10.1038/s41467-017-01967-6

Gerbe, F., Sidot, E., Smyth, D. J., Ohmoto, M., Matsumoto, I., Dardalhon, V., et al. (2016). Intestinal Epithelial Tuft Cells Initiate Type 2 Mucosal Immunity to Helminth Parasites. *Nature* 529, 226–230. doi:10.1038/nature16527

Giroux, V., and Rustgi, A. K. (2017). Metaplasia: Tissue Injury Adaptation and a Precursor to the Dysplasia-Cancer Sequence. *Nat. Rev. Cancer* 17, 594–604. doi:10.1038/nrc.2017.68

Grunddal, K. V., Tonack, S., Egerod, K. L., Thompson, J. J., Petersen, N., Engelstoft, M. S., et al. (2021). Adhesion Receptor ADGRG2/GPR64 Is in the GI-Tract Selectively Expressed in Mature Intestinal Tuft Cells. *Mol. Metab.* 51, 101231. doi:10.1016/j.molmet.2021.101231

Hart, N. J., Aramandla, R., Poffenberger, G., Fayolle, C., Thames, A. H., Bautista, A., et al. (2018). Cystic Fibrosis-Related Diabetes Is Caused by Islet Loss and Inflammation. *JCI Insight* 3. doi:10.1172/jci.insight.98240

Hingorani, S. R., Petricoin, E. F., Maitra, A., Rajapakse, V., King, C., Jacobetz, M. A., et al. (2003). Preinvasive and Invasive Ductal Pancreatic Cancer and its Early Detection in the Mouse. *Cancer Cell* 4, 437–450. doi:10.1016/s1535-6108(03)00309-x

Hingorani, S. R., Wang, L., Multani, A. S., Combs, C., Deramaudt, T. B., Hruban, R. H., et al. (2005). Trp53R172H and KrasG12D Cooperate to Promote Chromosomal Instability and Widely Metastatic Pancreatic Ductal Adenocarcinoma in Mice. *Cancer Cell* 7, 469–483. doi:10.1016/j.ccr.2005.04.023

Hruban, R. H., Adsay, N. V., Albores–Saavedra, J., Compton, C., Garrett, E. S., Goodman, S. N., et al. (2001). Pancreatic Intraepithelial Neoplasia. *Am. J. Surg. Pathol.* 25, 579–586. doi:10.1097/00000478-200105000-00003

Jiang, S.-H., Li, J., Dong, F.-Y., Yang, J.-Y., Liu, D.-J., Yang, X.-M., et al. (2017). Increased Serotonin Signaling Contributes to the Warburg Effect in Pancreatic Tumor Cells under Metabolic Stress and Promotes Growth of Pancreatic Tumors in Mice. *Gastroenterology* 153, 277–291. doi:10.1053/j.gastro.2017.03.008

Li, R., Zhang, X., Yu, L., Zou, X., and Zhao, H. (2016). Characterization of Insulin-Immunoreactive Cells and Endocrine Cells within the Duct System of the Adult Human Pancreas. *Pancreas* 45, 735–742. doi:10.1097/mpa.0000000000000555

Longnecker, D. S., Adsay, N. V., Castillo, C. F.-d., Hruban, R. H., Kasugai, T., Klimstra, D. S., et al. (2005). Histopathological Diagnosis of Pancreatic Intraepithelial Neoplasia and Intraductal Papillary-Mucinous Neoplasms: Interobserver Agreement. *Pancreas* 31, 344–349. doi:10.1097/01.mpa.0000186245.35716.18

Ma, Z., Lytle, N. K., Chen, B., Jyotsana, N., Novak, S. W., Cho, C. J., et al. (2021). Single-Cell Transcriptomics Reveals a Conserved Metaplasia Program in Pancreatic Injury. *Gastroenterology* 162, 604–620. doi:10.1053/j.gastro.2021.10.027

Manco, R., Averbukh, I., Porat, Z., Bahar Halpern, K., Amit, I., and Itzkovitz, S. (2021). Clump Sequencing Exposes the Spatial Expression Programs of Intestinal Secretory Cells. *Nat. Commun.* 12, 3074. doi:10.1038/s41467-021-23245-2

Ohta, Y., Kosaka, Y., Kishimoto, N., Wang, J., Smith, S. B., Honig, G., et al. (2011). Convergence of the Insulin and Serotonin Programs in the Pancreatic β-Cell. *Diabetes* 60, 3208–3216. doi:10.2337/db10-1192

Park, I.-S., and Bendayan, M. s. (1992). Characterization of the Endocrine Cells in the Pancreatic-Bile Duct System of the Rat. *Anat. Rec.* 232, 247–256. doi:10.1002/ar.1092320209

Perez-Frances, M., van Gurp, L., Abate, M. V., Cigliola, V., Furuyama, K., Bru-Tari, E., et al. (2021). Pancreatic Ppy-Expressing γ-Cells Display Mixed Phenotypic Traits and the Adaptive Plasticity to Engage Insulin Production. *Nat. Commun.* 12, 4458. doi:10.1038/s41467-021-24788-0

Petrescu, A. D. D., Grant, S., Williams, E., Frampton, G., Reinhart, E. H., Nguyen, A., et al. (2020). Ghrelin Reverses Ductular Reaction and Hepatic Fibrosis in a Rodent Model of Cholestasis. *Sci. Rep.* 10, 16024. doi:10.1038/s41598-020-72681-5

Poher, A.-L., Tschöp, M. H., and Müller, T. D. (2018). Ghrelin Regulation of Glucose Metabolism. *Peptides* 100, 236–242. doi:10.1016/j.peptides.2017.12.015

Rahib, L., Smith, B. D., Aizenberg, R., Rosenzweig, A. B., Fleshman, J. M., and Matrisian, L. M. (2014). Projecting Cancer Incidence and Deaths to 2030: The Unexpected burden of Thyroid, Liver, and Pancreas Cancers in the United States. *Cancer Res.* 74, 2913–2921. doi:10.1158/0008-5472.can-14-0155

Sakaki, M., Sano, T., Hirokawa, M., Takahashi, M., and Kiyoku, H. (2002). Immunohistochemical Study of Endocrine Cells in Ductal Adenocarcinoma of the Pancreas. *Virchows Arch.* 441, 249–255. doi:10.1007/s00428-002-0652-7

Sarrouilhe, D., and Mesnil, M. (2019). Serotonin and Human Cancer: A Critical View. *Biochimie* 161, 46–50. doi:10.1016/j.biochi.2018.06.016

Schlesinger, Y., Yosefov-Levi, O., Kolodkin-Gal, D., Granit, R. Z., Peters, L., Kalifa, R., et al. (2020). Single-Cell Transcriptomes of Pancreatic Preinvasive Lesions and Cancer Reveal Acinar Metaplastic Cells' Heterogeneity. *Nat. Commun.* 11, 4516. doi:10.1038/s41467-020-18207-z

Schneider, M. A., Heeb, L., Beffinger, M. M., Pantelyushin, S., Linecker, M., Roth, L., et al. (2021). Attenuation of Peripheral Serotonin Inhibits Tumor Growth and Enhances Immune Checkpoint Blockade Therapy in Murine Tumor Models. *Sci. Transl. Med.* 13, eabc8188. doi:10.1126/scitranslmed.abc8188

Sinha, S., Fu, Y.-Y., Grimont, A., Ketcham, M., Lafaro, K., Saglimbeni, J. A., et al. (2017). PanIN Neuroendocrine Cells Promote Tumorigenesis via Neuronal Cross-Talk. *Cancer Res.* 77, 1868–1879. doi:10.1158/0008-5472.can-16-0899-t

Soll, C., Jang, J. H., Riener, M.-O., Moritz, W., Wild, P. J., Graf, R., et al. (2010). Serotonin Promotes Tumor Growth in Human Hepatocellular Cancer. *Hepatology* 51, 1244–1254. doi:10.1002/hep.23441

Tong, J., Prigeon, R. L., Davis, H. W., Bidlingmaier, M., Kahn, S. E., Cummings, D. E., et al. (2010). Ghrelin Suppresses Glucose-Stimulated Insulin Secretion and Deteriorates Glucose Tolerance in Healthy Humans. *Diabetes* 59, 2145–2151. doi:10.2337/db10-0504

Wang, X., Li, B., Kim, Y. J., Wang, Y. C., Li, Z., Yu, J., et al. (2021). Targeting Monoamine Oxidase A for T Cell-Based Cancer Immunotherapy. *Sci. Immunol.* 6. doi:10.1126/sciimmunol.abh2383

Whitcomb, D. C., Taylor, I. L., and Vigna, S. R. (1990). Characterization of Saturable Binding Sites for Circulating Pancreatic Polypeptide in Rat Brain. *Am. J. Physiology-Gastrointestinal Liver Physiol.* 259, G687–G691. doi:10.1152/ajpgi.1990.259.4.g687

Wierup, N., Svensson, H., Mulder, H., and Sundler, F. (2002). The Ghrelin Cell: A Novel Developmentally Regulated Islet Cell in the Human Pancreas. *Regul. Peptides* 107, 63–69. doi:10.1016/s0167-0115(02)00067-8

Wren, A. M., Seal, L. J., Cohen, M. A., Brynes, A. E., Frost, G. S., Murphy, K. G., et al. (2001). Ghrelin Enhances Appetite and Increases Food Intake in Humans. *J. Clin. Endocrinol. Metab.* 86, 5992. doi:10.1210/jcem.86.12.8111

Yacoub, W., Thomson, A., Hooper, P., and Jewell, L. (1996). Immunocytochemical and Morphometric Studies of Gastrin-, Somatostatin- and Serotonin-Producing Cells in the Stomach and Duodenum of Patients with Acid Peptic Disorders. *Can. J. Gastroenterol.* 10, 395–400. doi:10.1155/1996/245908

Yamaguchi, J., Liss, A. S., Sontheimer, A., Mino-Kenudson, M., Castillo, C. F.-d., Warshaw, A. L., et al. (2015). Pancreatic Duct Glands (PDGs) Are a Progenitor Compartment Responsible for Pancreatic Ductal Epithelial Repair. *Stem Cell Res.* 15, 190–202. doi:10.1016/j.scr.2015.05.006

Yamaguchi, T., Yamashita, J., Ohmoto, M., Aoudé, I., Ogura, T., Luo, W., et al. (2014). Skn-1a/Pou2f3 Is Required for the Generation of Trpm5-Expressing Microvillous Cells in the Mouse Main Olfactory Epithelium. *BMC Neurosci.* 15, 13. doi:10.1186/1471-2202-15-13

Conflict of Interest: The authors declare that the research was conducted in the absence of any commercial or financial relationships that could be construed as a potential conflict of interest.

Publisher's Note: All claims expressed in this article are solely those of the authors and do not necessarily represent those of their affiliated organizations, or those of the publisher, the editors and the reviewers. Any product that may be evaluated in this article, or claim that may be made by its manufacturer, is not guaranteed or endorsed by the publisher.

frontiers | Frontiers in Oncology

ORIGINAL RESEARCH
published: 04 May 2022
doi: 10.3389/fonc.2022.878920

Cancer-Associated Fibroblasts and Squamous Epithelial Cells Constitute a Unique Microenvironment in a Mouse Model of Inflammation-Induced Colon Cancer

Paige N. Vega[1,2], Avlant Nilsson[3,4], Manu P. Kumar[3], Hiroaki Niitsu[2,5], Alan J. Simmons[1,2], James Ro[1,2], Jiawei Wang[1,2], Zhengyi Chen[1,2], Brian A. Joughin[3], Wei Li[2,5], Eliot T. McKinley[1,2], Qi Liu[6], Joseph T. Roland[2,7], M. Kay Washington[8], Robert J. Coffey[1,2,5], Douglas A. Lauffenburger[3] and Ken S. Lau[1,2,7]**

[1] Department of Cell and Developmental Biology and Program in Developmental Biology, Vanderbilt University, Nashville, TN, United States, [2] Epithelial Biology Center, Vanderbilt University Medical Center, Nashville, TN, United States, [3] Department of Biological Engineering and Koch Institute for Integrative Cancer Research, Massachusetts Institute of Technology, Cambridge, MA, United States, [4] Department of Biology and Biological Engineering, Chalmers University of Technology, Gothenburg, Sweden, [5] Department of Medicine, Division of Gastroenterology, Hepatology and Nutrition, Vanderbilt University Medical Center, Nashville, TN, United States, [6] Department of Biostatistics and Center for Quantitative Sciences, Vanderbilt University Medical Center, Nashville, TN, United States, [7] Department of Surgery, Vanderbilt University Medical Center, Nashville, TN, United States, [8] Department of Pathology, Microbiology, and Immunology, Vanderbilt University Medical Center, Nashville, TN, United States

The tumor microenvironment plays a key role in the pathogenesis of colorectal tumors and contains various cell types including epithelial, immune, and mesenchymal cells. Characterization of the interactions between these cell types is necessary for revealing the complex nature of tumors. In this study, we used single-cell RNA-seq (scRNA-seq) to compare the tumor microenvironments between a mouse model of sporadic colorectal adenoma (Lrig1$^{CreERT2/+}$;Apc$^{2lox14/+}$) and a mouse model of inflammation-driven colorectal cancer induced by azoxymethane and dextran sodium sulfate (AOM/DSS). While both models develop tumors in the distal colon, we found that the two tumor types have distinct microenvironments. AOM/DSS tumors have an increased abundance of two populations of cancer-associated fibroblasts (CAFs) compared with APC tumors, and we revealed their divergent spatial association with tumor cells using multiplex immunofluorescence (MxIF) imaging. We also identified a unique squamous cell population in AOM/DSS tumors, whose origins were distinct from anal squamous epithelial cells. These cells were in higher proportions upon administration of a chemotherapy regimen of 5-Fluorouracil/Irinotecan. We used computational inference algorithms to predict cell-cell communication mediated by ligand-receptor interactions

OPEN ACCESS

Edited by:
Natalie Luhtala, Salk Institute for Biological Studies, United States

Reviewed by:
Sophia Ran, Southern Illinois University Carbondale, United States
Akshay Narkar, United States Food and Drug Administration, United States

***Correspondence:**
Douglas A. Lauffenburger
lauffen@mit.edu
Ken S. Lau
ken.s.lau@vanderbilt.edu

Specialty section:
This article was submitted to Gastrointestinal Cancers: Colorectal Cancer, a section of the journal Frontiers in Oncology

Received: *18 February 2022*
Accepted: *06 April 2022*
Published: *04 May 2022*

Citation:
Vega PN, Nilsson A, Kumar MP, Niitsu H, Simmons AJ, Ro J, Wang J, Chen Z, Joughin BA, Li W, McKinley ET, Liu Q, Roland JT, Washington MK, Coffey RJ, Lauffenburger DA and Lau KS (2022) Cancer-Associated Fibroblasts and Squamous Epithelial Cells Constitute a Unique Microenvironment in a Mouse Model of Inflammation-Induced Colon Cancer. Front. Oncol. 12:878920. doi: 10.3389/fonc.2022.878920

and downstream pathway activation, and identified potential mechanistic connections between CAFs and tumor cells, as well as CAFs and squamous epithelial cells. This study provides important preclinical insight into the microenvironment of two distinct models of colorectal tumors and reveals unique roles for CAFs and squamous epithelial cells in the AOM/DSS model of inflammation-driven cancer.

Keywords: cancer associated fibroblasts (CAF), colorectal cancer, tumor microenvironment, squamous cells, adaptive immunity, stem cells, inflammation

INTRODUCTION

Polyp transition into colorectal cancer (CRC) can be modeled by an evolutionary selection of mutations favorable to tumor cell expansion (1–3). While the identities of these driver mutations have been revealed (4–7), there exists a myriad of factors that can influence mutational selection and tumor progression. According to Virchow's idea that cancers are wounds that do not heal, an aberrant wound healing process, where cells can maintain a regenerative or even embryonal state, drives tumor cell expansion. While aberrant cell states are eventually permanently fixed by mutations in oncogenic pathways, the initiation of these tumor-favorable states may be triggered by interaction with an abnormal tumor microenvironment (TME), the so-called sites of chronic irritation.

The role of the TME in CRC progression is well-supported by observations of increased microenvironmental complexity in CRC compared to less advanced lesions (8). More specifically, the increased abundance of cancer-associated fibroblasts (CAFs) in CRC is associated with more advanced disease, poor prognostic outcomes, and disease recurrence (9–12). Mouse models of CRC have also recapitulated this increased complexity associated with advanced lesions, which has been linked to growth factor, chemokine, and cytokine expression from CAFs (13–16). Indeed, a recent human tumor atlas study has identified "hubs" that consists of GREM1/RSPO3-expressing CAFs possibly co-occurring with stem-like cancer cells (17). However, there has been a lack of comparative studies describing changes in TME occurring right at the juncture between advanced adenoma and pre-invasive carcinoma. Here, we compare mouse models of advanced adenoma and early carcinoma to identify unique microenvironmental features that accompany this critical transition.

In the *Lrig1*$^{CreERT2/+}$;*Apc*$^{fl/+}$ model, a single copy of *Apc* is recombined in *Lrig1*-expressing stem cells, and tumors, mirroring the sporadic tumorigenesis process, are initiated when the second copy of *Apc* undergoes a stochastic loss-of-heterozygosity event (18). Colonic adenomatous polyps are generated from cells with these genetic perturbations in the distal colon approximately 12 weeks after tamoxifen-induced recombination; these tumors are histologically advanced but do not progress to carcinoma (18). In contrast, distal colonic tumors induced by chemical mutagenesis *via* azoxymethane (AOM) and dextran sodium sulfate (DSS) results from β-catenin mutations in colonic crypt cells (19, 20). These inflammation-induced tumors also form approximately 12 weeks post-induction and may lead to invasive carcinomas when left to progress (21). Our goal was to utilize single-cell RNA-sequencing (scRNA-seq) coupled with multiplex immunofluorescence (MxIF) to characterize TME components and their interactions in these two mouse models of colorectal tumorigenesis that differ in their stage of progression. We found increased TME complexity in the AOM/DSS model of CRC compared to the adenoma model driven by APC loss, with increased diversity of CAFs and unique squamous epithelial cells that can be modulated by conventional chemotherapy.

RESULTS

scRNA-seq Reveals the Complexity of the TME in AOM/DSS Colonic Tumorigenesis

We compared the cellular features between colonic tumors generated from the Lrig1$^{CreERT2/+}$;Apc$^{2lox14/+}$ (herein referred to as APC tumors) mice, which is a model of advanced sporadic colonic adenoma (18), to those generated by azoxymethane and dextran sodium sulfate (herein referred to as AOM/DSS tumors), which is a model of inflammation-driven CRC (19) (**Figure 1A**). We harvested tumors at 12 weeks post-induction, as documented previously to be a standard timepoint for these models and when tumor formation is routinely detected. Both sets of tumors were pedunculated and polypoid in nature, arose in the distal colon, and exhibited similar adenomatous features typical of these models (**Figure 1B**). To identify additional cellular and molecular differences between these colonic tumors, we performed inDrop scRNA-seq on multiple biological replicates (different mice) of AOM/DSS tumors, APC tumors and tumor adjacent colonic tissue, and wildtype (WT) normal colons (22). Approximately 13,000 cells across all conditions passed quality control and were co-embedded in UMAP space (**Figures 1C–E**). Density peak clustering of cell transcriptomes and subsequent automatic cell type annotation using the Mouse Cell Atlas reference revealed cell populations consistent with known biology (**Figure 1C**; **Figures S1**, **S2**) (23, 24). Normal colons from both WT and tumor-adjacent regions were virtually phenotypically identical, consisting of mostly epithelial cells with a small lymphocyte population, which we characterize below (**Figures 1C, D, F**). In contrast, tumors were composed of a much richer microenvironmental milieu (**Figures 1C, D, F**). Importantly, biological replicate data generated from different mice largely intermixed, demonstrating rigor and reproducibility (**Figure 1E**).

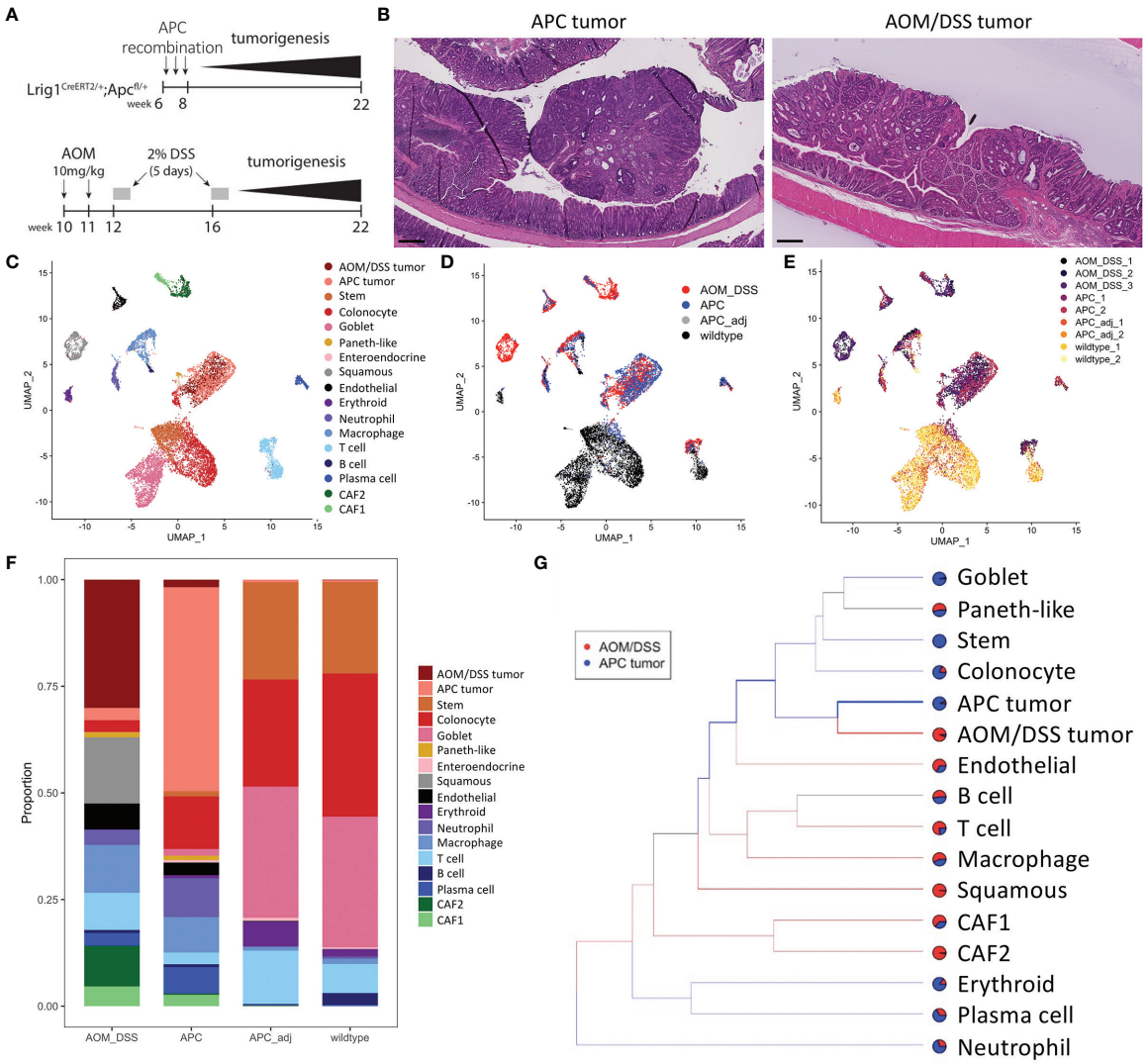

FIGURE 1 | Cell type composition of wildtype, APC tumor, APC adjacent normal, and AOM/DSS tumor samples assessed by scRNA-seq. **(A)** Experimental timeline for induction of APC tumors (top) and AOM/DSS tumors (bottom). **(B)** Representative H&E images of APC tumors and AOM/DSS tumors. Scale bars = 300 μm. UMAP co-embedding of wildtype, APC tumor, APC adjacent normal, and AOM/DSS tumor scRNA-seq samples with **(C)** cell type clustering overlay, **(D)** sample type overlay, and **(E)** replicate overlay, by color. **(F)** Bar graph of cell type proportions, broken down by sample type in scRNA-seq data. **(G)** sc-Unifrac analysis of APC tumor sample cell types compared to AOM/DSS tumor sample cell types from scRNA-seq data. Colored branches indicate statistically enriched cell population structures per sample type, with black branches indicating non-significance. Pie charts indicate the proportional representation between the two sample types. Thickness of branches represent level of enrichment sc-Unifrac distance values range from 0 to 1, with 0 representing complete overlap between two datasets sc-Unifrac distance = 0.35.

Examining epithelial cell types, normal colonic cells (WT and tumor adjacent) were composed of canonical stem, absorptive, and secretory cell lineages (**Figures 1C, D, F**). Tumor cells were largely distinct from normal epithelial cells. AOM/DSS tumors were devoid of goblet cells, consistent with DSS-induced inflammation that drives goblet cell loss (**Figure 1F**) (25). In addition, both tumor types displayed the emergence of metaplastic Paneth-like cells absent from the normal colon, as documented previously (26).

Within the non-epithelial compartment, tumors were enriched in neutrophils, macrophages, T cells, B cells, plasma cells, endothelial cells, and fibroblasts, compared to normal colonic samples (**Figure 1F**). We did not compare erythrocytes since their presence depends on the isolation procedure. sc-UniFrac analysis identified cell populations that were statistically enriched in AOM/DSS tumors compared to APC tumors (23). As expected, each tumor type was enriched in their respective APC or AOM/DSS tumor cell type (**Figure 1G**). Normal epithelial cells were further depleted in AOM/DSS tumors, supporting their more advanced progression stage (**Figure 1G**). Within the immune cell compartment, T cells and macrophages were enriched in AOM/DSS tumors, while plasma cells and

neutrophils were enriched in APC tumors. Two populations of cancer-associated fibroblasts (CAFs), CAF1 and CAF2, were enriched in AOM/DSS tumors compared to APC tumors, with CAF2s being mostly exclusive to AOM/DSS tumors (**Figure 1G**). In addition, an unexpected cell population expressing stratified epithelial markers, such as *Krt5* and *Krt14*, was present only in AOM/DSS tumors. Together, these data highlight the expansion of the stromal compartment in AOM/DSS tumors, consistent with their more advanced state compared to APC tumors.

CAFs and T cells in AOM/DSS Tumors Specify a Distinct Pro-Tumor TME

In addition to cell type annotation, we also examined molecular differences within cell types. To examine T cell subtypes, we performed sub-clustering on the T cells, population and identified four distinct T cells clusters that are condition-specific (**Figures 2A–C**). Normal colonic samples were expectedly enriched for *Cd8*+ T cells, identified as intraepithelial lymphocytes by expression of *Itgae* and *Trdc*, as observed previously (26–28) (**Figures 2D, E**). These cells express *Gzma* and *Gzmb* that play key roles in cytotoxicity, *Cd38* marking activation, and the killing effectors *Klre1*, *Cd244* (when expressed at the appropriate level), *Nkg7, Klrd1,* and *Xcl1* (29–31). In contrast, both tumor types contained low percentages of cytotoxic cells, but contained substantial percentages of *Cd4*+ T cells (**Figures 2A–C**). These cells expressed a different set of activation markers (*Tcf7, Lef1, Il7r*), and were also enriched for regulatory genes such as *Foxp3* and *Il2ra* (CD25) (**Figures 2D, E**). Tumors also contained a small population of proliferative T cells, which signifies immune activity. Comparing between tumor subtypes, AOM/DSS tumors possessed a unique population of dysfunctional inflammatory T cells (**Figures 2A–C**). These cells expressed markers of T cell exhaustion or anergy including *Prdm1, Havcr2*, and *Cish* (32, 33) (**Figures 2D, E**). Of note, *Pdcd1*, the gene encoding the immune checkpoint protein PD-1 (34), was highly upregulated in AOM/DSS tumor T cells. In contrast, *Ctla4* expression, a marker of exhausted T cells but also Tregs, was similar in APC and AOM/DSS tumor T cells (35). More importantly, AOM/DSS T cells highly expressed *Id2* downstream of TGFβ signaling, which has been shown to lead to RORα-dependent tumor-promoting inflammation, evident in this population by high *Rora* and *Il17a* expression (36) (**Figures 2D, E**). *Cd4* is downregulated but *Trdc* is characteristically upregulated, implicating that these are not Th17 cells, but are γδT cells that produce IL17 in an innate fashion to promote inflammation (37, 38). Thus, aside from immunosuppressive T cells, the TME of AOM/DSS tumor is further augmented by dysfunctional T cells that potentially induce tumor-promoting inflammation.

Within the B lymphocyte compartment, normal colonic samples were skewed toward B cells, with only a minor population of plasma cells, while both type of tumors exhibit the inverse relationship skewed towards plasma cells (**Figures 1C, D, F**). We did not notice any difference in marker genes expressed in B cells or plasma cells across normal colonic, APC tumor, and AOM/DSS samples (**Figure S3A**). Although there was an expanded myeloid compartment within both tumor types, we observed that markers of neutrophils and macrophages were largely consistent across normal colonic, APC tumor, and AOM/DSS tumor samples (**Figures 1C, D, F**; **Figure S3B**), with a few critical exceptions. Tumor associated macrophages were enriched in M2 genes, *Arg1, Il1rn*, and *Tgfb1* (**Figure S3B**). Moreover, AOM/DSS tumor associated macrophages uniquely express *Il10* and *Tnf*, implicating heightened tumor-promoting immunosuppression and inflammation. Taken together, both tumor types displayed an expansion in plasma cell, macrophage, and neutrophil compartments compared to normal colonic samples contributing to a pro-tumor TME.

There are relatively few fibroblasts in normal colonic mucosa compared to other cell types, and thus, they were not sampled in whole tissue dissociations from wildtype colonic samples. In contrast, we were able to detect one small population of CAFs, CAF1, in APC tumors, and two larger CAF populations, CAF1 and CAF2, in AOM/DSS tumors (**Figures 1C, D, F**). We used differential gene expression analysis to identify marker genes that were shared, as well as ones that distinguish the two fibroblast populations (**Figures 2F–I**). *Igfbp7*, an insulin-like growth factor binding protein and molecule involved in cell adhesion whose high expression is correlated with poor prognosis in CRC, was highly expressed in both CAF1 and CAF2 cells in APC and AOM/DSS samples (39). The CAF2 population had upregulated expression of tissue remodeling genes (*Mmp10, Mmp2, Mmp3, Mmp13, Timp2, Timp3)* and immune-related genes, including many cytokines and chemokines (*Il11, Il1rl1, Cxcl14*, and *Cxcl5*) (**Figures 2F, G**). We examined markers of recently described inflammatory CAFs (iCAFs), and found CAF2s express *Cxcl12* and *Il11* (**Figure 2H**) (40). Interestingly, iCAF markers *Il6* and *Cxcl1* were expressed at low levels in CAF1s from APC tumors, but were induced in CAF1s in AOM/DSS tumors. Similarly, we examined normal myofibroblast markers (*Acta2*, *Tagln, and Mylk*) as well as myCAF markers (*Acta2*, *Itgb1* (CD29), and *Thy1* (CD90)), and found high expression in CAF1s (**Figures 2G, H**) (31, 40). In addition to immune-related functions, we observed expression of *Grem1*, *Sfrp1*, and *Wnt5a* in the CAF2 population, all of which are reported CAF markers as well as secreted factors involved in BMP and WNT signaling, respectively (41, 42) (**Figures 2F, G**). We aimed to identify specific marker genes compatible with immunofluorescence imaging with readily available antibodies to distinguish these two fibroblast populations. *Vim* (Vimentin, VIM), *Acta2* (smooth muscle actin alpha 2, SMA), and *Pdgfrb* (platelet-derived growth factor receptor beta, PDGFRβ) were upregulated in CAF1s, with lower expression in CAF2s, and negligible expression in all other cell types, except for *Vim* (**Figure 2I**). In contrast, CAF2s were marked by upregulation of *Tnc* (tenascin-C, TNC), *Pdgfra* (platelet-derived growth factor receptor beta, PDGFRβ), and *Col1a1* (collagen type 1 alpha 1 chain). Consistent with findings that PDGF (platelet-derived growth factor) receptors form homodimers or heterodimers when bound to various PDGF ligands, *Pdgfrb* was expressed in both CAF populations, with higher expression in CAF1s, while

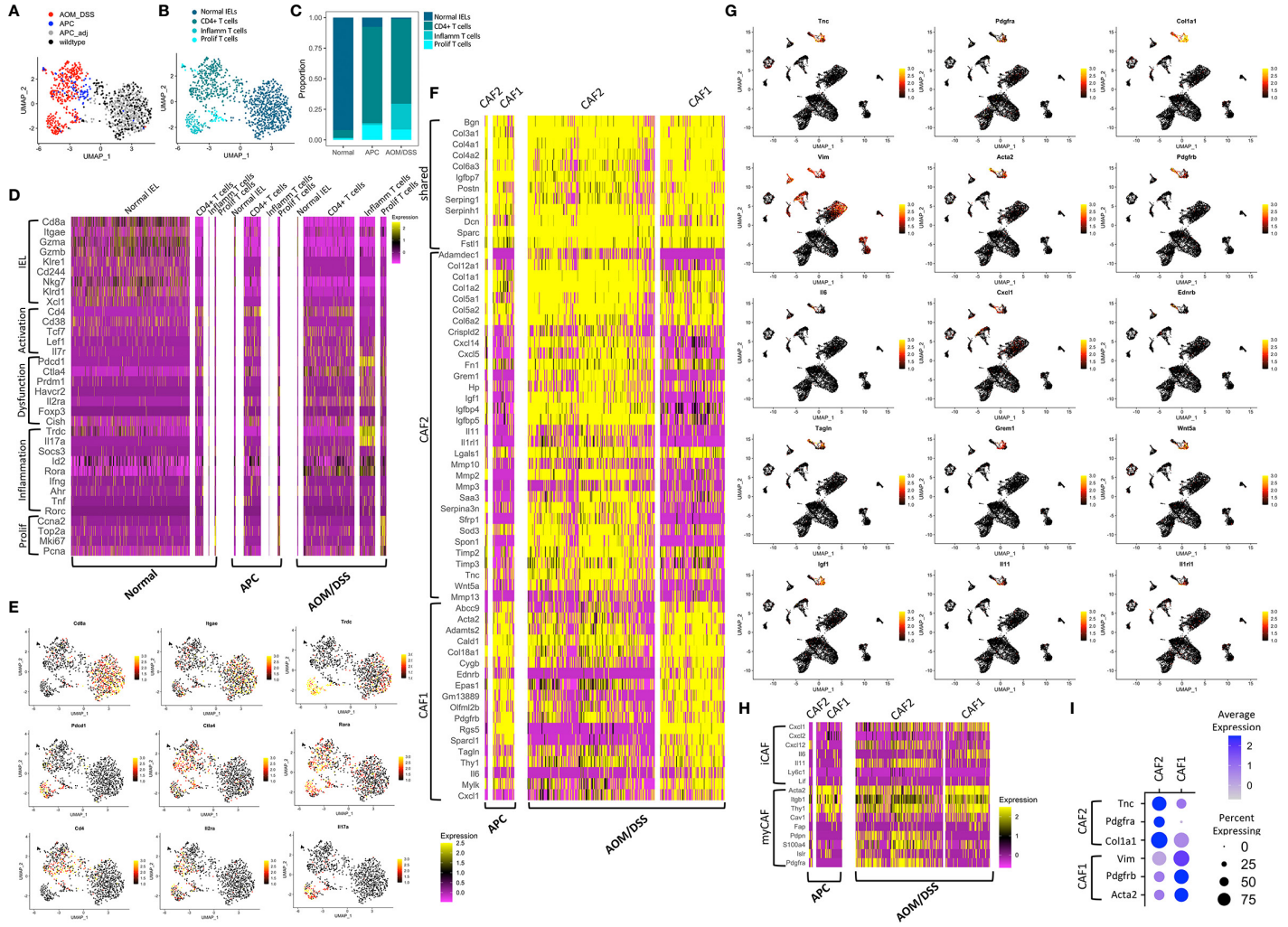

FIGURE 2 | Transcriptomic differences among microenvironmental cell types in normal colonic, APC tumor, and AOM/DSS tumor samples. UMAP co-embedding of the T cell cluster from wildtype, APC tumor, APC adjacent normal, and AOM/DSS tumor scRNA-seq samples with **(A)** sample type overlay **(B)** and cell type clustering overlay, by color. **(C)** Bar graph of T cell type proportions, broken down by subcluster and sample type in scRNA-seq data. **(D)** Heatmap of select T cell subtype marker expression in scRNA-seq data within the T cell clusters, split by sample type. Columns represent single cells. **(E)** UMAPs of scRNA-seq data with gene expression overlay, indicated by the color gradient, for select T cell subtype markers. **(F)** Heatmap of DEGs in fibroblast subtypes (CAF1, CAF2) in scRNA-seq data, split by fibroblast subtype and by sample type. Columns represent single cells. **(G)** UMAPs of scRNA-seq data with gene expression overlay, indicated by the color gradient, for select fibroblast subtype markers. **(H)** Heatmap of expression of markers of iCAFs and myCAFs described in literature in CAF1 and CAF2 populations in scRNA-seq data, broken down by tumor sample. Columns represent single cells. **(I)** Dot plot showing selected markers for fibroblast subtypes, CAF1 and CAF2, where clusters include cells from both APC tumor and AOM/DSS tumor samples.

Pdgfra was exclusive to CAF2s (43). These results demonstrate that the fibroblast compartment increases in complexity in AOM/DSS tumors as compared to APC tumors, with accompanied increased expression of tissue remodeling, inflammatory, and secreted factor genes in a subset of CAFs.

Fibroblasts from the normal colon were not sampled from whole tissue dissociations due to their paucity. Consequently, we developed another dissociation strategy that enriches for stromal cells. scRNA-seq using this strategy revealed substantial de-enrichment of epithelial cells, and enrichment of immune, glial, and endothelial cells, as well as five distinct mesenchymal populations all expressing *Vim* (**Figures S3C, D**). Pericytes were identified as a distinct cell population that expresses a set of four previously defined marker genes (*Abcc9, Kcnj8, Rgs5, Cspg4*) as well as *Pdgfrb* (31, 44, 45). These cells are distinct from fibroblasts in that they express much lower levels of CAF1 and CAF2 markers *Acta2*, *Tnc*, and *Pdgfra* (45). As described by others, we identified telocytes by expression of *Foxl1*, *Pdgfra*, and *Wnt5a*, and found that they also express *Tnc* (**Figure S3D**) (46). Similarly, we identified myofibroblasts by high *Acta2* expression, along with expression of previously defined marker genes (*Tagln, Actg2, Myh11, Mylk*) (31). These results demonstrate that the normal colon also possesses fibroblastic counterparts to CAF1 (myofibroblasts) and CAF2 (telocytes), although they exist in much lower numbers.

We hypothesized that CAFs may be activated in the context of an altered tumor microenvironment. Thus, we queried expression of signaling regulator genes comparing CAFs to their normal counterparts. While several CAF2 genes were maintained in telocytes (*Cxcl12, Mmp2, Timp2*) (**Figure S3D**), many were simply not expressed in any normal colonic fibroblasts (*Mmp3, Mmp10, Mmp13, Timp3, Il1rl1, Il11, Cxcl1, Cxcl5*) (data not shown). Furthermore, while *Grem1, Sfrp*, and *Wnt5a* were co-expressed in CAF2s, only *Wnt5a* was expressed in telocytes while the other two genes were expressed in the Fibro1 population in the normal colon. *Il6* was upregulated in AOM/DSS CAF1s but it was not expressed in myofibroblasts, but instead, was expressed in Fibro1 cells. CAF2 marker *Igf1* was more highly expressed in myofibroblasts than telocytes in the normal colon, inverse to the relationship of CAF1 to CAF2. Thus, we demonstrate that while counterparts of CAFs exist in the normal colon, their expression of signaling regulators is altered in tumors.

To determine whether CAF populations observed in mice translate to human, we examined CAF1 and CAF2 gene expression within fibroblast populations from human CRC scRNA-seq datasets. Multiple populations of CAFs were identified in a set of microsatellite stable (MSS) CRC samples (**Figure S3E**) and an another set of samples consisting of broader CRC subtypes (**Figure S3F**), with two datasets showing similar results (17, 31). Distinct populations of CAF1 (*ACTA2, TAGLN, MYLK*) and CAF2 (*PDGFRA*) analogs were identified, similar to our mouse models of tumorigenesis. Normal human colonic tissues and pre-cancerous colonic lesions contain a paucity of fibroblasts consistent with our observations in the mouse (data not shown) (26). Also consistent with our mouse models, CAF2 analogs expressed a rich set of signaling regulators including *CXCL12, GREM1, IGF1, IL11*, and *WNT5A*, with a subset of cells co-expressing *WNT5A* and *GREM1* and another subset co-expressing *CXCL12* and *IGF1*. These results validate the existence of CAF subpopulations in human CRCs correspond to those found in mouse colonic tumors.

The CAF2 Population Spatially Associates With Tumor Cells

We validated the presence and abundance of the CAF1 and CAF2 populations using MxIF imaging (47). As both APC and AOM/DSS tumors were induced by WNT signaling, increased cytoplasmic and nuclear staining for β-catenin was observed in tissue regions with characteristic tumor histologies (18, 48) (**Figure 3A**). Within tumor regions, we used markers informed by scRNA-seq analysis to identify CAF1 (SMA and VIM) or CAF2 (TNC and PDGFRα) populations (**Figure 2I**). By visual inspection, APC tumors were densely populated by epithelial cells, while AOM/DSS tumors had expanded inter-glandular stromal spaces occupied by non-epithelial cells (**Figure 3A**; **Figures S4**, **S5**). Consequently, AOM/DSS tumors had significantly higher levels of both fibroblast types compared to APC tumors, as quantified by normalized counts of pixels positive for markers of each CAF type (**Figures 3A–C**; **Figures S6**–**S8**). Although the CAF2s were undetected as a population in APC tumors by scRNA-seq, expression of CAF2 markers, *Tnc* and *Pdgfra,* was detected at lower levels in the CAF1 population, which is consistent with low protein expression of TNC and PDGFRα by immunostaining (**Figures 2I**, **3A–C**). As opposed to scRNA-seq where the spatial context is lost, MxIF revealed that myofibroblastic CAF1s reside in the center of the inter-glandular stromal regions, while PDGFRα+ CAF2s associate closely with the epithelial layers, lining the glands (**Figure 3D**). This result differs from the myCAF definition in pancreatic cancer, where it is the myofibroblastic CAFs that associate more closely with epithelial glands (49). These results validate our transcriptomic data and support the differential abundance of CAF1 in APC versus AOM/DSS tumors, while the CAF2 population is dramatically increased in AOM/DSS tumors and has a distinct spatial distribution.

AOM/DSS Tumors Consist of a Unique Squamous Epithelial Component

To decipher how differences in the TME can affect tumor cells, we examined gene programs that describe signaling pathways activated in epithelial cell populations. As expected, WNT signaling genes are upregulated in tumor cells from both AOM/DSS and APC tumors when compared to normal colonic stem and normal differentiated colonic epithelial cells (**Figure 4A**). Consistent with increased stemness in tumors, the stem cell marker *Lgr5* was upregulated compared to normal cells, while colonic identity and differentiation genes such as *Cdx2* and *Krt20*, were downregulated in both tumor types (50–58) (**Figures 4A, B**). The AOM/DSS-specific squamous epithelial cell population was devoid of WNT signaling and colonic epithelial cell type markers (**Figures 4A**; **Figure S2**).

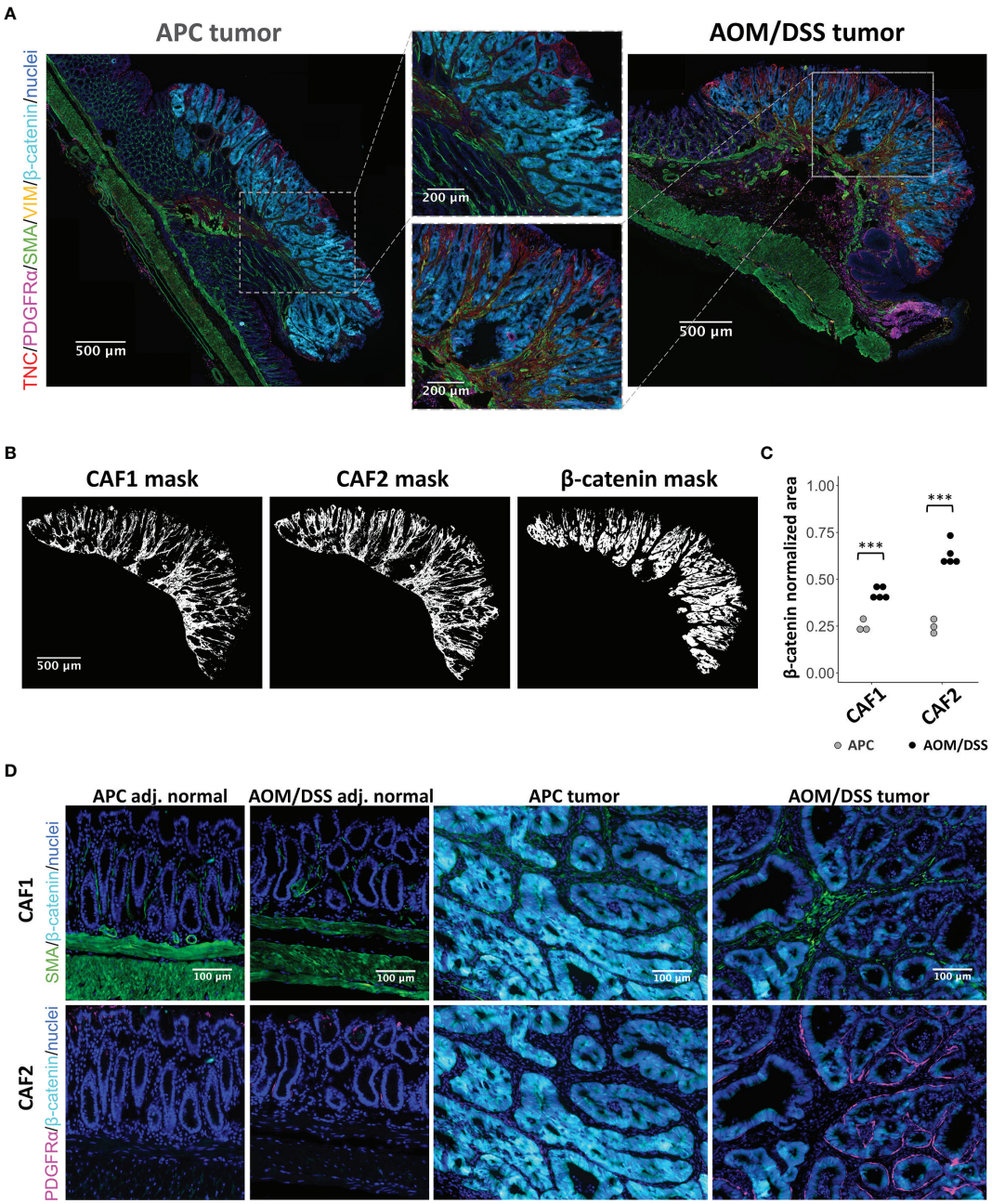

FIGURE 3 | MxIF of cancer-associated fibroblasts to reveal their spatial distributions in APC and AOM/DSS tumors. **(A)** Representative stitched MxIF images of APC tumors and AOM/DSS tumors immunostained for CAF1 (SMA, VIM) and CAF2 (TNC, PDGFRα) subtypes. Tumor regions are visualized using immunostaining for β-catenin. **(B)** Representative binary images (here, AOM/DSS tumor sample) and **(C)** quantification of CAF1 and CAF2 marker expression within tumor regions of APC and AOM/DSS samples. n = 5 AOM/DSS tumors, n = 3 APC tumors *** indicates $p < 0.001$. **(D)** Visualization of CAF1 (SMA) and CAF2 (PDGFRα) subtype proximity to β-catenin+ tumor cells in APC and AOM/DSS samples, including tumor regions and adjacent normal regions.

While metaplasia and damage gene lists used by Chen et al., 2021 did not show enrichment in the squamous cell population, fetal and embryonic genes were uniquely upregulated in squamous cells compared to all other epithelial cell populations, including tumor cells (**Figures 4C, D**) (26). Notably, several genes related to matrix composition and immune cell recruitment were upregulated in squamous cells (*Anxa1*, *Ecm1*, *Il1rn*, *Itgb4*), as well as genes that are reported to be tumor suppressors (*Serpin5b*, *Phlda3*) (59, 60). In contrast, *Hes1*, a Notch target gene normally associated with stemness and absorptive cell differentiation, and *Phlda2*, a growth restriction gene in development and a tumor suppressor, were upregulated in

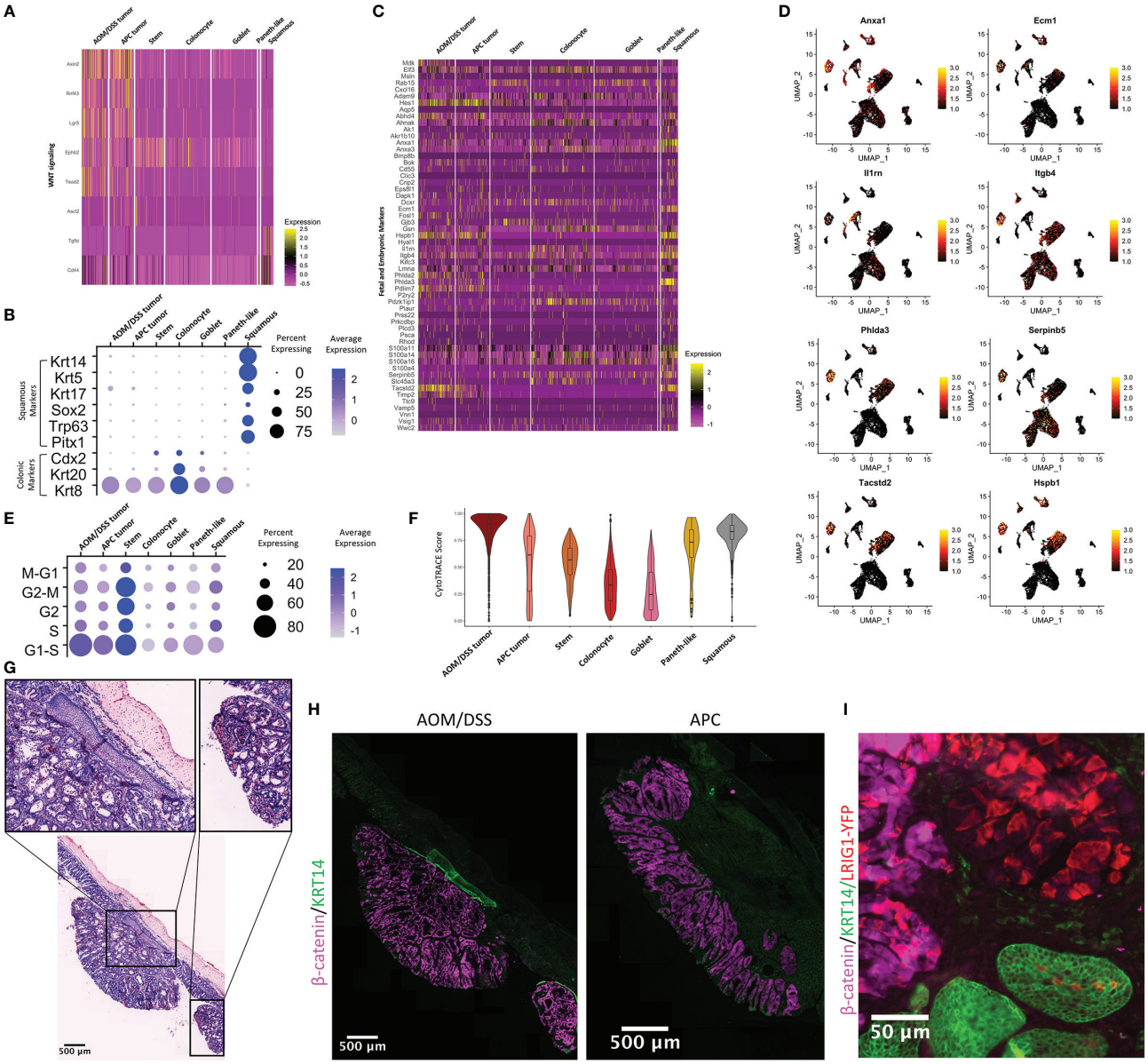

FIGURE 4 | Characterization of the squamous component present in AOM/DSS, but not APC, tumors. **(A)** Heatmap of genes related to WNT signaling and colonic stem cells. Columns represent single cells, arranged by epithelial cell type clusters. **(B)** Dot plot showing colonic or squamous identity genes for epithelial cell clusters, where clusters include cells from both APC tumor and AOM/DSS tumor samples. **(C)** Heatmap of fetal and embryonic programs. Columns represent single cells, arranged by epithelial cell type clusters. **(D)** UMAPs of scRNA-seq data with expression overlay, indicated by the color gradient, of selected fetal and embryonic genes. **(E)** Dot plot showing cell cycle meta-genes for each cell cycle phase in epithelial cell clusters. **(F)** CytoTRACE scores for epithelial cell types calculated from scRNA-seq data. **(G)** Representative H&E image of multiple AOM/DSS tumors within the same animals, with a focus on squamous components (insets). **(H)** Representative MxIF image of KRT14 in APC tumors and AOM/DSS tumors. Images were representative of n = 5 AOM/DSS tumors and n = 3 APC tumors. **(I)** Observation of *Lrig1*$^{CreERTe/+}$; *Rosa*$^{YFP/+}$ traced cells within a single squamous cell region of an AOM/DSS tumor.

APC and AOM/DSS tumor cells, but not in squamous cells (61–65). These observations are consistent with the association of tumor cells with colonic stem cell identity. Interestingly, *Tacstd2*, the gene encoding the TROP2 protein that is associated with transition to dysplasia but also expressed in some normal tissues, was highly upregulated in the squamous cell population as well as in AOM/DSS tumor cells (66, 67).

We aimed to elucidate the origin of the squamous cell population that was unique to AOM/DSS tumors. As this tumor type typically manifests in the distal colon, one possible source of this population could be re-epithelialization of damaged regions of columnar colonic epithelia by anal epithelium, as speculated by other groups (68). However, another potential origin could be the transdifferentiation of

columnar to squamous epithelial cell identity (69). We first observed that keratin expression (*Krt5*+, *Krt14*+, *Krt17*+, *Krt20*-, *Krt8*-) in scRNA-seq data was consistent with a basal squamous cell identity (**Figure 4B**). *Trp63*, a master regulator of a stratified epithelial identity whose aberrant expression results in embryonic subversion, squamous cell metaplasia, and squamous cell carcinoma, was expressed exclusively in the squamous population, along with other transcription factors regulating squamous cell identity (*Sox2* and *Pitx1)* (70–73). We examined cell cycle genes, and as expected, normal stem cells are actively cycling, as are APC tumor and AOM/DSS tumor cells to a lesser extent. (**Figure 4E**). Squamous cells cycle to the same extent as tumor cells, indicative of their abnormal state. We used CytoTRACE to predict epithelial cell stemness and found that AOM/DSS tumor cells have the highest average CytoTRACE score, followed by APC tumor and then normal stem cells, consistent with higher stemness in tumor cells versus normal stem cells (**Figure 4F**) (74). Paneth-like cells also have a high score, consistent with these cells being an abnormal metaplastic cell type in tumors. Additionally, the squamous cell population's average CytoTRACE score was similar to AOM/DSS tumor cells and above that of normal colonic epithelial stem cells, indicative of that these cells also have aberrant stemness similar to tumors. We then sought to determine whether we could locate the squamous cells spatially in tissue sections of AOM/DSS tumors, and we found examples of stratified squamous cell tissue that underlie pedunculated tumors in AOM/DSS, but not APC tumors (**Figure 4G**). Importantly, we found more than one instance where squamous components were found in multiple tumors, both distal and more proximal in the colon, within a single mouse, discounting the possibility that the squamous cells were from the anal epithelium adjacent to the tumor. Squamous components were positive for KRT14 staining, consistent with scRNA-seq results (**Figure 4H**).We then used lineage tracing from $Lrig1^{CreERT2/+}$;$Rosa^{YFP/+}$ mice, as *Lrig1* is a colonic stem cell marker, to investigate whether the squamous population might arise from transdifferentiation of columnar epithelium (75). We first confirmed that *Lrig1* is not expressed in the AOM/DSS-specific squamous cell cluster, but only in the tumor cell cluster, in our scRNA-seq data (**Figure S9A**). Next, fluorescence imaging of $Lrig1^{Apple/+}$ and $Lrig1^{CreERT2/+}$;$Rosa^{YFP/+}$ lineage traced mice revealed that LRIG1 is not expressed in normal anal squamous epithelia (**Figures S9B, C**). However, the same lineage tracing from AOM/DSS tumors resulted in YFP-positive cells in the squamous component in one instance (**Figure 4I**), suggesting a potential for rare cases of transdifferentiation. However, we cannot discount the possibility of leaky Cre recombinase activity, aberrant expression of *Lrig1* in anal epithelium in the context of AOM/DSS tumorigenesis, or other unknown factors. Moreover, squamous components were not observed in all AOM/DSS tumors, and in particular, those generated on a pure C57BL/6J background. Although we were unable to determine the origin of all squamous cells associated with tumors, we were able to validate the existence of a squamous population unique to AOM/DSS, but not APC, tumors, and whose transcriptomic signature indicates these cells have high stem potential, are actively cycling, and express several fetal and embryonic genes.

Chemotherapeutic Treatment Results in Expansion of Squamous Cells and Depletion of Stem Features in Tumors

We sought to determine how a chemotherapeutic regimen of Fluorouracil (5-FU) and Irinotecan affects the AOM/DSS TME. We treated AOM/DSS-induced tumor mice with a 5-FU and Irinotecan regimen for 1, 3, and 6 days and performed scRNA-seq on resulting tumors. To assess changes over the treatment timeline, we consider day 1 replicates as an "early treatment" timepoint, and days 3 and 6 as replicates for a "late treatment" timepoint. While chemotherapy is expected to induce cell death and tumor regression, our 5-FU/Irinotecan regimen coupled to the harvest time points did not result in reduction in tumor size, nor was there a reduction in cell numbers, which provides an opportunity to observe chemotherapy-induced changes within tumor cells. The tumor cells and squamous cells from days 1, 3, and 6 timepoints occupied different UMAP spaces, while stromal and immune cells from different timepoints largely overlapped (**Figures 5A, B**). Compared to the early treatment timepoint, we observed an expansion of squamous cells at late treatment timepoints (6 and 11% of total epithelial cells in early treatment, 21% and 27% of total epithelial cells in late treatment) (**Figure 5C**). However, differences in experimentalists and instrumentation prevent us from making comparisons of squamous cell percentages in the 5-FU/Irinotecan dataset to the untreated AOM/DSS dataset (**Figure 1F**). Histologically, we also observed squamous cell components located at the surface of the tumor, rather than underlying the tumor as in untreated AOM/DSS tumors, implicating a phenotypic transition (**Figure 5D**). Expansion of squamous cells was accompanied by increased expression of squamous identity transcription factors *Trp63* and *Sox2* (**Figure 5E**). Surprisingly, stem cell markers and associated WNT signaling genes, including *Lgr5*, decreased in tumor cells along the treatment timeline in a gradient-like manner (**Figure 5F**); this corresponded with increase in differentiated epithelial genes *Krt20* and *Krt8* (**Figure 5E**). Consistent with the loss of stemness upon treatment, tumor cells displayed an increase in cell cycle related genes at later timepoints and a decreased predicted stem potential, as determined by CytoTRACE score, whereas squamous cells increased proliferation genes and stem potential (**Figures 5G, H**). Using unsupervised differential gene expression analysis as well as examining selected marker genes, we observed an upregulation in antigen presentation (AP) genes in tumor cells from the day 6 timepoint, consistent with our previous finding of increased AP as a function of differentiation (**Figure 5I**) (26). Interestingly, squamous cells in day 3 and day 6 timepoints also upregulated interferon-induced genes *Ifi27* and *Ifitm3*, consistent with a change in the immune microenvironment. Together, we found that along a treatment timeline, 5-FU and Irinotecan treatment is associated with expansion of squamous cells and decreased stemness in tumor cells.

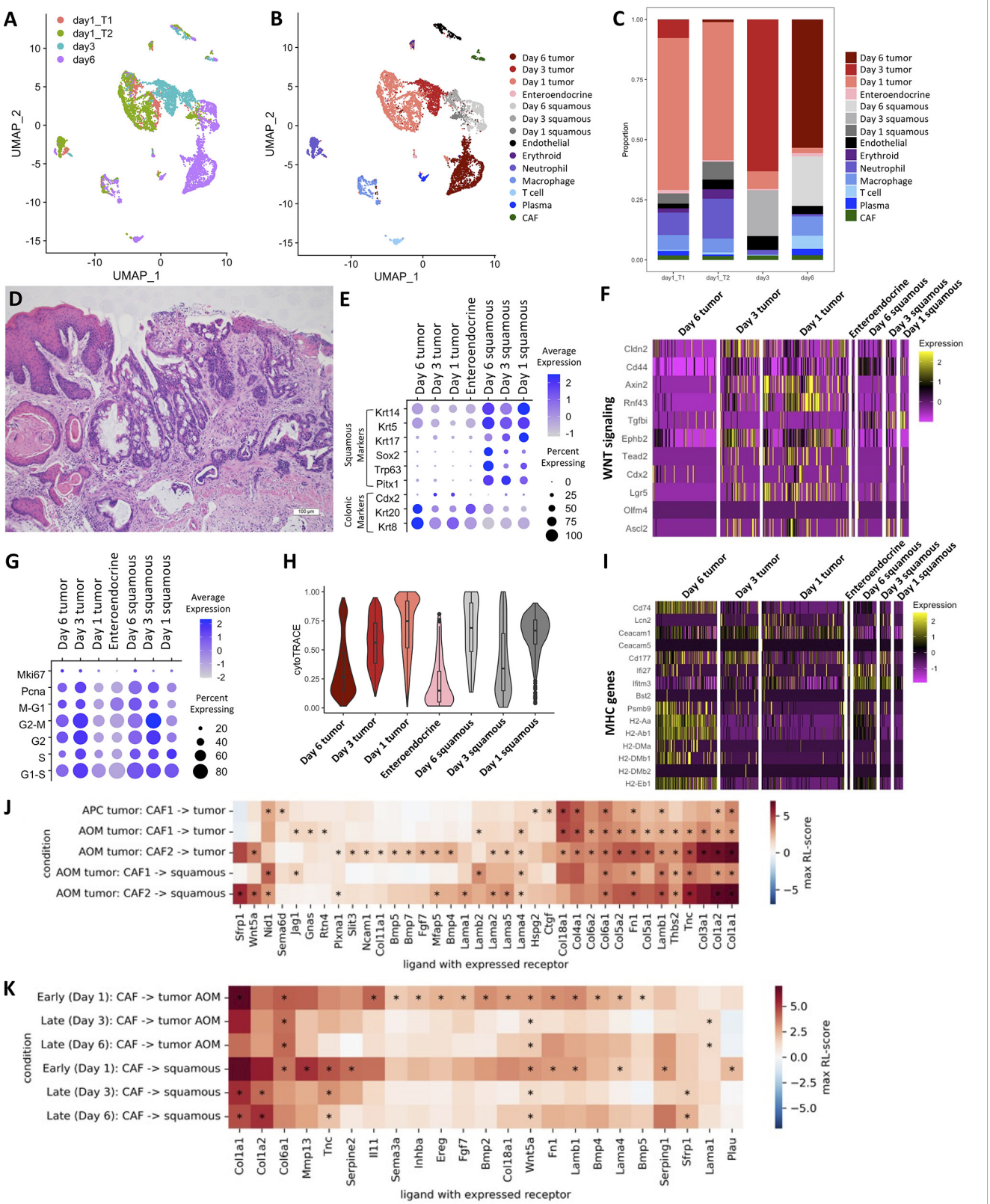

FIGURE 5 | Continued

FIGURE 5 | Changes in TME interactions within AOM/DSS tumors upon chemotherapy treatment. UMAP of scRNA-seq data from 5-FU and Irinotecan treated AOM/DSS tumor samples with timepoint overlay **(A)** and cell type clustering overlay **(B)**, by color. T1 and T2 indicate day 1 biological replicates (n = 2) that correspond to the "early treatment" timepoint, while day 3 and day6 are biological replicates (n =2) for the "late treatment" timepoint. **(C)** Bar graph of cell type proportions, broken down by sample type in timepoints of 5-FU and Irinotecan treated AOM/DSS tumor scRNA-seq data. **(D)** Representative H&E image of 5-FU and Irinotecan treated AOM/DSS tumors. Scale bar = 100 μm. **(E)** Dot plot showing colonic or squamous identity genes for epithelial cell clusters of 5-FU and Irinotecan treated AOM/DSS tumor scRNA-seq data timepoints. **(F)** Heatmap of genes related to WNT signaling and colonic stem cells. Columns represent single cells, arranged by epithelial cell type clusters in 5-FU and Irinotecan treated AOM/DSS tumor scRNA-seq data timepoints. **(G)** Dot plot showing cell cycle meta-genes for each cell cycle phase in epithelial cell clusters of 5-FU and Irinotecan treated AOM/DSS tumor scRNA-seq data timepoints. **(H)** CytoTRACE scores for epithelial cell types in 5-FU and Irinotecan treated AOM/DSS tumor scRNA-seq data timepoints. **(I)** Heatmap of select DEGs and marker genes related to AP. Columns represent single cells, arranged by epithelial cell type clusters in 5-FU and Irinotecan treated AOM/DSS tumor scRNA-seq data timepoints. **(J)** RL-scores for differentially expressed ligands in CAF cells with a receptor in squamous, AOM/DSS tumor, or APC tumor cells. **(K)** Ligands in CAF cells with a receptor in squamous or cancer cells early and late after treatment by 5-FU + Irinotecan. (*) indicates that both receptor and ligand are differentially expressed (adjusted p-value < 0.01) and that the log FC of the ligand is at least 0.5 for all samples of the same group.

To further evaluate how tumor cells may be influenced by the TME, we analyzed differences in cell-cell communication of AOM/DSS tumors as compared to APC tumors, and moreover, we identified differences in cell-cell communication among early vs late 5-FU/Irinotecan treatment timepoints in AOM/DSS tumors. We made use of established receptor and ligand (R-L) interactions from a prior knowledge database and, similar to previous work, we quantified these interactions by a R-L score based on the receptor and ligand expression (76, 77). We searched for cell types expressing ligands that could bind receptors expressed in the tumor cells (**Figures S10A–D**). We observed that compared to all other cell types, CAF populations, particularly CAF2s, dominate interactions with tumor cells by providing ligands that are binding partners with receptors expressed on tumor cells (**Figure 5J**; **Figures S10A–D**). Many receptors expressed by tumor cells were also expressed by squamous cells, resulting in similar scores, and suggesting that they may experience similar signals from the TME. Consistent with the observed increase in WNT related genes in tumor cells (**Figures 4A**, **5F**), we saw high scores for WNT-related interactions (ligands *Sfrp1* and *Wnt5a* and receptors *Fzd6*, *Fzd7* and *Lrp6*) and significant BMP-related interactions (e.g. from *Bmp4* with *Bmpr1a)*. Notably, *Fgf7* is upregulated in acute response to injury and thought to serve a protective role in DSS treated mice, however, it is also known to increase cell proliferation and may inadvertently act as a growth factor for tumor cells in the AOM/DSS setting (78, 79). For squamous cells, there was a significant *Lama1-Rpsa* interaction, which is an interaction associated with metastasis as *Rpsa* enables tumors to penetrate laminin tissue (80). These interactions were largely mirrored in the 5-FU and Irinotecan treated cells, and the treatment appeared to reduce the amplitude of these signatures over time, possibly resulting in decreased stemness (**Figure 5K**).

DISCUSSION

We describe differences between the TMEs of AOM/DSS tumors and APC tumors, as models for pre-invasive cancers and pre-cancerous adenomas, respectively. Using single-cell and computational approaches, we identified and validated two CAF populations that are increased in AOM/DSS tumors, with CAF2 being uniquely present and the main driver of differences in cell-cell communication between the two colonic tumor models. CAF2-derived ligands interact with receptors expressed on AOM/DSS tumor cells to increase WNT signaling, increase growth factor signaling, and remodel the extracellular matrix. We also revealed a unique squamous cell component in many AOM/DSS, but not APC, tumors, which are found to increase upon a chemotherapeutic regimen of 5-FU and Irinotecan.

While there are many different types of CAFs with diverse functions, in general, increases in CAFs accompany cancer progression (81). In CRC in particular, the consensus molecular subtype 4 (CMS4) is characterized by mesenchymal signatures (82), with the majority contributed by the presence of CAFs (83–85). CMS4 CRCs are more advanced and have poor prognoses (86, 87). There are a diverse set of mechanisms by which CAFs promote CRC progression including WNT modulation (17, 41, 88), inhibition of BMP signaling (89), or inducing tumor-promoting inflammation (89). Our study identifies two populations of CAFs, one of which (CAF2) was not detected in APC adenoma by scRNA-seq, but was abundant in AOM/DSS tumors. CAF2s closely associate with tumor cells, which mirrors the major CAF dichotomy in pancreatic cancer, where myCAFs closely associates with neoplastic cells while iCAFs are located more distantly (49). However, the phenotypes of these colonic CAFs seem to be distinct from those of pancreatic cancers, as it is the CAF1s, which are located more distantly to epithelial cells, that have more myofibroblastic features and some iCAF gene expression such as *Il6* and *Cxcl1*, while CAF2s also express iCAF genes such as *Il11, Cxcl12* and other chemokines (40). The induction of immune-related genes in either CAF populations is specific to AOM/DSS tumors and not APC adenomas, suggesting that immune-regulating function of CAFs may only be activated in the context of DSS inflammation. CAF2s, which are closely associated with epithelium, parallel pericryptal fibroblasts or telocytes in the normal gut (90). These cells provide signals that support a WNT signaling niche to maintain stem cell renewal during normal homeostasis (46), although *Grem1* and *Wnt5a* seem to be expressed in distinct stromal populations in the non-neoplastic

mouse colon (91–93). *Grem1/Wnt5a* co-expressing CAF2 may inhibit BMP while simultaneously stimulate WNT signaling, promoting stemness in more advanced tumors.

An unresolved question from this work is the origin of the squamous cells in AOM/DSS tumors. Similar histological findings of squamous cells in DSS colitis mouse models have been reported and were speculated to be a metaplastic event whereby the damaged colonic epithelium is re-epithelialized with stratified squamous epithelium (68). Squamous cell lesions of unknown origin have been observed in colonic polyps of CDX2-knockout mice, and likewise in SMAD3-depleted and SMAD3-knockout colonic tumors given DSS compared to DSS alone (94, 95). While squamous cell lesions could result from a simple re-epithelialization event, an alternative explanation is transdifferentiation of columnar colonic epithelial cells into stratified squamous epithelia, a process in reverse of normal colonic development. p63-positive pseudostratified embryonic epithelial cells from the endodermal lining of the primitive distal gut have been lineage traced to p63-negative adult colonic simple columnar epithelia (71). This supports the notion that some cancers, including colorectal cancer, may arise through embryonic subversion (96). In line with these observations, our data also showed an enrichment of fetal markers in the squamous tumor component absent from epithelial cells from both AOM/DSS and APC tumors, including genes expressed in primitive gut (*Trp63, Sox2, Pitx1)*, as well as metaplastic genes such as *Tacstd2.* We attempted to determine the origin of squamous lesions in AOM/DSS tumors using lineage tracing from *Lrig1*-expressing epithelial cells, since *Lrig1* is not expressed in the anal epithelium (75). We found rare lineage tracing events from *Lrig1*-expressing cells to a squamous lesion in an AOM/DSS tumor. While this result suggests the possibility of a transdifferentiation event, we cannot rule out sporadic, induced expression of *Lrig1* in the anal epithelium during re-epithelialization. We also observed AOM/DSS tumors, during a course of 5-FU and Irinotecan, expanded their squamous component. These cells exhibited more transcriptional similarity to tumor cells than those from untreated tumors, suggestive of transdifferentiation. However, this expansion could be due to the insensitivity of squamous cells to chemotherapy-induced cell death or drug-induced proliferation. Our L-R inference suggests that similar CAF-tumor interactions exist for CAF-squamous interactions. Moreover, we found that CAF2s lie in close proximity to not only AOM/DSS tumor cells, but also squamous lesions within tumors. The squamous transdifferentiation process has been shown to affect tumor cell interaction with CAFs in pancreatic cancer (69). We also found that differences in genetic backgrounds contribute profoundly to the development of squamous lesions, highlighting the complexity of factors that influence their development. Our findings implicate a role of squamous cells in colorectal tumorigenesis processes and provides insight into adenosquamous carcinomas in humans, a rare cancer type that is more aggressive and has a poorer prognosis when compared to adenocarcinoma, in part due to lack of mechanistic knowledge of their pathogenesis (97).

We also presented translationally relevant insights from our mouse studies. While checkpoint immunotherapies can result in long term responses, only a minority of cancer patients benefit (98). A positive immunotherapy response is largely dependent a favorable tumor microenvironment partly characterized by infiltration of adaptive immune cells (99–102). Some chemotherapies have been shown to stimulate the immune microenvironment, and thus, may boost the efficacy of immunotherapies when given as a combinatorial regimen. A major immunogenic mechanism is chemotherapy-induced immunogenic cell death, where tumor antigens and danger-associated molecular patterns are released into the microenvironment from a dying cell (103, 104). Our study proposes an additional mechanism, where a chemotherapy regimen of 5-FU and Irinotecan results in tumor cells with decreased WNT signaling, increased differentiation, and increased expression of AP machinery. MHC class I upregulation has been previously observed in a subcutaneous injection model of breast cancer under Irinotecan treatment (105), lending additional support to our observations. How this phenotype is achieved remains to be investigated, but a possibility may be that the chemotherapy kills highly proliferative stem cells while sparing less proliferative differentiated cells. Previous studies from our lab and others have demonstrated that tumor cell differentiation state controls antigen presentation and cytotoxic versus suppressive immunity (26, 106). However, cytotoxic T cells were not increased under 5-FU and Irinotecan despite increased expression of antigen presentation machinery, suggesting that additional immunosuppressive mechanisms may be activated. Indeed, previous studies show that Irinotecan treatment of AOM/DSS tumors blocks the apoptosis of MDSCs (107). Whereas chemotherapy regimens are non-targeted, further work in this area is required to discover therapeutic approaches to precisely establish and maintain a favorable immune microenvironment.

METHODS

Mouse Experiments

All animal experiments were performed under protocols approved by the Vanderbilt University Animal Care and Use Committee and in accordance with NIH guidelines. Animals of C57BL/6J; 129 mixed or C57BL/6J backgrounds of the appropriate size by weight (6-12 weeks old) were used at the start of experiments. Mice were housed (2 to 5 per cage) in a specific pathogen-free environment under a standard 12-hour daylight cycle, and were fed a standard rodent Lab Chow and provided water ad libitum. Littermate controls of both sexes were used for experiments when possible.

For the APC tumor model, $Lrig1^{CreERT2/+};Apc^{fl/+}$ mice were induced as documented previously (18). For the AOM/DSS tumor model, mice were injected twice with 10 mg/kg AOM with one week apart. A week after the second injection, mice were fed 2% DSS for a week, and then again after 3 weeks of rest.

For both models, tissues were harvested 12 weeks after the initial injection to initiate tumors, a timepoint where tumors are consistently present.

For lineage tracing studies, $Lrig1^{CreERT2/+}$;$Rosa26^{LSL\text{-}EYFP/+}$ mice were injected intraperitoneally (i.p.) for 3 consecutive days with 2.5 mg tamoxifen (Sigma-Aldrich; T5648) in corn oil. Mice were euthanized at the indicated timepoints for short and long-term lineage tracing.

For 5-FU and Irinotecan treatment, AOM/DSS tumors were first confirmed by colonoscopy after 12 weeks of induction. 50 mg/kg of Irinotecan hydrochloride (Millipore Sigma: 136572-09-3) was delivered intraperitoneally on day 1, followed by 50 mg/kg of 5-FU (Millipore Sigma: 51-21-8) on day 2, followed by 5 days of rest. Three cycles of this chemotherapy regimen were administered. Tissues were harvested according to timeline after the last cycle of treatment was given.

Whole Tissue Single-Cell RNA-Sequencing and Initial Processing

Dissociation of colonic tumors was performed in a two-phase process. In the first stage, colon adenomas were dissected from the distal colon and washed in ice-cold PBS. The tumors were digested in DMEM containing 2 mg/mL collagenase type II at 37°C for 1 hour or until fragments had dispersed. The tumor tissue suspension was washed in ice-cold PBS and filtered through a 40 μm filter. Tumor epithelial crypts retained by the filter were collected and resuspended in PBS while the flow-through was discarded. The tumor epithelial fraction was filtered again through a 100 μm filter to remove undigested fragments, and the flow-through was collected. In the second stage, isolated tumor epithelial crypts were further digested into single cells for encapsulation similar to above. Normal colonic tissues were digested according to a previous protocol (108). Single-cell encapsulation, library preparation, and sequencing were performed as previous (109). Raw sequencing data were aligned using dropEst to mouse GRCm38.85 resulting in count matrices (110). After obtaining the count matrices, we combined the data for each sample and removed low-quality cells. We defined low-quality as any cell with either less than 500 genes detected or with greater 15% of counts mapping to mitochondrial genes. In total, we retained sequencing data of approximately 19,000 cells across all samples.

Colonic Stroma Enrichment for Single-Cell RNA-Sequencing

Colon was isolated, flushed and washed briefly in DPBS (-ca/mg) with 20mM HEPES (DPBSH). Tissue was chelated at 37˚c for 20min with rotation in DPBSH with 5mM EDTA and 1mM DTT. After, the tissue was shaken in 10ml volumes of DPBSH to remove crypts. The remaining tissue (lamina propria and stroma) was then minced into ~2mm^2 pieces and digested for 30min at 37˚C in DPBSH with 1mg/ml collagenase and dispase. Digest was then stopped by adding an equal volume of DPBSH with 5% FBS and 2.5mM EDTA. Tissue was triturated using a p1000 pipette and passed through a 70μm filter into a 50ml tube, with 10 additional mL of DPBSH to rinse. Cells were pelleted at 500g and resuspended in 5ml of 40% percol and underlayed with 5ml of 90% percol, then centrifuged at 500g for 10 minutes with no brakes to allow separation of cells. Layers at the top of the 40% percol and 40%/90% interface were washed 3 times in DPBS and loaded onto inDrop for encapsulation.

Single-Cell RNA-Sequencing Data Analysis

Analysis of pre-processed murine scRNA-seq data was carried out in RStudio version 4.1.1 and Seurat version 4.0.4 (111). Functions use default arguments unless specified. Batch effects were minimal as seen from the intermixing of non-neoplastic cells, and therefore, no batch corrections were performed. After quality control and filtering steps, the following steps were performed for the following datasets: 1) APC tumor (n=2), AOM/DSS tumor (n=3), APC adjacent normal (n=2), and wildtype colon (n=2) samples (~13,000 total cells). 2) 5-FU and Irinotecan treated AOM/DSS tumor samples (n=2 for the "late treatment" timepoint from day 3 and 6 post-treatment, and n=2 for the "early treatment" timepoint from day 1 post-treatment, ~7,000 total cells). 3) Normal mouse colon enriched for fibroblasts (n=1), 1108 total cells, 465 of which are fibroblasts. A Seurat object was created using the CreateSeuratObject function and the number of genes, number of UMIs, and percent mitochondrial expression for all cells in the dataset were visualized. The NormalizeData, FindVariableFeatures (vst method with 2000 features), and ScaleData (using all genes) functions were used to normalize the data, find highly variable genes (HVGs), and scale and center the data. Principle component analysis (PCA) was performed using Seurat's RunPCA function using only HVGs as features for dimension reduction. The jackstraw method (Seurat's JackStraw function with 30 PCs) and the ElbowPlot function were used to determine the PCs to use for UMAP (Seurat's RunUMAP function) visualization. DPC clustering was performed on the APC, AOM/DSS, APC adjacent, and wildtype dataset to determine cell types, with the exception of subclustering of the T cells, for which we used Seurat's FindClusters function (112). For the 5-FU and Irinotecan-treated samples, we used Seurat's FindClusters function as well as manual subclustering based on sample type. To determine the appropriate number of clusters in each sample, the clustering resolution parameter was adjusted, and differential expression analysis was performed to identify known cell types based on marker gene expression. We used Seurat's FindMarkers function with standard parameters and log fold change thresholds above 2 to identify differentially expressed genes. Cell cycle analysis was performed as previously described (113). Sc-Unifrac was run with default parameters and using our clustering data, rather than the default hierarchical clustering, as previously described (23). The CytoTRACE web tool was used to calculate predicted stemness of single cells (74). Gene lists for metaplasia and damage, fetal and embryonic, and WNT signaling were used as previously described (26).

Analysis of human scRNA-seq data was performed in Python using scanpy, pandas, and numpy packages as previously described (26). Briefly, raw scRNA-seq counts were normalized by median library size, log-like transformed with Arcsinh, and Z-score standardized per gene. Cells annotated as mesenchymal cell

types were subset from the Samsung Medical Center dataset (31). Similarly, cell annotated as mesenchymal from only microsatellite stable (MSS) tumor status samples were subset from the Broad Institute Human Tumor Atlas Network dataset (17). UMAP visualization was based on normalized gene counts for the two datasets. All UMAP plot coordinates for individual cells were generated with the *scanpy.tl.umap* function. The input to this function was the normalized dataset, their 40 principal components, and a KNN graph with k equal to the square root of the number of cells in the dataset. The *scanpy.pl.umap* function was used to visualize select gene marker expressions as an overlay onto UMAP coordinates.

Immunofluorescence Imaging and MxIF

Colonic tissue was isolated, washed with 1X DPBS, spread longitudinally onto Whatman filter paper and fixed in 4% PFA (Thermo Scientific). Fixed tissues were washed with 1X DPBS, swiss-rolled, and stored in 70% EtOH until processing and paraffin embedding (formalin-fixed paraffin embedded, or "FFPE"), or were incubated in 30% sucrose in 1X PBS and embedded in cryo embedding media ("fixed frozen"). Tissues were sectioned at 5 or 7 um thick onto glass slides. FFPE tissue slides were processed for deparaffinization, rehydration, and antigen retrieval using citrate buffer (pH 6.0; Dako) for 20 minutes in a pressure cooker at 105°C followed by a 20-minute bench cool down. Endogenous background signal was reduced by incubating slides in 1% H_2O_2 (Sigma-Aldrich) for 10 minutes, before blocking for 30 minutes in 2.5% Normal Donkey Serum, 1% BSA in 1X DPBS prior to antibody staining. Primary antibodies against selected markers were incubated on the slides in a humidity chamber overnight, followed by three washes in PBS or dilute blocking buffer, and 1 hour incubation in Hoechst 33342 (Invitrogen), and compatible secondaries (1:500) conjugated to Invitrogen AlexaFluor-488, -555, or -647. Slides were washed in 1X DPBS or dilute blocking buffer, mounted in 50% glycerol/50% 1X PBS and imaged using a Zeiss Axio Imager M2 microscope with Axiovision digital imaging system (Zeiss; Jena GmBH). Multiplexed imaging using an immune cell-based antibody panel was performed by using a multiplex iterative staining and fluorescence-inactivation protocol, as previously described (47, 114), and imaged on an Olympus X81 inverted microscope with a motorized stage or Cytell Slide Imaging System (GE Healthcare) at 20X magnification. For histological analysis, slides were processed and stained for hematoxylin and eosin using standard approaches.

Quantification of CAF Subtypes in MxIF Images

Stitched images were generated of tumor sections stained for nuclei with Hoechst and with antibodies against VIM, SMA, PDGFRα, TNC, and β-catenin. For each antibody target, thresholding was used to generate a binary mask. Tumor areas were outlined by identifying areas with strong β-catenin signal. Within tumor areas, CAF1, CAF2, and β-catenin binary masks were generated. CAF1 area was determined by overlaying binary masks of VIM and SMA signal, while CAF2 area was determined by overlaying binary masks of PDGFRα and TNC. CAF1 and CAF2 abundance was determined by normalizing the area of positive signal in CAF1 and CAF2 binary masks, individually, to the area of positive signal in the β-catenin binary mask. Example quantification is shown in **Figure S6**, and all MxIF data and masks are shown in **Figure S7** for APC tumors and **Figure S8** for AOM/DSS tumors. Student's t-test was performed to determine statistical significance between 2 groups.

Computation of Receptor Ligand Interaction Scores

In similar vein to previous work (76), the analysis aimed to identify receptor-ligand (RL) interactions using prior knowledge of their interactions and differential expression in cell-type pairs of interest. Here quantified as a log transformed product of fold changes (FC), RL-score = $\log2(FC_{Ligand} \times FC_{Receptor})$. The interaction was taken to be significant if both the receptor and ligand were differentially expressed compared to background (see below). A multiple hypothesis corrected p-value threshold of 0.01 was used and results were also filtered for effect size using a cutoff of 0.5 log2 FC for ligands and cutoff of 0 (i.e. positive) for receptors. These results were further restricted to only include receptors and ligands where the filtering requirements were met for all samples within a group (n=3 for AOM/DSS, n=2 for APC and n=2 for early and late treatment by 5-FU + Irinotecan). A prior knowledge graph of receptor-ligand interactions was extracted from an online database (OmniPath) (77). The RL interactions were subset to ones with known mode of action and directionality. From this, lists of ligands and receptors were compiled and their differential gene expression was calculated. Gene expression was normalized on a cell by cell basis using the default method in the r-package Seurat (115), i.e. dividing the counts for each cell by the sum of counts, multiplying by 10000, and taking the log2(x+1) transformation. Differential gene expression and fold changes for different cell types was calculated on a sample-by-sample basis by comparing the gene expression of cells from one cell type and sample at a time against the background expression among all other cell types and samples. Differential gene expression was calculated with the FindMarkers function in Seurat using the MAST method (116) with filtering for fold change and percent gene expression set to 0. After computing p-values for all selected genes in all cell-types, multiple hypothesis testing adjusted p-values were calculated using the Benjamini & Hochberg method.

DATA AVAILABILITY STATEMENT

The datasets presented in this study can be found in online repositories. The names of the repository/repositories and accession number(s) can be found below: (https://www.ncbi.nlm.nih.gov/, GSE134255, GSE199999).

ETHICS STATEMENT

The animal study was reviewed and approved by Vanderbilt University Animal Care and Use Committee.

AUTHOR CONTRIBUTIONS

PV, RC, DL, and KL study design and conception. PV, HN, AS, JR, JW, and WL experiment conduction. PV, AN, MK, ZC data analysis and statistical analysis. EM, BJ, MW, and JR technical consultation. KL and PV writing manuscript. All authors have approved the final manuscript.

FUNDING

This work is funded by U01CA215798 to DL, R01DK103831 to KL, F31DK127687 to PV, R35CA197570 and P50CA236733 to RC, Vetenskapsrådet 2019-06349 to AN, T32HD007502 in support of PV, and P30CA068485 for cores used. RC acknowledges the generous support of the Nicholas Tierney GI Cancer Memorial Fund. The funders played no role in the research conducted.

ACKNOWLEDGMENTS

The authors wish to thank other contributing investigators, including Austin Southard-Smith, Marisol Ramirez-Solano, Bob Chen, Won Jae Huh, and Yanwen Xu, as well as members of the Vanderbilt Epithelial Biology Center for helpful discussions. We would also like to acknowledge Cores at Vanderbilt used in this study, including TPSR, DHSR, and VANTAGE.

SUPPLEMENTARY MATERIAL

The Supplementary Material for this article can be found online at: https://www.frontiersin.org/articles/10.3389/fonc.2022.878920/full#supplementary-material

REFERENCES

1. Greaves M, Maley CC. CLONAL EVOLUTION IN CANCER. *Nature* (2012) 481(7381):306. doi: 10.1038/NATURE10762
2. Nowell PC. The Clonal Evolution of Tumor Cell Populations. *Science* (1976) 194(4260):23–8. doi: 10.1126/SCIENCE.959840
3. Sottoriva A, Kang H, Ma Z, Graham TA, Salomon MP, Zhao J, et al. A Big Bang Model of Human Colorectal Tumor Growth HHS Public Access Author Manuscript. *Nat Genet* (2015) 47(3):209–16. doi: 10.1038/ng.3214
4. Wood LD, Parsons DW, Jones S, Lin J, Sjöblom T, Leary RJ, et al. The Genomic Landscapes of Human Breast and Colorectal Cancers. *Sci (New York N.Y.)* (2007) 318(5853):1108–13. doi: 10.1126/SCIENCE.1145720
5. Vogelstein B, Fearon ER, Hamilton SR, Kern SE, Preisinger AC, Leppert M, et al. Genetic Alterations During Colorectal-Tumor Development. (2010) 319(9):525–325. doi: 10.1056/NEJM198809013190901
6. Muzny DM, Bainbridge MN, Chang K, Dinh HH, Drummond JA, Fowler G, et al. Comprehensive Molecular Characterization of Human Colon and Rectal Cancer. *Nature* (2012) 487(7407):330–37. doi: 10.1038/nature11252
7. Vasaikar S, Huang C, Wang X, Petyuk VA, Savage SR, Wen B, et al. Proteogenomic Analysis of Human Colon Cancer Reveals New Therapeutic Opportunities. *Cell* (2019) 177(4):1035–1049.e19. doi: 10.1016/j.cell.2019.03.030
8. Fridman WH, Miller I, Sautès-Fridman C, Byrne AT. Therapeutic Targeting of the Colorectal Tumor Stroma. *Gastroenterology* (2020) 158(2):303–215. doi: 10.1053/j.gastro.2019.09.045
9. Tsujino T, Seshimo I, Yamamoto H, Chew YN, Ezumi K, Takemasa I, et al. Stromal Myofibroblasts Predict Disease Recurrence for Colorectal Cancer. *Clin Cancer Research: Off J Am Assoc Cancer Res* (2007) 13(7):2082–905. doi: 10.1158/1078-0432.CCR-06-2191
10. Herrera M, Herrera A, Domínguez G, Silva J, García V, García JM, et al. Cancer-Associated Fibroblast and M2 Macrophage Markers Together Predict Outcome in Colorectal Cancer Patients. *Cancer Sci* (2013) 104 (4):437–44. doi: 10.1111/CAS.12096
11. Herrera M, Berral-González A, López-Cade I, Galindo-Pumariño C, Bueno-Fortes S, Martín-Merino M, et al. Cancer-Associated Fibroblast-Derived Gene Signatures Determine Prognosis in Colon Cancer Patients. *Mol Cancer* (2021) 20(1):1–6. doi: 10.1186/S12943-021-01367-X/FIGURES/3
12. Nishishita R, Morohashi S, Seino H, Wu Y, Yoshizawa T, Haga T, et al. Expression of Cancer-Associated Fibroblast Markers in Advanced Colorectal Cancer. *Oncol Lett* (2018) 15(5):6195–62025. doi: 10.3892/OL.2018.8097
13. Heichler C, Scheibe K, Schmied A, Geppert CI, Schmid B, Wirtz S, et al. STAT3 Activation Through IL-6/IL-11 in Cancer-Associated Fibroblasts Promotes Colorectal Tumour Development and Correlates With Poor Prognosis. *Gut* (2020) 69(7):1269–82. doi: 10.1136/GUTJNL-2019-319200
14. Bai YP, Shang K, Chen H, Ding F, Wang Z, Liang C, et al. FGF-1/-3/FGFR4 Signaling in Cancer-Associated Fibroblasts Promotes Tumor Progression in Colon Cancer Through Erk and MMP-7. *Cancer Sci* (2015) 106(10):1278–875. doi: 10.1111/CAS.12745
15. Fujita M, Ito-Fujita Y, Iyoda T, Sasada M, Okada Y, Ishibashi K, et al. Peptide TNIIIA2 Derived From Tenascin-C Contributes to Malignant Progression in Colitis-Associated Colorectal Cancer via B1-Integrin Activation in Fibroblasts. *Int J Mol Sci* (2019) 20(11):27525. doi: 10.3390/IJMS20112752
16. Sasaki S, Baba T, Shinagawa K, Matsushima K, Mukaida N. Crucial Involvement of the CCL3-CCR5 Axis-Mediated Fibroblast Accumulation in Colitis-Associated Carcinogenesis in Mice. *Int J Cancer* (2014) 135 (6):1297–13065. doi: 10.1002/IJC.28779
17. Pelka K, Hofree M, Chen JH, Sarkizova S, Pirl JD, Jorgji V, et al. Spatially Organized Multicellular Immune Hubs in Human Colorectal Cancer. *Cell* (2021) 184(18):4734–4752.e20. doi: 10.1016/j.cell.2021.08.003
18. Powell AE, Vlacich G, Zhao Z-Y, McKinley ET, Washington MK, Manning HC, et al. Inducible Loss of One Apc Allele in Lrig1-Expressing Progenitor Cells Results in Multiple Distal Colonic Tumors With Features of Familial Adenomatous Polyposis. *Am J Physiol Gastrointest Liver Physiol* (2014) 307 (1):G16–23. doi: 10.1152/ajpgi.00358.2013
19. Robertis M, Massi E, Luana Poeta M, Carotti S, Morini S, Cecchetelli L, et al. The AOM/DSS Murine Model for the Study of Colon Carcinogenesis: From Pathways to Diagnosis and Therapy Studies. *J Carcinog* (2011) 10(March):9. doi: 10.4103/1477-3163.78279
20. Evans JP, Sutton PA, Winiarski BK, Fenwick SW, Malik HZ, Vimalachandran D, et al. From Mice to Men: Murine Models of Colorectal Cancer for Use in Translational Research. *Crit Rev Oncol/Hematol* (2016) 98:94–105. doi: 10.1016/j.critrevonc.2015.10.009
21. Tanaka T, Kohno H, Suzuki R, Yamada Y, Sugie S, Mori H. A Novel Inflammation-Related Mouse Colon Carcinogenesis Model Induced by Azoxymethane and Dextran Sodium Sulfate. *Cancer Sci* (2003) 94 (11):965–735. doi: 10.1111/j.1349-7006.2003.tb01386.x

22. Klein AM, Mazutis L, Akartuna I, Tallapragada N, Veres A, Li V, et al. Droplet Barcoding for Single-Cell Transcriptomics Applied to Embryonic Stem Cells. *Cell* (2015) 161(5):1187–12015. doi: 10.1016/j.cell.2015.04.044
23. Liu Q, Herring CA, Sheng Q, Ping J, Simmons AJ, Chen B, et al. Quantitative Assessment of Cell Population Diversity in Single-Cell Landscapes. *PloS Biol* (2018) 16(10):e2006687. doi: 10.1371/journal.pbio.2006687
24. Han X, Wang R, Zhou Y, Fei L, Sun H, Lai S, et al. Mapping the Mouse Cell Atlas by Microwell-Seq. *Cell* (2018) 172(5):1091–1107.e17. doi: 10.1016/j.cell.2018.02.001
25. Nakano S, Ohara S, Kubota T, Saigenji K, Hotta K. Compensatory Response of Colon Tissue to Dextran Sulfate Sodium-Induced Colitis. *J Gastroenterol* (1999) 34(2):207–14. doi: 10.1007/s005350050245
26. Chen B, Scurrah C'R, McKinley ET, Simmons AJ, Ramirez-Solano MA, Zhu X, et al. Differential Pre-Malignant Programs and Microenvironment Chart Distinct Paths to Malignancy in Human Colorectal Polyps. *Cell* (2021) 184 (26):6262–6280.e26. doi: 10.1016/j.cell.2021.11.031
27. Schön MP, Arya A, Murphy EA, Adams CM, Strauch UG, Agace WW, et al. Mucosal T Lymphocyte Numbers Are Selectively Reduced in Integrin Alpha E (CD103)-Deficient Mice. *J Immunol (Baltimore Md.: 1950)* (1999) 162 (11):6641–49.
28. Bonneville M, Janeway CA, Ito K, Haser W, Ishida I, Nakanishit N, et al. Intestinal Intraepithelial Lymphocytes Are a Distinct Set of Γδ T Cells. *Nature* (1988) 336(6198):479–81. doi: 10.1038/336479a0
29. Joshi NS, Cui W, Chandele A, Lee HK, Urso DR, Hagman J, et al. Inflammation Directs Memory Precursor and Short-Lived Effector CD8+ T Cell Fates via the Graded Expression of T-Bet Transcription Factor. *Immunity* (2007) 27(2):281–955. doi: 10.1016/J.IMMUNI.2007.07.010/ATTACHMENT/81A95BA8-80A4-44F7-A5B1-EF9960A25120/MMC1.PDF
30. Blackburn SD, Shin H, Nicholas Haining W, Zou T, Workman CJ, Polley A, et al. Coregulation of CD8+ T Cell Exhaustion by Multiple Inhibitory Receptors During Chronic Viral Infection. *Nat Immunol* (2008) 10(1):29–375. doi: 10.1038/ni.1679
31. Lee H-O, Hong Y, Etlioglu HE, Cho YB, Pomella V, den Bosch BV, et al. Lineage-Dependent Gene Expression Programs Influence the Immune Landscape of Colorectal Cancer. *Nat Genet* (2020) 52(6):594–603. doi: 10.1038/s41588-020-0636-z
32. Duckworth A, Glenn M, Slupsky JR, Packham G, Kalakonda N. Variable Induction of PRDM1 and Differentiation in Chronic Lymphocytic Leukemia Is Associated With Anergy. *Blood* (2014) 123(21):3277–855. doi: 10.1182/BLOOD-2013-11-539049
33. Anderson AC, Joller N, Kuchroo VK. Lag-3, Tim-3, and TIGIT: Co-Inhibitory Receptors With Specialized Functions in Immune Regulation. *Immunity* (2016) 44(5):989–10045. doi: 10.1016/J.IMMUNI.2016.05.001
34. Fife BT, Pauken KE, Eagar TN, Obu T, Wu J, Tang Q, et al. Interactions Between PD-1 and PD-L1 Promote Tolerance by Blocking the TCR–Induced Stop Signal. *Nat Immunol* (2009) 10(11):1185–925. doi: 10.1038/ni.1790
35. Greenwald RJ, Boussiotis VA, Lorsbach RB, Abbas AK, Sharpe AH. CTLA-4 Regulates Induction of Anergy In Vivo. *Immunity* (2001) 14(2):145–555. doi: 10.1016/S1074-7613(01)00097-8
36. Schwartz RH. T Cell Anergy. *Annu Rev Immunol* (2003) 21 (November):305–34. doi: 10.1146/annurev.immunol.21.120601.141110
37. McKenzie DR, Kara EE, Bastow CR, Tyllis TS, Fenix KA, Gregor CE, et al. IL-17-Producing Γδ T Cells Switch Migratory Patterns Between Resting and Activated States. *Nat Commun* (2017) 8:15632. doi: 10.1038/ncomms15632
38. Sutton CE, Lalor SJ, Sweeney CM, Brereton CF, Lavelle EC, Mills KHG. Interleukin-1 and IL-23 Induce Innate IL-17 Production From Gammadelta T Cells, Amplifying Th17 Responses and Autoimmunity. *Immunity* (2009) 31(2):331–415. doi: 10.1016/j.immuni.2009.08.001
39. Rupp C, Scherzer M, Rudisch A, Unger C, Haslinger C, Schweifer N, et al. IGFBP7, a Novel Tumor Stroma Marker, With Growth-Promoting Effects in Colon Cancer Through a Paracrine Tumor-Stroma Interaction. *Oncogene* (2015) 34(7):815–25. doi: 10.1038/ONC.2014.18
40. Barrett RL, Pure E. Cancer-Associated Fibroblasts and Their Influence on Tumor Immunity and Immunotherapy. *ELife* (2020) 9(December):1–20. doi: 10.7554/ELIFE.57243
41. Hirashima T, Karasawa H, Aizawa T, Suzuki T, Yamamura A, Suzuki H, et al. Wnt5a in Cancer-Associated Fibroblasts Promotes Colorectal Cancer Progression. *Biochem Biophys Res Commun* (2021) 568:37–42. doi: 10.1016/j.bbrc.2021.06.062
42. Kobayashi H, Gieniec KA, Lannagan TR, Wang T, Asai N, Mizutani Y, et al. The Origin and Contribution of Cancer-Associated Fibroblasts in Colorectal Carcinogenesis. *Gastroenterology* (2022) 162(3):890-906. doi: 10.1053/j.gastro.2021.11.037
43. Chen PH, Chen X, He X. Platelet-Derived Growth Factors and Their Receptors: Structural and Functional Perspectives. *Biochim Biophys Acta* (2013) 1834(10):2176. doi: 10.1016/J.BBAPAP.2012.10.015
44. Yamazaki T, Nalbandian A, Uchida Y, Li W, Arnold TD, Kubota Y, et al. Tissue Myeloid Progenitors Differentiate Into Pericytes Through TGF-β Signaling in Developing Skin Vasculature. *Cell Rep* (2017) 18(12):2991–30045. doi: 10.1016/J.CELREP.2017.02.069
45. Yamazaki T, Mukouyama YS. Tissue Specific Origin, Development, and Pathological Perspectives of Pericytes. *Front Cardiovasc Med* (2018) 5:78/BIBTEX(June). doi: 10.3389/FCVM.2018.00078/BIBTEX
46. Shoshkes-Carmel M, Wang YJ, Wangensteen KJ, Tóth B, Kondo A, Massassa EE, et al. Subepithelial Telocytes Are an Important Source of Wnts That Supports Intestinal Crypts. *Nature* (2018) 557(7704):242–46. doi: 10.1038/s41586-018-0084-4
47. McKinley ET, Sui Y, Al-Kofahi Y, Millis BA, Tyska MJ, Roland JT, et al. Optimized Multiplex Immunofluorescence Single-Cell Analysis Reveals Tuft Cell Heterogeneity. *JCI Insight* (2017) 2(11). doi: 10.1172/jci.insight.93487
48. Takahashi M, Wakabayashi K. Gene Mutations and Altered Gene Expression in Azoxymethane-Induced Colon Carcinogenesis in Rodents. *Cancer Sci* (2004) 95(6):475–805. doi: 10.1111/J.1349-7006.2004.TB03235.X
49. Öhlund D, Handly-Santana A, Biffi G, Elyada E, Almeida AS, Ponz-Sarvise M, et al. Distinct Populations of Inflammatory Fibroblasts and Myofibroblasts in Pancreatic Cancer. *J Exp Med* (2017) 214(3):579–96. doi: 10.1084/jem.20162024
50. Liu YS, Hsu HC, Tseng KC, Chen HC, Chen SJ. Lgr5 Promotes Cancer Stemness and Confers Chemoresistance Through ABCB1 in Colorectal Cancer. *Biomed Pharmacot = Biomed Pharmacot* (2013) 67(8):791–995. doi: 10.1016/J.BIOPHA.2013.08.001
51. Takahashi H, Ishii H, Nishida N, Takemasa I, Mizushima T, Ikeda M, et al. Significance of Lgr5+ve Cancer Stem Cells in the Colon and Rectum. *Ann Surg Oncol* (2010) 18(4):1166–74. doi: 10.1245/S10434-010-1373-9
52. Baba Y, Nosho K, Shima K, Freed E, Irahara N, Philips J, et al. Relationship of CDX2 Loss With Molecular Features and Prognosis in Colorectal Cancer. *Clin Cancer Research: Off J Am Assoc Cancer Res* (2009) 15(14):4665–73. doi: 10.1158/1078-0432.CCR-09-0401
53. Bae JM, Lee TH, Cho NY, Kim TY, Kang GH. Loss of CDX2 Expression Is Associated With Poor Prognosis in Colorectal Cancer Patients. *World J Gastroenterol* (2015) 21(5):1457–675. doi: 10.3748/WJG.V21.I5.1457
54. Lugli A, Tzankov A, Zlobec I, Terracciano LM. Differential Diagnostic and Functional Role of the Multi-Marker Phenotype CDX2/CK20/CK7 in Colorectal Cancer Stratified by Mismatch Repair Status. *Mod Pathology: Off J Unite States Can Acad Pathol Inc* (2008) 21(11):1403–125. doi: 10.1038/MODPATHOL.2008.117
55. Zhang BY, Jones JC, Briggler AM, Hubbard JM, Kipp BR, Sargent DJ, et al. Lack of Caudal-Type Homeobox Transcription Factor 2 Expression as a Prognostic Biomarker in Metastatic Colorectal Cancer. *Clin Colorectal Cancer* (2017) 16(2):124–285. doi: 10.1016/J.CLCC.2016.09.003
56. Mallo GV, Rechreche H, Frigerio J-M, Rocha D, Zweibaum A, Lacasa M, et al. Molecular Cloning, Sequencing and Expression of the MRNA Encoding Human Cdx1 and Cdx2 Homeobox. Down-Regulation of Cdx1 and Cdx2 MRNA Expression During Colorectal Carcinogenesis. *Int J Cancer (Pred. Oncol* (1996) 74(1):35–44. doi: 10.1002/(SICI)1097-0215(19970220)74:1
57. Qualtrough D, Hinoi T, Fearon E, Paraskeva C. Expression of CDX2 in Normal and Neoplastic Human Colon Tissue and During Differentiation of an in Vitro Model System. *Gut* (2002) 51(2):184–90. doi: 10.1136/GUT.51.2.184
58. Hinoi T, Loda M, Fearon ER. Silencing of CDX2 Expression in Colon Cancer via a Dominant Repression Pathway *. *J Biol Chem* (2003) 278(45):44608–165. doi: 10.1074/JBC.M307435200
59. Sheng S, Carey J, Seftor EA, Dias L, Hendrix MJC, Sager R. Maspin Acts at the Cell Membrane to Inhibit Invasion and Motility of Mammary and

Prostatic Cancer Cells. *Proc Natl Acad Sci USA* (1996) 93(21):11669–745. doi: 10.1073/PNAS.93.21.11669
60. Ohki R, Saito K, Chen Y, Kawase T, Hiraoka N, Saigawa R, et al. PHLDA3 Is a Novel Tumor Suppressor of Pancreatic Neuroendocrine Tumors. *Proc Natl Acad Sci USA* (2014) 111(23):E2404-13. doi: 10.1073/PNAS.1319962111/-/DCSUPPLEMENTAL/PNAS.1319962111.SAPP.PDF
61. VanDussen KL, Samuelson LC. Mouse Atonal Homolog 1 Directs Intestinal Progenitors to Secretory Cell Rather Than Absorptive Cell Fate. *Dev Biol* (2010) 346(2):2155. doi: 10.1016/J.YDBIO.2010.07.026
62. Sun L, Ke J, He Z, Chen Z, Huang Q, Ai W, et al. HES1 Promotes Colorectal Cancer Cell Resistance To 5-Fu by Inducing Of EMT and ABC Transporter Proteins. *J Cancer* (2017) 8(14):2802. doi: 10.7150/JCA.19142
63. Weng MT, Tsao PN, Lin HL, Tung CC, Change MC, Chang YT, et al. Hes1 Increases the Invasion Ability of Colorectal Cancer Cells *via* the STAT3-MMP14 Pathway. *PloS One* (2015) 10(12):e0144322-35. doi: 10.1371/JOURNAL.PONE.0144322
64. Rad R, Cadiñ J, Rad L, Varela I, Strong A, Kriegl L, et al. Cancer Cell Article A Genetic Progression Model of Braf V600E-Induced Intestinal Tumorigenesis Reveals Targets for Therapeutic Intervention. *Cancer Cell* (2013) 24:15–29. doi: 10.1016/j.ccr.2013.05.014
65. Wang X, Li G, Koul S, Ohki R, Maurer M, Borczuk A, et al. PHLDA2 Is a Key Oncogene-Induced Negative Feedback Inhibitor of EGFR/ErbB2 Signaling via Interference With AKT Signaling. *Oncotarget* (2018) 9(38):249145. doi: 10.18632/ONCOTARGET.3674
66. Shvartsur A, Bonavida B. Trop2 and Its Overexpression in Cancers: Regulation and Clinical/Therapeutic Implications. *Genes Cancer* (2015) 6 (3–4):84. doi: 10.18632/GENESANDCANCER.40
67. Riera KM, Jang B, Min J, Roland JT, Yang Q, Fesmire WT, et al. Trop2 Is Upregulated in the Transition to Dysplasia in the Metaplastic Gastric Mucosa. *J Pathol* (2020) 251(3):336–47. doi: 10.1002/path.5469
68. Perše M, Cerar A. Dextran Sodium Sulphate Colitis Mouse Model: Traps and Tricks. *J Biomed Biotechnol* (2012) 2012(718617):82–94. doi: 10.1155/2012/718617
69. Somerville T, Biffi G, Daßler-Plenker J, Hur SK, He X-Y, Vance KE, et al. Squamous Trans-Differentiation of Pancreatic Cancer Cells Promotes Stromal Inflammation. *ELife* (2020) 9:e53381-411. doi: 10.7554/eLife.53381
70. Yoh K, Prywes R. Pathway Regulation of P63, a Director of Epithelial Cell Fate. *Front Endocrinol* (2015) 6:51/BIBTEX(APR). doi: 10.3389/FENDO.2015.00051/BIBTEX
71. Pignon JC, Grisanzio C, Geng Y, Song J, Shivdasani RA, Signoretti S. P63-Expressing Cells Are the Stem Cells of Developing Prostate, Bladder, and Colorectal Epithelia. *Proc Natl Acad Sci USA* (2013) 110(20):8105–105. doi: 10.1073/PNAS.1221216110
72. Watanabe H, Ma Q, Peng S, Adelmant G, Swain D, Song W, et al. SOX2 and P63 Colocalize at Genetic Loci in Squamous Cell Carcinomas. *J Clin Invest* (2014) 124(4):1636–45. doi: 10.1172/JCI71545
73. Sastre-Perona A, Hoang-Phou S, Leitner MC, Okuniewska M, Meehan S, Schober M. *De Novo* PITX1 Expression Controls Bi-Stable Transcriptional Circuits to Govern Self-Renewal and Differentiation in Squamous Cell Carcinoma. *Cell Stem Cell* (2019) 24(3):390–4045.e8. doi: 10.1016/J.STEM.2019.01.003
74. Gulati GS, Sikandar SS, Wesche DJ, Manjunath A, Bharadwaj A, Berger MJ, et al. Single-Cell Transcriptional Diversity Is a Hallmark of Developmental Potential. *Sci (New York N.Y.)* (2020) 367(6476):405–11. doi: 10.1126/SCIENCE.AAX0249
75. Powell AE, Wang Y, Li Y, Poulin EJ, Means AL, Washington MK, et al. The Pan-ErbB Negative Regulator Lrig1 Is an Intestinal Stem Cell Marker That Functions as a Tumor Suppressor. *Cell* (2012) 149(1):146–58. doi: 10.1016/j.cell.2012.02.042
76. Kumar MP, Du J, Lagoudas G, Jiao Y, Sawyer A, Drummond DC, et al. Analysis of Single-Cell RNA-Seq Identifies Cell-Cell Communication Associated With Tumor Characteristics. *Cell Rep* (2018) 25(6):1458–14685.e4. doi: 10.1016/j.celrep.2018.10.047
77. Türei D, Korcsmáros T, Saez-Rodriguez J. OmniPath: Guidelines and Gateway for Literature-Curated Signaling Pathway Resources. *Nat Methods* (2016) 13(12):966–67. doi: 10.1038/nmeth.4077
78. Cheng X, Lai H, Luo W, Zhang M, Miao J, Song W, et al. Single-Cell Analysis Reveals Urothelial Cell Heterogeneity and Regenerative Cues Following Cyclophosphamide-Induced Bladder Injury. *Cell Death Dis* (2021) 12 (5):1–155. doi: 10.1038/s41419-021-03740-6
79. Danopoulos S, Schlieve CR, Grikscheit TC, Al Alam D. Fibroblast Growth Factors in the Gastrointestinal Tract: Twists and Turns. *Dev Dynam* (2017) 246(4):344–525. doi: 10.1002/DVDY.24491
80. Digiacomo V, Meruelo D. Looking Into Laminin Receptor: Critical Discussion Regarding the Non-Integrin 37/67-KDa Laminin Receptor/RPSA Protein. *Biol Rev Cambridge Philos Soc* (2016) 91(2):2885. doi: 10.1111/BRV.12170
81. Sahai E, Astsaturov I, Cukierman E, DeNardo DG, Egeblad M, Evans RM, et al. A Framework for Advancing Our Understanding of Cancer-Associated Fibroblasts. *Nat Rev Cancer* (2020) 20(3):174–86. doi: 10.1038/s41568-019-0238-1
82. Guinney J, Dienstmann R, Wang X, de Reyniès A, Schlicker A, Soneson C, et al. The Consensus Molecular Subtypes of Colorectal Cancer. *Nat Med* (2015) 21(11):1350–56. doi: 10.1038/nm.3967
83. Calon A, Lonardo E, Berenguer-llergo A, Espinet E, Hernando-momblona X, Iglesias M, et al. Stromal Gene Expression Defines Poor-Prognosis Subtypes in Colorectal Cancer. *Nat Genet* (2015) 47(February):320–29. doi: 10.1038/ng.3225
84. Isella C, Terrasi A, Bellomo SE, Petti C, Galatola G, Muratore A, et al. Stromal Contribution to the Colorectal Cancer Transcriptome. *Nat Genet* (2015) 47(4):312–19. doi: 10.1038/ng.3224
85. McCorry A, Loughrey MB, Longley DB, Lawler M, Dunne PD. Epithelial-To-Mesenchymal Transition Signature Assessment in Colorectal Cancer Quantifies Tumour Stromal Content Rather Than True Transition. *J Pathol* (2018) 246(4):422–265. doi: 10.1002/path.5155
86. Dienstmann R, Vermeulen L, Guinney J, Kopetz S, Tejpar S, Tabernero J. Consensus Molecular Subtypes and the Evolution of Precision Medicine in Colorectal Cancer. *Nat Rev Cancer* (2017) 17(2):79–925. doi: 10.1038/nrc.2016.126
87. Becht E, de Reyniès A, Giraldo NA, Pilati C, Buttard B, Lacroix L, et al. Immune and Stromal Classification of Colorectal Cancer Is Associated With Molecular Subtypes and Relevant for Precision Immunotherapy. *Clin Cancer Research: Off J Am Assoc Cancer Res* (2016) 22(16):4057–665. doi: 10.1158/1078-0432.CCR-15-2879
88. Aizawa T, Karasawa H, Funayama R, Shirota M, Suzuki T, Maeda S, et al. Cancer-Associated Fibroblasts Secrete Wnt2 to Promote Cancer Progression in Colorectal Cancer. *Cancer Med* (2019) 8(14):6370–82. doi: 10.1002/cam4.2523
89. Kobayashi H, Gieniec KA, Wright JA, Wang T, Asai N, Mizutani Y, et al. The Balance of Stromal BMP Signaling Mediated by GREM1 and ISLR Drives Colorectal Carcinogenesis. *Gastroenterology* (2021) 160(4):1224–1239.e30. doi: 10.1053/j.gastro.2020.11.011
90. Aoki R, Shoshkes-Carmel M, Gao N, Shin S, May CL, Golson ML, et al. Foxl1-Expressing Mesenchymal Cells Constitute the Intestinal Stem Cell Niche. *CMGH* (2016) 2(2):175–88. doi: 10.1016/j.jcmgh.2015.12.004
91. Brügger MD, Valenta T, Fazilaty H, Hausmann G, Basler K. Distinct Populations of Crypt-Associated Fibroblasts Act as Signaling Hubs to Control Colon Homeostasis. *PloS Biol* (2020) 18(12):e30010325. doi: 10.1371/journal.pbio.3001032
92. Kinchen J, Chen HH, Parikh K, Antanaviciute A, Jagielowicz M, Fawkner-Corbett D, et al. Structural Remodeling of the Human Colonic Mesenchyme in Inflammatory Bowel Disease. *Cell* (2018) 175(2):372–386.e17. doi: 10.1016/j.cell.2018.08.067
93. Koppens MAJ, Davis H, Valbuena GN, Mulholland EJ, Nasreddin N, Colombe M, et al. Bone Morphogenetic Protein Pathway Antagonism by Grem1 Regulates Epithelial Cell Fate in Intestinal Regeneration. *Gastroenterology* (2021) 161 (1):239–254.e9. doi: 10.1053/j.gastro.2021.03.052
94. Chawiengsaksophak K, James R, Hammond VE, Köntgen F, Beck F. Homeosis and Intestinal Tumours in Cdx2 Mutant Mice. *Nature* (1997) 386(6620):84–7. doi: 10.1038/386084A0
95. Seamons A, Treuting PM, Brabb T, Maggio-Price L. Characterization of Dextran Sodium Sulfate-Induced Inflammation and Colonic Tumorigenesis in Smad3−/− Mice With Dysregulated TGFb. *PloS One* (2013) 8(11): p.e79182-96. doi: 10.1371/journal.pone.0079182
96. Kaiser S, Park YK, Franklin JL, Halberg RB, Yu M, Jessen WJ, et al. Transcriptional Recapitulation and Subversion of Embryonic Colon Development by Mouse Colon Tumor Models and Human Colon Cancer. *Genome Biol* (2007) 8(7):1–26. doi: 10.1186/GB-2007-8-7-R131

97. Kang DB, Oh JT, Jo HJ, Park WC. Primary Adenosquamous Carcinoma of the Colon. *J Kor Surg Soc* (2011) 80(Suppl 1):S31. doi: 10.4174/JKSS.2011.80.SUPPL1.S31
98. Robert C. A Decade of Immune-Checkpoint Inhibitors in Cancer Therapy. *Nat Commun* (2020) 11(1):1–3. doi: 10.1038/s41467-020-17670-y
99. Llosa NJ, Cruise M, Tam A, Wicks EC, Hechenbleikner EM, Taube JM, et al. The Vigorous Immune Microenvironment of Microsatellite Instable Colon Cancer Is Balanced by Multiple Counter-Inhibitory Checkpoints. *Cancer Discov* (2015) 5(1):43–51. doi: 10.1158/2159-8290.CD-14-0863
100. Mlecnik B, Bindea G, Angell HK, Maby P, Angelova M, Tougeron D, et al. Integrative Analyses of Colorectal Cancer Show Immunoscore Is a Stronger Predictor of Patient Survival Than Microsatellite Instability. *Immunity* (2016) 44(3):698–711. doi: 10.1016/j.immuni.2016.02.025
101. Bruni D, Angell HK, Galon J. The Immune Contexture and Immunoscore in Cancer Prognosis and Therapeutic Efficacy. *Nat Rev Cancer* (2020) 20 (11):662–805. doi: 10.1038/s41568-020-0285-7
102. Tumeh PC, Harview CL, Yearley JH, Shintaku IP, Taylor EJM, Robert L, et al. PD-1 Blockade Induces Responses by Inhibiting Adaptive Immune Resistance. *Nature* (2014) 515(7528):568–71. doi: 10.1038/nature13954
103. Emens LA, Middleton G. The Interplay of Immunotherapy and Chemotherapy: Harnessing Potential Synergies. *Cancer Immunol Res* (2015) 3(5):436–5. doi: 10.1158/2326-6066.CIR-15-0064
104. Kepp O, Galluzzi L, Martins I, Schlemmer F, Adjemian S, Michaud M, et al. Molecular Determinants of Immunogenic Cell Death Elicited by Anticancer Chemotherapy. *Cancer Metastasis Rev* (2011) 30(1):61–695. doi: 10.1007/s10555-011-9273-4
105. Iwai T, Sugimoto M, Wakita D, Yorozu K, Kurasawa M, Yamamoto K. Topoisomerase I Inhibitor, Irinotecan, Depletes Regulatory T Cells and Up-Regulates MHC Class I and PD-L1 Expression, Resulting in a Supra-Additive Antitumor Effect When Combined With Anti-PD-L1 Antibodies. *Oncotarget* (2018) 9(59):31411–215. doi: 10.18632/oncotarget.25830
106. Biton M, Haber AL, Rogel N, Burgin G, Beyaz S, Schnell A, et al. T Helper Cell Cytokines Modulate Intestinal Stem Cell Renewal and Differentiation. *Cell* (2018) 175(5):1307–1320.e22. doi: 10.1016/j.cell.2018.10.008
107. Kanterman J, Sade-Feldman M, Biton M, Ish-Shalom E, Lasry A, Goldshtein A, et al. Adverse Immunoregulatory Effects of 5FU and CPT11 Chemotherapy on Myeloid-Derived Suppressor Cells and Colorectal Cancer Outcomes. *Cancer Res* (2014) 74(21):6022–355. doi: 10.1158/0008-5472.CAN-14-0657
108. Herring CA, Banerjee A, McKinley ET, Simmons AJ, Ping J, Roland JT, et al. Unsupervised Trajectory Analysis of Single-Cell RNA-Seq and Imaging Data Reveals Alternative Tuft Cell Origins in the Gut. *Cell Syst* (2018) 6(1):37–51.e9. doi: 10.1016/j.cels.2017.10.012
109. Banerjee A, Herring CA, Chen B, Kim H, Simmons AJ, Southard-Smith AN, et al. Succinate Produced by Intestinal Microbes Promotes Specification of Tuft Cells to Suppress Ileal Inflammation. *Gastroenterology* (2020) 159 (6):2101–2115.e5. doi: 10.1053/j.gastro.2020.08.029
110. Petukhov V, Guo J, Baryawno N, Severe N, Scadden DT, Samsonova MG, et al. DropEst: Pipeline for Accurate Estimation of Molecular Counts in Droplet-Based Single-Cell RNA-Seq Experiments. *Genome Biol* (2018) 19 (1):785. doi: 10.1186/s13059-018-1449-6
111. Butler A, Hoffman P, Smibert P, Papalexi E, Satija R. Integrating Single-Cell Transcriptomic Data Across Different Conditions, Technologies, and Species. *Nat Biotechnol* (2018) 36(5):411–205. doi: 10.1038/nbt.4096
112. Laio A, Rodriguez A. Clustering by Fast Search and Find of Density Peaks. *Science* (2014) 344(6191):1492–96. doi: 10.1126/science.1242072
113. Min J, Vega PN, Engevik AC, Williams JA, Yang Q, Patterson LM, et al. Heterogeneity and Dynamics of Active Kras-Induced Dysplastic Lineages From Mouse Corpus Stomach. *Nat Commun* (2019) 10(1):5549. doi: 10.1038/s41467-019-13479-6
114. McKinley ET, Shao J, Ellis ST, Heiser CN, Roland JT, Macedonia MC, et al. MIRIAM: A Machine and Deep Learning Single-Cell Segmentation and Quantification Pipeline for Multi-Dimensional Tissue Images. *Cytometry Part A* (2022) BioRxiv preprint.
115. Hafemeister C, Satija R. Normalization and Variance Stabilization of Single-Cell RNA-Seq Data Using Regularized Negative Binomial Regression. *Genome Biol* (2019) 20(1):2965. doi: 10.1186/s13059-019-1874-1
116. Finak G, McDavid A, Yajima M, Deng J, Gersuk V, Shalek AK, et al. MAST: A Flexible Statistical Framework for Assessing Transcriptional Changes and Characterizing Heterogeneity in Single-Cell RNA Sequencing Data. *Genome Biol* (2015) 16(1):278. doi: 10.1186/s13059-015-0844-5

Conflict of Interest: The authors declare that the research was conducted in the absence of any commercial or financial relationships that could be construed as a potential conflict of interest.

frontiers | Frontiers in Physiology

ORIGINAL RESEARCH
published: 24 May 2022
doi: 10.3389/fphys.2022.880024

Acinetobacter calcoaceticus is Well Adapted to Withstand Intestinal Stressors and Modulate the Gut Epithelium

Janiece S. Glover[1], *Brittney D. Browning*[2], *Taylor D. Ticer*[3], *Amy C. Engevik*[1] *and Melinda A. Engevik*[1,3]*

[1]Department of Regenerative Medicine and Cell Biology, Medical University of South Carolina, Charleston, SC, United States, [2]Department of Psychiatry and Behavioral Sciences, Medical University of South Carolina, Charleston, SC, United States, [3]Department of Microbiology and Immunology, Medical University of South Carolina, Charleston, SC, United States

Background: The gastrointestinal tract has been speculated to serve as a reservoir for *Acinetobacter*, however little is known about the ecological fitness of *Acinetobacter* strains in the gut. Likewise, not much is known about the ability of *Acinetobacter* to consume dietary, or host derived nutrients or their capacity to modulate host gene expression. Given the increasing prevalence of *Acinetobacter* in the clinical setting, we sought to characterize how *A. calcoaceticus* responds to gut-related stressors and identify potential microbe-host interactions.

Materials and Methods: To accomplish these aims, we grew clinical isolates and commercially available strains of *A. calcoaceticus* in minimal media with different levels of pH, osmolarity, ethanol and hydrogen peroxide. Utilization of nutrients was examined using Biolog phenotypic microarrays. To examine the interactions of *A. calcoaceticus* with the host, inverted murine organoids where the apical membrane is exposed to bacteria, were incubated with live *A. calcoaceticus,* and gene expression was examined by qPCR.

Results: All strains grew modestly at pH 6, 5 and 4; indicating that these strains could tolerate passage through the gastrointestinal tract. All strains had robust growth in 0.1 and 0.5 M NaCl concentrations which mirror the small intestine, but differences were observed between strains in response to 1 M NaCl. Additionally, all strains tolerated up to 5% ethanol and 0.1% hydrogen peroxide. Biolog phenotypic microarrays revealed that *A. calcoaceticus* strains could use a range of nutrient sources, including monosaccharides, disaccharides, polymers, glycosides, acids, and amino acids. Interestingly, the commercially available *A. calcoaceticus* strains and one clinical isolate stimulated the pro-inflammatory cytokines *Tnf*, *Kc*, and *Mcp-1* while all strains suppressed *Muc13* and *Muc2*.

Conclusion: Collectively, these data demonstrate that *A. calcoaceticus* is well adapted to dealing with environmental stressors of the gastrointestinal system. This data also points to the potential for *Acinetobacter* to influence the gut epithelium.

Keywords: *Acinetobacter*, intestine, organoid, *Acinetobacter calcoaceticus*, metabolism

OPEN ACCESS

Edited by:
Kathleen E. DelGiorno, Vanderbilt University, United States

Reviewed by:
Oscar Medina-Contreras, Federico Gómez Children's Hospital, Mexico
Arno R. Bourgonje, University Medical Center Groningen, Netherlands

***Correspondence:**
Melinda A. Engevik
engevik@musc.edu

Specialty section:
This article was submitted to Gastrointestinal Sciences, a section of the journal Frontiers in Physiology

Received: *20 February 2022*
Accepted: *12 April 2022*
Published: *24 May 2022*

Citation:
Glover JS, Browning BD, Ticer TD, Engevik AC and Engevik MA (2022) Acinetobacter calcoaceticus is Well Adapted to Withstand Intestinal Stressors and Modulate the Gut Epithelium. Front. Physiol. 13:880024. doi: 10.3389/fphys.2022.880024

INTRODUCTION

Acinetobacter is a Gram-negative nonfermenting coccobacillus that is widely distributed in nature. Certain *Acinetobacter* species are classified as opportunistic pathogens and are commonly associated with healthcare associated infections (Peleg et al., 2008; Nemec et al., 2015; Mancilla-Rojano et al., 2020). The *Acinetobacter* species that are considered to be pathogens include *A. baumannii*, *A. pittii* and *A. nosocomialis* (Mancilla-Rojano et al., 2020). These species cause infections like bacteremia, ventilator-associated pneumonia, urinary tract infection, meningitis, and wound infection. *A. baumannii* is the most frequently isolated and best studied of the *Acinetobacter* species. In contrast to *A. baumannii*, *A. calcoaceticus* has been considered to have a lower virulence since colonization is more frequently noted than infection (Glew et al., 1977). However, *A. calcoaceticus* can still cause infection and understanding the mechanism by which *A. calcoaceticus* interacts with the host remains an important topic.

Acinetobacter species are capable of occupying several ecological niches, including the mammalian intestine. *Acinetobacter* species have been identified in the human fecal microbiota and it has been speculated that the gut could serve as a potential reservoir for *Acinetobacter* infection (Timsit et al., 1993; Xavier et al., 1996; Ayats et al., 1997; Dijkshoorn et al., 2005; Roy et al., 2010; Pandey et al., 2012; Aljindan et al., 2015; Cheng et al., 2015; Li et al., 2015; Braun et al., 2017; Li et al., 2019). Consistent with this hypothesis, *A. baumannii* can bind to rabbit small intestinal glycosphingolipids (Madar Johansson et al., 2020) and colonize the mouse gastrointestinal tract in a secretory IgA dependent manner (Coron et al., 2017; Ketter et al., 2018). Moreover, ampicillin treatment of mice has been shown to elevate *A. baumannii* and *A. calcoaceticus* fecal levels, suggesting that antibiotic selection could allow the outgrowth of endogenous strains (Raplee et al., 2021). Apart from these studies, little is known regarding the factors that influence *Acinetobacter* colonization and little data exists on the effects of *A. calcoaceticus*. The importance of *Acinetobacter* in the gut is highlighted by the fact that *Acinetobacter* species are elevated in certain disease states including ulcerative colitis, a subset of inflammatory bowel disease (IBD) (Gophna et al., 2006; Lucke et al., 2006; Leung et al., 2014; Kevans et al., 2015; Tang et al., 2015; Sjoberg et al., 2017; Sekido et al., 2020; He et al., 2021; Qi et al., 2022). In this study, we sought to examine the ability of *A. calcoaceticus* strains to survive environmental stressors found in the gut, interact with other gut microbes and utilize dietary components. We also examined the reciprocal interactions of *A. calcoaceticus* strains on the host using intestinal organoids.

METHODS

General Bacterial Culturing Techniques

Acinetobacter calcoaceticus ATCC 23055 (American Type Culture Collection) and *A. calcoaceticus* CB1 (Carolina Biological Supply) were purchased from commercial sources. Four clinical isolates of *A. calcoaceticus* strains that were isolated from ventricular fluid of pediatric patients were provided by Dr. James Versalovic. All *A. calcoaceticus* strains were cultured aerobically in brain-heart-infusion (BHI) medium (ThermoFisher) at 37°C. Overnight cultures were sub-cultured into M9 minimal media containing glucose at an optical density (OD_{600nm}) = 0.1. To model environmental stressors, M9 media was supplemented with NaCl (0.1, 0.5, or 1 M), H_2O_2 (0.05, 0.1, 0.2%), or ethanol (1, 2.5 or 5%). M9 was also adjusted to varying pH values (4, 5, 6, 7). Growth was monitored after 18 h incubation by OD_{600nm}.

To examine nutrient uptake, *A. calcoaceticus* strains were added to M9 media lacking glucose at OD_{600nm} = 0.1. Then 100 µL of this culture was added to each well of a 96-well Biolog Phenotype Microarrays for Microbial Cells (PM1 and PM2 plates). Growth was monitored at 18 h by OD_{600nm} on a Synergy HT BioTek plate reader. Stool-based bioreactors were generated as previously described (Engevik et al., 2021). Briefly, stool samples were cultured anaerobically for 24 h to allow microbes to establish stable communities, then inoculated with *A. calcoaceticus* strains at an OD_{600nm} = 0.05. After 48 h of incubation with *A. calcoaceticus* strains, samples were collected for gDNA isolation. For imaging purposes, *A. calcoaceticus* strains were fluorescently tagged with CFDA-SE (ThermoFisher) as previously described (Engevik et al., 2021). Briefly, *A. calcoaceticus* strains were washed 2x with sterile PBS and incubated for 1 h aerobically at 37°C with 10 µM CFDA-SE. After the incubation, bacteria were washed 3–5x with sterile PBS to remove any unused CFDA-SE. Bacteria were then ready for incubation with organoids.

Organoid Generation

Intestinal organoids were generated from four adult (8–12 weeks) C57B6/J mice as previously described (Engevik et al., 2013). The jejunum was rapidly dissected, washed with ice-cold PBS (PBS; Gibco) and opened longitudinally. The jejunum was then cut into ~1-cm length pieces and placed in a 15-ml conical tube containing 5 ml of ice-cold PBS, 43.4 mM sucrose, 0.5 mM DTT and 3 mM EDTA (Gibco). The tissue was incubated at 4°C rocking for 30 min. Crypts were mechanically disrupted by shaking in 5 ml of ice-cold PBS with D-sorbitol and sucrose and collected following filtration with a 70-µm cell strainer (Corning cat# 431,751). Crypts were centrifuged, resuspended in Matrigel (Corning), and incubated with complex media containing WNT, R-spondin, Noggin and EGF. Organoids were passaged >2 times to ensure no tissue fragments remained. Organoids were differentiated and grown inside-out by adding split organoids directly to complex media without Wnt and incubated at 37°C with 5% CO2 for 5 days before use.

For imaging purposes, live fluorescently tagged *A. calcoaceticus* was incubated with inside-out organoids for 3 h. Organoids were then washed with PBS, fixed with 4% paraformaldehyde for 30 min, incubated in 30% sucrose/PBS overnight and frozen embedded. Sections were stained with phospho-ezrin, radixin, moesin (1:200 dilution, Rabbit Ab, Cell Signaling #3726S) overnight at 4°C. After washing, sections were incubated with donkey-anti-rabbit Alexa Fluor 555 (1:1,000 dilution, ThermoFisher # A31572) for 1 h at

TABLE 1 | Two Way ANOVA statistics from bacterial growth in the presence of stressors. All comparisons were made against *A. calcoaceticus* ATCC 23055. Significant *p* values ($p < 0.05$) are colored in blue.

	NaCl				pH				ETOH				H_2O_2	
Strain	0 M	0.1 M	0.5 M	1 M	pH 7	pH 6	pH 5	pH 4	0%	1%	2.50%	5%	0%	0.05%	0.10%	0.20%
CB1	0.1379	0.1097	<0.0001	<0.0001	0.0148	0.0003	0.4224	0.2573	0.079	<0.0001	<0.0001	0.0204	0.2819	0.163	0.2286	0.5514
M3	0.9269	0.4824	0.0126	0.0136	0.1814	0.3755	0.0133	0.0827	0.31	<0.0001	0.0023	0.0594	0.2781	0.0335	<0.0001	<0.0001
T82	0.2879	0.0218	0.9543	0.0013	0.034	0.7245	0.6418	0.4756	0.8335	0.0001	<0.0001	0.0003	0.2543	0.2975	0.0393	0.002
M5	0.577	0.0131	<0.0001	<0.0001	0.8767	0.0002	0.2652	0.2672	0.1845	<0.0001	0.0018	<0.0001	0.0775	0.0083	0.0734	0.0007
X75	0.1106	0.3661	<0.0001	0.0002	0.2573	0.0002	0.0003	0.0017	0.4996	<0.0001	<0.0001	<0.0001	0.0833	0.0199	<0.0001	<0.0001

room temperature and counter stained with Hoechst 33,342 (Invitrogen) for 10 min at room temperature. Slides were cover-slipped with mounting media (Life Technologies) and imaged using a Zeiss AxioScan at ×20 (Zeiss). The relative fluorescence intensity of adhered bacteria was quantified using FIJI (Formerly ImageJ) software (NIH) and reported as relative fluorescence. Three regions of interests per image and four images per slide were used for semi-quantitation of stain intensity.

For gene expression analysis, inside-out organoids were incubated with live *A. calcoaceticus* strains adjusted to an OD_{600nm} = 1.0 for 3 h at 37°C (n = 4 different mouse organoids; performed in replicates per mouse). After incubation, organoids were centrifuged at 300 × g for 5 min and the organoid pellet was resuspended in 400 µL TRIZOL. Organoids were stored in TRIZOL at −80°C until the RNA was isolated.

RNA Isolation, cDNA Generation, gDNA Isolation and qPCR

Total RNA was extractr'ed from organoids in TRIZOL according to manufactures instructions, with the addition of glycogen. cDNA was generated from 500 ng RNA via the Verso cDNA synthesis kit (ThermoFisher #AB-1453). gDNA was isolated from 1 ml aliquots of stool-based bioreactors using the Zymo Quick-DNA Fecal/Soil Microbe Kits according to the manufacturer's instructions. Quantitative real time PCR (qPCR) was performed using a Bio-Rad CFX96 Real Time qPCR machine (Bio-Rad). Forward and reverse primers were added to SYBR Green mastermix (Genesee Scientific #17-501DP) and cDNA. Epithelial genes were normalized to the housekeeping gene 18S and relative expression was calculated using the ddCT method. Bacterial colony forming units (CFUs) were calculated from CT values based on standard curves as previously described (Engevik et al., 2013).

Statistics

Data are presented as mean ± standard deviation, with points representing individual bacteria strain growth rate with a n = 4 (repeated 3 independent times). Comparisons within groups were made with One-way Analysis of Variance (ANOVA) and comparisons between groups were made with a Two-way ANOVA (**Table 1**). All analyses were corrected for multiple comparisons by controlling the False Discovery Rate. GraphPad version 9.3 was used to generate graphs and statistics (GraphPad Software, Inc. La Jolla, CA). A $^*p < 0.05$ value was considered significant while n is the number of experiments performed.

RESULTS

It has been speculated that the gut may be a site for *Acinetobacter* colonization and thus could be a source of endemic infections (Timsit et al., 1993; Xavier et al., 1996; Ayats et al., 1997; Dijkshoorn et al., 2005; Roy et al., 2010; Pandey et al., 2012; Aljindan et al., 2015; Cheng et al., 2015; Li et al., 2015; Braun et al.,

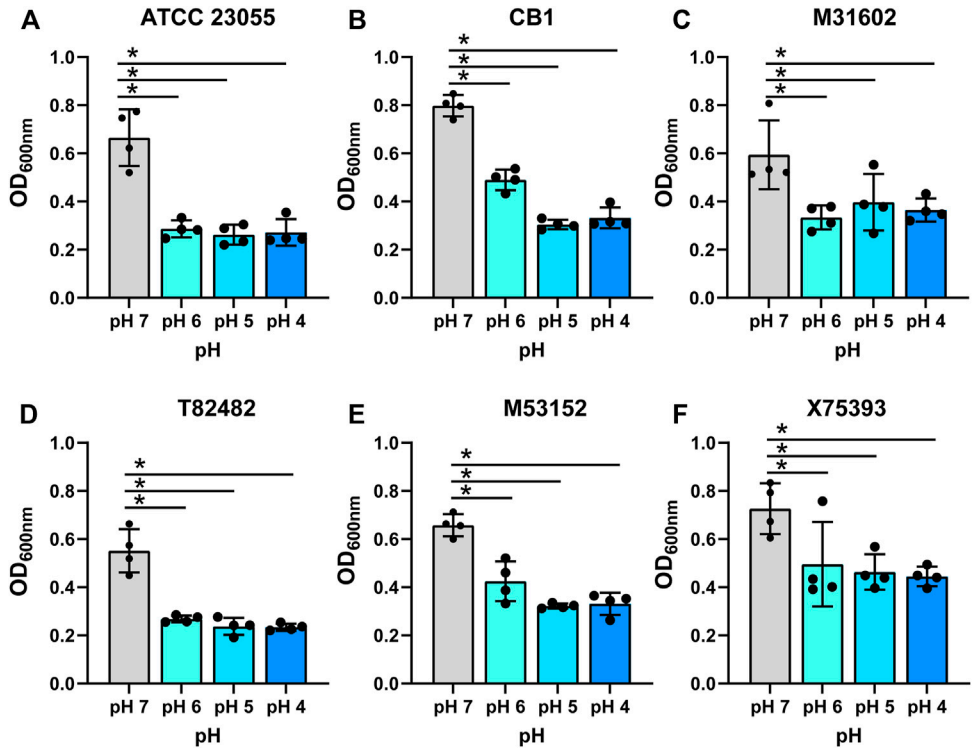

FIGURE 1 | Growth of **(A)** *calcoaceticus* in various pHs. Growth of *A. calcoaceticus* strains as measured by OD_{600nm} after 18 h of incubation. Growth was examined in the following strains: **(A)** ATCC 23055, **(B)** CB1; clinical isolates: **(C)** M31602, **(D)** T82482, **(E)** M53152, and **(F)** X75,393). *$p < 0.05$, One Way ANOVA.

2017; Li et al., 2019). To examine the efficiency of *A. calcoaceticus* strains to withstand the conditions of the gastrointestinal tract, we grew commercially available and clinical isolates of *A. calcoaceticus* in minimal media at pH 7, 6, 5, and 4. Cultures were seeded with $OD_{600n} = 0.1$ and growth was considered to be above an $OD_{600nm} = 0.2$. As expected, we observed robust growth of the commercially available *A. calcoaceticus* strains (ATCC 23055, CB1) and clinical isolates (M31602, T82482, M53152, and X75393) in pH 7 media (**Figures 1A–F**; **Table 1**). We observed growth ($OD_{600nm} > 0.2$) of all strains at pH 6, pH 5, and pH 4; although growth was significantly reduced compared to pH 7. These findings suggest that *A. calcoaceticus* is well adapted to withstand varying intestinal pHs.

The intestine harbors varying ranges of osmolarity, with the small intestinal villi encountering 400–700 mM (Overduin et al., 2014). To model the gut, we added increasing concentrations of NaCl (0.1, 0.5 and 1 M) to minimal media and examined the growth of *A. calcoaceticus* (**Figures 2A–F**; **Table 1**). All strains were found to have similar growth at 0.1 and 0.5 M as media controls. Decreased growth was observed at 1 M NaCl with all but the T82482 strain. We observed that the ATCC 23055 strain exhibited the most significant decline in growth (**Figure 2A**). These data highlight that *A. calcoaceticus* can grow well in various osmolarities which mirror the gut environment.

In the gut, commensal microbes such as Lactobacilli can generate ethanol and hydrogen peroxide (Engevik and Versalovic, 2017) and microbes occupying the same niche must adapt to these stressors. To model the production of localized ethanol and hydrogen peroxide, we supplemented minimal media with ethanol (1, 2.5 or 5%) (**Figures 3A–F**; **Table 1**) or hydrogen peroxide (0.05, 0.1 or 0.2%) (**Figures 4A–F**; **Table 1**). Impressively, all *A. calcoaceticus* strains could grow in up to 5% ethanol. Our commercially available ATCC 23055 strain was the most sensitive strain to ethanol, exhibiting a ~2-fold decrease in growth in 1% ethanol compared to media controls (**Figure 3A**). In contrast, clinical isolates T82482 (**Figure 3D**), M53152 (**Figure 3E**), and X75,393 (**Figure 3F**) exhibited only a slight decline in growth at the higher ethanol concentrations; suggesting that these clinical isolates are highly resistant to ethanol. When *A. calcoaceticus* was treated with hydrogen peroxide (**Figures 4A–F**), all strains could grow with 0.05 and 0.1% hydrogen peroxide. The commercially available ATCC 23055 and CB1 were the most tolerant to 0.2% hydrogen peroxide (**Figures 4A,B**); exhibiting a less than 2-fold decrease in growth compared to the no hydrogen peroxide controls. In contrast, the clinical isolates M31602 (**Figure 4C**), T82482 (**Figure 4D**), M53152 (**Figure 4E**), and X75,393 (**Figure 4F**) were sensitive to 0.2% hydrogen peroxide and did not grow above the seeded density of $OD_{600nm} = 0.1$. Collectively, these data with stressors indicate that *A. calcoaceticus* is well adapted for the environmental stressors associated with gut colonization.

Next, we sought to examine the potential nutrient sources for *A. calcoaceticus* within the intestine. To address this, we grew *A. calcoaceticus* strains in minimal media lacking glucose in Biolog

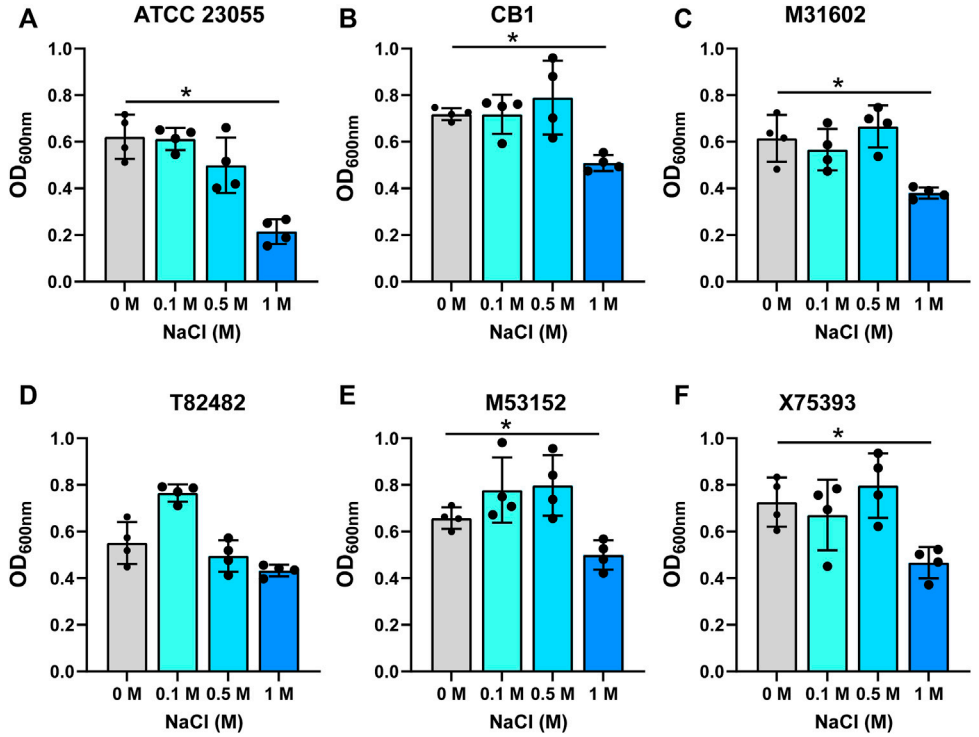

FIGURE 2 | Growth of **(A)**. *calcoaceticus* at varying osmolarity. Growth of *A. calcoaceticus* strains as measured by OD_{600nm} after 18 h of incubation. Growth was examined in the following strains: **(A)** ATCC 23055, **(B)** CB1; clinical isolates: **(C)** M31602, **(D)** T82482, **(E)** M53152, and **(F)** X75,393). *$p < 0.05$, One Way ANOVA.

phenotypic microarrays (**Figures 5**, **6**). Growth was considered to be > 1.5 fold change. Compared to growth in a media without a carbon source, *A. calcoaceticus* had improved growth in the presence of glucose (**Figure 5A**). Since *A. calcoaceticus* had improved growth with glucose, we first examined monosaccharides (**Figure 5A**). ATCC 23055 and CB1 grew well with L-arabinose, D-galactose, D-mannose, D-fructose, D-tagatose, D-glucosamine, D-ribose, and N-acetyl-D-glucosamine. Interestingly, clinical isolates M31602, T82482 and M53152 did not grow with arabinose and exhibited strain-dependent growth with D-mannose, D-fructose, S-tagatose, D-ribose and N-acetyl-D-glucosamine. M53152 alone grew with L-glucose, B-D-allose, D-fucose, and L-sorbose, highlighting strain-specific nutrient preferences. When we examined alcohol sugars (**Figure 5B**), we found that all strains could use adonitol and no strains could use D-mannitol, L-arabitol, i-erythritol, or dulcitol.

In terms of growth with disaccharides (**Figure 5C**), we found that all strains used gentiobiose and no strains used lactulose or turnanose. For the other disaccharides and trisaccharides, we observed strain-dependent growth. For example, M53152 grew with D-melbiose, D-trehalose, maltose, D-melibiose, sucrose, D-cellbiose, D-raffinose, stachyose and maltotriose, while T82482 only grew with D-palatinose, D-melezitose, D-raffinose and stachyose. When we examined polysaccharide utilization, we found very similar profiles between ATCC 23055 and M53152. Both strains were highly efficient at using laminarin, mannan, pectin, α-Cyclodextrin, β-Cyclodextrin, γ-cyclodextrin and dextrin (**Figure 5D**). In general, most strains grew well with dietary polysaccharides. In the nucleosides (**Figure 5E**) and glycosides (**Figure 5F**) classification, we found strain-dependent use of specific compounds. ATCC 23055 and M53152 exhibited the highest fold change in growth with chondroitin sulfate C, 2,3-butanedione and 3-hydroxy 2-butanone.

Of the acids (**Figure 6A**), we found that all strains could use a-keto-glutaric acid. ATCC 23055 and M53152 responded to the largest number of acids, including B-methyl-D-glucuronic acid, γ-amino butryic acid, butryic acid, capric acid, 4-hydroxy benzoic acid and acetamide. Unique profiles were observed with the other acids examined depending on the strain. Even without a carbon source, we found that all *A. calcoaceticus* strains had improved growth with L-glutamine and ATCC 23055 and M53152 used L-lysine, L-methionine, L-Ornithine, L-Phenylalanine and L-valine (**Figure 6B**), indicating that select amino acids could be used as an alternative to carbon. Tween can be employed as a stool emulsifier and tween enemas have been used to treat fecal mass obstructions (Wood and Katzberg, 1978). None of the *A. calcoaceticus* strains responded to tween with improved growth (**Figure 6C**). These data indicate that *A. calcoaceticus* can use a wide range of nutrients sources, ranging from sugars to amino acids.

In addition to stressors and nutrients, *Acinetobacter* species encounter a complex community of micro-organisms when colonizing the gastrointestinal tract. To confirm that *A. calcoaceticus* could proliferate in this competitive environment,

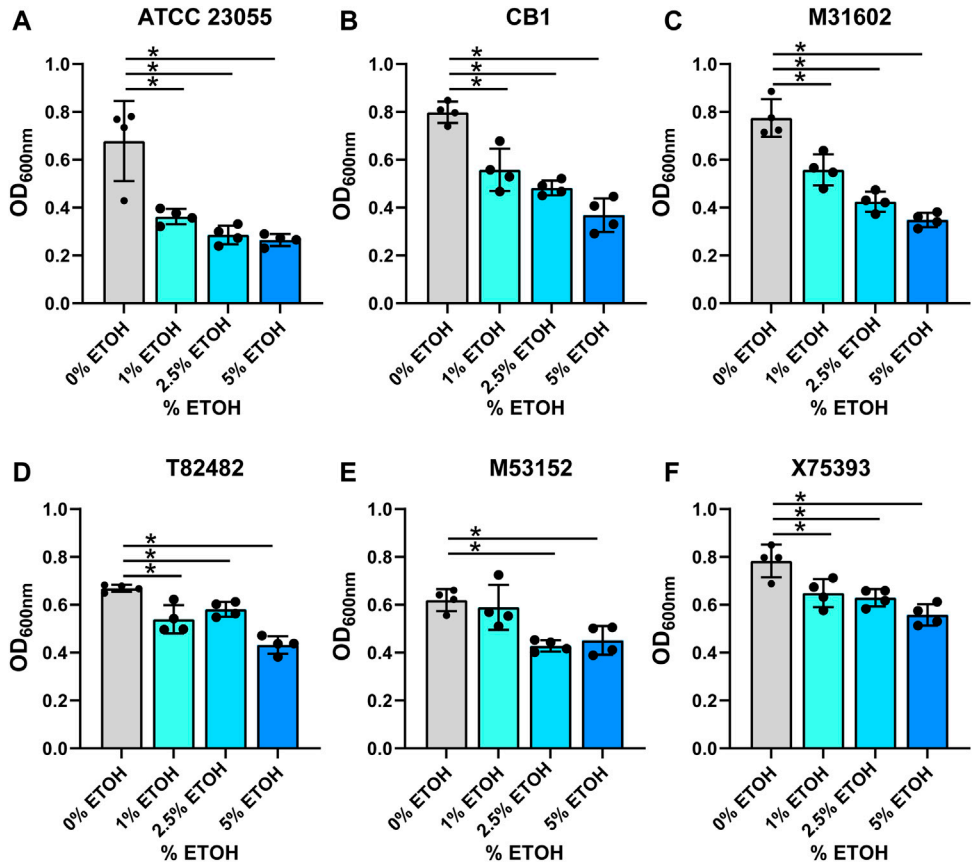

FIGURE 3 | (A) *calcoaceticus* growth in percentages of ethanol. Growth of *A. calcoaceticus* strains as measured by OD_{600nm} after 18 h of incubation. Growth was examined in the following strains: **(A)** ATCC 23055, **(B)** CB1; clinical isolates: **(C)** M31602, **(D)** T82482, **(E)** M53152, and **(F)** X75,393). *$p < 0.05$, One Way ANOVA.

we cultured stool-based bioreactors and introduced *A. calcoaceticus* strains. After 48 h of culturing, we examined the presence of *A. calcoaceticus* in the bioreactors by qPCR (**Supplementary Figure S1A**). We found that all strains effectively colonized the bioreactors, indicating that *A. calcoaceticus* could be present within the intestinal milieu. Next, we sought to examine how *A. calcoaceticus* interacted with the intestinal epithelium. To test whether *A. calcoaceticus* was able to stimulate epithelial responses, we incubated live *A. calcoaceticus* strains with apical side-out intestinal organoids for 3 h. By immunostaining, we found that some *A. calcoaceticus* microbes adhered to the organoids (**Figure 7A**). A similar level of bacteria was observed on all organoids regardless of the strain (**Supplementary Figure S1B**). Analysis of pro-inflammatory cytokines by qPCR revealed that the commercially available strains ATCC 23055 and CB1 and one of our clinical isolates T82482 increased the expression of *Tnf* (**Figure 7B**), *Kc* (**Figure 7C**) and *Mcp-1* (**Figure 7D**) compared to media controls. The T82482 strain also increased the expression of *IL-1α* (**Figure 7E**). Inflammation is known to regulate intestinal mucus, so we also examined adherent mucins *Muc1* and *Muc13* and secreted mucins *Muc2* in our organoid model. T82482 was the only strain that upregulated *Muc1* (**Figure 7F**), but all strains suppressed *Muc13* levels (**Figure 7G**) compared to media controls. Likewise, all strains suppressed *Muc2* expression (**Figure 7H**). We also examined an antimicrobial protein secreted by goblet cells, Relmβ, and we observed that *Relmβ* expression was increased in response to T82482 (**Figure 7I**), suggesting that goblet cells were not decreased in this model despite decreased *Muc2*. Together these findings highlight that *A. calcoaceticus* strains are adept at dealing with environmental stressors, are able to consume multiple nutrient sources, colonize in the presence of other microbes, and can elicit pro-inflammatory signaling pathways.

DISCUSSION

The digestive tract is proposed to be a reservoir for *Acinetobacter* spp. (Timsit et al., 1993; Corbella et al., 1996; Agusti et al., 2002; Dijkshoorn et al., 2005; Thom et al., 2010; Lim et al., 2014). In this study, we confirmed the ability of *A. calcoaceticus* strains to withstand conditions that recapitulate the gastrointestinal tract luminal environment and use various nutritional sources found in the intestine. We identified that *A. calcoaceticus* strains are fairly resistant to changing pH, osmolarity, ethanol and hydrogen

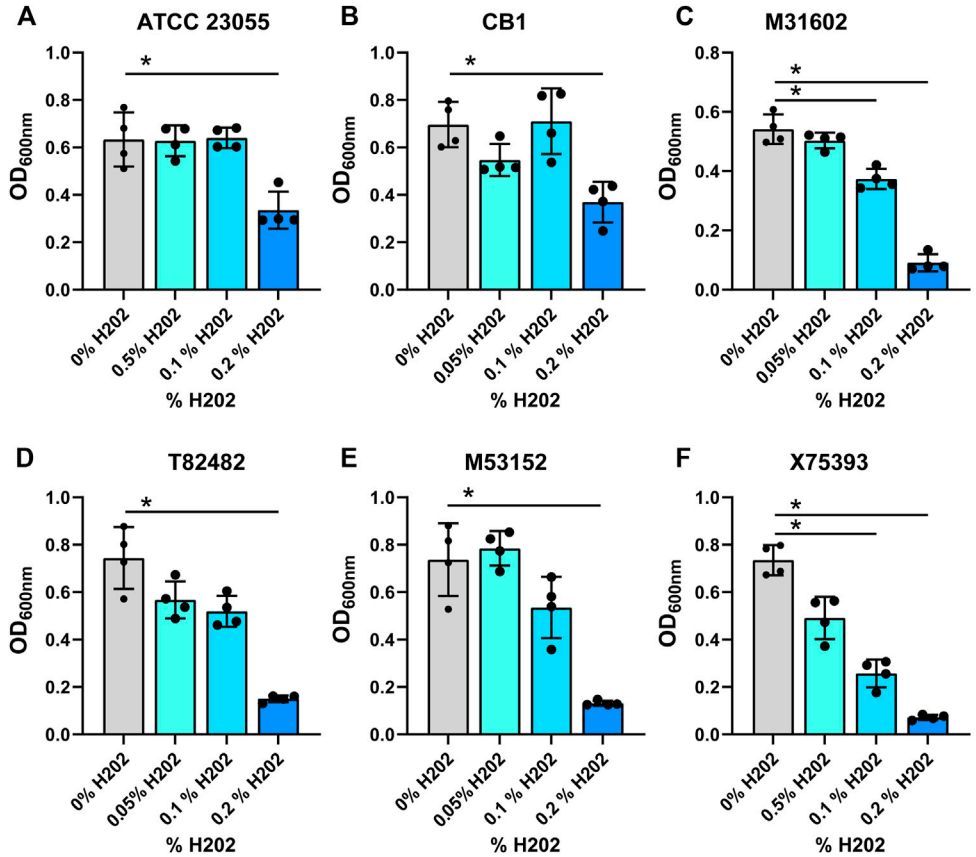

FIGURE 4 | (A) *calcoaceticus* growth in hydrogen peroxide. Growth of *A. calcoaceticus* strains as measured by OD_{600nm} after 18 h of incubation. Growth was examined in the following strains: **(A)** ATCC 23055, **(B)** CB1; clinical isolates: **(C)** M31602, **(D)** T82482, **(E)** M53152, and **(F)** X75,393). *$p < 0.05$, One Way ANOVA.

peroxide levels. We also found that the majority of *A. calcoaceticus* strains used glucose, L-arabinose, D-galactose, D-mannose, D-fructose and N-acetyl-D-glucosamine, D-trehalose, adonitol, mannan, pectin, α-Cyclodextrin, β-Cyclodextrin, γ-cyclodextrin, dextrin, D-ribose and α-keto-glutaric acid and L-glutamine. These data indicate that *A. calcoaceticus* can use a wide range of nutrients sources. Bioreactor experiments confirmed that *A. calcoaceticus* could colonize with other gut microbes. This work adds to existing research and suggests that *Acinetobacter* spp. are well adapted for survival in the gastrointestinal tract.

Entry of *Acinetobacter* spp. into the gut has recently been examined by Coron et al. (2017). The authors found that intranasal administration of *A. baumannii* in mice, which mimicked the major method by which ventilated patients in ICUs commonly become infected with *Acinetobacter*, resulted in digestive-tract colonization. This data suggests that patients could become colonized with *Acinetobacter* spp. in hospital settings and this gut colonization could be the precursor of severe infections. Consistent with this notion, Corbella *et al.* identified that patients colonized with *A. baumannii* in their digestive system had a positive association for blood infections with multidrug-resistant *A. baumannii* strains compared to patients without colonization (Corbella et al., 1996). Similarly, Medina *et al.* found that *A. baumannii* gut colonization was an independent risk factor for the development of *A. baumannii* respiratory infections (Medina-Presentado et al., 2013). Wisplinghof *et al.* reported that the portal of entry was not identified in 48.6% of the *A. baumannii* bloodstream infections, suggesting that a significant proportion of these infections could be due to intestinal carriage (Wisplinghoff et al., 2000; Coron et al., 2017). Our work complements these findings by demonstrating that *Acinetobacter* species are equipped to colonize the gastrointestinal tract, where they could serve as a reservoir for infection.

In animal models, *A. baumannii* colonized both the small and large intestine (Coron et al., 2017; Ketter et al., 2018). In these models, intestinal inflammation was not specifically examined. However, our apical inside-out organoid model revealed that certain strains of *A. calcoaceticus* stimulated pro-inflammatory cytokines. This data can be interpreted in several ways. First, it is possible that in the setting of a complex gut microbiota *in vivo*, other microbes may dampen pro-inflammatory signatures associated with *Acinetobacter*. Second, the existing *in vivo* studies used *A. baumannii* and this study focused on *A. calcoaceticus*. It is therefore possible that differences may exist between the species. Third, our data suggests that pro-inflammatory responses are strain dependent and these strain

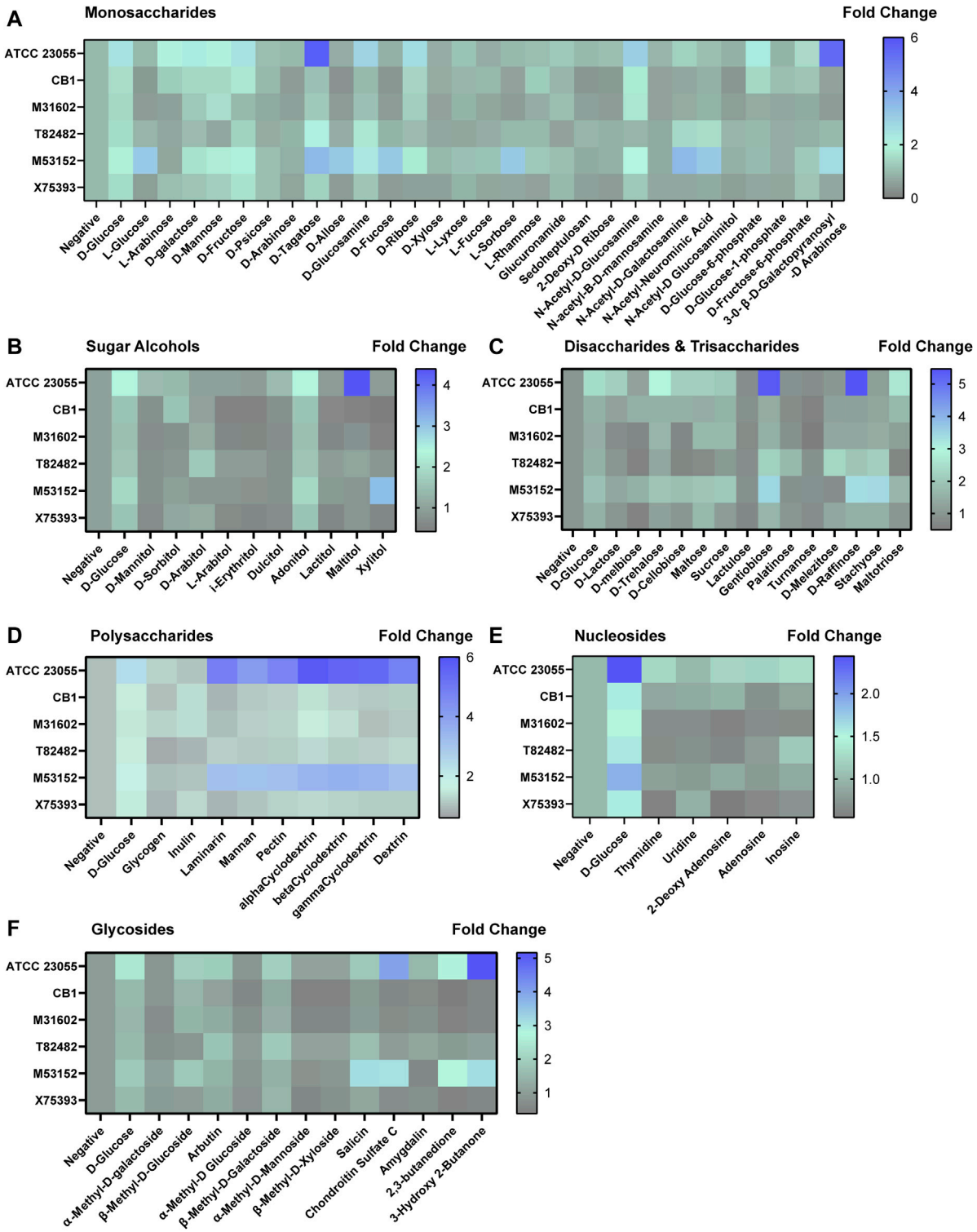

FIGURE 5 | *Acinetobacter* growth in varying carbon sources. Heat maps representing fold change in growth with the negative control (no added nutrients) set at 1. Growth was examined with **(A)** monosaccharides, **(B)** sugar alcohols, **(C)** disaccharides and trisaccharides, **(D)** polysaccharides, **(E)** nucleosides and **(F)** glycosides after 18 h incubation.

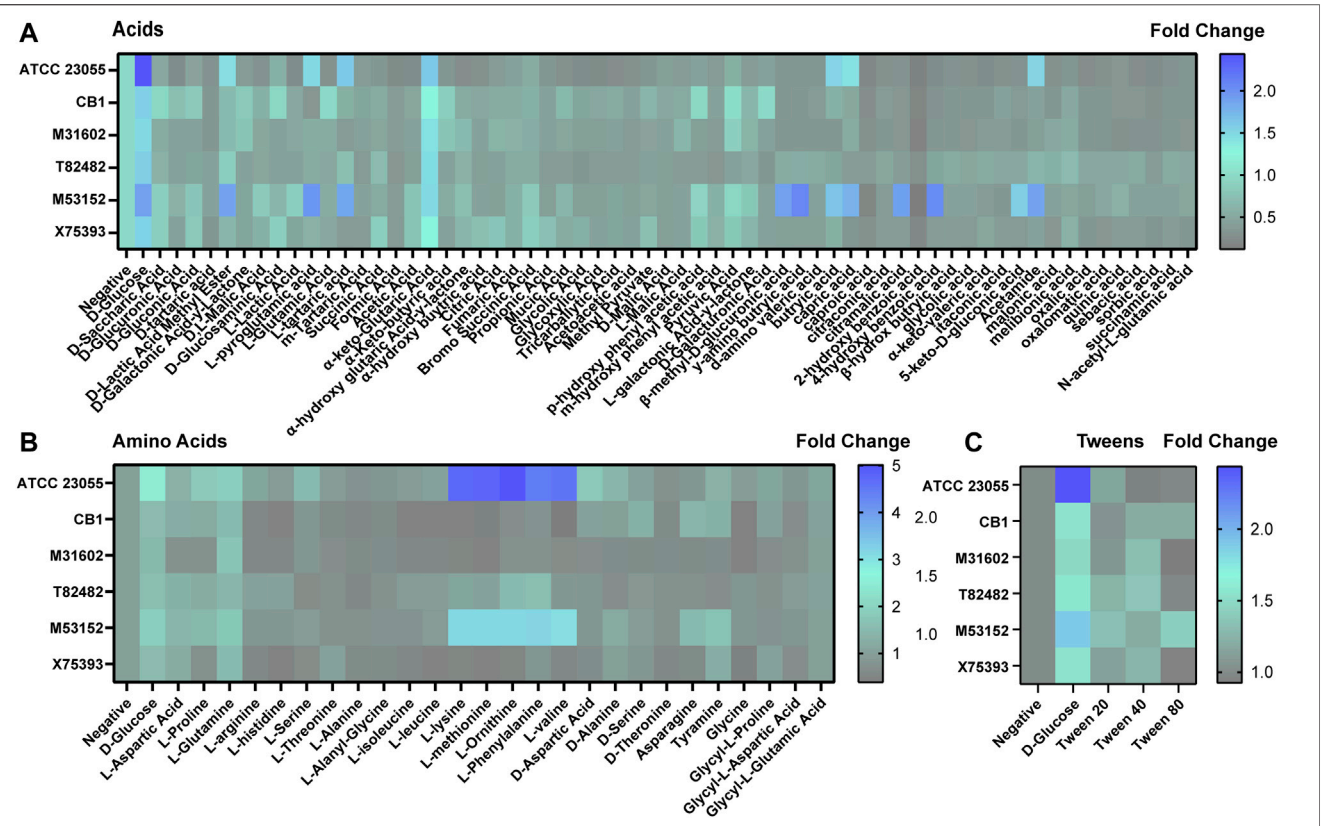

FIGURE 6 | *Acinetobacter* growth in acids, amino acids and tweens. Heat maps representing fold change in growth with the negative control (no added nutrients) set at 1. Growth was examined with **(A)** acids, **(B)** amino acids, and **(C)** tweens after 18 h incubation.

differences may also exist for *A. baumannii* strains. Future studies using mouse models are warranted to fully dissect the colonization capacity and epithelial crosstalk with *A. calcoaceticus*.

Elevated levels of *Acinetobacter* in the setting of IBD has been observed in several studies (Gophna et al., 2006; Lucke et al., 2006; Leung et al., 2014; Kevans et al., 2015; Tang et al., 2015; Sjoberg et al., 2017; Sekido et al., 2020; He et al., 2021; Qi et al., 2022). Two studies found high abundance of *Acinetobacter* in pediatric patients with newly diagnosed ulcerative colitis (Kevans et al., 2015; Sjoberg et al., 2017); providing potential evidence that *Acinetobacter* species could be contributing to the onset of intestinal inflammation in genetically susceptible patients. Another study found that *Acinetobacter* was enriched in the mucosa-associated bacteria during active colitis in ulcerative colitis patients (Tang et al., 2015). This study found that *Acinetobacter* levels significantly correlated with microbial pathways in actively inflamed colitis tissue, suggesting a potential causal relationship between *Acinetobacter* and intestinal inflammation. Another study identified *Acinetobacter* in the $CD14^{+}CD11c$ + CD163low subset macrophages in the lamina propia of ulcerative colitis patients (Sekido et al., 2020), which indicates these microbes were able to bypass the epithelial barrier. In our intestinal organoid model, we found that several *A. calcoaceticus* strains stimulated pro-inflammatory cytokine expression and suppressed mucin production. These findings mirror what has been observed in ulcerative colitis patients (Trabucchi et al., 1986; Raouf et al., 1992; Pullan et al., 1994; Tytgat et al., 1996; Hanski et al., 1999; Heazlewood et al., 2008; Zhao et al., 2010; Larsson et al., 2011; Antoni et al., 2014; Johansson et al., 2014; Wenzel et al., 2014). Our findings provide further evidence for the potential link between *Acinetobacter*, intestinal inflammation and IBD. In the future, we plan to dissect the mechanisms of how *A. calcoaceticus* initiates inflammation in more depth.

Another observation from our organoid model was that not all the clinical isolates stimulated pro-inflammation cytokine expression. Gram-negative bacteria such as *Acinetobacter* can activate TLR4 on host cells via the cell wall component lipopolysaccharide (LPS) (Pelletier et al., 2013). LPS is comprised of lipid A, the core oligosaccharide, and the O-specific antigen. Lipid A is considered the bioactive component of LPS and is responsible for activating immune responses (Pelletier et al., 2013). *A. baumannii* has been shown to modify their lipid A with the addition of positively charged residues including ethanolamine, phosphoethanolamine, aminoarabinose, and glucosamine (Moskowitz et al., 2004; Arroyo et al., 2011; Basheer et al., 2011; Beceiro et al., 2011; Llobet et al., 2011; Pelletier et al., 2013). These modifications enhance the resistance of *A. baumannii* to the antibiotic

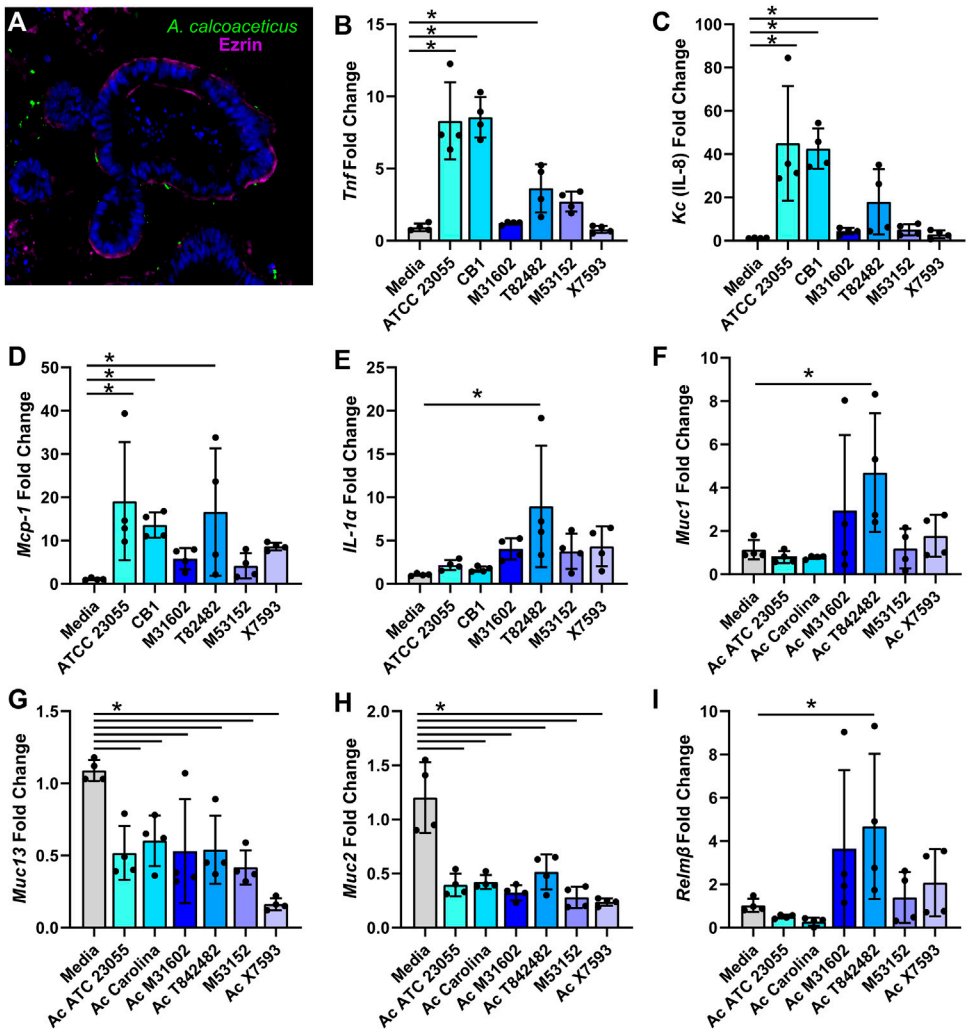

FIGURE 7 | (A) *calcoaceticus* induces inflammatory responses in intestinal organoids. **(A)** Inside-out organoids incubated with live fluorescently tagged *A. calcoaceticus* and immunostained with the apical marker phospho-Ezrin. qPCR analysis of organoids after 3 h of incubation examining expression of **(B)** *Tnf*, **(C)** *IL-18*, **(D)** *Mcp-1*, **(E)** *IL-1alpha*, and **(F)** *Muc1*, **(G)** *Muc13*, **(H)** *Muc2*, and **(I)** *Relmβ*.

colistin and suppresses their immunostimulatory capacity (Pelletier et al., 2013). In addition to modifying LPS, some clinical strains of *A. baumannii* have been identified with loss-of-function mutations in genes in the LPS biosynthetic pathway (Moffatt et al., 2010; Nagy et al., 2019); resulting in strains which completely lack LPS. Although *A. baumannii* can survive in the absence of LPS, these microbes have distinct morphological defects and growth alterations under laboratory conditions (Nagy et al., 2019; Beceiro et al., 2011; Bojkovic et al., 2015; Powers et al., 2018; Boll et al., 2016). All of our *A. calcoaceticus* strains were resistant to colistin (*data not shown*) suggesting that some LPS modification might have occurred in these microbes. Since we didn't observe significant morphological or growth differences between our strains, we think that all our stains harbor LPS, but we speculate that their may be different modifications between our *A. calcoaceticus* strains which could account for the variability in cytokine stimulation. We plan in future studies to examine the LPS structures of our *A. calcoaceticus* strains.

Interestingly we noted differences between our commercially available strains and clinical isolates in many of our results. For example, the clinical isolates were more adapted at survival in high concentrations of ethanol and NaCl than the lab adapted strains. The growth of the clinical isolates was also not as robust as the ATCC 23055 strain in utilizing many of the carbon sources, such as glucose, L-arbinose, D-trehalose, GluNAc, galactose, mannose and fructose. In our organoid model, we found that lab adapted ATCC 23055 and CB1 and one clinical isolate T82482 stimulate multiple pro-inflammatory cytokines, while the other strains had minimal stimulation of cytokines. A number of groups have begun to question the adequacy of laboratory-adapted reference strains to represent "real world" pathogenesis (Fux et al., 2005). Some laboratory strains have been sub-cultured for years, which may result in the loss of

important pathophysiological characteristics or the dependence on lab-specific media components. This limitation can be overcome by including multiple strains, including clinical isolates, and examining their collective behavior. While we did note several differences, in general we found that all strains were fairly resistant to environmental stressors (pH, osmolarity, ethanol, and hydrogen peroxide) and we found several common nutrient sources across strains. Based on these studies, we believe that *A. calcoaceticus* species are well adapted to colonize the gastrointestinal tract and can consume a variety of nutritional sources. We also believe this work highlights the benefits of incorporating clinical isolates into future work.

There are several strengths in our study. To the best of our knowledge, this is the only study that has examined the ability of *A. calcoaceticus* to withstand conditions of the gastrointestinal tract and the first show that *A. calcoaceticus* can colonize human stool communities and modulate the gut epithelium. We incorporated several clinical isolates, which has allowed us to identify some global attributes of *A. calcoaceticus*. However, there are also several limitations. This work was all done *in vitro* and *in vivo* studies are necessary to truly identify the colonization capacity of *A. calcoaceticus*. Although we hypothesize that *A. calcoaceticus* activates TLR4 on the gut epithelium to drive inflammatory signatures, this work did not identify a specific mechanism and more work is needed to delineate how *A. calcoaceticus* modulates the intestinal epithelium and immune cells.

In summary, we demonstrate that *A. calcoaceticus* strains can withstand intestinal conditions and thrive with several dietary sources. We believe these attributes make *Acinetobacter* spp. ecologically fit for colonizing the gut. This information is clinically important since the gut likely serves as a reservoir for secondary *Acinetobacter* spp. infections. Thus, it might be possible to prevent secondary infections, like blood stream infections or pneumonia, by inhibiting *Acinetobacter* gut colonization and we believe this is an exciting area for future studies.

DATA AVAILABILITY STATEMENT

The raw data supporting the conclusion of this article will be made available by the authors, without undue reservation.

AUTHOR CONTRIBUTIONS

Concept and design JG and ME; intellectual contribution JG, BB, TT, AE, and ME; data acquisition JG, BB, TT, AE, and ME; data analysis, statistics, and interpretation JG, BB, and ME; drafting manuscript JG; funding AE and ME.

FUNDING

T32GM132055-01 (JG), T32DK124191-01A1 (TT), K01DK121869 (AE), and K01K123195-01 (ME).

SUPPLEMENTARY MATERIAL

The Supplementary Material for this article can be found online at: https://www.frontiersin.org/articles/10.3389/fphys.2022.880024/full#supplementary-material

REFERENCES

Agusti, C., Pujol, M., Argerich, M. J., Ayats, J., Badia, M., Dominguez, M. A., et al. (2002). Short-term Effect of the Application of Selective Decontamination of the Digestive Tract on Different Body Site Reservoir ICU Patients Colonized by Multi-Resistant Acinetobacter Baumannii. *J. Antimicrob. Chemother.* 49, 205–208. doi:10.1093/jac/49.1.205

Aljindan, R., Bukharie, H., Alomar, A., and Abdalhamid, B. (2015). Prevalence of Digestive Tract Colonization of Carbapenem-Resistant Acinetobacter Baumannii in Hospitals in Saudi Arabia. *J. Med. Microbiol.* 64, 400–406. doi:10.1099/jmm.0.000033

Antoni, L., Nuding, S., Wehkamp, J., and Stange, E. F. (2014). Intestinal Barrier in Inflammatory Bowel Disease. *Wjg* 20, 1165–1179. doi:10.3748/wjg.v20.i5.1165

Arroyo, L. A., Herrera, C. M., Fernandez, L., Hankins, J. V., Trent, M. S., and Hancock, R. E. W. (2011). The pmrCAB Operon Mediates Polymyxin Resistance in Acinetobacter Baumannii ATCC 17978 and Clinical Isolates through Phosphoethanolamine Modification of Lipid A. *Antimicrob. Agents Chemother.* 55, 3743–3751. doi:10.1128/aac.00256-11

Ayats, J., Corbella, X., Ardanuy, C., Domínguez, M. A., Ricart, A., Ariza, J., et al. (1997). Epidemiological Significance of Cutaneous, Pharyngeal, and Digestive Tract Colonization by Multiresistant Acinetobacter Baumannii in ICU Patients. *J. Hosp. Infect.* 37, 287–295. doi:10.1016/s0195-6701(97)90145-6

Basheer, S. M., Guiso, N., Tirsoaga, A., Caroff, M., and Novikov, A. (2011). Structural Modifications Occurring in Lipid A of Bordetella Bronchiseptica Clinical Isolates as Demonstrated by Matrix-Assisted Laser Desorption/ionization Time-Of-Flight Mass Spectrometry. *Rapid Commun. Mass Spectrom.* 25, 1075–1081. doi:10.1002/rcm.4960

Beceiro, A., Llobet, E., Aranda, J., Bengoechea, J. A., Doumith, M., Hornsey, M., et al. (2011). Phosphoethanolamine Modification of Lipid A in Colistin-Resistant Variants of Acinetobacter Baumannii Mediated by the pmrAB Two-Component Regulatory System. *Antimicrob. Agents Chemother.* 55, 3370–3379. doi:10.1128/aac.00079-11

Bojkovic, J., Richie, D. L., Six, D. A., Rath, C. M., Sawyer, W. S., Hu, Q., et al. (2015). Characterization of an Acinetobacter baumannii lptD Deletion Strain: Permeability Defects and Response to Inhibition of Lipopolysaccharide and Fatty Acid Biosynthesis. *J. Bacteriol.* 198, 731–741.

Boll, J. M., Crofts, A. A., Peters, K., Cattoir, V., Vollmer, W., Davies, B. W., et al. (2016). A Penicillin-Binding Protein Inhibits Selection of Colistin-Resistant, Lipooligosaccharide-Deficient *Acinetobacter baumannii*. *Proc Natl Acad Sci U S A* 113, E6228–e6237.

Braun, T., Di Segni, A., Benshoshan, M., Asaf, R., Squires, J. E., Farage Barhom, S., et al. (2017). Fecal Microbial Characterization of Hospitalized Patients with Suspected Infectious Diarrhea Shows Significant Dysbiosis. *Sci. Rep.* 7, 1088. doi:10.1038/s41598-017-01217-1

Cheng, V. C. C., Chen, J. H. K., So, S. Y. C., Wong, S. C. Y., Yan, M. K., Chau, P. H., et al. (2015). Use of Fluoroquinolones Is the Single Most Important Risk Factor for the High Bacterial Load in Patients with Nasal and Gastrointestinal Colonization by Multidrug-Resistant Acinetobacter Baumannii. *Eur. J. Clin. Microbiol. Infect. Dis.* 34, 2359–2366. doi:10.1007/s10096-015-2489-4

Corbella, X., Pujol, M., Ayats, J., Sendra, M., Ardanuy, C., Dominguez, M. A., et al. (1996). Relevance of Digestive Tract Colonization in the Epidemiology of Nosocomial Infections Due to Multiresistant Acinetobacter Baumannii. *Clin. Infect. Dis.* 23, 329–334. doi:10.1093/clinids/23.2.329

Coron, N., Pavlickova, S., Godefroy, A., Pailhoriès, H., Kempf, M., Cassisa, V., et al. (2017). Mouse Model of Colonization of the Digestive Tract with Acinetobacter Baumannii and Subsequent Pneumonia. *Future Microbiol.* 12, 707–719. doi:10.2217/fmb-2016-0203

Dijkshoorn, L., Van Aken, E., Shunburne, L., Van Der Reijden, T. J. K., Bernards, A. T., Nemec, A., et al. (2005). Prevalence of Acinetobacter Baumannii and Other Acinetobacter Spp. In Faecal Samples from Non-hospitalised Individuals. *Clin. Microbiol. Infect.* 11, 329–332. doi:10.1111/j.1469-0691.2005.01093.x

Engevik, M. A., and Versalovic, J. (2017). Biochemical Features of Beneficial Microbes: Foundations for Therapeutic Microbiology. *Microbiol. Spectr.* 1, 3-47. doi:10.1128/microbiolspec.BAD-0012-2016

Engevik, M. A., Aihara, E., Montrose, M. H., Shull, G. E., Hassett, D. J., and Worrell, R. T. (2013). Loss of NHE3 Alters Gut Microbiota Composition and influencesBacteroides Thetaiotaomicrongrowth. *Am. J. Physiology-Gastrointestinal Liver Physiology* 305, G697–G711. doi:10.1152/ajpgi.00184.2013

Engevik, M. A., Danhof, H. A., Auchtung, J., Endres, B. T., Ruan, W., Bassères, E., et al. (2021). Fusobacterium Nucleatum Adheres to Clostridioides Difficile via the RadD Adhesin to Enhance Biofilm Formation in Intestinal Mucus. *Gastroenterology* 160, 1301–1314. e1308. doi:10.1053/j.gastro.2020.11.034

Fux, C. A., Shirtliff, M., Stoodley, P., and Costerton, J. W. (2005). Can Laboratory Reference Strains Mirror 'real-World' Pathogenesis? *Trends Microbiol.* 13, 58–63. doi:10.1016/j.tim.2004.11.001

Glew, R. H., Moellering, R. C., Jr., and Kunz, L. J. (1977). Infections with Acinetobacter Calcoaceticus (Herellea Vaginicola). *Medicine* 56, 79–98. doi:10.1097/00005792-197703000-00001

Gophna, U., Sommerfeld, K., Gophna, S., Doolittle, W. F., and Veldhuyzen Van Zanten, S. J. O. (2006). Differences between Tissue-Associated Intestinal Microfloras of Patients with Crohn's Disease and Ulcerative Colitis. *J. Clin. Microbiol.* 44, 4136–4141. doi:10.1128/jcm.01004-06

Hanski, C., Born, M., Foss, H. D., Marowski, B., Mansmann, U., Arasteh, K., et al. (1999). Defective Post-transcriptional Processing of MUC2 Mucin in Ulcerative Colitis and in Crohn's Disease Increases Detectability of the MUC2 Protein Core. *J. Pathol.* 188, 304–311. doi:10.1002/(sici)1096-9896(199907)188:3<304:aid-path375>3.0.co;2-a

He, X.-X., Li, Y.-H., Yan, P.-G., Meng, X.-C., Chen, C.-Y., Li, K.-M., et al. (2021). Relationship between Clinical Features and Intestinal Microbiota in Chinese Patients with Ulcerative Colitis. *Wjg* 27, 4722–4737. doi:10.3748/wjg.v27.i28.4722

Heazlewood, C. K., Cook, M. C., Eri, R., Price, G. R., Tauro, S. B., Taupin, D., et al. (2008). Aberrant Mucin Assembly in Mice Causes Endoplasmic Reticulum Stress and Spontaneous Inflammation Resembling Ulcerative Colitis. *PLoS Med.* 5, e54. doi:10.1371/journal.pmed.0050054

Johansson, M. E. V., Gustafsson, J. K., Holmén-Larsson, J., Jabbar, K. S., Xia, L., Xu, H., et al. (2014). Bacteria Penetrate the Normally Impenetrable Inner Colon Mucus Layer in Both Murine Colitis Models and Patients with Ulcerative Colitis. *Gut* 63, 281–291. doi:10.1136/gutjnl-2012-303207

Ketter, P. M., Yu, J. J., Guentzel, M. N., May, H. C., Gupta, R., Eppinger, M., et al. (2018). Acinetobacter Baumannii Gastrointestinal Colonization Is Facilitated by Secretory IgA Which Is Reductively Dissociated by Bacterial Thioredoxin A. *mBio* 9, e01298. doi:10.1128/mBio.01298-18

Kevans, D., Tyler, A. D., Holm, K., Jørgensen, K. K., Vatn, M. H., Karlsen, T. H., et al. (2015). Characterization of Intestinal Microbiota in Ulcerative Colitis Patients with and without Primary Sclerosing Cholangitis. *Eccojc* 10, 330–337. doi:10.1093/ecco-jcc/jjv204

Larsson, J. M. H., Karlsson, H., Crespo, J. G., Johansson, M. E. V., Eklund, L., Sjövall, H., et al. (2011). Altered O-Glycosylation Profile of MUC2 Mucin Occurs in Active Ulcerative Colitis and Is Associated with Increased Inflammation. *Inflamm. Bowel Dis.* 17, 2299–2307. doi:10.1002/ibd.21625

Leung, J. M., Davenport, M., Wolff, M. J., Wiens, K. E., Abidi, W. M., Poles, M. A., et al. (2014). IL-22-producing CD4+ Cells Are Depleted in Actively Inflamed Colitis Tissue. *Mucosal Immunol.* 7, 124–133. doi:10.1038/mi.2013.31

Li, G., Yang, M., Zhou, K., Zhang, L., Tian, L., Lv, S., et al. (2015). Diversity of Duodenal and Rectal Microbiota in Biopsy Tissues and Luminal Contents in Healthy Volunteers. *J. Microbiol. Biotechnol.* 25, 1136–1145. doi:10.4014/jmb.1412.12047

Li, S., Duan, X., Peng, Y., and Rui, Y. (2019). Molecular Characteristics of Carbapenem-Resistant Acinetobacter Spp. From Clinical Infection Samples and Fecal Survey Samples in Southern China. *BMC Infect. Dis.* 19, 900. doi:10.1186/s12879-019-4423-3

Lim, C. J., Cheng, A. C., Kennon, J., Spelman, D., Hale, D., Melican, G., et al. (2014). Prevalence of Multidrug-Resistant Organisms and Risk Factors for Carriage in Long-Term Care Facilities: a Nested Case-Control Study. *J. Antimicrob. Chemother.* 69, 1972–1980. doi:10.1093/jac/dku077

Llobet, E., Campos, M. A., Giménez, P., Moranta, D., and Bengoechea, J. A. (2011). Analysis of the Networks Controlling the Antimicrobial-peptide-dependent Induction of *Klebsiella pneumoniae* Virulence Factors. *Infect. Immun.* 79, 3718–3732. doi:10.1128/iai.05226-11

Lucke, K., Miehlke, S., Jacobs, E., and Schuppler, M. (2006). Prevalence of Bacteroides and Prevotella Spp. In Ulcerative Colitis. *J. Med. Microbiol.* 55, 617–624. doi:10.1099/jmm.0.46198-0

Madar Johansson, M., Azzouz, M., Häggendal, B., Säljö, K., Malmi, H., Zaviolov, A., et al. (2020). Glycosphingolipids Recognized by Acinetobacter Baumannii. *Microorganisms* 8, 612. doi:10.3390/microorganisms8040612

Mancilla-Rojano, J., Ochoa, S. A., Reyes-Grajeda, J. P., Flores, V., Medina-Contreras, O., Espinosa-Mazariego, K., et al. (2020). Molecular Epidemiology of Acinetobacter calcoaceticus-Acinetobacter baumannii Complex Isolated From Children at the Hospital Infantil de México Federico Gómez. *Front. Microbiol.* 11, 576673. doi:10.3389/fmicb.2020.576673

Medina-Presentado, J. C., Seija, V., Vignoli, R., Pontet, J., Robino, L., Cordeiro, N. F., et al. (2013). Polyclonal Endemicity of Acinetobacter Baumannii in Ventilated Patients in an Intensive Care Unit in Uruguay. *Int. J. Infect. Dis.* 17, e422–e427. doi:10.1016/j.ijid.2012.12.025

Moffatt, J. H., Harper, M., Harrison, P., Hale, J. D. F., Vinogradov, E., Seemann, T., et al. (2010). Colistin Resistance in Acinetobacter Baumannii Is Mediated by Complete Loss of Lipopolysaccharide Production. *Antimicrob. Agents Chemother.* 54, 4971–4977. doi:10.1128/aac.00834-10

Moskowitz, S. M., Ernst, R. K., and Miller, S. I. (2004). PmrAB, a Two-Component Regulatory System of *Pseudomonas aeruginosa* that Modulates Resistance to Cationic Antimicrobial Peptides and Addition of Aminoarabinose to Lipid A. *J. Bacteriol.* 186, 575–579. doi:10.1128/jb.186.2.575-579.2004

Nagy, E., Losick, R., and Kahne, D. (2019). Robust Suppression of Lipopolysaccharide Deficiency in Acinetobacter Baumannii by Growth in Minimal Medium. *J. Bacteriol.* 201, e00420. doi:10.1128/JB.00420-19

Nemec, A., Krizova, L., Maixnerova, M., Sedo, O., Brisse, S., and Higgins, P. G. (2015). Acinetobacter Seifertii Sp. nov., a Member of the Acinetobacter Calcoaceticus-Acinetobacter Baumannii Complex Isolated from Human Clinical Specimens. *Int. J. Syst. Evol. Microbiol.* 65, 934–942. doi:10.1099/ijs.0.000043

Overduin, J., Tylee, T. S., Frayo, R. S., and Cummings, D. E. (2014). Hyperosmolarity in the Small Intestine Contributes to Postprandial Ghrelin Suppression. *Am. J. Physiology-Gastrointestinal Liver Physiology* 306, G1108–G1116. doi:10.1152/ajpgi.00072.2014

Pandey, P. K., Verma, P., Kumar, H., Bavdekar, A., Patole, M. S., and Shouche, Y. S. (2012). Comparative Analysis of Fecal Microflora of Healthy Full-Term Indian Infants Born with Different Methods of Delivery (Vaginal vs Cesarean): Acinetobacter Sp. Prevalence in Vaginally Born Infants. *J. Biosci.* 37, 989–998. doi:10.1007/s12038-012-9268-5

Peleg, A. Y., Seifert, H., and Paterson, D. L. (2008). Acinetobacter Baumannii : Emergence of a Successful Pathogen. *Clin. Microbiol. Rev.* 21, 538–582. doi:10.1128/cmr.00058-07

Pelletier, M. R., Casella, L. G., Jones, J. W., Adams, M. D., Zurawski, D. V., Hazlett, K. R. O., et al. (2013). Unique Structural Modifications Are Present in the Lipopolysaccharide from Colistin-Resistant Strains of Acinetobacter Baumannii. *Antimicrob. Agents Chemother.* 57, 4831–4840. doi:10.1128/aac.00865-13

Powers, M. J., and Trent, M. S. (2018). Expanding the Paradigm for the Outer Membrane: *Acinetobacter baumannii* in the Absence of Endotoxin. *Mol. Microbiol.* 107, 47–56.

Pullan, R. D., Thomas, G. A., Rhodes, M., Newcombe, R. G., Williams, G. T., Allen, A., et al. (1994). Thickness of Adherent Mucus Gel on Colonic Mucosa in Humans and its Relevance to Colitis. *Gut* 35, 353–359. doi:10.1136/gut.35.3.353

Qi, Q., Liu, Y.-N., Lv, S.-Y., Wu, H.-G., Zhang, L.-S., Cao, Z., et al. (2022). Gut Microbiome Alterations in Colitis Rats after Moxibustion at Bilateral Tianshu Acupoints. *BMC Gastroenterol.* 22, 62. doi:10.1186/s12876-022-02115-1

Raouf, A. H., Tsai, H. H., Parker, N., Hoffman, J., Walker, R. J., and Rhodes, J. M. (1992). Sulphation of Colonic and Rectal Mucin in Inflammatory Bowel Disease: Reduced Sulphation of Rectal Mucus in Ulcerative Colitis. *Clin. Sci. (Lond)* 83, 623–626. doi:10.1042/cs0830623

Raplee, I., Walker, L., Xu, L., Surathu, A., Chockalingam, A., Stewart, S., et al. (2021). Emergence of Nosocomial Associated Opportunistic Pathogens in the Gut Microbiome after Antibiotic Treatment. *Antimicrob. Resist Infect. Control* 10, 36. doi:10.1186/s13756-021-00903-0

Roy, S., Viswanathan, R., Singh, A., Das, P., and Basu, S. (2010). Gut Colonization by Multidrug-Resistant and Carbapenem-Resistant Acinetobacter Baumannii in Neonates. *Eur. J. Clin. Microbiol. Infect. Dis.* 29, 1495–1500. doi:10.1007/s10096-010-1030-z

Sekido, Y., Nishimura, J., Nakano, K., Osu, T., Chow, C.-E. T., Matsuno, H., et al. (2020). Some Gammaproteobacteria Are Enriched within CD14+ Macrophages from Intestinal Lamina Propria of Crohn's Disease Patients versus Mucus. *Sci. Rep.* 10, 2988. doi:10.1038/s41598-020-59937-w

Sjöberg, F., Barkman, C., Nookaew, I., Östman, S., Adlerberth, I., Saalman, R., et al. (2017). Low-complexity Microbiota in the Duodenum of Children with Newly Diagnosed Ulcerative Colitis. *PLoS One* 12, e0186178. doi:10.1371/journal.pone.0186178

Tang, M. S., Poles, J., Leung, J. M., Wolff, M. J., Davenport, M., Lee, S. C., et al. (2015). Inferred Metagenomic Comparison of Mucosal and Fecal Microbiota from Individuals Undergoing Routine Screening Colonoscopy Reveals Similar Differences Observed during Active Inflammation. *Gut Microbes* 6, 48–56. doi:10.1080/19490976.2014.1000080

Thom, K. A., Hsiao, W. W. L., Harris, A. D., Stine, O. C., Rasko, D. A., and Johnson, J. K. (2010). Patients with Acinetobacter Baumannii Bloodstream Infections Are Colonized in the Gastrointestinal Tract with Identical Strains. *Am. J. Infect. Control* 38, 751–753. doi:10.1016/j.ajic.2010.03.005

Timsit, J.-F., Garrait, V., Misset, B., Goldstein, F. W., Renaud, B., Carlet, J., et al. (1993). The Digestive Tract Is a Major Site for Acinetobacter Baumannii Colonization in Intensive Care Unit Patients. *J. Infect. Dis.* 168, 1336–1337. doi:10.1093/infdis/168.5.1336

Trabucchi, E., Mukenge, S., Baratti, C., Colombo, R., Fregoni, F., and Montorsi, W. (1986). Differential Diagnosis of Crohn's Disease of the Colon from Ulcerative Colitis: Ultrastructure Study with the Scanning Electron Microscope. *Int. J. Tissue React.* 8, 79–84.

Tytgat, K. M. A. J., Van Der Wal, J.-W. G., Einerhand, A. W. C., Büller, H. A., and Dekker, J. (1996). Quantitative Analysis of MUC2 Synthesis in Ulcerative Colitis. *Biochem. Biophysical Res. Commun.* 224, 397–405. doi:10.1006/bbrc.1996.1039

Wenzel, U. A., Magnusson, M. K., Rydström, A., Jonstrand, C., Hengst, J., Johansson, M. E., et al. (2014). Spontaneous Colitis in Muc2-Deficient Mice Reflects Clinical and Cellular Features of Active Ulcerative Colitis. *PLoS One* 9, e100217. doi:10.1371/journal.pone.0100217

Wisplinghoff, H., Edmond, M. B., Pfaller, M. A., Jones, R. N., Wenzel, R. P., and Seifert, H. (2000). Nosocomial Bloodstream Infections Caused by Acinetobacter Species in United States Hospitals: Clinical Features, Molecular Epidemiology, and Antimicrobial Susceptibility. *Clin. Infect. Dis.* 31, 690–697. doi:10.1086/314040

Wood, B., and Katzberg, R. (1978). Tween 80/diatrizoate Enemas in Bowel Obstruction. *Am. J. Roentgenol.* 130, 747–750. doi:10.2214/ajr.130.4.747

Xavier, C., Miquel, P., Josefina, A., Montserrat, S., Carmen, A., Dom, X., et al. (1996). Relevance of Digestive Tract Colonization in the Epidemiology of Nosocomial Infections Due to Multiresistant Acinetobacter Baumannii. *Clin. Infect. Dis.* 23, 329–334.

Zhao, F., Edwards, R., Dizon, D., Afrasiabi, K., Mastroianni, J. R., Geyfman, M., et al. (2010). Disruption of Paneth and Goblet Cell Homeostasis and Increased Endoplasmic Reticulum Stress in Agr2−/− Mice. *Dev. Biol.* 338, 270–279. doi:10.1016/j.ydbio.2009.12.008

Conflict of Interest: The authors declare that the research was conducted in the absence of any commercial or financial relationships that could be construed as a potential conflict of interest.

Publisher's Note: All claims expressed in this article are solely those of the authors and do not necessarily represent those of their affiliated organizations, or those of the publisher, the editors, and the reviewers. Any product that may be evaluated in this article, or claim that may be made by its manufacturer, is not guaranteed or endorsed by the publisher.

frontiers | Frontiers in Physiology

ORIGINAL RESEARCH
published: 31 May 2022
doi: 10.3389/fphys.2022.866945

A Pilot Study to Assess Opportunistic Use of CT-Scan for Osteoporosis Screening in Chronic Pancreatitis

*Julia McNabb-Baltar[1], Hanisha R. Manickavasagan[2], Darwin L. Conwell[2], Andrew Lu[3], Dhiraj Yadav[4], Philip A. Hart[2], Luis F. Lara[2], Zobeida Cruz-Monserrate[2], Steven Ing[5], Alice Hinton[6], Thomas A. Mace[2], David Bradley[5] and Zarine K. Shah[3]**

[1]Brigham and Women's Hospital, Harvard Medical School, Division of Gastroenterology, Hepatology, and Endoscopy, Boston, MA, United States, [2]The Ohio State University Wexner Medical Center, Division of Gastroenterology, Hepatology, and Nutrition, Columbus, OH, United States, [3]The Ohio State University Wexner Medical Center, Department of Radiology, Columbus, OH, United States, [4]University of Pittsburgh Medical Center, Division of GI, Hepatology and Nutrition, Columbus, OH, United States, [5]The Ohio State University Wexner Medical Center, Division of Endocrinology, Diabetes and Metabolism, Columbus, OH, United States, [6]Division of Biostatistics, College of Public Health, The Ohio State University, Columbus, OH, United States

OPEN ACCESS

Edited by:
Natalie Luhtala,
Salk Institute for Biological Studies, United States

Reviewed by:
Asger Reinstrup Bihlet, Nordic Bioscience, Denmark
Shin Hamada, Tohoku University, Japan

***Correspondence:**
Zarine K. Shah
zarine.shah@osumc.edu

Specialty section:
This article was submitted to Gastrointestinal Sciences, a section of the journal Frontiers in Physiology

Received: 31 January 2022
Accepted: 22 April 2022
Published: 31 May 2022

Citation:
McNabb-Baltar J, Manickavasagan HR, Conwell DL, Lu A, Yadav D, Hart PA, Lara LF, Cruz-Monserrate Z, Ing S, Hinton A, Mace TA, Bradley D and Shah ZK (2022) A Pilot Study to Assess Opportunistic Use of CT-Scan for Osteoporosis Screening in Chronic Pancreatitis. Front. Physiol. 13:866945. doi: 10.3389/fphys.2022.866945

Objectives: CT scans are commonly performed in patients with chronic pancreatitis (CP). Osteopathy and fractures are recognized in CP but no osteoporosis screening guidelines are recommended. "Opportunistic" CT scan-derived bone density thresholds are assessed for identifying osteoporosis in CP.

Methods: Retrospective pilot cohort study. CP subjects who had CT scans and dual-energy x-ray absorptiometry (DXA) within 1 year were included. CT-derived bone density was measured at the L1 level. Pearson's correlation was performed between age and CT-derived bone density in Hounsfield unit (HU). Univariate analysis using HU to identify osteoporosis was performed at various thresholds of bone density. The discriminatory ability of the model was evaluated with the area under the receiver operating characteristic (ROC) curve (AUC). Several HU thresholds were tested.

Results: Twenty-seven CP subjects were included, of whom 11 had normal bone density, 12 osteopenia, and four osteoporosis on DXA. The mean age was 59.9 years (SD 13.0). There was a negative correlation of age with HU ($r = -0.519$, $p = 0.006$). CT-derived bone density predicted DXA-based osteoporosis in the univariable analysis (Odds Ratio (OR) = 0.97 95% Confidence Interval (CI) 0.94–1.00, $p = 0.03$). HU thresholds were tested. A threshold of 106 HU maximized the accuracy (AUC of 0.870).

Conclusions: CT scan may be repurposed for "opportunistic" screening to rule out osteoporosis in CP. A larger study is warranted to confirm these results.

Keywords: chronic pancreatitis (CP), osteoporosis, DXA (dual-energy X-ray absorptiometry), opportunistic screening, CT scan

INTRODUCTION

Chronic pancreatitis (CP) predisposes to metabolic bone disease (osteopenia and osteoporosis) and low trauma fracture. The prevalence of osteoporosis or osteopenia in CP is estimated to be 65% (Duggan et al., 2014). We have reported that CP subjects are at high risk for osteoporotic fracture compared to other "high-risk" gastrointestinal conditions for which screening guidelines are in place (Tignor et al., 2010). Yet, only a fraction of CP subjects receive dual-energy X-ray absorptiometry (DXA) imaging testing (Srivoleti et al., 2021). Identification of metabolic bone disease by DXA in CP may lead to interventions that lower fracture risk. However, there are no societal guidelines recommended for osteoporosis screening in CP; thus, insurance carriers do not universally cover costs of DXA "solely" for CP. Therefore, a cost-effective alternative screening method may identify those at risk of fracture (Anderson et al., 2018).

Opportunistic screening for osteoporosis with computerized tomography (CT) scans has been proposed as a no added cost strategy (Pickhardt et al., 2013; Zysset et al., 2015; Jang et al., 2019). Opportunistic use of CT scan is not a substitute for DXA scan but aids in the identification of subjects who are not, otherwise, suspected to be at risk of fracture or osteoporosis. There is grade-A evidence (Pickhardt et al., 2011; Pickhardt et al., 2013; Pickhardt et al., 2015; Schreiber et al., 2015; Zysset et al., 2015; Lee et al., 2016; Gausden et al., 2017; Gerety et al., 2017) that CT opportunistic screening is reproducible and valid compared with DXA to identify osteoporosis (Wright, 2006).

Chronic pancreatitis subjects have numerous CT scans during their lifetime for disease management, which potentially could be repurposed for osteoporosis risk assessment (Mortele et al., 2011). Retrieval of bone density data from CT scans ordered for other indications requires no additional cost, subject time, equipment, or radiation exposure. In addition, data can be obtained retrospectively or prospectively (Wright, 2006; Buckens et al., 2015; Gausden et al., 2017; Lee et al., 2017; Lenchik et al., 2018). Integration of opportunistic CT screening into the evaluation of CP subjects could markedly expand screening efforts in the population and improve our understanding of the burden of bone disease in CP.

The aim of the pilot study was to investigate CT-derived bone density thresholds from a cohort of CP subjects and test their added value for predicting osteoporosis in DXA-derived bone density measurements (lowest axial skeleton T-score). Diagnostic performance of CT-derived bone density (sensitivity, specificity, and accuracy) at different cut points for osteoporosis was calculated to determine its feasibility as an option for opportunistic screening in CP and is compared to thresholds in the medical literature.

METHODS

Subjects with chronic pancreatitis, 18 years and older, followed at the outpatient Pancreas Clinic at The Ohio State University who underwent both a CT [Siemens scanner (SOMATOM Definition Flash, 128 slice CT] and DXA (GE scanner Lunar, Lunar Prodigy or iDXA) scan within 1 year were identified for inclusion into this retrospective pilot study. Using these criteria, we identified 27 subjects with both abdominal CT scans and DXA for analysis. The correlation between CT-derived bone density measured in Hounsfield Units (HUs) at the L1 vertebral level vs. DXA T-score was assessed.

Demographics, laboratory, and imaging findings were abstracted, including age, gender, race, smoking, excessive alcohol use (defined as >2 drinks/day male; >1 drink/day female), use of pancreatic enzyme replacement therapy (PERT), diabetes, and vitamin A, D, and E values, when available. Diagnosis of chronic pancreatitis was based on the Cambridge classification (Axon et al., 1984). Study approval was obtained from The Ohio State University Institutional Board Review 2019H0353.

A region of interest (ROI) was drawn manually at the L1 vertebral body. It is the first non–rib-bearing vertebra and can be seen on both abdominal and thoracic CT scans. The L1 vertebra avoids most degenerative processes, and HU thresholds have been determined for L1 with excellent interobserver agreement. The HU value was determined by drawing an ellipse as large as possible on the axial and the midsagittal reconstruction in the anterior two-thirds of the vertebral body (**Figure 1**). This avoids venous channels in the posterior vertebra and should only include the trabecular bone. Additional images were assessed for occult vertebral fracture. The average of the mean HU values from the ROIs was recorded. Care was taken to note the model and voltage of the CT image and standardization of images and reviewed by a single abdominal radiologist (ZS).

DXA scan results were interpreted by a certified clinical densitometrist (CCD) as per The International Society for Clinical Densitometry (ISCD) guidelines and were recorded for comparison. Osteoporosis, osteopenia, and normal bone density were defined according to DXA results (Zysset et al., 2015).

Statistical Methods: Statistical analysis was conducted using SAS, version 9.4 (SAS Institute, North Carolina, US). The means and standard deviation (SD) were generated for continuously coded variables, whereas frequencies and proportions were generated for categorical variables. The association with CT-derived bone densities at L1 was evaluated with Pearson's correlations for age. A univariable logistic regression model was fit for osteoporosis to evaluate the contribution of L1 density. The discriminatory ability of the model was evaluated with the area under the receiver operating characteristic (ROC) curve (AUC), and the maximum of the sum of sensitivity and specificity was used to determine the optimal L1 density threshold for distinguishing between normal/osteopenia and osteoporosis. Sensitivity, specificity, positive predictive value (PPV), and negative predictive value (NPV) were calculated using different thresholds to indicate osteoporosis, including a CT derived bone density in HU threshold ≤110, ≤135, ≤160, all derived from previously published literature and the threshold derived from the ROC curve maximizing the sum of sensitivity and specificity in our dataset. (Wright, 2006; Pickhardt et al., 2011; Pickhardt et al., 2013; Pickhardt et al., 2015; Schreiber et al., 2015; Zysset

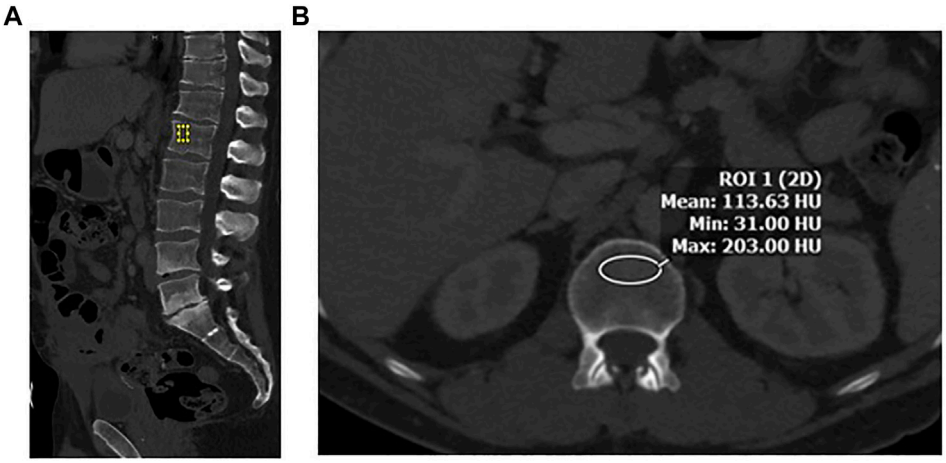

FIGURE 1 | (A) Sagittal image in bone windows demonstrating placement of an elliptical region of interest at L1 along the anterior aspect of the vertebral body. **(B)** Axial image at the L1 level along the superior aspect, with an elliptical region of interest to measure CT-derived bone density in Hounsfield Units (HU).

TABLE 1 | Summary of the population of CP subjects with both CT and DXA scans and within each of the three cohorts: normal, osteopenia, and osteoporosis.

	Overall (*n* = 27)		Normal (*n* = 11)		Osteopenia (*n* = 12)		Osteoporosis (*n* = 4)	
Age (*mean, SD*)	59.9	13.0	62.7	11.8	56.8	14.4	61.5	12.5
Female (*n, %*)	7	25.9	2	18.2	3	25.0	2	50.0
White race (*n, %*)	22	81.5	10	90.9	9	75.0	3	75.0
Smoking (*n, %*)	19	70.4	8	72.7	7	58.3	4	100.0
Excessive alcohol use (*n, %*)	11	40.7	4	36.4	6	50.0	1	25.0
PERT use (*n, %*)	24	88.9	10	90.9	10	83.3	4	100.0
Diabetes	21	77.8	10	90.9	8	66.7	3	75.0
Vitamin D (*mean, SD*)	28.5	12.6	27.2	12.5	27.5	12.6	35.3	13.9
Vitamin A (*mean, SD*)	42.9	23.3	39.5	20.5	41.9	18.0	55.5	43.0
Vitamin E (*mean, SD*)	7.9	3.7	7.9	4.5	7.8	2.8	8.5	4.9

PERT, pancreatic enzyme replacement therapy.

et al., 2015; Lee et al., 2016; Gausden et al., 2017; Gerety et al., 2017; Jang et al., 2019). All tests were two-sided with a statistical significance set at $p < 0.05$.

RESULTS

Demographics and Study Population

A total of 27 subjects were included in this study, of whom 11 had normal bone density, 12 osteopenia, and four osteoporosis on DXA. **Table 1** shows the summary demographics of the study population. The mean age was 59.9 years (SD 13.0). Overall, seven subjects were female (25.9%), 2/11 with normal bone density (18.2%), 3/12 with osteopenia (25.0%) and 2/4 with osteoporosis (50.0%). The majority of the study population were white (81.5%), smoking (70.4%), had diabetes (77.8%), and (88.9%) were on PERT, including all the subjects with osteoporosis. The mean levels of fat-soluble vitamins were also recorded and were not statistically significantly different according to the bone health cohorts. **Figure 2** shows the correlation and scatterplot of age- and CT scan–derived L1 HU density. Age (r = −0.519, p = 0.006) was associated with L1 density in a moderate negative linear relationship.

CT-Derived Bone Density Compared to Dual-Energy X-Ray Absorptiometry

Figures 3, **4** show the CT-derived bone density within each bone health cohort. A univariable logistic regression model assessing the association between HU and osteoporosis in CP was performed. For every one unit of HU rise, the odds of osteoporosis decreases by 0.03 Odds Ratio (OR) = 0.97 95% Confidence Interval (CI) 0.94–1.0, p = 0.03. **Figure 5** shows the ROC curve (AUC of 0.87), where a threshold of 106 HU maximizes the sum of sensitivity and specificity within this data.

Evaluation of CT-Derived Bone Density Thresholds for Osteoporosis

Sensitivity, specificity, PPV, and NPV were assessed according to various thresholds to indicate osteoporosis when applied to our dataset (**Table 2**). Based on this, a threshold of 106 HU maximizes the sum of

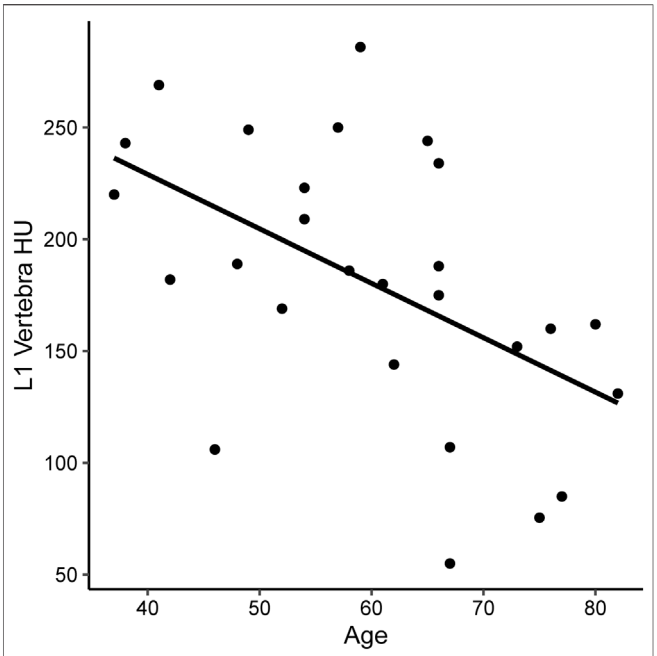

FIGURE 2 | Scatterplot of CT-derived bone density [measures in Hounsfield Units (HU) at the L1 vertebra] in subjects with CP.

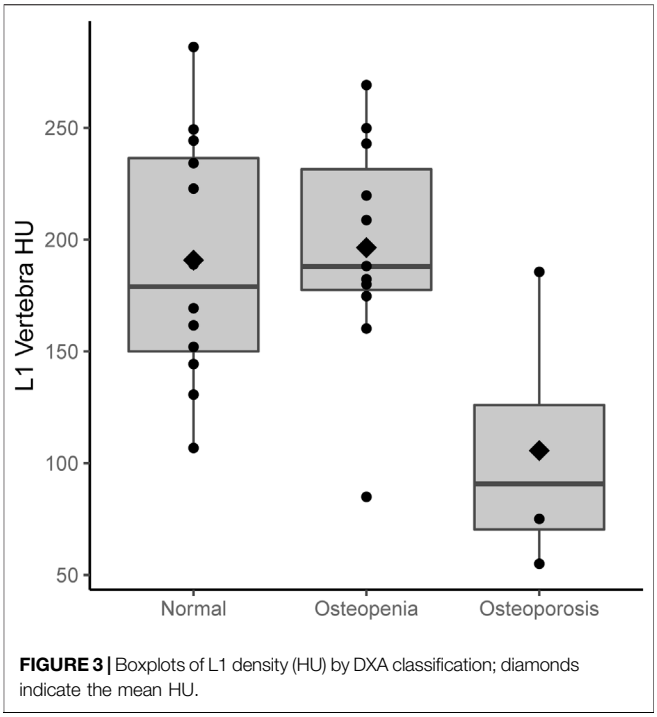

FIGURE 3 | Boxplots of L1 density (HU) by DXA classification; diamonds indicate the mean HU.

sensitivity and specificity. Values at or below 106 classify subjects as having osteoporosis and values >106 as not having osteoporosis. A highly accurate threshold to rule in osteoporosis is difficult to identify with this pilot data as only four subjects had osteoporosis. The four subjects with osteoporosis had L1 densities of 55, 75.7, 106, and 186.

DISCUSSION

To our knowledge, this is the first report of CT-derived bone density screening in osteoporosis in CP. In this pilot study, we have found that CT has the potential to be repurposed as a screening tool in the setting of CP. We assessed multiple thresholds described in the literature and found that a threshold of 106 HU maximized the sum of sensitivity and specificity. This value is similar to a threshold of 110 which has been advanced as a cut point conferring high specificity to rule in osteoporosis (Pickhardt et al., 2013). Since this dataset contained identical sensitivity values at each threshold, we do not arrive at a cut point to rule out osteoporosis. A larger study is needed to validate the findings.

TABLE 2 | Sensitivity, specificity, and positive and negative predictive values of various L1 density thresholds indicate osteoporosis when applied to our dataset. The 106 and 130 thresholds were derived from the OSU data, while the other thresholds are found in the literature.

Threshold	Sensitivity (%)	Specificity (%)	PPV (%)	NPV (%)
≤106	75	96	75	96
≤110	75	91	60	95
≤130	75	91	60	95
≤135	75	90	50	95
≤160	75	74	33	94

People with CP have multiple risk factors for osteopathy, including vitamin D malabsorption, malnutrition, exocrine pancreatic insufficiency, smoking, alcohol abuse, and chronic inflammation, and half are female, all of which contribute to bone mineral density loss and fractures (Duggan et al., 2014; Hart et al., 2021). In addition, several reports from our research group have described fractures and osteopathy in CP subjects (Tignor et al., 2010; Munigala et al., 2016; Hart et al., 2021). Since DXA screening for osteoporosis is not universally covered by insurance, an alternative strategy is needed to identify CP subjects at risk for fracture. Opportunistic CT screening may provide a viable, no-cost alternative.

More than 30 million CT scans were performed in the US in 2013, most of which contain information that can be repurposed (Mettler, 2019). In this context, a low or no-cost alternative screening method would be a major advancement in the field of pancreatology. In essence, CT scans ordered for other indications such as trauma and abdominal pain have been repurposed to screen for osteoporosis by measuring linear X-ray attenuation coefficient in Hounsfield Units (HUs). X-ray attenuation is proportional to the atomic mass and atom density of the tissue subjected to irradiation. For bone, HU is proportional to the mineral density. HU is presented on a grayscale for visualization and is easily determined numerically for any planar region of interest (ROI) using radiology software in routine clinical use. CT-derived HU measurements have been shown to strongly correlate with bone mineral density in the general population, and thresholds have been derived to rule in or

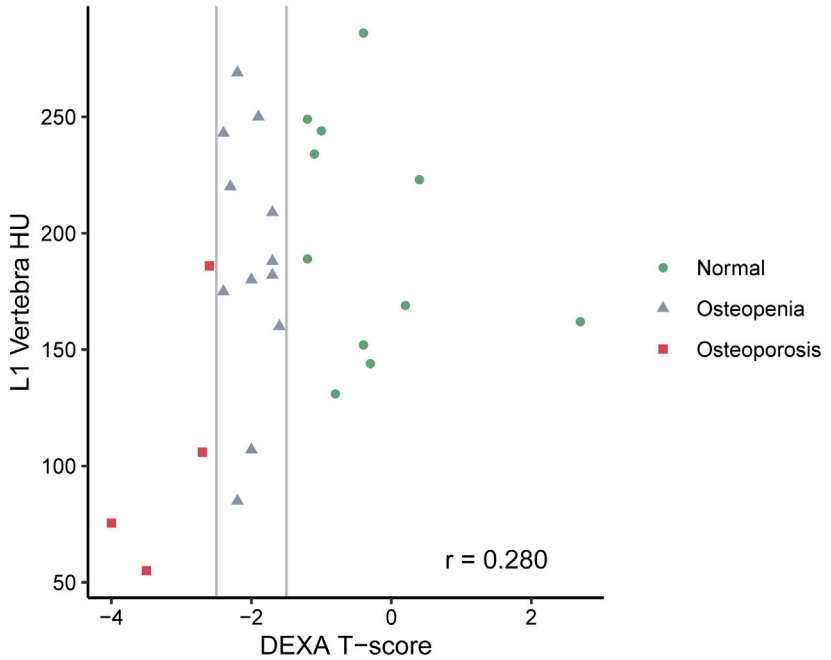

FIGURE 4 | Scatterplot of L1 density (HU) by DXA classification.

rule out osteoporosis. A threshold of <110 HU indicates a risk for osteoporosis (Pickhardt et al., 2013). Our pilot data are in-line with prior data on a nonCP population.

Opportunistic CT screening is carried out at the L1 vertebrae. This vertebra is the optimal site to draw an ROI and screen for osteoporosis, especially since this level is in the field of view on both thoracic and abdominal CT scans. Population-based, age-related bone density measured at L1 is fairly constant and predictable. Also, postmenopausal women and men have similar trabecular L1 attenuation values (Jang et al., 2019). Standardized protocols and methods have been established, including measurements of HU at a standard 120 kilovolts (kV) (the most common CT scan setting) (Garner et al., 2017). There is no significant difference between L1 HU measurement for scans performed without or with IV contrast material (Pickhardt et al., 2013; Pickhardt et al., 2016; Jang et al., 2019) for middle-aged subjects or for the elderly. Variations in HU at L1 without and with IV contrast have been reported, but the clinical impact of this difference is not likely to be significant when utilizing CT as an opportunistic screening tool for osteoporosis in high-risk subjects such as those with CP. (Wright, 2006; Pickhardt et al., 2016).

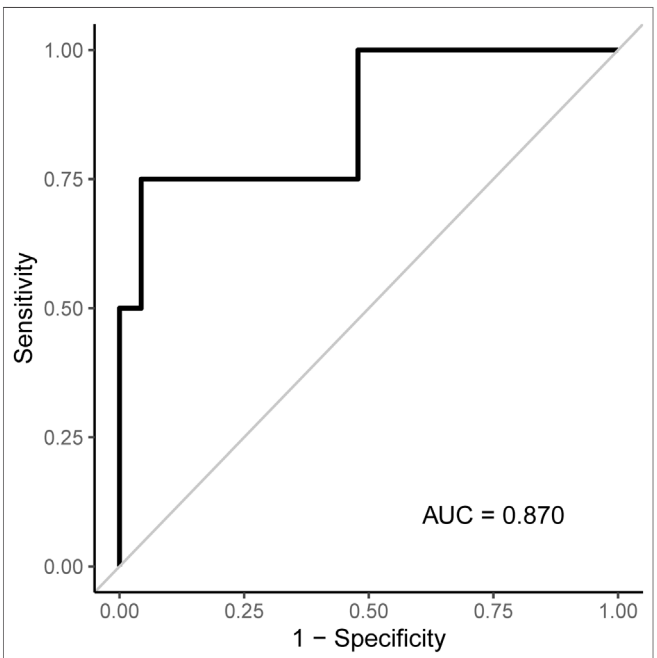

FIGURE 5 | ROC curve associated with the logistic regression model for osteoporosis shown in **Table 2**. An L1 density threshold of ≤106 to indicate osteoporosis maximizes the sum of sensitivity and specificity within this data.

We report that HU can be used to screen for osteoporosis in CP with a high correlation to T-scores on DXA, which corroborates previously published literature in other patient populations (Wright, 2006). CP subjects may receive multiple CT scans during the course of their disease, either to assess complications of CP or as a screening tool for early detection of pancreatic cancer. These CT scans obtained as standard of care can be used as an opportunistic screening tool to look for bone loss, which would put these subjects at increased risk for fractures. This can guide clinicians to obtain DXA scans for diagnosis and allow timely treatment interventions to reduce further bone loss.

In our study, population age was moderately inversely correlated with L1 HU, which provided biological plausibility to our findings. Increased age has been associated with decreased bone density (Barkaoui et al., 2017). Multiple factors can play a

role in this change, including alterations in the dynamics of bone cells, which can result in alterations in the bone formation and resorption process, changes in the bone architecture, and disparities in the concentration of deposited mineral, leading to hypo-mineralized areas. Some changes in the calcium and phosphate regulation also change with age including increases in parathyroid hormones and decrease in the vitamin D3 active metabolites. Finally, a decrease in physical activity and dietary inadequacies will lead to bone loss (Kiebzak, 1991).

The major limitation of this pilot study is the small number of subjects and those with osteoporosis. Given this, identifying a threshold to rule in osteoporosis cannot be confidently performed at this stage. Due to the limited sample size, we were unable to control for confounders in the analysis. Also, since the reported HU thresholds in the literature may not be applicable to CP subjects, we tested established thresholds and derived CP-specific thresholds for osteoporosis prediction. Factors that can cause variability in HU measurement include variations in CT manufacturers (coefficient of variation 4.9%), day-to-day fluctuations, administration of contrast (can increase HU by 11 units), CT tube voltage (130 kV has an 18% lower HU value than the standard 120 kV), and patient positioning (prone vs. supine) (Wright, 2006). Since CT scans in our study came from one academic center to account for this minor variability, the manufacturer, voltage, and administration of contrast were recorded and assessed for confounding. As opportunistic CT is a screening and not a diagnostic tool, these known variations in HU have been shown to have little impact (Wright, 2006).

To our knowledge, this is the first report of opportunistic CT screening in CP. This screening method may be especially helpful in the context of chronic pancreatitis where current societal guidelines do not currently recommend DXA testing and insurance carriers do not universally cover the expense. Despite its limitations, this retrospective pilot cohort study adds important evidence on expanding the use of opportunistic CT screening for osteoporosis in chronic pancreatitis. CT-derived bone density is correlated with age and T-scores on DXA. A larger cohort study in CP is needed to validate these findings.

DATA AVAILABILITY STATEMENT

The raw data supporting the conclusion of this article will be made available by the authors, without undue reservation.

ETHICS STATEMENT

The studies involving human participants were reviewed and approved by the Institutional Board Review of The Ohio State University Medical Center. Written informed consent for participation was not required for this study in accordance with the national legislation and the institutional requirements.

AUTHOR CONTRIBUTIONS

JM-B: analysis, original draft preparation, reviewing, and editing. HM: data collection and analysis. DC: conceptualization, analysis, and reviewing. AL: reviewing and editing. DY: analysis, reviewing, and editing. PH: analysis, reviewing, and editing. LL: reviewing and editing. ZC-M: reviewing and editing. SI: reviewing and editing. AH: analysis, reviewing, and editing. TM: reviewing and editing. DB: analysis, reviewing, and editing. ZS: conceptualization, data collection, analysis, reviewing, and editing.

FUNDING

Research reported in this publication was supported by the National Cancer Institute and the National Institute of Diabetes and Digestive and Kidney Diseases under award numbers: U01DK108327: DC, PH, DB, ZS, ZC-M, and LL U01DK108306: DY. The content is solely the responsibility of the authors and does not necessarily represent the official views of the National Institutes of Health.

REFERENCES

Anderson, P. A., Polly, D. W., Binkley, N. C., and Pickhardt, P. J. (2018). Clinical Use of Opportunistic Computed Tomography Screening for Osteoporosis. *J. Bone Jt. Surg.* 100 (23), 2073–2081. doi:10.2106/jbjs.17.01376

Axon, A. T., Classen, M., Cotton, P. B., Cremer, M., Freeny, P. C., and Lees, W. R. (1984). Pancreatography in Chronic Pancreatitis: International Definitions. *Gut* 25 (10), 1107–1112. doi:10.1136/gut.25.10.1107

Barkaoui, A., Ben Kahla, R., Merzouki, T., and Hambli, R. (2017). Age and Gender Effects on Bone Mass Density Variation: Finite Elements Simulation. *Biomech. Model Mechanobiol.* 16, 521–535. doi:10.1007/s10237-016-0834-x

Buckens, C. F., Dijkhuis, G., de Keizer, B., Verhaar, H. J., and de Jong, P. A. (2015). Opportunistic Screening for Osteoporosis on Routine Computed Tomography? an External Validation Study. *Eur. Radiol.* 25 (7), 2074–2079. doi:10.1007/s00330-014-3584-0

Duggan, S. N., Smyth, N. D., Murphy, A., MacNaughton, D., O'Keefe, S. J. D., and Conlon, K. C. (2014). High Prevalence of Osteoporosis in Patients with Chronic Pancreatitis: a Systematic Review and Meta-Analysis. *Clin. Gastroenterology Hepatology* 12 (2), 219–228. doi:10.1016/j.cgh.2013.06.016

Garner, H. W., Paturzo, M. M., Gaudier, G., Pickhardt, P. J., and Wessell, D. E. (2017). Variation in Attenuation in L1 Trabecular Bone at Different Tube Voltages: Caution Is Warranted when Screening for Osteoporosis with the Use of Opportunistic CT. *Am. J. Roentgenol.* 208 (1), 165–170. doi:10.2214/ajr.16.16744

Gausden, E. B., Nwachukwu, B. U., Schreiber, J. J., Lorich, D. G., and Lane, J. M. (2017). Opportunistic Use of CT Imaging for Osteoporosis Screening and Bone Density Assessment. *J. Bone Jt. Surg.* 99 (18), 1580–1590. doi:10.2106/jbjs.16.00749

Gerety, E. L., Hopper, M. A., and Bearcroft, P. W. (2017). The Reliability of Measuring the Density of the L1 Vertebral Body on CT Imaging as a Predictor of Bone Mineral Density. *Clin. Radiol.* 72 (2), e9–e15. doi:10.1016/j.crad.2016.09.022

Hart, P. A., Yadav, D., Li, L., Appana, S., Fisher, W., Fogel, E., et al. (2021). High Prevalence of Osteopathy in Chronic Pancreatitis: A Cross-Sectional Analysis from the PROCEED Study. *Clin. Gastroenterol. Hepatol.* 3565 (21), 01040. doi:10.1016/j.cgh.2021.09.026

Jang, S., Graffy, P. M., Ziemlewicz, T. J., Lee, S. J., Summers, R. M., and Pickhardt, P. J. (2019). Opportunistic Osteoporosis Screening at Routine Abdominal and Thoracic CT: Normative L1 Trabecular Attenuation Values in More Than 20 000 Adults. *Radiology* 291 (2), 360–367. doi:10.1148/radiol.2019181648

Kiebzak, G. M. (1991). Age-related Bone Changes. *Exp. Gerontol.* 26 (2-3), 171–187. doi:10.1016/0531-5565(91)90010-j

Lee, S. J., Anderson, P. A., and Pickhardt, P. J. (2017). Predicting Future Hip Fractures on Routine Abdominal CT Using Opportunistic Osteoporosis Screening Measures: A Matched Case-Control Study. *Am. J. Roentgenol.* 209 (2), 395–402. doi:10.2214/ajr.17.17820

Lee, S. J., Binkley, N., Lubner, M. G., Bruce, R. J., Ziemlewicz, T. J., and Pickhardt, P. J. (2016). Opportunistic Screening for Osteoporosis Using the Sagittal Reconstruction from Routine Abdominal CT for Combined Assessment of Vertebral Fractures and Density. *Osteoporos. Int.* 27 (3), 1131–1136. doi:10.1007/s00198-015-3318-4

Lenchik, L., Weaver, A. A., Ward, R. J., Boone, J. M., and Boutin, R. D. (2018). Opportunistic Screening for Osteoporosis Using Computed Tomography: State of the Art and Argument for Paradigm Shift. *Curr. Rheumatol. Rep.* 20 (12), 74. doi:10.1007/s11926-018-0784-7

Mettler, F. A. (2019). Medical Radiation Exposure in the United States: 2006-2016 Trends. *Health Phys.* 116 (2), 126–128. doi:10.1097/hp.0000000000000996

Mortele, K. J., Ip, I. K., Wu, B. U., Conwell, D. L., Banks, P. A., and Khorasani, R. (2011). Acute Pancreatitis: Imaging Utilization Practices in an Urban Teaching Hospital-Analysis of Trends with Assessment of Independent Predictors in Correlation with Patient Outcomes. *Radiology* 258 (1), 174–181. doi:10.1148/radiol.10100320

Munigala, S., Agarwal, B., Gelrud, A., and Conwell, D. L. (2016). Chronic Pancreatitis and Fracture: A Retrospective, Population-Based Veterans Administration Study. *Pancreas* 45 (3), 355–361. doi:10.1097/mpa.0000000000000381

Pickhardt, P. J., Bodeen, G., Brett, A., Brown, J. K., and Binkley, N. (2015). Comparison of Femoral Neck BMD Evaluation Obtained Using Lunar DXA and QCT with Asynchronous Calibration from CT Colonography. *J. Clin. Densitom.* 18 (1), 5–12. doi:10.1016/j.jocd.2014.03.002

Pickhardt, P. J., Lauder, T., Pooler, B. D., Muñoz del Rio, A., Rosas, H., Bruce, R. J., et al. (2016). Effect of IV Contrast on Lumbar Trabecular Attenuation at Routine Abdominal CT: Correlation with DXA and Implications for Opportunistic Osteoporosis Screening. *Osteoporos. Int.* 27 (1), 147–152. doi:10.1007/s00198-015-3224-9

Pickhardt, P. J., Lee, L. J., Muñoz del Rio, A., Lauder, T., Bruce, R. J., Summers, R. M., et al. (2011). Simultaneous Screening for Osteoporosis at CT Colonography: Bone Mineral Density Assessment Using MDCT Attenuation Techniques Compared with the DXA Reference Standard. *J. Bone Min. Res.* 26 (9), 2194–2203. doi:10.1002/jbmr.428

Pickhardt, P. J., Pooler, B. D., Lauder, T., del Rio, A. M., Bruce, R. J., and Binkley, N. (2013). Opportunistic Screening for Osteoporosis Using Abdominal Computed Tomography Scans Obtained for Other Indications. *Ann. Intern Med.* 158 (8), 588–595. doi:10.7326/0003-4819-158-8-201304160-00003

Schreiber, J. J., Gausden, E. B., Anderson, P. A., Carlson, M. G., and Weiland, A. J. (2015). Opportunistic Osteoporosis Screening- Gleaning Additional Information from Diagnostic Wrist CT Scans. *J. Bone Jt. Surg.* 97 (13), 1095–1100. doi:10.2106/jbjs.n.01230

Srivoleti, P., Yang, A. L., Jin, D. X., Banks, P. A., and McNabb-Baltar, J. (2021). Does Provider Type Affect Bone Health Surveillance in Chronic Pancreatitis? *Dig. Dis. Sci.* 66 (7), 2235–2239. doi:10.1007/s10620-020-06542-6

Tignor, A. S., Wu, B. U., Whitlock, T. L., Lopez, R., Repas, K., Banks, P. A., et al. (2010). High Prevalence of Low-Trauma Fracture in Chronic Pancreatitis. *Am. J. Gastroenterol.* 105 (12), 2680–2686. doi:10.1038/ajg.2010.325

Wright, J. G. (2006). Revised Grades of Recommendation for Summaries or Reviews of Orthopaedic Surgical Studies. *J. Bone & Jt. Surg.* 88 (5), 1161–1162. doi:10.2106/00004623-200605000-00036

Zysset, P., Qin, L., Lang, T., Khosla, S., Leslie, W. D., Shepherd, J. A., et al. (2015). Clinical Use of Quantitative Computed Tomography-Based Finite Element Analysis of the Hip and Spine in the Management of Osteoporosis in Adults: the 2015 ISCD Official Positions-Part II. *J. Clin. Densitom.* 18 (3), 359–392. doi:10.1016/j.jocd.2015.06.011

Conflict of Interest: The authors declare that the research was conducted in the absence of any commercial or financial relationships that could be construed as a potential conflict of interest.

Publisher's Note: All claims expressed in this article are solely those of the authors and do not necessarily represent those of their affiliated organizations, or those of the publisher, the editors, and the reviewers. Any product that may be evaluated in this article, or claim that may be made by its manufacturer, is not guaranteed or endorsed by the publisher.

Advantages of publishing in Frontiers

OPEN ACCESS
Articles are free to read for greatest visibility and readership

FAST PUBLICATION
Around 90 days from submission to decision

HIGH QUALITY PEER-REVIEW
Rigorous, collaborative, and constructive peer-review

TRANSPARENT PEER-REVIEW
Editors and reviewers acknowledged by name on published articles

Frontiers
Avenue du Tribunal-Fédéral 34
1005 Lausanne | Switzerland

Visit us: www.frontiersin.org
Contact us: frontiersin.org/about/contact

REPRODUCIBILITY OF RESEARCH
Support open data and methods to enhance research reproducibility

DIGITAL PUBLISHING
Articles designed for optimal readership across devices

FOLLOW US
@frontiersin

IMPACT METRICS
Advanced article metrics track visibility across digital media

EXTENSIVE PROMOTION
Marketing and promotion of impactful research

LOOP RESEARCH NETWORK
Our network increases your article's readership